The Influence of Matrix Stoichiometry on Interfacial Adhesion in Composites for Wind Turbine Applications

A thesis in fulfilment of the requirements for the degree of Doctor of Philosophy

By

Ross Forbes Minty

Department of Mechanical and Aerospace Engineering
University of Strathclyde
Glasgow
Scotland
UK
2018

Declaration of Authenticity and Author's Rights

This thesis is the result of the author's original research. It has been composed by the author and has not been previously submitted for examination which has led to the award of a degree.

Signed:

Date:

Acknowledgements

I would first like to express my thanks to my primary supervisor, Professor Jim Thomason, for providing me with all the necessary guidance and support during the course of my studies. In addition, I would like to thank my secondary supervisor, Dr Liu Yang, for his advice and aid on many of the techniques developed and employed for this thesis.

I gratefully acknowledge the financial support my studies received from University of Strathclyde, Nippon Electric Glass and from the Engineering and Physical Sciences Research Council (EPSRC) through project EP/M506643/1.

I am thankful for the assistance provided to me by Dr John Liggat of the Department of Pure & Applied Chemistry. Dr Liggat's advice regarding the epoxy polymer chemistry employed in my research was invaluable to me in constructing this thesis and in helping me to explain my findings.

I wish to also thank Dr Walter Stanley and Mr Ananda Roy of the University of Limerick for providing me with the time and opportunity to work with their rheometer.

I would also like to take this opportunity to thank the various members of the Advanced Composites Group for providing a valuable source of friendship and advice that helped me during the completion of this thesis.

As well as my colleagues in the Advanced Composites Group I would also like to thank Dr Fiona Sillars for her help with my activities in the Advanced Materials Research Laboratory as well as James Kelly for his aid in microscopy and sample preparation.

Finally, I owe a lot to my parents, my brother and Eilidh for their continual support throughout the length of my studies.

Abstract

It is well known that the fibre-matrix interface plays a key role in defining the mechanical properties of fibre composite materials. The ability to efficiently transfer stress between the matrix and the fibres is critical in ensuring the required performance level needed for advanced composite materials. Stress transfer across the fibre-matrix interface is often reduced to a discussion of 'adhesion'. Past discussions of thermosetting matrices have typically focussed on the chemistry of the matrix system, specifically the task of maximising the level of chemical bonding between the fibre and the matrix to produce the strongest interface. However, many authors have also commented on the potential for residual radial compressive stresses formed at the interface to be a significant contributor to the strength of the interface. There is still a significant weight of opinion that holds that even if these residual stresses at the interface can contribute to the stress transfer capability, then chemistry and chemical reactions must play an active role in defining their magnitude. As such it was the objective of this thesis to develop an understanding of how chemistry and residual stresses formed at the interface could be interrelated to influence the stress transfer capability of the interface.

First an understanding was established of how the amine-to-epoxy group ratio (R) of an amine cured epoxy influences the thermomechanical properties of the matrix. Overall it was shown that the R value had a major influence over all of the thermomechanical properties studied. The glass transition temperature (T_g) was shown to change significantly depending on the R value, with a maximum of 87.3 °C observed at a value ($R \approx 1.25$) slightly above the stoichiometric point. The matrix T_g decreased as the R value deviated from this value, approaching room temperature for the extreme ratios. Above T_g, the linear coefficient of thermal expansion (LCTE) was shown to reach a minimum at the stoichiometric ratio due to this ratio inducing

the highest crosslink density. Below T_g, the R value appeared to have a less clear influence. The storage modulus (E') of the matrix was also shown to be affected by the R value, with the stoichiometric ratio possessing the largest magnitude of E' for temperatures 20 °C above T_g. However, for temperatures 20 °C below T_g the storage modulus decreased in magnitude the closer the R value was to R ≈ 1.25. This was the ratio measured to possess the largest T_g value and thus the highest temperature at which E' was plotted relative to the other ratios.

The effect of changing the R value on the interfacial shear strength (IFSS) was investigated using the microbond test. This was done in combination with changing the surface chemistry of the glass fibre and purity of the hardener. Results showed the magnitude of IFSS to be significantly affected by the R value, independent of the fibre sizing applied. The chemistry of the fibre sizing was shown to influence the maximum IFSS achievable and the R value at which it would occur, however the magnitude differences were not as significant. From these results it was concluded that the R value of the matrix has a greater influence than the chemistry of the fibre sizing in defining the level of adhesion at the fibre-matrix interface.

The changes in IFSS were shown to correlate with T_g and the decrease in the contribution of residual thermal stresses at the interface. However, this contribution only represented a portion of the total IFSS value measured. It was concluded that other mechanisms, such as cure shrinkage stresses, must provide the remaining portion of IFSS shown. To expand upon this, the influence of temperature in combination with the other variables discussed was studied using the microbond test within a thermomechanical analyser. At lower temperatures the maximum IFSS value was shown to occur at R ≈ 1.0. The magnitude of IFSS was then shown to decrease as the R value deviated further from this value, again independent of the chemistry of the fibre sizing. Above T_g it was observed that a small value of IFSS remained which

appeared to possess a linear relationship with the level of amine present within the R ratio. It was hypothesized that the magnitude of IFSS being greater for excess amine ratios (R > 1) resulted from a combination of an increase in the level of hydrogen bonding and a variation in the shear failure behaviour of the matrix due to the differing crosslink densities.

Using Nairn's model, a correlation was shown to exist between the IFSS values measured and the potential total contribution of residual stresses for R ≈ 1.0. However, as the ratios deviated further from R ≈ 1.0 the degree of correlation was shown to decrease. It was concluded that assumptions made by the model regarding the contribution of cure shrinkage stresses appeared to be oversimplifications once the R value deviated significantly from R ≈ 1.0.

To address this a novel technique using hot-stage microscopy was used to measure the cure shrinkage of a minute epoxy droplet upon a single fibre during the curing process. The results showed that as the R value was increased, the level of cure shrinkage increased. Rheometry was then used to study the influence of the R value on the gel time of the matrix and applied to the data collected using the hot-stage method. This cure shrinkage data was then reapplied to the model where again good correlation was shown for R ≈ 1.0, yet the discrepancies regarding off-stoichiometric ratios remained. It was concluded that this may be due to a lack of understanding regarding the T_g of a microdroplet and the adhesion mechanisms of a rubbery state polymer. Overall it was concluded that Nairn's model supports the hypothesis that residual radial compressive stresses at the interface can contribute significantly to the stress transfer capability of the interface. Since these stresses were shown to be affected by the R value it would also satisfy the need for chemistry to be involved significantly in some role.

Contents

Nomenclature

α	Linear coefficient of thermal expansion
γ_1	Surface free energy of the liquid
γ_{12}	Difference between the γ_1 and γ_2
γ_2	Surface free energy of the solid
γ_{LV}	Surface free energies for the liquid – vapour interface
γ_{SL}	Surface free energies for the solid – liquid interface
γ_{SV}	Surface free energies for the solid – vapour interface
ΔH	Reaction enthalpy
ΔL	Change in length
ΔT	Difference between two given temperatures
ε_V	Normalised volumetric change
Θ	Contact angle
μ_s	Coefficient of static friction
σ_{fu}	Fibre strength
σ_R	Interfacial thermal residual stresses
τ_{app}	Apparent interfacial shear stress
τ_R	Contribution of RTS to interfacial shear stress
Φ	Heating rate
a	Dimension of major axis used for hot-stage sample
b	Dimension of minor axis used for hot-stage sample
D_f	Diameter of fibre
E’	Storage modulus

E''	Loss modulus
E_0	Concentrations of epoxy groups present initially
E_a	Activation energy
E	Young's modulus
E_t	Concentrations of epoxy groups present after time t
$_f$	Subscript for fibre
F_{max}	Maximum force recorded at full interfacial de-bonding
G'	Elastic modulus
G''	Viscous modulus
h	Thickness at time t of sample
h_0	Initial thickness of sample
$_L$	Subscript for longitudinal
L	Original length of TMA samples
L_c	Critical fibre length
L_{Co}	Corrected embedded length
L_e	Droplet embedded length
L_m	Length of remaining meniscus
$_m$	Subscript for matrix
r	Radius of fibre
R	Ratio of amine to epoxy groups within the system
R_g	Universal gas constant
S	Spreading parameter
$_T$	Subscript for transverse

T_c	Cure temperature
T_g	Glass transition temperature
T_{ge}	End of glass transition range
T_{gf}	Beginning of glass transition range
T_{onset}	Onset temperature
T_p	Peak temperature
T_s	Stress-free temperature
T_t	Testing temperature
V_0	Initial volume of hot-stage sample
V_{acc}	Accelerating voltage
V_f	Fibre volume fraction
V_t	Volume of hot-stage sample after time t
W_A	Negative work of de-adhesion
APS	Aminopropyltriethoxysilane
CTE	Thermal Expansion Coefficient
DGEBA	Diglycidyl Ether of Bisphenol A
DMA	Dynamic Mechanical Analysis
DSC	Differential Scanning Calorimetry
FEA	Finite Element Analysis
FT-IR	Fourier Transform Infrared Spectroscopy
GF	Glass Fibre
GPS	Glycidoxypropyltrimethoxysilane
HPTETA	High Purity TETA

IFSS	Interfacial Shear strength
ILSS	Interlaminar Shear Strength
IPN	Interpenetrating Network
LCTE	Linear Coefficient of Thermal Expansion
MBT	Microbond Test
mIR	Mid-Infrared Analysis
MPS	Methacryloxypropyltrimethoxysilane
nIR	Near-Infrared Analysis
pph	Parts Per Hundred
RTS	Residual Thermal Stress
SEM	Scanning Electron Microscopy
SFFT	Single Fibre Fragmentation Test
SFPoT	Single Fibre Push-out Test
SFPT	Single Fibre Pull-out Test
StdTETA	Standard Purity TETA
TETA	Triethylenetetramine
TMA	Thermal Mechanical Analysis
TTT	Time-Temperature Transformation diagram
UD	Unidirectional

List of figures

List of tables

Chapter 1. Introduction

1.1 Background

The term “composite material” was coined during the 1950’s before becoming a much more widely used term during the 1960’s [1]. This coincided with the first major increase in demand and production of composite materials as their use became commercialised on a large scale, rather than being restricted to more niche applications such as those within the military sector. Since then there has been a rapid growth in demand for, and development of, fibre-reinforced composite materials for use in high performance applications.

As the composites industry has expanded glass fibres have continued to be the most common fibre reinforcement selected for engineering applications [2]. The versatility of glass fibres is due to the structure of glass possessing several key bulk properties such as hardness, transparency, chemical resistance, stability and inertness. In fibre form the glass may gain additional positive properties such as strength, flexibility and stiffness [3]. It is this overall versatility, combined with low cost, which has led to glass fibre continuing to be used instead of other comparable fibres such as carbon, aramid and natural fibres [4].

Wind turbine producers are continually challenged by the need to develop longer, better performing, turbine blades. The exposure of wind turbine blades to high static and dynamic loads over a broad temperature range requires high performance composite materials which will perform reliably over the lifetime of the structure. Optimization of the fibre-matrix interface is critical to achieving the required performance level of these advanced composite materials [5–8]. It is clear that the fibre surface and any coating on the fibre must play a significant role in the formation

of the properties of the composite interface. All reinforcement fibres are surface treated to increase their interaction with polymer matrices. The ability to efficiently characterise the influence of these surface treatments on the interface stress transfer capability is critical to the development of the next generation of higher performing advanced composites.

Stress transfer across the fibre-matrix interface in these composites is often reduced to a discussion of ‘adhesion’ and one of the generally accepted manifestations of adhesion is the mechanically-measured value of interfacial shear strength (IFSS). Past discussions about the interface in composites have typically focussed on the chemistry of the matrix system and the necessity to maximise the level of chemical bonding between the fibre and the matrix through the use of a fibre surface coating – or sizing [6,9–13]. However, a number of authors have also commented on the potential role that shrinkage stresses may have in influencing the stress transfer capability of the interface [14–20]. Specifically, that residual radial compressive stresses formed at the interface may be a significant contributor to the measured strength of the interface.

Thermal compressive radial stresses form during the cooling process due to differences in the thermal expansion coefficients of the matrix polymer and the reinforcement fibre. Thermosetting matrices also undergo volume change during polymerisation, known as cure shrinkage. Due to the increase of the glass transition temperature as the thermoset matrix reacts and shrinks it is possible for some level of this cure shrinkage to be “frozen” into the system, creating additional residual stresses at the interface.

Despite the correlation shown between IFSS and the potential residual stress contribution for both thermoplastic and thermosetting matrices in [14,15] there is still

a significant weight of opinion that holds that even if the residual stresses at the interface do contribute to the stress transfer capability, then chemistry and chemical reactions must also play an active role in defining the magnitude of these stresses [21–25]. In addition to this it is known that glass fibre sizings often utilise chemicals containing unreacted amine and epoxy groups to facilitate good adhesion between the glass fibre and epoxy matrix. In practice however, the level of sizing applied to a coated fibre may vary along the length of the fibre. This has the potential to influence the amine-to-epoxy group ratio at the interface and lead to variations in the formation and performance of the fibre-matrix interface. Given that these two important aspects are in debate, it was considered necessary to study how chemistry and the residual radial compressive stresses formed at the interface could be interrelated to influence the stress transfer capability of the interface.

1.2 Aims and objectives of thesis

As described above, to produce advanced composites with improved mechanical performance we must improve our understanding of the mechanisms of interfacial adhesion. The primary goal of this thesis was to conduct a fundamental study into the influence of the amine-to-epoxy group ratio (R) on the properties of the bulk matrix and fibre-matrix interface through systematically changing the hardener-to-epoxy ratio of an epoxy matrix system. This would allow for the contribution of residual stresses to the IFSS value at different R values to be understood. The potential role of sizing chemistry would also need to be investigated to understand the potential for the sizing to change the R value of the matrix locally at the interface and the resulting effect on interfacial adhesion. To achieve these goals, the following objectives were defined:

1. To study the influence of the R value on the thermomechanical properties of the epoxy system chosen as the matrix material for study.

2. To study how the interfacial adhesion of a GF/Epoxy composite is affected by the R value of the epoxy system.
3. To study the influence of the chemistry of the fibre surface coating on the interfacial adhesion of a GF/Epoxy composite.
4. To study the influence of the R value on the resulting residual stresses formed at the interface during the curing process and the potential contribution of these stresses to the stress transfer capability of the interface.

1.3 Outline of thesis

This chapter provides a brief introduction and background to the reader as well as the objectives and the structure of this thesis. The second chapter presents an in-depth discussion of the literature relevant to the studies undertaken in this thesis. The discussion is broken down into three main sections: Glass Fibre Reinforced Composites, Polymer Matrices and the Glass Fibre-Matrix Interface, each of which consists of further subchapters. 0 provides a detailed description of the materials and methods that were used to generate and analyse the data for this thesis. Chapter 4 outlines the findings of the investigation into the influence of the R value on the thermomechanical properties of the matrix. In Chapter 5 the influence of the R value and the chemistry of the fibre sizing on the apparent IFSS is discussed. An initial model showing the influence of the R value on the magnitude and contribution of thermal residual stresses is also discussed. Chapter 6 presents the findings on the influence of the R value, fibre sizing and testing temperature on the apparent IFSS. A more in-depth model is constructed and discussed regarding the potential contribution of both thermal and cure shrinkage residual stresses to the apparent IFSS value for different R values. Chapter 7 provides a detailed discussion into the influence of the R value on the level of shrinkage that occurs during curing and how this would affect the contribution to the apparent IFSS. The role of the R value in defining the gel point

of the system, along with its place in defining the contribution of residual stresses at the interface, is also discussed in Chapter 7. This results in a final updated model showing the potential contribution of the thermal and cure shrinkage stresses to the stress transfer capability of the interface. The conclusions of this thesis and suggestions for future work can be found in Chapter 8.

Chapter 2. Literature Review

2.1 Glass Fibre Reinforced Composites

2.1.1 Definition of a composite

The term “composite material” was coined during the 1950’s before becoming a much more widely used term during the 1960’s [1]. This coincided with the first major increase in demand and production of composite materials as their use became more mainstream rather than being constricted to more niche applications like for the defence industry. Since then the use of composites has progressively increased in many industries including space, automotive, aerospace, furniture and wind energy.

The internal structure of a composite consists of three basic physical phases [1]: -

i. The polymer matrix phase, which is continuous throughout the composite material;
ii. The reinforcement phase, which is distributed in and surrounded by the matrix phase;
iii. The so-called composite’s interphase which exists as a “phase” between the reinforcement and the matrix.

An older and simpler concept for portraying the phase that exists between the bulk polymer and bulk reinforcement is as a two-dimensional “interface” boundary that separates the two. Each phase listed above will interact with the other, with the interface acting as the simplified representation of the link between the matrix and the reinforcement, allowing loads to be shared and transferred between the two. The actual three-dimensional interphase however is not entirely consistent throughout; it is now accepted that the sections nearest the fibre/matrix interface will vary structurally from the bulk of each respective phase. This leads to the formation of the

third phase listed, the interphase. This concept is supported by the fact that the structure and morphology of the fibre-matrix interface has been found to influence the macroscopic performance of the overall composite material. This means that the microscopic area that exists between the matrix and fibre must change in both structure and properties from the bulk of the rest of the material [1].

A composite material is, therefore, constructed from two different components: the matrix and the reinforcement, with the interphase forming due to their interaction with each other. The structure and nature of all three phases, their configuration and interaction in relation to each other, as well as their relative content can all affect the overall performance of each composite. As such, developing a better understanding of the interphase and how to optimise the stress transfer capability of the interface region is crucial if composite development is to continue to progress.

2.1.2 Mechanical behaviour of fibre reinforced composites

One of the distinct advantages of composite materials is that they possess many characteristics which differ greatly from the more conventional materials typically used for engineering purposes, such as metals and ceramics. Some characteristics are merely modifications of more conventional behaviour while others are new and specific to composite materials alone.

For instance, composite materials are typically neither homogeneous nor isotropic, instead being inhomogeneous (also known as heterogeneous) and non-isotropic (either orthotropic or anisotropic). As one would expect, an inhomogeneous material possesses properties that change depending on the location within the material at which the properties are being measured. Meanwhile orthotropic materials typically possess properties that are different in three mutually perpendicular directions at a point within the body of material, whilst also possessing three perpendicular planes

of material property symmetry. Thus, the properties are dependent on the orientation of a point within the material.

Since composites are inhomogeneous, applying an external force can lead to shear deformation to a lesser or greater extent depending on the direction of the reinforcement, as shown in Figure 2.1.

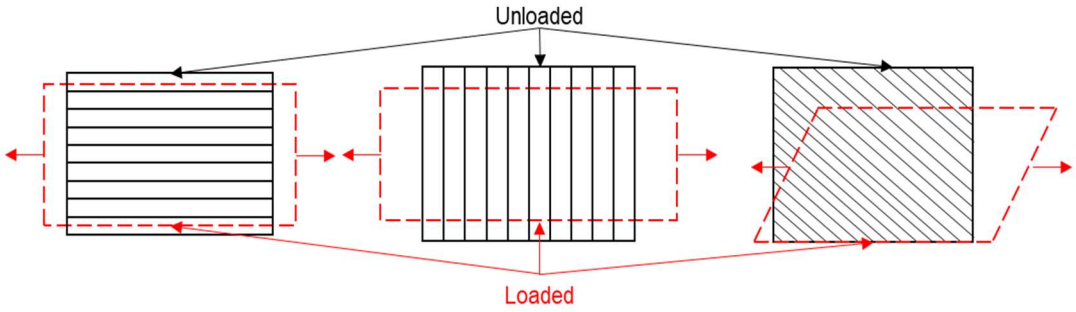

Figure 2.1 - The deformation depending on the fibre orientation: longitudinal, transverse and 45° angled.

Composites using continuous fibres possess superior mechanical properties in the direction parallel to the fibres (longitudinal direction) compared to the directions perpendicular to the fibres (transverse direction), where the matrix provides the bulk of the strength. In the manufacture of wind turbine blades glass fibres are primarily introduced to a composite material in the form of thin sheet constructions known as laminates. Laminates are made by stacking unidirectional layers (plies or laminae) in predetermined directions and thicknesses to give a tailored stiffness and strength properties. The fibres can be laid up in either unidirectional (UD), biaxial or random orientation. Often a combination of differently orientated fabrics is used to produce the strongest structure. UD laminates possessing a lay-up, where all the fibres are oriented in one single direction, produce a composite material with strong mechanical properties in the longitudinal direction. However, such a material is then unable to withstand any loading in the transverse direction, due to the relative weakness of the matrix. This transverse weakness, relative to the orientation of the

fibres, can be readily addressed by constructing the composite using a lay-up of differently orientated fibres, for instance by using 45 ° oriented fibres. This will result in a laminate possessing improved properties in the transverse directions [26].

Due to the heterogeneous nature of composites, studies focus on two points of analysis: micromechanics and/or macromechanics. Micromechanics is the study of composite behaviour where the interactions of the component phases are examined on a microscopic scale. Macromechanics is the study of composite behaviour where the material is presumed to be homogeneous but not isotropic, with the effects of the different component phases detected as the averaged apparent properties of the overall composite material in any particular direction of loading [1].

2.2 Polymer Matrices

Polymers have become a key matrix material in the world of engineering composites, now established in a wide variety of different fields with many different uses. These materials can be highly complex in both composition and structure, their performance under engineering situations being governed by several factors. These factors include: (i) the method of polymerisation, i.e. use of a curing agent/catalyst, (ii) the effect of the functionality of the monomer, (iii) the effect of symmetry and the size of the groups bonded to the polymer backbone, (iv) the effect of molar mass and finally (v) the polymer blend and existence of copolymers. Each of these can influence the mechanical properties of the polymer matrix, and as such the properties of the final composite material [4].

2.2.1 Thermoset versus Thermoplastic

Two of the primary types of polymer used for the manufacture of composites materials are thermosetting resin systems, also known as thermosets, and thermoplastic resin systems. Both possess advantages and disadvantages over the other due to the

nature of the specific matrix structure which they possess. As a result, thermoplastics and thermosets are typically used for different applications.

Thermoplastic matrices are pre-polymerised, high molecular weight polymers. These polymers exist initially as solids and must be heated in order to lower their viscosity sufficiently to achieve composite processing. Thermoplastic polymers can be split into two distinct types: amorphous polymers and semi-crystalline polymers. Amorphous polymers consist of a large number of interpenetrating random coiled molecules that make up the structure of the matrix. Semi-crystalline polymers consist of regions of molecular alignment and increased intramolecular interaction. The crystalline regions within these polymers act as physical crosslinks, similar to those found in thermosets, which improve many of the mechanical/thermal properties.

Some advantages of thermoplastics include their greater ductility and ability to recycled. However, this comes at the cost of some of the mechanical properties such as lower modulus and higher creep values when compared to thermosets. The high melt viscosity required for impregnation can also lead to elevated temperatures sometimes being required during manufacture, thus raising the cost. Examples of thermoplastic polymers in polypropylene (PP) and nylon.

Thermosetting matrices are mixtures of two (or more) chemically reactive, low molecular weight compounds that cross-link together during the curing process to form an irreversible chemical bond. In its initial phase, a thermoset matrix is typically a relatively low viscosity liquid which requires heating to initiate polymerisation. The curing reaction typically involves the use of a curing agent, or hardener, which is added to the resin to facilitate the bonding process between the monomers and oligomers of the thermoset to form crosslinks between the growing chains. These crosslinks will continue to form until a full crosslinked network consisting of tightly

linked polymer chains is created. This molecular network is permanent and as such thermosets cannot be recycled in the manner that thermoplastic polymers can. However, this is offset by the high mechanical and physical strength produced by the network when compared to thermoplastics. Examples of thermosetting polymers include epoxy and polyester resin systems.

2.2.2 Epoxides

Epoxy resin is today one of the most widely used polymeric materials in the composites industry. Epoxy resin systems can generally be thought of as a molecule containing at least one reactive three-membered oxirane ring, consisting of one oxygen atom and two carbon atoms, known as an epoxide (Figure 2.2). Although the first epoxy resins were synthesised as early as 1891 it was not until the independent work of Pierre Castan in Switzerland and Sylvan Greene in the United States that commercial epoxy resins were marketed in the 1940s [27].

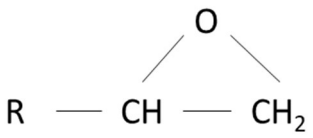

Figure 2.2 - Basic chemical structure of an epoxy group.

Overall, there are two main types of epoxy resin used: glycidyl epoxy and non-glycidyl epoxy. Each type can then be further divided with glycidyl epoxies being one of: amine, ester or ether, while non-glycidyl epoxies are aliphatic or cycloaliphatic. The primary epoxy resin of interest for this thesis was a diglycidyl ether of bisphenol A (DGEBA or BADGE) which is normally synthesised through reacting a large excess of epichlorohydrin with bisphenol A [27]. Figure 2.3 shows the basic chemical structure of DGEBA.

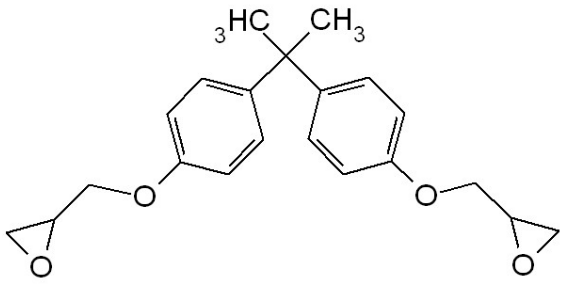

Figure 2.3 - Chemical structure of DGEBA taken from [28].

Curing of epoxy can be achieved using curing agents or hardeners, with commonly used hardeners typically based upon amines [29]. In polymerising the reactive epoxy groups with an amine curing agent, the epoxy ring is opened to form both a secondary amine and secondary alcohol (Figure 2.4).

The secondary amine produced by this reaction can then react with another epoxy group, producing a tertiary amine and another secondary alcohol (Figure 2.5).

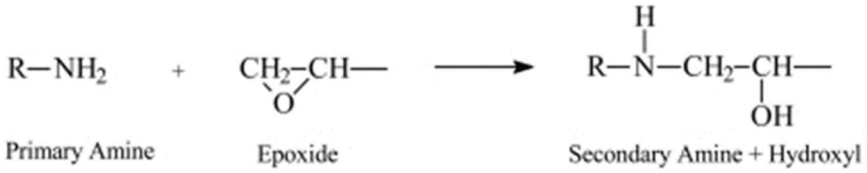

Figure 2.4 - Primary amine and epoxide reaction taken from [30].

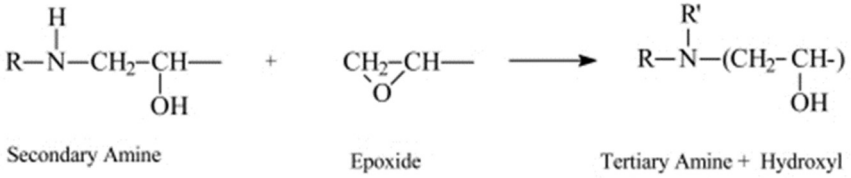

Figure 2.5 - Secondary amine and epoxide reaction taken from [30].

In theory this process will continue until all the amine within the system has been used up. Ideally, there should be one amine hydrogen per epoxy group amongst the reactants to produce a molecular structure with the highest crosslink density. This ratio is defined as the stoichiometric ratio. With each crosslinking reaction, the secondary amine produced is less reactive than the original used in the reaction i.e.

primary amines are more reactive than secondary amines and so on. Depending on the stoichiometry of amine to epoxy, there may also be further reaction of the secondary alcohols with epoxy groups, producing an ether linkage. This is usually very limited within the resin system, unless there are excess epoxy groups, a catalyst such as a tertiary amine, or high cure temperatures are employed [31–34]. The role of the R value in influencing the etherification reaction was explored by Simon and Gillham [35] and can have a major impact on the mechanical properties of the final material.

2.2.3 Cure Kinetics of Epoxides

The cure kinetics of epoxy resins has been extensively studied. Although the cure of an epoxy resin involves the reaction between the epoxy groups and curing agent reactive groups, the full characterization of the process requires understanding many other factors [31]. During the curing process the initially liquid hardener-resin mixture will be converted into a solid. The points of interest during this are the gelation point and the onset of vitrification. The former is the point at which the viscosity of the liquid begins to exponentially increase towards infinity as it transforms into a solid. The latter effect occurs as the glass transition temperature (T_g) of the epoxy polymer approaches the cure temperature (T_c). T_g itself is noted to be a function of the extent of the reaction X_e [31]:

$$X_e = \frac{E_0 - E_t}{E_0} \qquad 2.1$$

with E_0 and E_t being the concentrations of epoxy groups present initially and at cure time t. This allows for the extent of reaction to be quantified. Initially, whilst $T_c > T_g$ (0) the rate of curing is chemically kinetically controlled. As the reaction progresses, with the formation of larger branched molecules, a critical point is reached where a three-dimensional crosslinked network is formed. This critical point is termed the gel point.

As T_g approaches T_c, the curing reaction will become diffusion controlled due to the lack of molecular mobility. Curing may still occur once $T_g > T_c$, but to a much smaller degree. However, if the T_c is too low, then vitrification may occur before the gel point has been reached. This would prevent any further reaction from occurring and limit the properties of the cured matrix.

Extensive research has been conducted by Gillham et al. [35–39] into understanding and classifying the curing process of epoxy resin systems. One outcome from this research was the time-temperature transformation (TTT) diagram (Figure 2.6). A TTT diagram provides a more visual representation of how an epoxy resin system can change with temperature. It also highlights the key characteristic features that will occur.

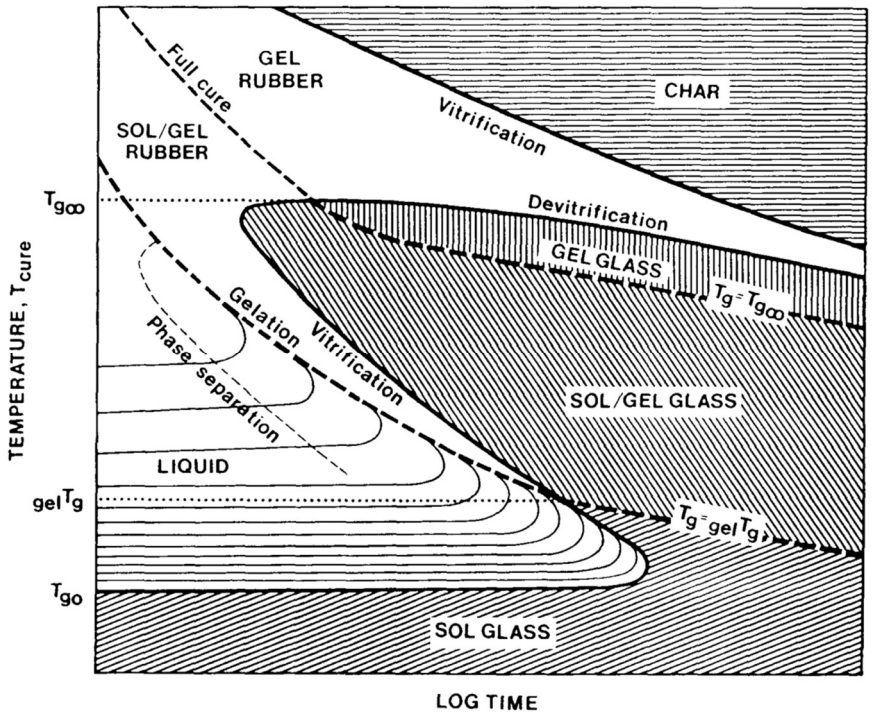

Figure 2.6 - Time-Temperature-Transformation of an Epoxy Resin taken from [37].

From Figure 2.6 it can be seen how variables such as T_c, T_g as well as the heating rate during cure could influence the final properties of the matrix. This has led to extensive studies to evaluate the degree of influence of each of these variables.

Ramos et al. [25] more recently proposed a model for better understanding of cure kinetics and the shrinkage of an epoxy/amine system. The model was primarily based around the results of DSC and pressure-volume-temperature (PVT) experiments. The model proposed was designed to obtain kinetic constants, based on volume shrinkage through curing. The investigators found that both temperature and pressure increased the reaction rate. The kinetic constant of the model was found to be strongly dependent on the cure temperature, whereas the influence of pressure was found to be smaller.

2.2.3.1 Isothermal Cure Studies

Montserrat studied the curing kinetics of a DGEBA-phthalic anhydride system cured at isothermal temperatures between 30 and 130 °C [40] using differential scanning calorimetry (DSC). The samples were cured at certain temperatures for various periods of time before being placed into DSC. Samples were heated and scanned twice to measure the degree of cure achieved and glass transition temperatures. Vitrification phenomena and further structural relaxation were observed when the epoxy was cured at curing temperatures lower than the maximum T_g value, under which the material stayed in a glassy state. This process may significantly affect an isothermal curing reaction system. By examining the extent of curing, the time needed before vitrification and the extent of relaxation were found to depend on the crosslink density of the network.

Koike investigated the isothermal curing process of an epoxy resin by a dielectric measurement and DSC at temperatures below T_g. He concluded that the relaxation during isothermal curing could be caused by the transformation of the matrices from

a liquid state to an un-gelled glassy state as a result of an increase of molecular weight [41]. The T_g was then shown to increase with time using isothermal curing at 80 °C.

Wang et al. [42] compared the isothermal curing of an epoxy-amine system with glass fibre reinforcement at different temperatures from 75 to 110 °C via near-infrared spectroscopy and DSC. It was found that the light transmittance decreased with the increase of viscosity. The epoxy conversion degree was related to the gel point where the light transmittance started to decrease. DSC scanning of the post-cure after isothermal curing indicated that the effect of using different isothermal curing temperatures disappeared, and that the final network of the epoxy resin was affected to some extent by the different pre-cure temperatures. Relaxation of non-equilibrated structures was also found to occur during post-cure.

Consequently, the isothermal curing process of epoxy resins was shown to affect some physical processes such as gelation, vitrification and structural relaxation. However, previous studies mainly focused on the effects on relatively high curing temperatures close to T_g. Thus, more could be done to address what and how much effect the curing time has on isothermal curing reaction of an epoxy-amine system at lower temperatures, such as room temperature (20 °C).

2.2.3.2 Curing schedule and heating rate studies

Studies of non-isothermal curing often focus on the thermal and mechanical performance of the cured epoxy resin. As such the thermal history of curing, especially the heating rate, would be interesting to research to fully understand the resin used for much of this thesis.

Sharma et al. [43] compared the curing processes of an epoxy/amine system at four different heating rates (5, 10, 15 and 20 °C/min) using imide-amines synthesized within their laboratory. To observe whether the trend of the activation energy and

reaction peak temperature changed with heating rate, curing processes of different heating rates were compared by superposition of the heat flow curves. It was observed that the peak temperature during the curing process increased with any increase in heating rate. They concluded that this may be due to the slower heating process allowing more time for physical interactions to occur among the different functional groups of the amine and epoxy. Rosu et al. [44] achieved similar results at different heating rates for two different epoxy/amine curing systems. This suggested that this phenomenon would occur regardless of the epoxy/amine system used. To help analyse their curing systems both studies examined the activation energy by using Arrhenius plots.

The curing kinetics at four heating rates were studied by Zvetkov [45] who constructed reaction models by numerical and experimental methods. It was found that an epoxy/amine system, cured under elevated temperature, achieved higher conversion of epoxy groups when a lower heating rate was used. After experimental analysis and numerical analysis, a side reaction was found to decrease the T_g and reaction enthalpy with higher heating rate when the system possessed a high degree of conversion. Although a lower heating rate may reduce the effect of side reaction, it was pointed out that there may be a possibility of diffusion controlling the overall main reaction.

Dang et al. [28] looked at the influence of the curing schedule on the mechanical properties and water absorption behaviour of an DGEBA/Triethylenetetramine (TETA) network. It was found that, by changing the curing schedule, the free volume distribution within the network could be affected. If the curing temperature was below T_g then the heterogenous network would form with soft and hard crosslinked zones. Yet if the curing temperature was above T_g then a homogenous network would form. The lower curing temperatures would also result in physical ageing of the sample

leading to a decrease in free volume, enthalpy and entropy due to the relaxation of the crosslinked network. The difference in networks and free volume was found to be responsible for changes in the water absorption level with a higher curing temperature found to increase the level of water absorption. This is in agreement with a study previously conducted by Pethrick et al. [46].

To summarise, it has been found that a lower heating rate for curing can increase the conversion of epoxy groups to some degree. Numerical models have been built to predict the reaction. Deviation of T_g and reaction enthalpy has been shown to be a direct result of using a higher heating rate. With this information in mind it would be of value to study the effect of heating rate on the epoxy system used during this thesis to study its volatility and to ensure that the standard cure schedule used was satisfactory.

2.2.3.3 Influence of reactants on cure kinetics

The non-isothermal curing reaction can also be affected by the characteristics of the reactants, i.e. the base structure of the epoxy and hardener. Besides molecular weight, functionality and structure of the reactants, the ratio of hardener-to-epoxy has been shown to have a significant effect on the extent of curing.

Besides a comparison of curing with different heating rates, Sharma et al. [43] also investigated the curing behaviour of DGEBA with various molar ratios of imide-amines as well as 4, 4’ -diaminodiphenyl sulfone (DDS) as the curing agent. Curing agents with higher molecular weight were observed to possess higher activation energies to achieve the full curing of the epoxy. This resulted in a higher stoichiometric concentration of amine being needed to fully cure the epoxy. This increase in the stoichiometric ratio was found to potentially increase the viscosity of the system and decrease the availability of amino groups for the curing reaction.

Skourlis and McCullough [47] investigated the effect of epoxy prepolymer molecular weight and epoxy/amine stoichiometry on the curing reaction. Four epoxy resins with the same basic structure (DGEBA) but different molecular weights were used as prepolymers. A cyclo-aliphatic diamine was used as the curing agent for each resin. It was found that at the optimum stoichiometry ratio of epoxy and amine, the system possessed the highest crosslink density. In addition, increases in the molecular weight of the prepolymer was found to decrease T_g due to the decrease of the systems crosslink density.

The effects of stoichiometry and thermal history were also studied by Meyer et al. [48]. Curing of matrices with three amine-to-epoxy group ratios and several thermal histories of curing were compared by thermal and mechanical tests. Their conclusion on the influence of matrix stoichiometry agreed with that of Skourlis and McCullough [47]. The matrices at the stoichiometric ratio were shown to possess the highest T_g, rubbery modulus and molecular weight values because of the high crosslink density. The effect of different thermal histories during curing was found to be removable by post-curing. This agreed with the conclusion obtained by Wang et al. [42]. In addition, residual epoxy groups were found in all systems after curing, which indicated that the epoxy groups could not fully convert due to the topological constraints of the network in the latter stages of curing.

Garcia et al. [49] studied the mechanical properties and thermal relaxation of a DGEBA resin cured using four linear aliphatic amines and two cyclic aliphatic amines. DSC analysis and tensile, flexural and fracture tests were used in this study. It was concluded that under the same conditions, the functionality of the curing agent determines the performance of the epoxy. This was due to the resulting increase in the crosslink density of the system. Their conclusions provide an additional explanation to Skourlis and McCullough's study [47] that characteristics of a cured

epoxy resin are significantly affected by the crosslink density of the matrix. This in turn can be affected by the type and amount of hardener, the molecular weight of the reactants and the thermal history of curing.

Dynamic and mechanical properties have also been measured to analyse the curing process of an epoxy resin. Fernandez-Nograd et al. [50] investigated the effect of stoichiometry by analysing its effect on stiffness, toughness, strength and ductility. The T_g was found to be obtainable from changes to the modulus and loss factor. Differences of these properties were found to also reflect the network structure of epoxy resin and the extent of curing. The influence of the chain extension and steric hindrance of the curing agent to crosslink density was also confirmed. A higher T_g value was found at the stoichiometric ratio. It was also pointed out that excess of amine may be necessary to achieve maximum conversion of epoxy groups, agreeing with the findings of Meyer [48].

Despite the difference of research objectives in the studies above, they all focused on the effect of curing reactants at different heating rates on the final epoxy resin network. From these studies it can be concluded that for an epoxy resin system cured with the same base structure and curing agent, the crosslink density may be primarily influenced by the amine-to-epoxy group ratio as well as the thermal history of curing. The curing behaviour for a wide range of different stoichiometric ratios will be required to fully understand the cure kinetics of any epoxy resin system used in research reported in this thesis. This will provide a meaningful reference for the matrices thermal properties which can then be compared to any similar change that occurs for the interface.

Overall, relatively more studies have been done on the effects of the hardener-to-epoxy ratio on a non-isothermal curing process. The effect of heating rate on non-

isothermal curing was typically studied at the stoichiometry ratio. The effect of the curing time on an isothermal curing process has been studied mainly at higher curing temperatures. The study of curing is often related to the activation energy, crosslink density, T_g and physical transition of state during curing. DSC has been shown to be an appropriate method to investigate the curing kinetics and thermal properties of an epoxy/amine system.

2.2.4 The influence of matrix stoichiometry on thermal and mechanical properties

The influence of matrix stoichiometry has also been studied in terms of its effect on the mechanical properties of the final cured polymer. Vanlandingham et al. [51] conducted an investigation based on dynamic analysis and phase images to understand the structure of the EPON 828 epoxy thermally cured with the PACM20 amine curing agent. It was found that this system possessed a two-phase structure, with a hard, heavily crosslinked, microgel phase and a dispersed phase of soft, unreacted or partially reacted material. Stoichiometric mixtures were shown to consist of mostly the hard microgel phase although they did still contain a small degree of the softer dispersed phase. This small degree was found to be sufficient to decrease the measured T_g. However post-curing was shown to remove the dispersed phase by causing the unreacted or partially reacted material to cure. This resulted in the T_g value increasing significantly. The size of these two phases was shown to be highly influenced by the amine-to-epoxy group ratio of the system. Vanlandingham hypothesised that amine rich mixtures located at the interphase may lead to its microstructure to contain a large amount of the soft phase. As such it could be hypothesised that the phases discussed may form at the fibre/matrix interface due to local changes in matrix stoichiometry. This would lead to changes in both the thermal and mechanical properties of the composite material.

D'Almeida et al. [52–56] conducted a number of different studies into the influence of matrix stoichiometry on the mechanical properties of epoxy/amine systems. Each study found that the amine-to-epoxy group ratio of the system would affect different properties of the cured polymer. One study involved ageing samples at room temperature (23 ± 3 °C) and relative humidity of 65 to 70% for six months before comparing them with samples tested just after fabrication [56]. Ageing of off-stoichiometric ratios was found to influence the deformability of the polymer differently. Epoxy rich formulations were found to become much more brittle due to the recrystallization of unreacted epoxy monomers and homo-polymerisation of the unreacted epoxy rings by secondary OH groups. These formulations possessed a rigid and tight macromolecular structure due to complete exhaustion of all the reactive groups on the amine molecule [56]. Amine-rich mixtures were found to possess much more stable tensile properties. However, their deformability was found to significantly increase [56]. This difference in deformability was also observed to occur in both compressive and tensile studies with no ageing [53,55]. D'Almeida concluded that composites fabricated from excess hardener ratios typically possess the best compromise between stress and strain for low volume fraction composites, because this matrix formulation showed greater deformability [52]. Overall the results from these studies emphasise the influence that matrix stoichiometry may have on the mechanical properties of the composite. As such it could be expected to influence the fibre/matrix interface similarly.

Palmese and McCullough [57] studied the influence of the amine-to-epoxy group ratio on the material properties of a cured resin. They found that the stoichiometric ratio possessed the highest T_g value as well as the lowest coefficient of thermal expansion above T_g. This was attributed to the stoichiometric ratio possessing the highest

crosslink density, agreeing with the conclusions made by Meyer [48] and Fernandez-Nogrado [50].

The effect of matrix stoichiometry on nano-filled epoxies has also been studied by various authors. Bignotti et al. [58] studied the influence of the amine-to-epoxy group ratio on the curing structure and T_g value of an epoxy-clay nanocomposite. The addition of the organoclay was found to not significantly change the crosslink density of the system through DSC analysis. The results suggested that, as the amine-to-epoxy group ratio was raised, the nanocomposite resins behaved as if they became more densely crosslinked. The data for T_g indicated a similar conclusion. Bignotti [58] concluded that the increase in ratio was not only increasing the crosslink density but also the apparent level of adhesion between the nanoclay filler and the matrix.

Gude et al. [59] studied the effect of different amine-to-epoxy group ratios on different properties of a carbon nanotube (CNT)/ DGEBA epoxy composite. They found that an excess of epoxy groups produced the stiffest material, agreeing with the findings of D'Almeida [53,55]. The stoichiometric ratio was again shown to possess the highest T_g value. However, the effect of CNT was much greater for epoxy-rich ratios, which possessed larger values for the T_g and the elastic modulus. For stoichiometric and amine-rich resins, the effect of CNTs was found to be almost negligible [59]. These results would suggest that the reinforcement effect of CNT is higher in the stiffer and less crosslinked network, while in highly crosslinked epoxy networks they are not able to improve the resin properties significantly. Overall the main conclusion was that changes to the matrix stoichiometry had a greater effect on the properties of the epoxy resin than the addition of the carbon nanotubes.

To summarise, many of the studies conducted on the influence of matrix stoichiometry have focussed primarily on the effect on mechanical properties of the resulting cured

polymer. The findings have shown that the amine-to-epoxy group ratio of the system can greatly influence many mechanical properties associated with composite performance. These findings reinforce the hypothesis that the mixture ratio at the fibre surface may have the potential to influence the stress transfer capability of the interface significantly. As such an in-depth study of this relationship would be valuable to better understanding the complex mechanisms at work at the fibre/matrix interface.

2.2.5 Cure Shrinkage

One significant difference between thermosetting and thermoplastic systems is that thermosets will undergo chemical shrinkage during the curing process due to the polymerization reaction. This cure shrinkage can result in significant volumetric changes, applying a large degree of strain to the system. This strain can potentially lead to the formation of voids and deformations [23] as well the formation of residual stresses that are ‘frozen’ into the network.

As a result, many investigations have been conducted into how the level of cure shrinkage may be influenced by the curing temperature as well as evaluating potential techniques for its measurement. Both Shah et al. [60] and Khoun et al. [61] provided studies evaluating techniques for studying cure shrinkage. Nawab et al. [62] also provided a further review of potential techniques, including the use of dynamic mechanical analysis (DMA) [63] and thermal mechanical analysis (TMA) [64].They all agreed that a modified rheometry method could be applicable for studying the level of cure shrinkage at different curing temperatures. Alternatively, the use of a gas pycnometer or the gravimetric method have been shown to be equally be viable for studying cure shrinkage.

Shah’s [60] investigation provides valuable information regarding the techniques themselves. However, it did not study the cure shrinkage that occurred. Instead it

quantified and compared it at consistent values to measure and report the accuracy of the methods employed. Khoun [61] briefly studied the effect of changing the curing temperature, showing that an increase in temperature would cause the shrinkage to occur earlier and, overall, to reach a higher value. Hoa et al. [65] studied the effect of different hardener ratios on the level of shrinkage and modulus development for a common epoxy resin. The study was based around an ultrasonic technique, with the change in the time of travel of longitudinal ultrasonic waves in a couplant to determine the change in height of a column of resin [65]. They found that as more hardener was added to the system, the level of cure shrinkage would increase.

Other than the studies discussed above, little in-depth work has been done to investigate the variables that may affect the level of cure shrinkage that occurs. Studies looking at the effect of the curing temperature appear more common than the other variables, with samples typically studied at the stoichiometric ratio. Reflecting on the clear effect that matrix stoichiometry was shown to have on the material properties of the cured resin and the results shown by Hoa [65], it would be of interest to study whether this shrinkage would occur similarly for a microdroplet sample. This would be valuable in evaluating whether cure shrinkage, in collaboration with thermal shrinkage, could provide the necessary residual stresses at the interface to significantly influence the stress transfer capability.

2.3 Glass Fibre-Epoxy Interface

The interfaces that form within fibre composites exist due to the material's inherent heterogeneous nature. The fibres and polymer, although linked, remain separate entities to some degree, separated by a boundary that holds the two together. This surface, formed by a common boundary, represents the established definition of the

two-dimensional interface in fibre composites [66]. It is in contact with both the fibre and the matrix, supporting the link that exists between the two thus allowing for the effective transfer of loads. It possesses physical and mechanical properties that are derived from a combination of the two constituents. As understanding of this subject area has increased, the original two-dimensional concept has been extended to form a full three-dimensional phase that exists between the fibre and matrix respectively, as touched upon in subchapter 2.1. Defined as the interphase, it is considered to be the geometrical surface of the classic fibre-matrix contact, as well as the region of finite volume extending on both sides of the interface into both the fibre and matrix [67]. Chemical, physical and mechanical properties of this intervening phase can vary either continuously or in a stepwise manner between those of the bulk fibre and matrix material [66]. Ultimately this will lead to properties varying as you go from one extreme to the other. As such, the nature of the interphase is highly variable, being influenced by the atomic arrangement, fibre topography, molecular conformation and chemical make-up of both the fibre and the matrix [7]. In addition, the morphology of the glass fibre and the ability of elements of each constituent to diffuse into each other can influence its formation [7]. This means that each interphase can be notably different from another composed from different components.

2.3.1 Theories of Adhesion and Bonding

The term ‘adhesion’ is commonly used to describe and analyse the stress transfer capability of the interface. It represents a greatly simplified term used to describe the combination of complex mechanisms at work between the glass fibre and the polymer matrix across the interface. The more established interactions range from adsorption, wettability, electrostatic attraction, chemical bonding, reaction bonding and exchange reaction bonding [7]. These typically represent the major interactions at work, however smaller, less powerful, chemical interactions such as hydrogen bonding and

Van der Waals forces may also influence the formation of the final link between the fibre and the matrix.

2.3.1.1 Wetting and Adsorption

The study of surface wettability has been around since the last century, with Bartell and Osterhof [68] studying the wettability of a solid by a liquid in 1927. The concept of how to treat the contact angle of liquid is even older, with Thomas Young [69] having proposed it in 1805. As understanding has improved it has been established that for successful impregnation of fibres within a polymer resin there must exist good wettability between the two components involved i.e. the resin will spread rapidly over the surface of the fibres and not ball up to avoid contact with the surface. Without good wetting, the resin would not be able to remain in contact with the fibre and thus would not be able to form a bond. Bonding due to wetting is a mechanism that involves very short-range interactions of electrons on an atomic scale that only develops when the atoms of both constituents are in close proximity with each other [7]. Wetting may be expressed in terms of the negative work of de-adhesion (W_A) for a liquid to solid interaction using the Dupre equation as shown in Equation 2.2 [7].

$$W_A = \gamma_1 + \gamma_2 - \gamma_{12} \qquad 2.2$$

W_A represents the energy required to create two separate surfaces and in so doing, destroy the interface that exists between the two with γ_1 representing the surface free energy of the liquid (the resin), γ_2 the surface free energy of the solid (the fibre) and γ_{12} the difference between the two.

It is possible to resolve the forces of work in the horizontal direction at a point where three phases meet i.e. where the droplet of resin is on the fibre. This gives Young's equation shown in Equation 2.3 [7,69] where γ_{SV} , γ_{SL} and γ_{LV} represent the surface

free energies for the solid - vapour, solid – liquid and liquid – vapour interfaces respectively. θ represents the contact angle as shown in Figure 2.7 [7].

$$\gamma_{SV} = \gamma_{SL} + \gamma_{LV} \cos\theta \quad (2.3)$$

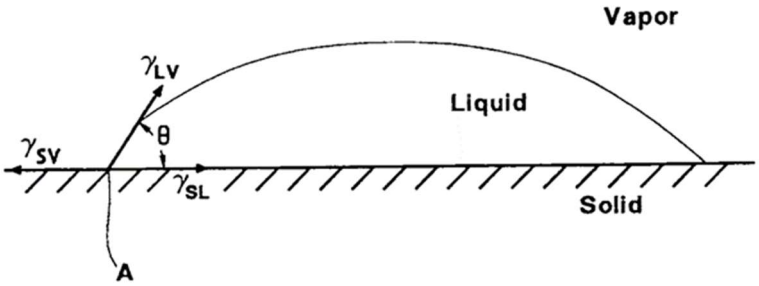

Figure 2.7 - Contact angle θ, and surface energies γ_{SV} , γ_{SL} and γ_{LV} for a liquid drop on a solid surface taken from [7].

Equations 2.2 and 2.3 may then be combined to give Equation 2.4 [7].

$$W_A = \gamma_{LV}(1 + \cos\theta) \quad (2.4)$$

Thus, in theory the higher the work of adhesion is, the larger the interactions will be and the stronger the theoretical bond that should form between the fibre and the polymer. Both the interfacial tension and work of adhesion can be defined using contact angle measurements [70–76]. The interfacial tension is of particular importance since if the wetting of the system is poor then it can lead to the formation of voids [77].

Another important parameter linked to wettability is the spreading parameter S defined in Equation 2.5.

$$S = \gamma_{SV} - (\gamma_{SL} + \gamma_{LV}) \quad (2.5)$$

It gauges the degree of wetting which has occurred. If S > 0 then spontaneous "spreading" will occur, meaning that the surface will be completely wetted by the liquid.

If S ≤ 0 then spontaneous spreading will not occur, leading to only partial wetting. This can be combined with Young's equation to give Equation 2.6 [78].

$$W_A = \gamma_{LV}(\cos\theta - 1) \quad 2.6$$

2.3.1.2 Interdiffusion

Interdiffusion is a phenomenon where atoms or molecules from each constituent mix together across the interface between the two forming an interpenetrating network (IPN) and as such the interphase. A simplified figure illustrating the structure of an IPN is provided in Figure 2.8 [79] and Figure 2.9 [5].

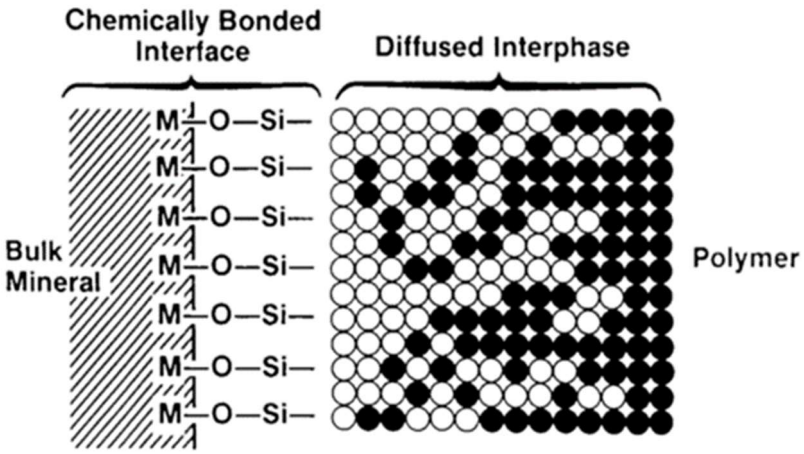

Figure 2.8 - Interphase structure in a silane-coated glass fibre-polymer matrix composite taken from [79].

In general, the degree of molecular entanglement between the two components, the number of molecules involved and the strength of the bonds that form between the entangled molecules all influence the strength of the bond created by this mechanism. The interphase region that forms is large enough to exist as a separate phase from the bulk fibre and bulk matrix, possessing properties that are a combination of the two. As such the chemical, physical and mechanical properties of this region can vary either continuously or in a stepwise manner between those of the bulk fibre and matrix material [66,67]. Typically, sections of the interphase will be significantly softer than

the bulk polymer matrix due to the interference of the “surface-active” fibres on the polymerisation reaction during the curing process [80,81]. Williams et al. [80] also hypothesised that this effect was combined with the fibre being potentially surrounded by matrix material possessing a lower glass transition temperature than the bulk matrix. However, overall it was shown that the presence of the reinforcing fibres caused the net stiffness of the interphase to be greater than that of the bulk matrix in areas located around the fibres [6,7].

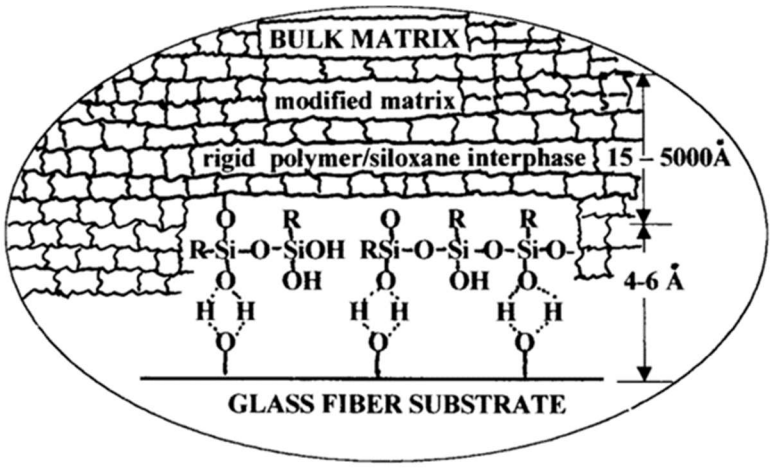

Figure 2.9 - Concept of a Polymer/Siloxane/Glass Interphase taken from [5].

2.3.1.3 Electrostatic Attraction

Electrostatic attraction occurs if there are differences in electrostatic charge between the fibre and the matrix at the interface. As such, this can lead to an attraction bond forming, the strength of which will depend on the charge density i.e. the difference in charge between the fibre and the matrix. Typically, this mechanism is not solely responsible for the formation of an interface since, in comparison to the other mechanisms, its strength is relatively low. Hence it is usually only a minor contributor amongst the other mechanisms. Electrostatic attraction does however become more important with the application of a surface coating, in the form of a coupling agent, to the glass fibre surface. The application can lead to changes in surface properties, including charge. This theory may potentially explain why silane coatings are able to

work especially well with certain acidic or neutral reinforcements but not so much with alkaline surfaces [7].

2.3.1.4 Chemical Bonding

Chemical bonding currently represents the oldest and most widely accepted mechanism for adhesion and bonding due to its nature [7,79,82,83]. The physical adsorption theories strongly depend on Van der Waal's forces or the reaction that occurs between an acid and a base. However, the primary foundation of chemical bonding is the idea of there being a primary covalent bond across the interface that physically holds the two constituents together [7]. Theory presents this mechanism of adhesion as being a bond that forms between a chemical group that exists on the surface of the glass fibre and another chemically compatible group that exists within the polymer matrix. For epoxy systems the two groups are either reactive epoxy groups or reactive amines, depending on the chemistry coating of the fibre. This bond typically forms due to a thermally activated chemical reaction [7].

For a lengthy period, chemical bonding was the main adhesive mechanism proposed for explaining the interaction that exists between the fibre and the matrix. However, as time has passed, more complex phenomena have been discovered which cannot be explained by chemical bonding alone. For instance, the ability of γ-aminopropyltriethoxysilane (γ-APS) to produce a strong interphase under conditions where chemical bonding through the amino group cannot be optimized [6]. This has led to a number of authors commenting on the potential role of shrinkage stresses contributing to the stress transfer capability of the interface [14,16–20,84,85]. This subject will be covered in more detail in subchapter 2.3.3.

2.3.1.5 Mechanical Bonding

As the name would suggest, mechanical bonding involves mechanical interlocking which takes place at the surface of the reinforcing fibre. For instance, mechanical

bonding created using surface oxidation treatments is widely used for bonding carbon fibre-polymer matrix composites due to it producing a significant number of corrugations and pits over a wide surface area of the carbon fibre [7]. The strength of such an interface may not be very strong in transverse tension but it is strong in longitudinal shear, the principal loading mechanism for most applications.

Along with the simple geometrical aspects of mechanical bonding there are also multiple different types of internal stresses that exist within the material. These arise due to the shrinkage of the matrix material during curing as well as the thermal expansion that occurs between the fibre and the matrix when cooling takes place [111]. This leads into subchapter 2.3.3.

2.3.2 Fibre Surface Coatings

Since its inception, the glass fibre industry has continued to grow and expand as its products have found more applications due to the fibres possessing a unique combination of strength, stiffness, light weight and low cost, due to the nature of glass chemistry [86]. However, to extract the full potential from glass fibres in a fibre reinforced composite it was necessary to ensure that the inorganic glass fibre and the organic polymer would successfully interact and bond to form the composite material.

Within the composite material, the physical and chemical interactions between the glass fibre and the polymer matrix always takes place at an interface, where the link between the two exists. However, the relative contribution of each of the phases to the stress transfer capability depends significantly on the formation of stronger interactions if they are to truly bond together. Such interactions include acid-base interactions and covalent bonds [13]. These adhesive interactions between the fibre and the matrix can only form if “intimate contact between the two phases is achieved” [13].

Overall, the finished composite interface will depend strongly on maximising contact between the two phases as well as on the presence of any flaws located at the interface. The interface challenge is that due to the chemical dissimilarities between a glass fibre and polymer resin, the stress transfer capability will not be optimised without the addition of an external surface coating. Hence manufacturers apply a chemical coating to the surface of the fibre, a sizing. Each sizing is tailored for the specific fibre and the polymer resin, to promote as much “adhesion” between the two as possible. The objective is to allow a typically heterogeneous material to act as one single homogeneous structure [86].

2.3.2.1 Sizings

In most instances, the application of the sizing to glass fibres occurs just after the fibre formation process but before the individual filaments are gathered into a strand below the bushing [3,87]. Typically, the most common sizing formulations are water-based mixtures of molecular species such as adhesion promoters, film formers, lubricants and other processing aids as shown in Table 2.1 [86]. As such, the goal of designers is to create sizing formulations that deliver efficient manufacturing processes as well as providing the maximum level of adhesion between the fibre and the polymer matrix to optimize the performance of the interface. A further goal of sizings is to protect fibres from environmental damage such as water ingress and damage through contact with other fibres. Commercial sizing formulations used on glass fibres are typically confidential; the manufacturers do not want to disclose their secret formulations to their competitors. However, in many cases the basic composition of a standard sizing is known in rough detail, with the approximate percentages of each component being known, just not the exact values.

It is important to note that the characterization of the sizing as well as the glass fibre is critical to determining whether the final glass-reinforced composite will be a success

[88]. As a result, interest has grown in understanding the interface, with many standardized tests developed and acknowledged by ASTM and ISO for analysing interfacial adhesion, interfacial shear stress, tensile stress modulus and hydrolytic stability.

Classification	Functionality
Coupling Agents	Adhesion promoters that bond or couple the glass surface with specific matrix resin systems; May also provide excellent filament protection as well increasing the dry fibre and strand breaking strength.
Film Formers	Holds filaments together and provides protection for the glass fibre strand.
Film Modifiers	Alters how the film forms to increase strength, flexibility or adhesion properties.
External Lubricants	Helps provide resistance to abrasion damage at external contact points, an example being strand guides in downstream processes.
Internal Lubricants	Helps reduce the filament-to-filament abrasion within the glass fibre strand.
Emulsifiers/Surfactants	Forms stable suspensions or emulsions of immiscible ingredients, typically in water-based systems.
Other Process Aids	Used when required to control foam, wetting, static behaviour, biological activity as well as any other special requirements by a specific end-use or internal processing need.

Table 2.1 - Typical Size Components.

Due to the importance of the sizing in promoting adhesion between the glass fibre and the polymer matrix, a significant amount of research has been invested into better understanding how different sizings can result in different levels of adhesion and as such composite performance. Saidpour et al. [89] studied the effect of applying several different sizing systems to the surface of glass fibres and identifying those that gave the optimum mechanical properties. The investigation revolved around the use of fibre coatings, consisting of only four different silane coupling agents and one titanate coupling-agent, at three different concentrations, which were applied to glass fibres used in vinyl ester composites. They found that the different coatings did indeed result in changes to the interfacial bond strength, with several interesting notes. Firstly, sizes designed for polyester matrices were found to provide the best performance in terms of tensile strength and interlaminar shear strength (ILSS). Next, they found that good performance seemed linked to the formation of strong styrene bridges between double bond unsaturation in both the coupling agent and the vinyl ester. Furthermore, the number of siloxane bridges at the interface between the coating and the fibre heavily influenced performance. The final note found that the poor ILSS values for some samples was linked to coupling agents that possessed a lower general reactivity. They concluded that this was due to the higher degree of mobility within these coupling agents, which may allow for more distribution in, and hence weakening of, the interphase region, thus damaging the performance of the composite [89]. However, since this investigation was only conducted using silane/titanate coatings, the results produced may not be fully relevant regarding the performance of a full commercial sizing.

Zhuang et al. [90] investigated the influence of the sizing distribution on the properties of sized glass fibres and corresponding polypropylene (PP) composites by using a two –stage sizing application process. This involved applying the silane coupling-

agent and a polymeric film former at separate stages, in different sequences, to see the net effect, if any. For reference, a one-stage application process would involve both the coupling agent and film former applied at the same time in a single mixture. The study focussed on the surface properties of the sized glass fibres as well as the transverse tensile strength of constructed unidirectional glass fibre reinforced composites using surface and interface analysis methods and tensile testing respectively [90]. Their results highlighted that the sizing application conditions did influence the formation of the dried sizing layer that formed upon the fibres and as such the stress transfer capability of the interface. For the two-stage technique, which involved applying the APS first, at conditions matching those found in industry, they measured a low interface strength value. This was attributed to there being little uptake of APS. They found however that this effect could be solved by increasing the uptake of APS by increasing the applicator speed which produced a composite with mechanical properties a little lower than those found in composites produced by the one stage sizing process. It was concluded that this must be attributed to enhanced covalent bonding as well as a stronger base-acid interaction between the amino group of the sizing (APS) and the anhydride group of the matrix modifier applied which was maleic anhydride grafted polypropylene (MaPP).

In terms of sizings designed for epoxy compatibility, research has been conducted to gauge their effect on the formation of the interface for both glass and carbon fibres. Fernández et al. [91] studied the influence that epoxy sizings had on the fracture behaviour of woven carbon fibre tetra-functional epoxy composites. The first sizing was based on a DGEBA resin, supplied by Dow Chemical (DER 332) whilst the second type was based on tetraglycidyl methylenedianiline (TGDDM). Several different techniques including atomic force microscopy (AFM), DMA, and scanning electron microscopy (SEM) were used to analyse different fibre/epoxy composite

combinations along with a wettability study to investigate adhesion. Further tests carried out included macro-mechanical tests such as three-point flexural and short beam shear to measure any change in the mechanical properties of the composites. They found that the application of the epoxy coating led to notable improvements in the mechanical properties of the composite due to what they concluded as an increase in the level of adhesion between the fibre and matrix.

Regarding the effect of different sizings, Dey et al. [10] studied a series of fibre sizing formulations with the goal being to identify the influence of the silane coupling agent and film former on the properties of a glass fibre/ epoxy resin interphase using the microbond test. Specifically, they were interested in the role of the film former. They found that the chemical reactivity and wettability of the film former influenced the strength and energy absorption of the interphase, with this being assigned to improvements in chemical bond formation as well as decreasing the surface roughness of the fibre. Thus, it appeared that both the film former and coupling agent play a positive role in the formation of the interphase.

Dai et al. [92] studied the effect of applying an epoxy sizing to a carbon fibre through the use of various techniques. These included X-ray photoelectron spectroscopy (XPS), the microbond test and inverse gas chromatography (IGC). Their goal was to identify key differences between the sized and de-sized carbon fibres, primarily the interfacial adhesion between the fibre and matrix. They studied changes in the surface chemical properties using XPS while changes in the surface energy and acid-base interaction were investigated by IGC. Surprisingly, results showed that fibres de-sized using acetone extraction possessed a higher interfacial strength, which coupled with the fact that the acid parameter of the carbon fibres reduces, improves the bonding strength at the interface. They concluded that the interfacial shear strength was dependent on not just chemical bonding but also the physical and adhesive

interactions occurring at the interface. Such interactions could potentially include the existence of residual stresses at the interface. These findings would suggest that it would be beneficial to study the potential influence that fibre sizings have on the local stoichiometry of the interface and how this may result in changes to the interfacial shear strength. This was one of the research goals for this thesis.

Plonka et al. [13] investigated the effect of ageing different sizes and applying them to glass fibres. The sizes included γ-aminopropyltriethoxysilane (APS) along with combinations of APS with either polyurethane (PU) or epoxy (EP). Several different aging treatments were studied against a reference value to study different surface properties produced from zeta potential, inverse gas chromatography (IGC), wetting techniques and atomic force microscopy. The interface was analysed using both single fibre pull-out and cyclic loading tests. The ageing of the sizing showed a clear effect on the surface properties of the fibre, and as such performance dropping off over time. The interfacial strength of the composite was found to be strongly dependent on the formulation of the sizing applied along with the topography of the fibre surface after application. Therefore, it was concluded that there was a need to further analyse this interaction between the fibre – sizing – matrix since although the variations in performance were clear, the specific reasons why were not. This remains a current theme in continuing research, with the focus being to understand the interaction that occurs at the interface.

Overall, much of the research conducted on the influence of sizings has concluded that they improve the stress transfer capability of the interface through improvement of the ‘adhesion’ between the fibre and the matrix [10,13,91–95]. The term adhesion represents a simplified term for encompassing the multiple complex mechanisms that exist at the interface and contribute to its strength. Yet, this generalised term can lead to misinterpretation when it comes to understanding the fibre-matrix interface, since it

can potentially mean different things depending on the readers' viewpoint. This would suggest that the application of sizings may potentially improve multiple adhesion mechanisms, although it is difficult to determine specifically which ones. The theory of adhesion and the potential mechanisms at work was discussed in more detail in subchapter 2.3.1.

2.3.2.2 Silane Coupling Agents

a) Definition of a silane coupling agent

As has been established, optimising the interaction between the inorganic glass fibre and the organic polymer matrix is vital in terms of producing a composite material with the desired mechanical properties. This interaction is influenced by many different mechanisms, such as the chemical/molecular features, the atomic composition of the specific glass fibre surface and its topography.

Typically, the chemical composition of the surface of a glass fibre consists of both weakly adsorbed materials that can be removed by heat treatment including hydroxyl groups, silicon and aluminium [96], as well as strongly adsorbed materials that are strongly bonded to the surface through covalent bonds, i.e. the fibre sizing. As such, both types of adsorbed material play a major role in the interaction between the fibre and the polymer. Furthermore, the topography of the fibre can play a role in the interaction since it can govern the level of mechanical bonding that occurs between the fibre surface and the matrix resin depending on the properties and nature of the surface imperfections [97].

It is commonly assumed that the foundation block of a good glass fibre sizing system revolves around the selection of an appropriate adhesion promoter, also known as a coupling agent, which provides the necessary platform between the inorganic glass fibre surface and the reactive sites located in the polymer matrix system. Currently, the most used coupling agents are organosilanes. This species of chemicals is

designed to both promote the reaction between the silanol sites located on the glass fibre surface and on the organosilane molecule as well as to provide an organic group for interaction (bonding) with the matrix polymer [7]. Beginning with the creation of organofunctional silane coupling agents, a vast amount of research has been dedicated to investigating this interaction between the fibre and the matrix in order to identify chemical compounds which may increase the stress transfer capability [24,97,106–108,98–105]. The focus has primarily been on studying the link between chemical bonding and the level of 'adhesion' between the fibre and the epoxy matrix. The conclusion is that, typically, more chemical bonds across the interface will lead to a stronger link. In comparison, little work has been done to study the effect that the various components of the sizing will have on the properties of the interphase due to it theoretically altering the local mixture ratio of the epoxy system.

Silane coupling agents are valued for their ability to form a durable bond between two chemically dissimilar materials, typically one that is inorganic and another which is organic. The general formula for a silane coupling agent typically contains two different classes of functionality, as shown in Equation 2.7 where R is the organofunctional group, CH_2 is the linker, Si is a silicon atom and X_3 are hydrolysable groups.

$$R - (CH_2)_n - Si - X_3 \qquad 2.7$$

It is these hydrolysable groups that are involved in the reaction with the inorganic substrate, being typically alkoxy groups, primarily methoxy or ethoxy. When hydrolysed they form a reactive silanol group that can then condense with other silanol groups, creating strong siloxane linkages. The R group represents the organofunctional group which is a "nonhydrolyzable organic radical". These possess a functionality that allows the silane to bond with organic resins and polymers.

To conclude, the manner in which the fibre surface is coated is highly dependent on the coating used as well as the matrix material it is designed to bond with. If the interphase region between the fibre and the matrix is to be accurately analysed, then it is necessary to understand the chemical nature/microstructure of the glass fibres investigated [66]. As such, in today's composites industry, conducting accurate investigations into the status of interfaces modified by surface treatments and their effect on the resulting composite is just as valuable as creating new analysis techniques [97].

b) The functionality of silane coupling-agents

Overall, a significant level of research has gone into why silane coupling-agents influence the interface bonding methods between the two components. This has resulted in the proposal of several different theories, with the most established theory revolving around the concept of chemical bonding [24,97,106–108,98–105]. Other theories highlighted by Kim et al. [97] link with preferential absorption, restrained layer, coefficient of friction, wettability and the surface energy effect. All of these theories have their specific benefits, however none are as established and widely accepted as chemical bonding. In turn, the industry has focussed on designing silane coupling-agents specifically revolving around their chemical reactivity with both the inorganic substrate, in this case glass fibre, and the organic polymer resin. Since multiple different combinations of fibre and polymer may be used this has led to the design of several different silanes which contain organofunctional groups. It is these groups that are vital to the theory of chemical bonding, thus allowing for a more in-depth discussion of what occurs. Despite this diversity, analysis has been conducted by Thomason [2,109] which highlighted that only three or four different silanes are used by the glass fibre industry.

c) Role in chemical bonding theory

As described by Kim et al. [97], the organofunctional groups can act as a link between the inorganic glass and the organic resin, creating a “chemical bond with the surface of the glass through a siloxane bridge, while its organofunctional group bonds to the polymer resin.” Koenig and Emadipour [110] proposed that it is this co-reactivity that allows for the molecular structure of the interface to be continuously normal to the fibre surface.

Hull and Clyne [111] provided a simple model for the function of silane coupling agents, as shown in Equation 2.8, with Kim et al. [97] breaking down in chemical detail what exactly occurs between the silane coupling agent and the glass fibre surface and polymer matrix.

$$R - SiX_3 + H_2O \rightarrow R - Si(OH)_3 + 3HX \qquad 2.8$$

Overall, the choice of which organofunctional group and the pH of the solution present will have significant control over the compositional form the silane will take when it is in solution. Plueddemann [79,112] postulated that, after the process of coating, a reversible condensation reaction will occur between the silanol coating and the M-OH groups on the surface of the glass fibre. This reaction will create a polysiloxane layer which bonds to the glass fibre surface, holding the two together.

Hence, once the silane coating is bonded to the fibre surface, if the treated glass fibres are then exposed to uncured resins then the R-group will react with the functional groups present within the polymer resin, creating strong covalent bonds. Naturally, it is necessary to ensure that the functional groups within the silane and the resin are compatible and thus can react together, hence why different coupling agents are used for different resins. If both reactions successfully occur then the coupling agent has succeeded in creating an increased level of adhesion between the two dissimilar

materials through a large density of strong chemical bonds which will contribute significantly to the stress transfer capability of the interface [97].

The topic of the interaction that exists between different glass fibres, polymer resins and silane coupling agents can be considered significantly complex due to the influence which several different properties of the coupling agent have over the mechanical and physical properties of the resulting composite material. Even now, much work still needs to be done if we are to gain a better understanding. The techniques most commonly used in the past have been Fourier transform infrared spectroscopy (FT-IR) [113–121], nuclear magnetic resonance spectroscopy (NMR) [120,122,123] and more recently XPS [124–128].

d) Role in formation of interpenetrating polymer networks

Although the chemical bonding theory does successfully encompass many of the phenomena found within fibre-reinforced composites, there may exist other mechanisms that are acting within the interphase since the application of a silane coupling-agent may not produce the maximum degree of performance if applied alone.

A well-established view is that bonding between the fibre and matrix will occur through multiple means other than just chemical bonding. This link to interdiffusion and interpenetrating networks (IPN) was proposed by Plueddemann [129,130] as well as Ishida et al. [119]. Schrader [131] made the discovery that the interface between the coupling agent and the epoxy polymer matrix will act as a diffusion boundary, where the interphase forms. The epoxy resin was shown to penetrate the chemisorbed silane layers, while the resin has physisorbed silane molecules integrated into its structure. The combined effect of both chemical bonding and IPN reaction methods have a

major influence on the performance of thermoset composites in terms of interfacial bond strength [97].

As previously noted, the phase that exists between the bulk fibre and bulk polymer possesses properties that can differ greatly from the bulk properties of the two different components. One instance, for example, is the glass transition temperature (T_g), with the interphase typically possessing a lower T_g than that of the bulk materials. Drown et al. [93] confirmed this by plotting a graph comparing T_g vs the degree of size applied to the stoichiometric mixture. It was shown that as more size was applied, the T_g dropped accordingly. Kim et al. [97] suggested that this was due to the silane and other components within the sizing breaking down the cross-linking density of the mixture. However, in some cases the T_g of the interphase is larger than that of the bulk material. For instance, the addition of nanoparticles to the interface of a fibre-reinforced composite can alter its thermal properties. Haque et al. [132] found that significant improvements could be made in both the mechanical and thermal properties of the finished composite through the addition of nanoclay particles. Similar improvements have been found through the addition of nanoparticles to different systems or via modelling of such additions [133–135].

2.3.3 Residual Stress

As mentioned in subchapter 2.3.1 discussions about the composite interface have primarily focussed on the chemistry of the matrix system and fibre surface coating to ensure the optimum formation of chemical bonds [6,9–13,136]. In particular there has been extensive study of fibre sizings to better understand the specific mechanisms influencing the link between the inorganic glass fibre and the organic polymer matrix system [5,79,98,99,101,103,105,129,137]. However, a number of authors have also commented on the potential role of shrinkage stresses contributing to the stress transfer capability of the interface [126–133]. Specifically, it has been suggested that

residual radial compressive stresses at the interface may contribute significantly to the stress transfer capability of the interface. The primary goal of research focussed on residual stress is to maximise our understanding of it and to utilise this knowledge to then maximise mechanical performance. For this thesis, the main motive was to show that chemistry, in the form of matrix stoichiometry, and residual stresses at the interface were in some manner interrelated. Thus, residual stresses could be shown to significantly contribute to the stress transfer capability of the interface whilst meeting the observed demands that chemistry must be in some way involved.

2.3.3.1 Formation of residual stresses

The residual stresses that form within fibre epoxy composites can be classified into two categories based on their nature of formation as well as magnitude. Thermal radial residual compressive stresses can form during the cooling process due to differences in the thermal expansion coefficients (CTE) of the matrix polymer and the reinforcement fibre. As such residual thermal stress (RTS) can be defined as a residual stress introduced within a body resulting from any change in temperature. Due to fibre epoxy composites typically requiring curing to achieve full structural integrity, this process often involves the composite being exposed to an elevated temperature for an extended period. As a result, this process induces residual thermal stress to build up in the composite when at a temperature different from its process temperature [67,138]. The magnitude of RTS is considered to primarily depend on four parameters: (i) the temperature difference between testing temperature and stress-free temperature (T_g for epoxy [143,146]); (ii) the CTE of the fibre and matrix; (iii) the thermo-elastic properties of the fibre and matrix as well as (iv) the fibre volume fraction of the composite [67]. Glass fibre properties have been found to be temperature dependent, but typically to a much lesser degree than that of the matrix [139]. Thus, any major differences in RTS are likely to originate in changes in the

properties of the polymer. It has been shown previously that the T_g and CTE of an epoxy resin can be influenced by the hardener-epoxy ratio of the system [51,57]. Maximum RTS would be expected to occur at the stoichiometric ratio due to the optimized nature of the T_g and CTE values. Deviating from this value would thus lower RTS.

One significant difference between thermosetting and thermoplastic systems is that thermosets will undergo chemical shrinkage during the curing process due to the polymerization reaction. This cure shrinkage can result in significant volumetric changes, applying a large degree of strain to the system [21,84]. Jakobsen et al. [21] have previously discussed the possibility that cure shrinkage may actually provide the bulk of the residual stresses when compared to thermal shrinkage stresses in thermoset systems. However, any cure shrinkage that occurs before the gel point of the system can potentially relax away. This can be attributed to the low molecular weight and liquid nature of the matrix in this state. Gelation is defined as the liquid–solid transition of an epoxy resin that occurs when the average molecular weight approaches infinity. One can reasonably assume that any strain induced by cure shrinkage will require more time to relax away as the system approaches the gel point. Thus, once the gel point is exceeded then any further cure shrinkage related residual strain will be locked into the epoxy network. As the system is cooled back through T_g the residual stress from the cure shrinkage strain will increase in proportion to the increase in the matrix modulus [84,85,140]. The research studying the topic of cure shrinkage within epoxy matrices was covered in more detail in subchapter 2.2.5.

2.3.3.2 Modelling residual stresses

Several models have been proposed [16,17,22,141,142] to calculate the residual thermal stresses, with Nairn [16] having proposed a model showing significant normal stresses at the interface as shown in Equation 2.9. The benefit of Nairn's model is

that it accounts for the effects of differences in axial and transverse fibre properties exhibited by many reinforcements.

$$\sigma_R = A_1\left(1 - \frac{b^2}{r^2}\right) \tag{2.9}$$

where A_1 is a constant and the result of the calculation shown in Equation 2.10.

$$\begin{bmatrix} X_{11} & X_{12} \\ X_{21} & X_{22} \end{bmatrix} \begin{bmatrix} A_1 \\ A_3 \end{bmatrix} = \begin{bmatrix} (\alpha_m - \alpha_{fT})\Delta T \\ (\alpha_m - \alpha_{fL})\Delta T \end{bmatrix} \tag{2.10}$$

The model shown in Equation 2.10 represents a simplification of the composite cylinder model proposed in [16]. Nairn assumed the volume fraction of the interphase to be zero which allowed for the equation to be reduced to a two by two linear system. The X terms represent elements of the matrix that can be calculated if certain material properties of the fibre and matrix are known, such as modulus, Poisson's ratio and volume fraction. These expressions are detailed in [16].

Of the variables presented, b is a function of the fibre volume ratio (V_f), r is the radius of the fibre, α is the linear coefficient of thermal expansion, ΔT represents the difference between the stress-free temperature (T_s) and the testing temperature (T_t) and f, m, L and T are subscripts for the fibre, matrix, longitudinal and transverse respectively. From the form of Equation 2.10 it can be seen that the interfacial thermal residual stresses (σ_R) are directly influenced by changes in ΔT. For thermosetting systems, the stress-free temperature is accepted as being the glass transition temperature T_g [141,143]. The data produced by Equation 2.10, in combination with a coefficient of static friction value μ_s may then be used to calculate the contribution to the interfacial stress transfer capability (τ_R) [14,67,84,144].

$$\tau_R = \mu_s \sigma_R \tag{2.11}$$

2.3.3.3 Effect of residual stresses

The existence of residual stresses within a fibre epoxy composite can have both beneficial and detrimental effects on the properties depending on certain parameters. In unidirectional lamina, the residual stresses often leave fibres under compression and the matrix under tension in the fibre longitudinal direction [67]. As such any potential stress transfer between the fibre and the matrix would occur at the interface. In the radial direction, any residual stresses present will place both the fibres and the matrix under a state of compression [67]. In addition to this, compressive and tensile hoop stresses may form in the fibre and the matrix respectively due to RTS [16]. Due to the presence of these stresses, the properties of the matrix and interface may all be subject to change. Typically, if the residual stresses and the stresses due to external loads are equal in sign then the maximum allowable external stress will decrease. For instance, if there is a compressive residual stress located in the fibre then there will be a reduction in compressive strength. However due to the difference in signs this means there will also be an increase in the tensile strength in the fibre direction [67,141].

If the build-up of residual stresses within the matrix is sufficient, defects may form within the composite structure due to both RTS and cure shrinkage stress [23]. Designers attempt to minimise any such defects since their failure mechanisms are acknowledged as being very difficult to predict [145]. Compressive stress in the fibre may lead to ‘fibre waviness’, a term describing when fibres deviate from the mean direction of the laminate and form a pattern that typically takes the form of a sine wave [67]. Residual stresses are also known to potentially initiate an interfacial crack at the fibre-matrix interface that can result in fatigue failure and deterioration in ply material properties. The presence of voids would increase the chances of any such deterioration. The form of flaw will depend on the nature of the interface. If the

interface is relatively weak, cracks will propagate along the length of interface. However, if the fibre-matrix interface is strong then any such cracks will instead propagate into the bulk matrix [67]. Both can grow to form microcracks, which may then develop into transverse ply cracks if left unchecked. Any ply possessing a transverse crack would represent a point of stress concentration and weakness within a laminate. As a result such a flaw could initiate delamination and subsequently the ultimate failure of the laminate [67].

The effect of residual stresses on fibre-matrix 'adhesion' has been examined through both analytical analyses and experimental studies. Di Landro and Pegoraro [22] proposed a procedure that would evaluate RTS in polymer matrix composites. Their work focussed on the study of residual stresses acting around a carbon fibre for both thermoplastic and thermoset matrices. They made use of the model by Nairn [16] to calculate the stresses generated by a step-by-step cooling process of a single anisotropic fibre embedded in a matrix, from the glass transition temperature to a final set temperature. These estimations were then compared to experimental tests done at different temperatures and after different cooling cycles. The results showed that the processing parameters (temperatures and cooling rates) possessed major influence over the radial stresses at the fibre-matrix interface in the case of both thermoplastic and thermoset polymers. Furthermore, such stresses were shown to make a significant contribution to the fibre-matrix adhesion. Overall it was shown that the stress transfer capability of the interface decreased in all cases with decreasing radial stress. However thermoset interfaces were shown to maintain some level of interface strength once the residual stresses reached virtually zero. This was attributed to the possible presence of chemical bonds between the polymer matrix and fibre surface which would not have been present for thermoplastics.

Jakobsen et al. [21] characterised the in-plane thermo-mechanical properties and residual stresses of a CSM E-glass/Epoxy material. The data was then used to generate material models which describe the mechanical behaviour as a function of conversion and temperature. Comparing the values for the in-plane thermal expansion coefficient and chemical cure shrinkage measurements they found that chemical bonds between the polymer matrix and the glass fibres are formed prior to shrinkage of the epoxy matrix. This would suggest that composites possessing low residual stresses would likely be due to the interaction between the matrix and fibre sizing, not the matrix cure properties. As such they concluded that residual stresses within a composite material are mainly a result of restricted cure shrinkage rather than a difference in thermal expansion coefficients.

Thomason and Yang [14] studied the overall effect which temperature has on the apparent interfacial shear strength (IFSS) within GFPP composites. Their goal was to characterize the interface using the microbond test within a temperature-controlled environment, in this case a thermo-mechanical analyser (TMA). Specifically, the study looked to highlight the existence of residual stresses that existed at the interface. These residual stresses typically form from shrinkage stresses and static frictional stresses [14].

Overall, the results produced by the study showed that there was a temperature dependence of the apparent interfacial shear strength in GFPP between the range of -40°C to 100°C. This dependence was distinctly inverse, with major increases in the IFSS around the glass transition region of the PP matrix. This was due to an increase in the residual radial compressive stresses that exist at the interface as the temperature was lowered. Adding to this, analysis showed that these residual compressive stresses could be responsible for around 70% of the IFSS measured at room temperature thus supporting the hypothesis that residual thermal stresses

dominate the interface within a GFPP system [14]. This would agree with the findings of Di Landro and Pegoraro [144].

This work was then expanded upon to look at the influence of temperature on the interface strength of an epoxy/glass fibre composite [84], with clear correlation shown between the apparent IFSS value measured and the contribution of the residual stresses, (combination of both thermal and chemical cure), theoretically at the interface. In agreement with Jakobsen [21] they also found that the contribution due to chemical shrinkage was significantly larger than that of the RTS. The conclusion was that this characteristic could significantly contribute to the stress transfer capability of the interface. This result was somewhat controversial since it suggested another possible theory to how a strong interface forms without accounting for chemistry. However, there is still a significant body of opinion that holds that even if residual stresses formed at the interface do contribute to the stress transfer capability, then chemistry and chemical reactions must still play a direct role in determining the IFSS [34,102,140,143]. As such the need to carry out a similar investigation while studying the role of chemical variables such as matrix stoichiometry and fibre sizing is required.

Kim and Hahn [146] analysed the build-up of residual stresses within graphite/epoxy composites during the processing stage. This was achieved by intermittent curing of an unsymmetrical laminate to monitor the residual stress development. The resulting warpage of the laminate was measured to assess the extent of residual stresses present. They found that the level of warpage changed in a comparable manner to the degree of cure. It was shown that the level of residual stress increased rapidly after the gel point, in unison with key mechanical properties such as strength and modulus, suggesting a link between the two. This would agree with the interface contribution hypothesis described by Thomason and Yang [84].

Cowley and Beaumont [147] studied the residual stress in a thermoplastic matrix and a toughened thermosetting matrix, both reinforced with carbon fibre. Their experiments focussed on analysing the level of curvature of laminates during cooling, similar to the work of Kim and Hahn [151]. Other experiments involved measurement of the first-ply cracking stress. They concluded that residual stresses in laminates can be adequately predicted by using classical lamination theory, if the thermal expansion coefficients and the elastic moduli are known as a function of temperature. This provides a technique for measuring residual stresses on a macro-level, compared to the micromechanical model proposed by Nairn [16] which focussed on a single fibre.

Palmese et al. [148] proposed a method for predicting the formation and influence of interphase regions in composites materials. The method was illustrated by studying the influence of the sizing-induced interphase regions to the development of RTS within a carbon fibre epoxy/amine composite. The analysis showed that the formation of RTS could be significantly influenced by variations in the modulus of the different regions within the interphase. As such it could be hypothesised that changes to the properties of both constituents could influence the magnitude of both the RTS and cure shrinkage stress. In particular, changes to the matrix stoichiometry as a result of inconsistent sizing application along the length of the fibre as well as changes to the fibre sizing chemistry could both influence the contribution of the residual stresses as suggested by Thomason and Yang [84]. Again, this topic requires further investigation.

Zhao et al. [133] conducted a micromechanical study of residual stress and its effect on transverse failure in polymer-matrix composites through use of a finite element model. They emphasised that the determination of residual stress within polymer-matrix composites should include the contributions from both chemical cure shrinkage as well as RTS. Their results showed that for tension-dominated transverse loading,

residual stresses could be detrimental or beneficial depending on the magnitude of the residual stress and the material strength. Specifically, they found that it was detrimental for low resin strength composites but beneficial for relatively high resin strength composites. They also notably concluded that residual stress is always detrimental for pure shear loading. The results, although interesting, focus primarily on the effect of residual stresses on a single glass fibre embedded in the polymer matrix. It does not account for the interface interaction between the two and thus the potential contribution to its stress transfer capability suggested by the findings of Thomason and Yang [84].

In conclusion, it can be seen that a large degree of research has been conducted into the influence of residual stresses on the performance of fibre reinforced composites. Both macromechanical and micromechanical tests have been used to evaluate this influence, with the macromechanical providing a seemingly broader approximation based on properties like ply curvature. Overall the work focussing on the effect at the interface does suggest that there is a potential link between the contribution of these residual stresses and the interfacial strength value. However, the role of chemistry in this scenario is still unclear and requires an in-depth study to ascertain exactly where it fits in this picture, in particular, the role of matrix stoichiometry in determining the contribution of residual stresses to the stress transfer capability of the interface.

2.3.4 Characterisation of Fibre-Matrix Interface

Since the interface exerts a major influence on the mechanical characteristics of the resulting composite, the need to analyse this interaction between the polymer matrix and glass fibre has become a major area of research over the past decades. As a result, many different techniques have been developed to study the stress transfer capability of the interface. In general, these techniques fall into two categories depending on the nature of samples used and the scale of testing: micromechanical

or macromechanical. Micromechanical tests typically involve a single fibre sample being used to provide direct measurements of interface properties. Macromechanical tests generally involve bulk composite specimens being used to measure the interlaminar/intralaminar properties, from which the fibre-matrix interface properties are then inferred [67].

2.3.4.1 Micromechanical Tests

Over the past four decades, several different micromechanical tests have been developed to investigate the quality of the fibre-matrix interface by measuring the interfacial shear strength (IFSS). Such tests include the single fibre pull-out test (SFPT), microbond test (MBT), fragmentation test and single fibre push-out test [149]. Each test possesses positives and negatives when it comes to interface analysis with these traits typically depending on the materials under study. Overall there is still a degree of discussion as to the accuracy of micromechanical techniques when the measured values are scaled up to the macro-level [150,151].

a) Microbond Test

As significant research has been invested into studying the interface between the glass fibre and the polymer matrix, there must be a quantifiable property that may be used to measure the strength of the fibre-matrix interface. One accepted mechanically measurable value for quantifying fibre-matrix adhesion is the IFSS. The IFSS value represents the shear stress required to produce shear failure locally at a point located at the interface. When the IFSS is obtained under the assumption that the interfacial shear stress is uniformly distributed along the embedded length of the droplet, then it is regarded as the apparent IFSS, τ_{app} [67].

One of the common methods for measuring the IFSS is the microbond test which has been used to analyse the interface between multiple different fibres and polymers. [84,152–159]. First proposed by Miller et al. [160] in the 1980's, the microbond method

is based around shearing a minute matrix droplet on a single fibre through the application of an external force. The recorded maximum force at the point of debond is then used to quantify the IFSS value. Nevertheless, this technique does suffer limitations based on the nature of the microdroplet specimen and testing procedure itself. The sample preparation for microbond test samples can suffer from multiple issues in terms of consistency. Ensuring the formation of consistently axi-symmetrical droplets before curing is extremely difficult, with a typical remedy being to apply multiple droplets to allow multiple chances of producing the desired shape.

However, this can also lead to more difficulties, such as varying droplet embedded length. The embedded fibre length represents a key property that governs the IFSS of the droplet, and thus ideally would be maintained constant throughout testing for a direct comparison. The meniscus formed around the fibre for samples makes accurate measurement of this property even more difficult at times. Moreover, the microscale of the test prevents in situ observation of the failure process, with post-test analysis typically required. For thermosetting matrices there is also the potential for the mechanical properties of the droplet to vary with sample size due to variations of concentration of the curing agent and sizing of the fibre [67]. Overall data scatter is also recognized as being a major limitation of the technique [160–162].

The presence of these limitations has led to extensive study of the parameters associated with the microbond test involving analytical models, experiments and finite element analysis [161,162,171,163–170]. These studies have emphasised the importance of parameters associated with the microbond test rig, such as the vice angle [163] and gap [169]. For example, Ash et al. [172] set out to build a finite element model of the microbond test, with the goal being to study several key stresses that occur during the test and identifying the factors that influence them. They identified significant differences in the stress field that occur near the fibre/ droplet contact point,

with these differences being due to the geometry and z-location of the vice. The interface properties and vice angle were varied to identify their effect on the stresses. Overall, Ash found that the state of stress would drop considerably when the vice angle was increased. The interface appeared to possess less effect, but it still caused variations to occur in terms of stress at the fibre/droplet contact point. The final variable they studied was the geometry of the droplet, specifically which shape would perform best when under load, with major variations in performance recorded. The best performing droplet was the shape proposed by Carroll [173], which differs from an elliptical and circular shape as shown in Figure 2.10 [173].

Yet, as discussed previously, it can be challenging to try to control the droplet shape during the application process, so this information is primarily applicable to judging droplet shapes which have formed and cured previously, allowing for the selection of the optimum droplets.

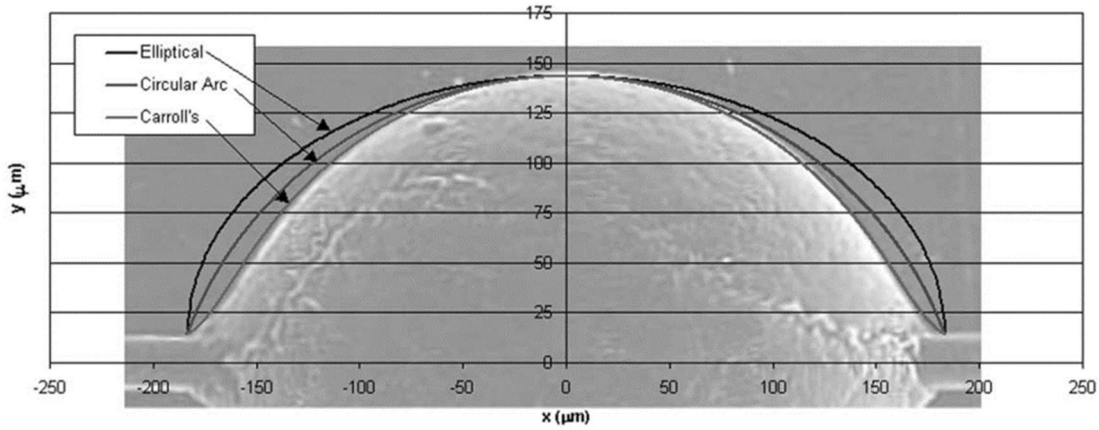

Figure 2.10 - Comparison of elliptical fit, circular arc fit, and Carroll's fit to an actual polyester bead on a thin-clad glass fibre taken from [172].

Despite the limitations listed, the measured values for the IFSS recorded in the literature confirmed that the microbond test was sufficiently sensitive to allow the study of changes in sample preparation conditions. In addition, the IFSS values obtained appeared comparable to the mechanical properties of full laminate composites.

Working from the findings of the various analytical studies, it is judged that the microbond test is useful for studying fibre-matrix adhesion, as long as variables such as the vice angle and droplet geometry are sufficiently accounted for during the analysis.

b) Single Fibre Pull-out Test

The principles of the single fibre pull-out test (SFPT) are similar to that of the microbond test. A fibre is partially embedded within a polymer matrix which is placed under some form of constraint, whilst the fibre is loaded in tension [149]. Essentially the main difference between the two tests relates to the scale and geometry of the tests, with the embedded interfacial area of the microbond test being significantly smaller than that found in SFPT.

Instead of minute droplets of the matrix, the SFPT makes use of larger plates/discs that the fibre is embedded in. This disc is then constrained, with a tensile load placed upon the fibre. The bond strength between the fibre and matrix is calculated using the bond peak force and the embedded area as shown in Figure 2.11 [9]. The technique has been used extensively to study fibre-matrix adhesion for a variety of different systems [13,99,136,174–179]. Piggott [180] provided an in-depth report of the technique, summarising its advantages and interpretation.

However, like the microbond test, SFPT possesses several potential difficulties and flaws that can lead to data spread and the potential for unreliable results. The difficulties primarily revolve around inaccurate measurements, especially regarding important parameters such as the embedded fibre depth, alignment of the fibre (which may not necessarily be perfectly straight) and end effects [9]. As with the microbond test, the limitations of the test has led to a number of studies to analyse the accuracy and applicability of the technique [176,181–186].

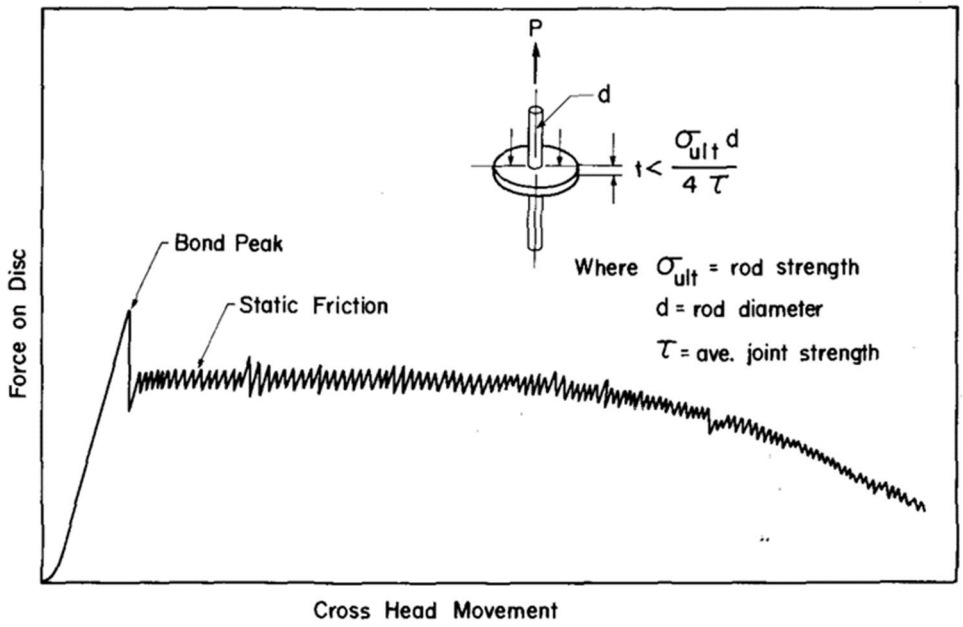

Figure 2.11 - Typical load-displacement curve for rod-disk joint strength specimen taken from [9].

c) Single Fibre Fragmentation Test

The single fibre fragmentation test (SFFT) is another popular technique used for studying the interface. The test is based around applying an external stress to a single fibre fully embedded in a matrix, with the tensile stress transferring to the fibre through interfacial shear strength as shown in Figure 2.12. As this tensile load is increased, the tensile strain in the fibre begins to increase until eventually the fibre fractures. This process continues multiple times, with the fibre fracturing into smaller sections several more times before the fragment lengths become too short to fracture (known as the saturation point in the fibre fragmentation process). This minimum fibre length for fracture is known as the critical fibre length [187].

The critical fibre length is used in conjunction with the fibre diameter and the fibre strength at the critical fibre length to calculate the average interfacial shear strength as shown in Equation 2.12:

$$\tau = \frac{\sigma_{fu} d}{2 l_c} \quad (2.12)$$

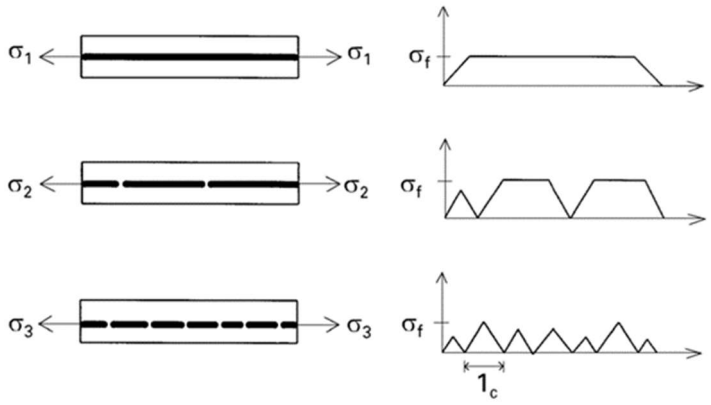

Figure 2.12 - Schematic drawing of the fragmentation test taken from [192].

The fragmentation test has been used extensively for the study of fibre matrix composites [141,188–193], particularly for natural fibre composites [194–196] and carbon fibre [187,189,197–200]. The fragmentation test does have limitations. The main problem is that its use is limited by the lack of a data reduction parameter linked to changes in the surface chemistry of the fibre and the mechanical properties of the resulting composite [187,201]. Furthermore, the addition of a sizing to the fibre surface modifies the matrix resin within the stress transfer region (interphase), impacting the accuracy of the test more than other techniques.

d) Single Fibre Push-out Test

The single fibre push-out test (SFPoT) is another technique used to measure the strength of the fibre-matrix interface. The test involves pushing individual fibres embedded in a matrix out of the matrix, typically using a tungsten carbide punch. The load-displacement curve produced by this procedure generally consists of four different stages that reflect the strength of the interface [202] as shown in Figure 2.13: (i) the linear elastic loading phase with perfect interface; (ii) the decrease of stiffness due to the interface cracking and this crack then propagating; (iii) the abrupt load drop

due to the complete interfacial de-bond and (iv) the frictional sliding of the fibre that takes place.

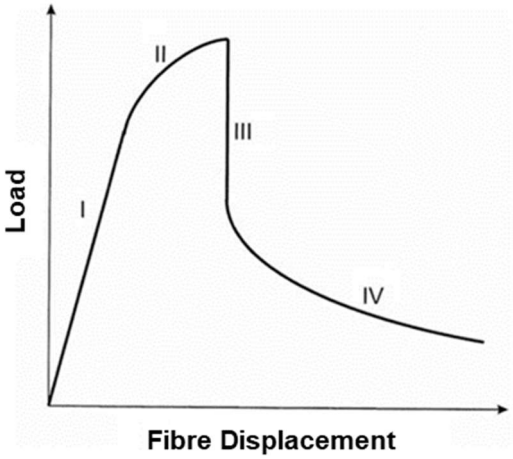

Figure 2.13 - Typical load-displacement curve for a fibre push-out test on a thick single-fibre specimen taken from [202].

Although this technique appears to be very popular, its use is very dependent on the type of matrix and fibre used, with much of the work being done with metallic matrix composites (MMCs) or intermetallic matrix composites (IMCs) [191,203–209]. Little work has been done using either glass fibres or an epoxy matrix for this method since it would be extremely difficult to manufacture the necessary samples needed for testing using those materials.

2.3.4.2 Macromechanical Tests

Along with micromechanical tests, the strength of the fibre-matrix interface may be studied by analysing the interlaminar/intralaminar properties of bulk composite specimens. As such a number of testing techniques have been devised to study the fibre-matrix interface bond quality by inference from the gross mechanical properties, such as interlaminar shear strength (ILSS), translaminar or in-plane shear strength, and transverse tensile strength [210].The short beam shear test may be used to measure the interlaminar shear properties of the macrocomposites. It involves loading

a beam fabricated from unidirectional laminate composites in three-point bending as outlined in ASTM D 2344 [211]. Various other techniques, such as the Iosipescu shear test, $[+45°]_s$ tensile test, the [10°] off-axis tensile test, rail-shear tests, cross-beam sandwich test and the thin-walled tube torsion test have been used for translaminar or in-plane strength measurements [210].

Biaxial testing using a cruciform specimen is an example of a relatively modern macromechanical technique that has been used to study interfacial debonding [212–217]. The test involves a transverse tensile test of the samples, with interfacial debonding initiating at the middle of the sample. Since the centre of the sample is free of initial stress singularities it can provide valid interfacial tensile strength data. The interfacial tensile strength is then calculated by the value of stress concentration factor at the interface multiplied by the specimen stress [212].

Macromechanical tests are limited compared to micromechanical tests in that they require the position and modes of failure to be consistent with those originally designed for the composite in order for a specific test to be valid [210]. The process of validating the test by examining the onset of failure during the experiment can be a time-consuming task since assumptions cannot be made regarding the nature of failure for a given loading condition. For instance, for apparent interlaminar shear failure the failure may occur at multiple different points within the composite depending on two factors, the first being the loading direction relative to the interface concerned. The second and, more crucial factor, is the relative strength of the fibre-matrix interface and the shear strength of the matrix material. Both govern the nature of the resulting failure mechanism. This leads to experimental data interpretation being more complicated and time consuming due to the requirement to conduct detailed micromechanics analysis in combination with prior knowledge of the matrix properties [210].

2.3.4.3 Summary

Having studied the various potential techniques for analysing the fibre-matrix interface, it appears that either the microbond test or SFPT technique would be the most suitable for studying a glass fibre epoxy composite in relation to the factors of residual stress and chemistry. Although the SFFT has been used for the study of epoxy composites, the fact that the results can be influenced by fibre sizing would undermine the potential findings of a study into changes to the mixture ratio of the resin. The SFPoT technique is primarily used for metallic matrix composites, making it inappropriate for researching glass fibre epoxy composites. Macromechanical tests may also be useful in studying the influence of matrix stoichiometry on the properties of composite material and how this could be related to the interface. This would expand upon the work completed primarily by D'Almeida et al. [30,31,33] but with more focus on how it relates to the interface.

Overall, the use of micromechanical test methods would appear preferable when studying the influence of chemical factors at the interface level. Specifically, the microbond test appears the most acceptable for studying the consequences of changing the mixture ratio of the epoxy system, primarily because the literature has shown the test to possess the required sensitivity to analyse changing sample preparation conditions. The IFSS values obtained using the technique have also been shown to be more comparable to the mechanical properties of full laminate composites than the other micromechanical tests, thus enabling a more accurate interpretation of how the data gathered may scale from a single fibre up to a full laminate composite.

Chapter 3. Experimental

3.1 Materials

Boron free E-glass (Advantex) fibres sized with different silane coupling agents supplied by Owens Corning were investigated in this project. Five different rovings were studied, two of which had the same silane coating. All fibre rovings were produced on the same pilot scale bushing and were received as 20kg continuous single-end square edge packages. The rovings possessed a nominal tex of 1200 g/km and an average fibre diameter of 17.5 μm. No sizing was applied to the bare fibres which had only been water sprayed by the cooling sprays beneath the bushing; these fibres are referred to as having been water sized or unsized. Immediately following the cooling step discussed previously the chosen sizing was applied to the sized fibres with a normal rotating cylinder applicator. In this project five sets of fibres were studied with three different silane sizings applied:

i. Fibres 1 and 2 were coated with aminopropyltriethoxysilane (APS);
ii. Fibre 3 was coated with glycidoxypropyltrimethoxysilane (GPS);
iii. Fibre 4 was coated with methacryloxypropyltrimethoxysilane (MPS);
iv. Fibre 5 was water sized.

The silane only coating process produces fibres with a significantly lower weight percentage of coating compared to commercially available glass fibre products. After coating all fibre packages were dried at 105 °C for 24 hours. Fibres near the bottom and top of the packages were likely to have been damaged during packing, storage, and transportation thus only the strands from the middle of the packages were selected for testing.

Two fibres with an APS coating were studied due to concerns that the silane coating

on the aged fibre 1 may have deteriorated over time. As such, a new roving of E – glass fibres with the same APS coating was acquired to allow for comparison. For ease of reference the fibre numbers and applied silane sizings are summarised in Table 3.1.

Fibre Number	Sizing Applied
Fibre 1	APS
Fibre 2	APS
Fibre 3	GPS
Fibre 4	MPS
Fibre 5	Water

Table 3.1 - Fibre designation table.

Araldite® 506, purchased from Sigma Aldrich, was used as the epoxy resin. This resin is a modified Bisphenol-A based epoxy resin, containing approximately 75-100% of Bisphenol-A-(epichlorhydrin) epoxy resin (CAS: 25068-38-6) and 10-25% butyl glycidyl ether (CAS: 2426-08-6), allowing the resin to have a very low viscosity. The equivalent epoxide weight of the resin was 172-185 g/mol. The molecular structure of bisphenol-A diglycidyl ether epoxy (DGEBA), the product of Bisphenol-A and epichlorhydrin, is shown in Figure 3.1 where n denotes the number of polymerized sub units. The molecular structure of the additive, butyl glycidyl ether, is shown in Figure 3.2.

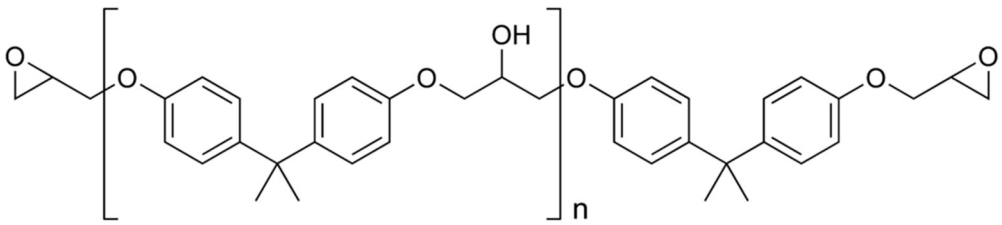

Figure 3.1 – Molecular structure of bisphenol-A diglycidyl ether epoxy.

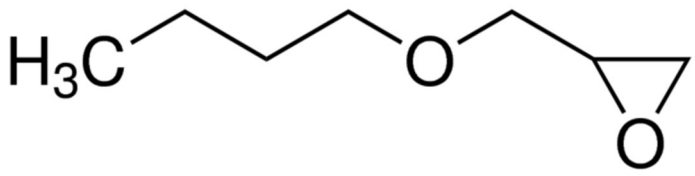

Figure 3.2 - Molecular structure of butyl glycidyl ether.

The curing agent, also known as the hardener, selected was triethylenetetramine (TETA), an aliphatic amine and this was also purchased from Sigma Aldrich. The curing agent consists of a mixture of four TETA ethyleneamines including linear, branched and two cyclic molecules. These compounds are: triethylenetetramine (CAS: 000112-24-3), piperazine-1,4-diethylamine (CAS: 006531-38-0), N-[2-(1-piperazinyl)ethyl]ethylenediamine (CAS: 24028-46-4) and tris(2-aminoethyl)amine (CAS: 004097-89-6). Two levels of purity were used during the study, with the bulk of the work having been conducted using TETA with a technical grade of 60% (standard purity TETA) whilst some comparable work was conducted using TETA with a technical grade of 99% (high purity TETA). The primary difference between the two being that the standard TETA consists of 60% of the TETA molecule shown in Figure 3.3 whilst the high purity TETA consists of 99% of the TETA molecule. The corresponding 40% and 1% remaining consists of the three other TETA ethyleneamines discussed. The average molecular weight of the hardener was 146.24 g/mol and it possessed a functionality of 6. The molecular structure for TETA is shown in Figure 3.3. The molecular structures of the other components are shown in Figure 3.4 - Figure 3.6. Both the epoxy and hardener were used as received.

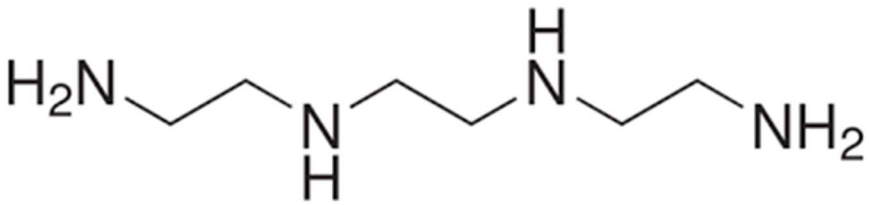

Figure 3.3 - Molecular structure of TETA.

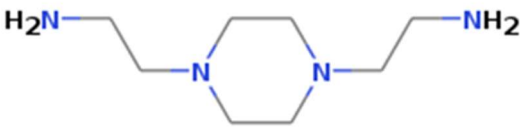

Figure 3.4 - Molecular structure of piperazine-1,4-diethylamine.

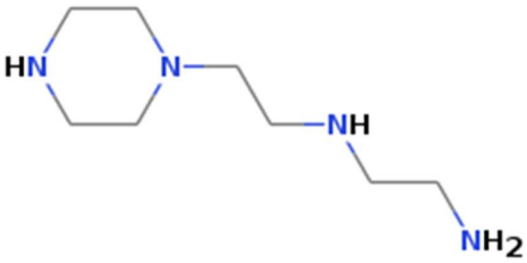

Figure.3.5 - Molecular structure of N-[2-(1-piperazinyl)ethyl]ethylenediamine.

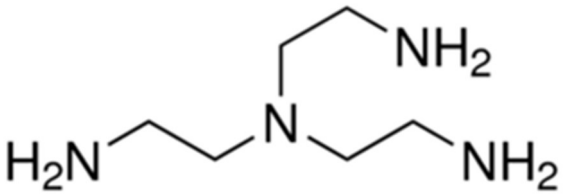

Figure 3.6 - Molecular structure of tris(2-aminoethyl)amine.

Due to the primary focus of the project being on the effects of varying the hardener-to-epoxy ratio it was necessary to calculate the stoichiometric ratio. To obtain the stoichiometric ratio, the ratio of reactive epoxy groups to reactive hydrogens amongst the reactants should be 1:1. Since there are six reactive hydrogen atoms per TETA molecule and two epoxy groups per epoxy molecule the ratio thus should be 1:3. That

is, for every mole of TETA added, 3 moles of epoxy molecules would be required in order to ensure the completion of the reaction as shown in Equation 3.1.

$$\text{Stoichiometric ratio} = \frac{\left(\frac{\text{molecular weight of TETA}}{\text{equivalent weight of DGEBA}}\right)}{\text{functionality of TETA}} \quad 3.1$$

Since the equivalent weight of the resin was shown to vary between 172 g/mol up to 185 g/mol it was assumed that the stoichiometric ratio would apply for any ratio that existed between these two limits. Assuming the equivalent weight was 172 g/mol the stoichiometric ratio is given by:

$$= \frac{146.24}{172\ x\ 6}\ x\ 100 \quad 3.2$$

$$= 14.170\ parts\ per\ TETA\ per\ 100\ parts\ epoxy$$

Equation 3.3 shows the calculation when the epoxy equivalent weight is taken as 185 g/mol.

$$= \frac{146.24}{185\ \text{x}\ 6}\ \text{x}\ 100 \quad 3.3$$

$$= 13.175\ \text{parts per TETA per 100 parts epoxy}$$

Thus, the stoichiometric ratio was taken as any ratio value between 13.175 parts per hundred, up to 14.17 parts per hundred (pph). Throughout the course of this thesis the hardener-to-epoxy ratio was calculated as measured as the percentage of TETA hardener to epoxy resin weight. This meant converting the parts per hundred values to a percentage ratio. This was achieved using Equation 3.4:

$$\text{Hardener} - \text{to} - \text{epoxy ratio}\ (\%) = \frac{100\ \text{x pph ratio}}{(100 + \text{pph ratio})} \quad 3.4$$

Hence the stoichiometric ratio of 13.18 – 14.17 pph equated to a ratio of 11.65% -

12.41% TETA. For ease of understanding regarding the chemistry within the matrix all data will be presented as the apparent ratio (R) of the number of amine to epoxy groups within the system. This was achieved by using Equation 3.5 with an amine-to-epoxy group ratio of 1 equating to the stoichiometric value.

$$R = \frac{\text{functionality of TETA x pph ratio x equivalent weight of DGEBA}}{(\text{molecular weight of TETA x } 100)} \qquad 3.5$$

The ratio is apparent due to the different functionalities of the four TETA ethyleneamines present in the hardener. Since the exact quantity of each ethyleneamine was not known, the baseline functionality of six was chosen.

3.2 Thermal Analysis Techniques

Thermal analysis of the epoxy polymer matrix is a major focus of the work presented in this thesis. In order to quantify the role of the amine-to-epoxy group ratio in defining several key thermal properties of the matrix a number of different pieces of equipment were used.

3.2.1 Differential Scanning Calorimetry (DSC)

One of the most common methods for studying the thermal properties of a polymer material, such as epoxy resin, is differential scanning calorimetry (DSC). The technique is typically used to study the variation of specific thermal properties of the material with temperature. It is based around measuring the difference of heat flow between a specimen and a reference to achieve the same temperature during a cooling or heating process. This difference is then recorded as a function of time or temperature. From this, properties such as the heat capacity of the material, activation energy, glass transition temperature and degree of cure can be calculated.

A Q20 differential scanning calorimeter was used for all DSC tests described in this thesis, as shown in Figure 3.7. The instrument was coupled with the refrigerated cooling system RSC90 to allow testing at sub-ambient temperature. Both devices were manufactured by TA Instruments. A flow of 50 mL/min of dry nitrogen over the oven was recommended by TA for the following reasons:

i. The flow of purge gas helps to remove moisture and oxygen which may accumulate and damage the DSC over time;
ii. The purge gas acts as a smooth thermal “blanket” for the sample, eliminating localized hot-spots which can lead to artificial heat flow;
iii. The purge gas allows for more efficient heat transfer between the constantan disc of the DSC and the sample pan, resulting in more sensitivity and a faster response time;
iv. Finally, the purge gas aids in the cooling of the DSC, allowing for faster cooling rates to be achieved with a wider modulation of parameters.

Figure 3.7 - Q20 differential scanning calorimeter.

3.2.1.1 Glass Transition Temperature Measurement

DSC testing to assign the glass transition temperature (T_g) was carried out in accordance with ASTM standard E1356-08; '*Standard Test Method for Assignment of the Glass Transition Temperatures by Differential Scanning Calorimetry*' [218]. The standard is applicable to stable materials that pass through a glass transition within the region between -120 and 500 °C and is equivalent to ISO 11357-2.

The DSC instrument was used to measure the heat flow to the material as the temperature was increased at a constant rate. The glass transition temperature could then be assigned from a clear step change visible on the resultant thermal curve of heat flow plotted against temperature using TA Universal Analysis software with a typical example shown in Figure 3.8.

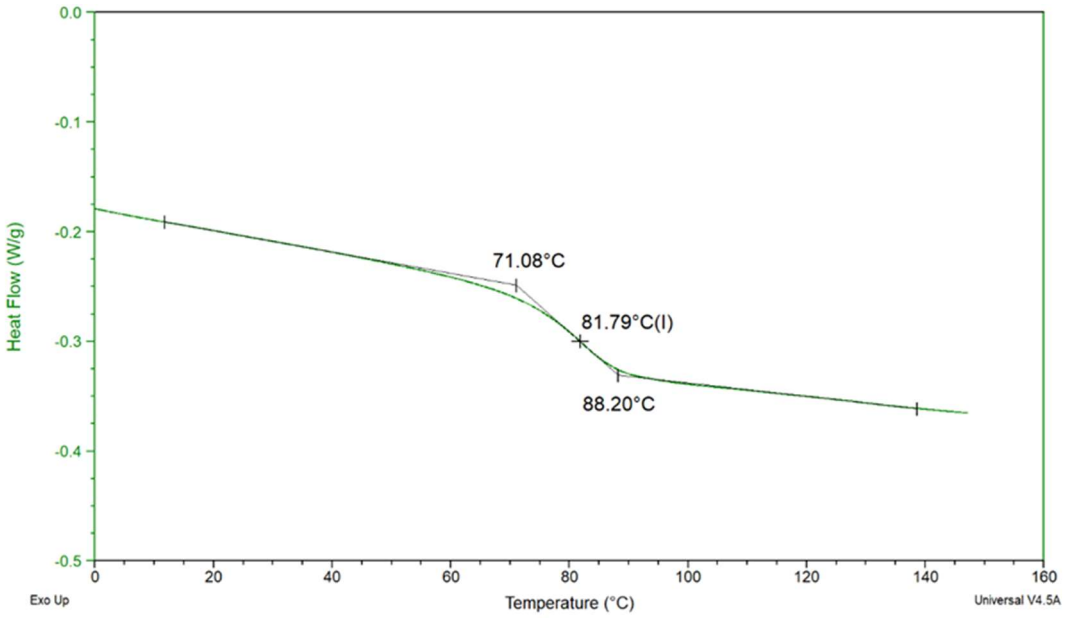

Figure 3.8 - Typical example of obtaining glass transition temperature values during a heating ramp.

Two temperature schedules were used for the work presented in this thesis, with the only difference being the final set temperature of the heat ramp being set to 150 °C or 180 °C respectively. The procedure was as follows:

i. Equilibrated at – 10 °C;
ii. Held isothermally for 10 minutes;
iii. Temperature ramped up to 150 °C (or 180 °C) at a rate of 10 °C/minute;
iv. Held isothermally for 10 minutes;
v. Temperature ramped down to -10 °C at a rate of 20 °C/minute;
vi. Held isothermally for 10 minutes;
vii. Temperature ramped up to 150 °C (or 180 °C) at a rate of 10 °C/minute.

The second heat ramp was conducted in order to account for any thermal lag that could occur during the first run.

The procedure could be carried out for specimens that had already cured as well as for specimens that would cure during the process, with the glass transition temperature being measured during the second temperature ramp. The difference between the two forms of analysis was the type of pan used, with cured specimens using standard aluminium pans purchased from TA while curing specimens required sealed aluminium hermetic pans purchased from Mettler Toledo. Curing specimens were also exposed to the higher final temperature of 180 °C during the DSC run to ensure full curing of the polymer was obtained.

The pre-cured specimens were cured prior to the analysis using the recommended curing schedule for the epoxy system which was used throughout this project as shown in Figure 3.9:

i. Temperature ramped up from 20 °C to 60 °C at a rate of 2 °C/minute;
ii. Held isothermally for 60 minutes;
iii. Temperature ramped up from 60 °C to 120 °C at a rate of 2 °C/minute;
iv. Held isothermally for 120 minutes;
v. Specimens then left to cool within the oven overnight.

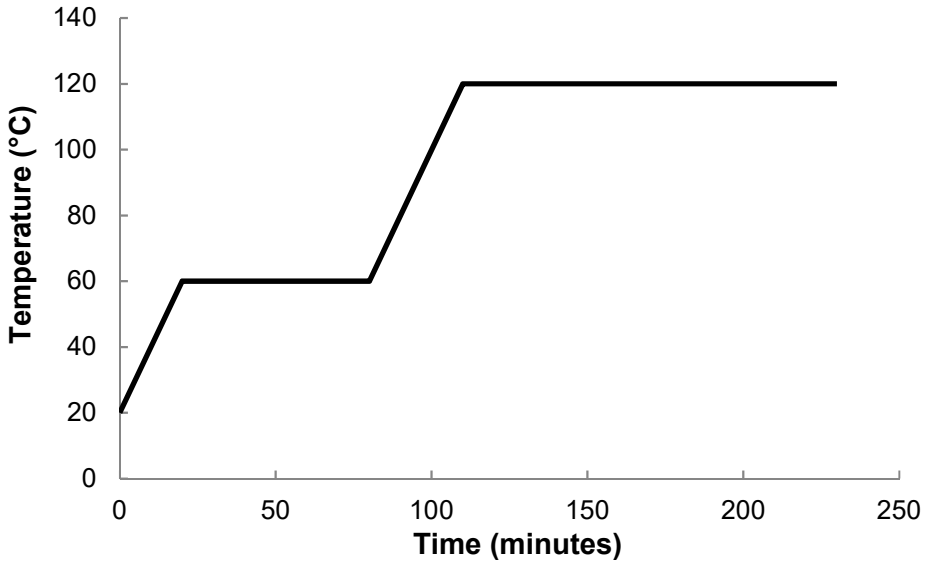

Figure 3.9 - Temperature profile of oven during curing schedule.

These pre-cured specimens were manufactured from larger TMA/DMA samples and sanded down to small flat discs with a mass in the range of 15 - 20 mg. As such nine-different hardener-to-epoxy ratios were studied. The pre-cured specimens were then placed in the standard aluminium pans and analysed in the DSC. Although the specimen sizes differed, the individual masses were measured to the nearest 0.01 mg using a XSE 205 Dual Range analytical balance, manufactured by Mettler Toledo. This information was used to ensure that all values of heat flow were in units of W/g and therefore specimens with different masses could be compared.

Uncured specimens were prepared by measuring out the pre-calculated values of epoxy and hardener required for the specified ratios in a small container. The system was then mixed and degassed for approximately 15 minutes before measuring out a mass in the range of 10-20 mg into a hermetic pan through use of a syringe. The pan was then sealed and placed in the DSC along with a hermetic reference pan.

3.2.1.2 Activation Energy Measurement

DSC testing to study the activation energy of the curing reaction was carried out in accordance to ASTM standard E698; '*Kinetic Parameters for Thermally Unstable Materials Using Differential Scanning Calorimetry and the Flynn/Wall/Ozawa Method*' [219]. Specimens of the stoichiometric ratio were cured at different heating rates of 1, 2, 5 or 10 °C/minute to allow for Ozawa's method to be applied where an Arrhenius plot is used to determine the activation energy. As such specimens were prepared using the same method discussed in 3.2.1.1 for uncured specimens. The approach assumes that the curing reaction obeys Arrhenius' equation and follows the first order kinetics [220].

To calculate the activation energy (E_a), the logarithms of heating rates were plotted as a function of the reciprocal of the four-peak temperature in the unit of Kelvin. A straight trend line was then made from the plot with its corresponding equation. The slope of the trend line would be used to calculate E_a by the following equation:

$$E_a = -2.19R_g \frac{d(\log \Phi)}{d\left(\frac{1}{T_p}\right)} \qquad 3.6$$

Where Φ is the heating rate, T_p is the peak temperature during curing and R_g is the gas constant R_g = 8.314 J / mol. K.

During this work other variables such as the onset temperature (T_{onset}), peak temperature (T_p) and reaction enthalpy (∆H) were also calculated from the plots for the different heating rates. T_p was defined as the maximum temperature recorded at the peak of the exothermic reaction during the curing process whilst T_{onset} was obtained by extrapolation of the steepest part of the rising curve. ∆H was calculated by the measuring the area under exothermic peak. An example of each is presented in Figure 3.10.

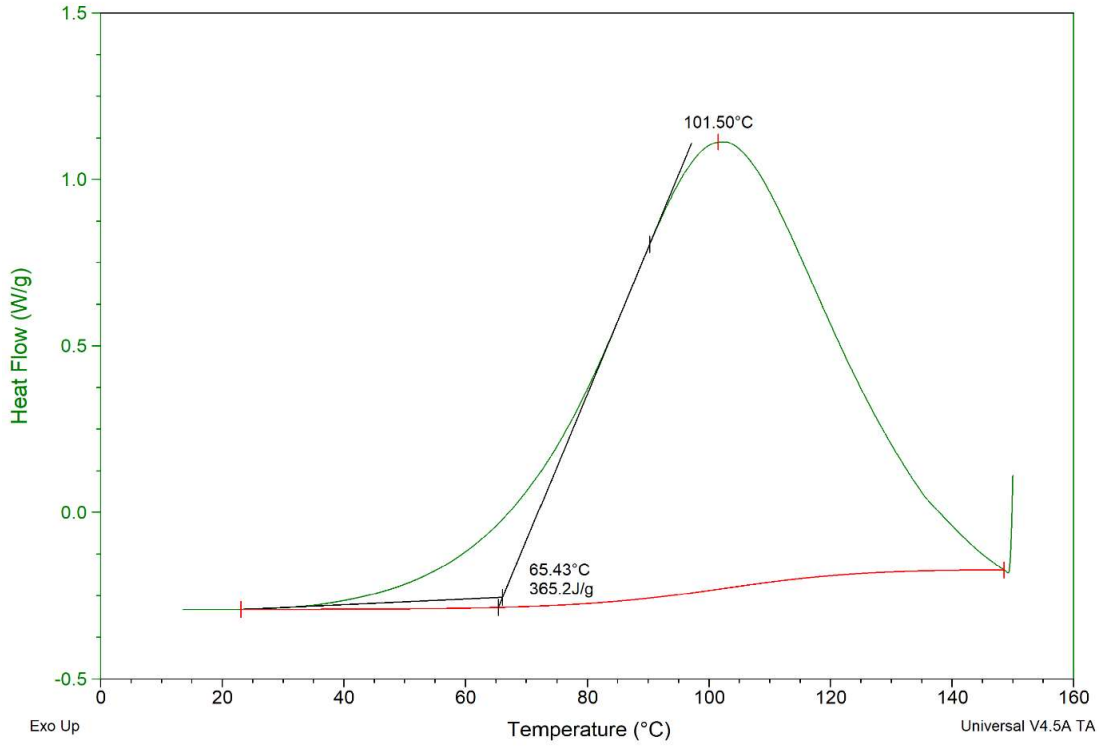

Figure 3.10 - DSC Plot including peak temperature, onset temperature and reaction enthalpy.

3.2.1.3 Degree of Cure Measurement

TA Universal Analysis software was used to analyse specimens cured within the DSC similar to those discussed in 3.2.1.1 in order to study the influence of the hardener-to-epoxy ratio on the degree of cure of the polymer whilst using a constant curing program. This was accomplished by using the running integral function available within the software to calculate the degree of cure as a function of temperature and time.

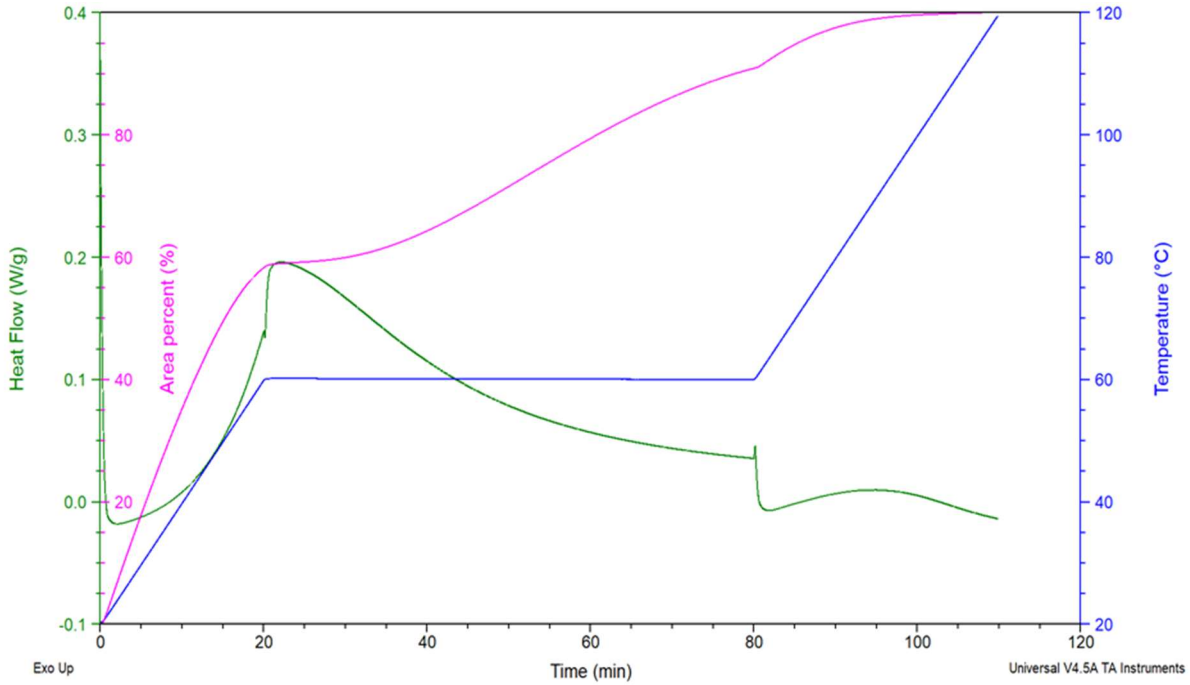

Figure 3.11 – Degree of cure plot using TA Universal Analysis.

Seven different amine-to-epoxy group ratios were investigated, ranging from R ≈ 0.5 systematically up to R ≈ 2.0 in increases of 0.25. The temperature program of the DSC was set up to follow the recommended curing schedule discussed in 3.2.1.1, with the limits for the running integral calculation being set at the start of the curing process (20 °C) and then at the end of the 120 °C isothermal step respectively. An example of such a plot is shown in Figure 3.11. The degree of cure was then calculated using the running integral function to graph, as an area percent, the integral of the data based on peak integration.

3.2.2 Thermo-mechanical Analysis (TMA)

Thermo-mechanical analysis was carried out in accordance with ASTM standard E831-12; '*Standard Test Method for Linear Thermal Expansion of Solid Materials by Thermo-mechanical Analysis*' [221]. The test requires a solid material with a linear coefficient of thermal expansion (LCTE) above 5 µm / °C and is applicable to a temperature range between -120 and 900 °C. This technique is related to ISO 11359-

2. The test results were also used to determine the glass transition temperature (T_g), following ASTM standard E1545-11; '*Standard Test Method for Assignment of the Glass Transition Temperature by Thermomechanical Analysis*' [222]. This test requires material rigid enough to prevent indentation during expansion, is applicable between -100 and 600 °C and is related to ISO 11359-2 and IEC 61006.

The analysis process constantly measured the change in length of the specimen as a function of temperature, during a constant heat ramp. The effects of altering the hardener-to-epoxy ratio upon these properties were then investigated.

A TA Q400EM in combination with a mechanical cooling accessory MCA70 was used for all TMA experiments as shown in Figure 3.12. This provided a potential temperature range from – 150 °C to 1000 °C, with a precision of ±1 °C. The probes used by the TMA possessed a sensing element with a sensitivity of 15 nm and were able to generate a constant load of between 0.001 and 2 N.

The technique required the specimens used to be of square shape with a constant dimension of 5 mm for the length, breadth and height respectively. These specimens were prepared in conjunction with the preparation of the specimens used for the dynamic mechanical analysis since both used the same silicon mould.

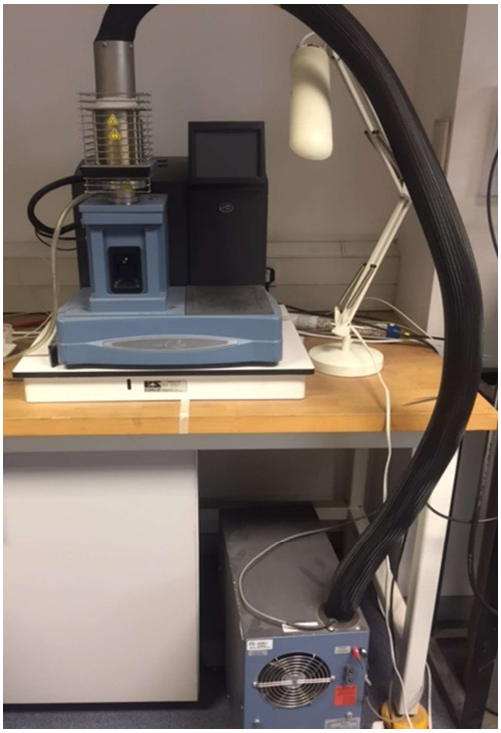

Figure 3.12 - TA Q400EM with the MCA70 accessory.

3.2.2.1 Silicone Mould Manufacture

In order to produce the specimens required for the thermo-mechanical and dynamic analysis, a simple method for manufacturing silicone moulds was required to mass produce specimens of adequate dimension and quality. As part of his undergraduate project, a 4th year student (Alistair Price) had previously designed a master mould manufactured from aluminium to be used to produce silicone moulds.

The master mould was initially designed using the modelling software Creo Parametric and then produced internally within the Mechanical and Aerospace Engineering workshop at the University of Strathclyde. The process involved the machining down of a 14 mm thick aluminium plate until the required protruding sections were formed. These sections were equivalent to the desired shape of the future specimens. The plate consisted of two sets of five protruding sections, the first set being roughly 5 mm^3 for the thermo-mechanical specimens and the second set being 64 x 13 x 3 mm^3 for the dynamic analysis specimens respectively. Four

removable sides were also made to encase the plate, producing the finished master mould as shown in Figure 3.13.

Alchemie RTV134, a two-component silicone rubber ordered from Allscott Ltd, was poured into the master moulds and cured at room temperature. Complying with the steps stated in the materials technical data sheet, the following process was conducted:

i. The master mould was cleaned, ensuring no dirt was present;
ii. Alchemie R6 release agent was applied to the inside of the aluminium master mould;
iii. The two components, the silicone rubber and the catalyst, were then poured in to a container at a ratio of 100:5 g in favour of the rubber;
iv. The components were mixed thoroughly in a container which had to possess overall volume at least 5 times the volume of the mixture to account for its expansion during the de-gassing process;
v. The mixture was then vacuumed for ten minutes, during which time the mixture expanded dramatically before collapsing back to its original volume;
vi. The de-gassed mixture was then poured into the master mould and left on a level surface to cure for 24 hours;

Figure 3.13 - Aluminium master mould.

To help increase the mould's life span it was then placed within a convection oven, heated up to 150 °C and held at that temperature for 2 hours. De-gassing the mixture for the correct amount of time proved a key step in the production process. Too short a time would leave the silicone rubber with air pockets, causing deformations to form within the mould. Too long would leave the mixture far too viscous to pour into the mould.

Overall the silicone rubber moulds proved to be successful, due to the ease of manufacture, its high tear strength properties and its non-stick qualities. It was found that typically each mould would last roughly three to four curing schedules before the silicon became worn down and started to tear. It was noticeable that when curing epoxy below the ideal stoichiometric ratio there was a higher negative impact on the moulds, as the cured epoxy would not peel away from the silicone rubber without tearing the surface. A comparison of a new mould with two older moulds is shown in Figure 3.14. Clear discolouring within the mould typically signified the end of its working life since this was the point at which specimens would begin to stick to the surface, making extraction difficult. The quality of the specimen surfaces would also deteriorate at this point.

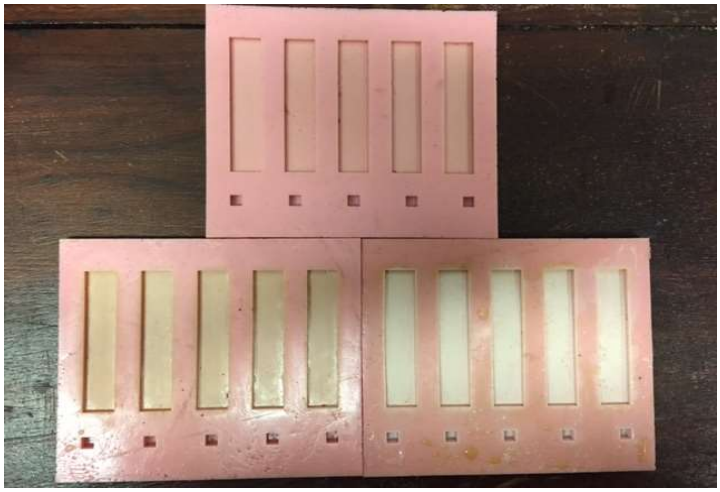

Figure 3.14 - Comparison of new and older silicone moulds.

3.2.2.2 TMA Expansion Specimen Preparation

With the silicone moulds now prepared it was possible to produce the specimens required for the thermo-mechanical analysis. The preparation and handling of the epoxy resin and hardener was the same as described in 3.2.1.1. In total, nine different ratios were studied ranging from R ≈ 0.31 up to R ≈ 3.13. The resin was then applied to the silicone mould using a syringe and placed in a convection oven to cure. The curing schedule used was the same as that described for the pre-cured DSC specimens in 3.2.1.1.

Due to the nature of the analysis being conducted, the surface of the cured specimens had to be carefully sanded to ensure good contact with the movable probe of the TMA. During the curing process it was possible for sharp edges to have formed on the surface of the specimens, particularly once the silicone mould used began to age. These edges had the potential to protrude minutely from the rest of the surface of the specimen, thus impeding contact with the probe and the resulting accuracy of the test. Hence it was important to ensure that the specimen edges were sanded to ensure that the surface sat as parallel to the stationary quartz probe as possible. Examples of specimens used for analysis are shown in Figure 3.15. The exact cube length varied, 5 ± 0.135 mm, however the instrument was able to measure the length in question to the nearest 0.0001 mm.

Figure 3.15 - TMA specimen cubes with an amine-to-epoxy group ratio of R ≈ 1.25.

3.2.2.3 TMA Expansion Technique

The movable quartz probe selected for the test was the expansion probe with the setup shown in Figure 3.16. Expansion measurements allow for the measurement of a material's linear coefficient of thermal expansion (LCTE), glass transition temperature (T_g), and compression modulus. A flat-tipped standard expansion probe was placed on the specimen, under a small constant load and the specimen subjected to a temperature program. Any movement of the probe will record specimen expansion or contraction.

The technique began with ensuring the TMA had been properly calibrated for the type of probe in use, with the movable probe having been zeroed onto the stationary quartz platform. Following this the specimens shown in Figure 3.15 would be placed onto the stationary platform and its initial length at room temperature measured under a constant load of 0.1 N. The thermocouple was then placed as close as possible to the specimen, without being in contact with the material itself. Ensuring that the thermocouple placement was constant throughout the analysis was a key task in minimising any potential errors occurring within the temperature measurement.

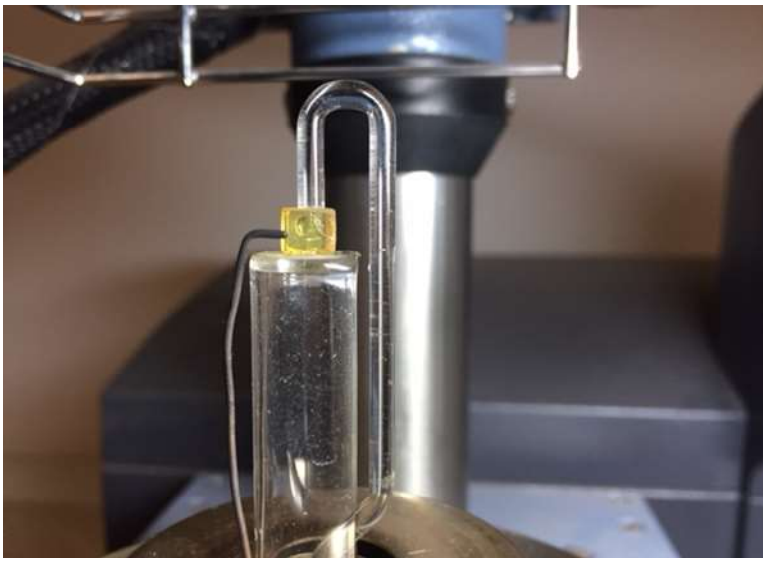

Figure 3.16- TMA Expansion Setup.

Once set up, the furnace of the TMA was closed, and the following temperature program followed:

i. Equilibrated at – 10 °C;
ii. Held isothermally for 5 minutes;
iii. Temperature ramped up to 150 °C at a rate of 2 °C/minute;
iv. Equilibrate at – 10 °C;
v. Held isothermally for 5 minutes;
vi. Temperature ramped up to 150 °C at a rate of 2 °C/minute.

Throughout the test the furnace was provided with a dry nitrogen flow of 50 mL/min.

The temperature increase rate of 2°C per minute, which differed from the recommended rate of 5 °C (by the ASTM standards), was chosen due to the relatively thick specimen sizes. Each specimen underwent two heat ramping stages, as the first often resulted in visible disturbance just before the T_g. This was due to settling along with residual stresses within the specimen relaxing. The first run in each test was therefore discarded. This procedure also ensured that the thermal history of each specimen was identical. An example of the potential differences in result for the same sample depending on the run number is presented in Figure 3.17.

The plot for the second run shown in Figure 3.17 shows two clear regions approximately above and below 70 °C, each portraying a relatively constant gradient but differing from each other. The intersection of these two gradients, the point of change, was taken as the position where the glass transition occurred. The two constant gradients on either side of the T_g were each used to calculate the linear coefficient of thermal expansion. The determination of the T_g value and the gradients was conducted using TA Universal Analysis software, with an example shown in Figure 3.18.

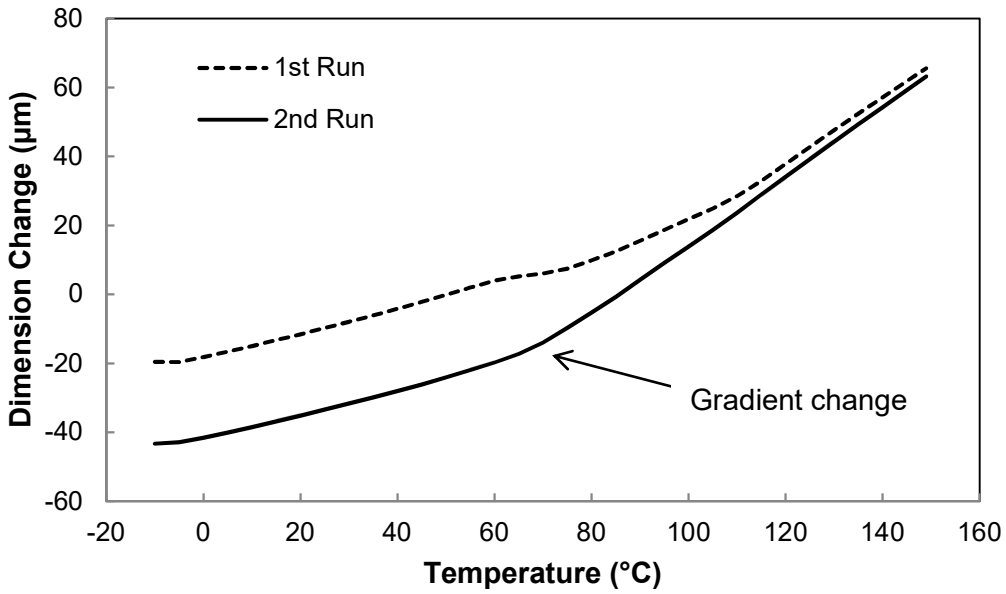

Figure 3.17 - Comparison of runs on the same specimen with a ratio of R ≈ 1.5.

The mean LCTE for a designated temperature range was calculated from Equation 3.7, from plots of change in length as a function of temperature like those shown in Figure 3.18:

$$LCTE = \frac{\Delta L}{\Delta T \; x \; L} = \frac{gradient}{L} \qquad 3.7$$

Where L is the original length of the specimen at room temperature, ΔL is the change in length and ΔT is the change in temperature respectively.

The values for T_g were evaluated directly from the plot as the intersection point of the two gradients, before and after T_g as shown in Figure 3.18. TA Universal Analysis was also used to plot the gradient of the dimension change variable as a function of temperature as shown in Figure 3.19. The discussed transition that occurs before and after T_g can clearly be seen in Figure 3.19. Such plots allowed for LCTE values to calculated for each temperature value, rather than the average that would be calculated from Figure 3.18.

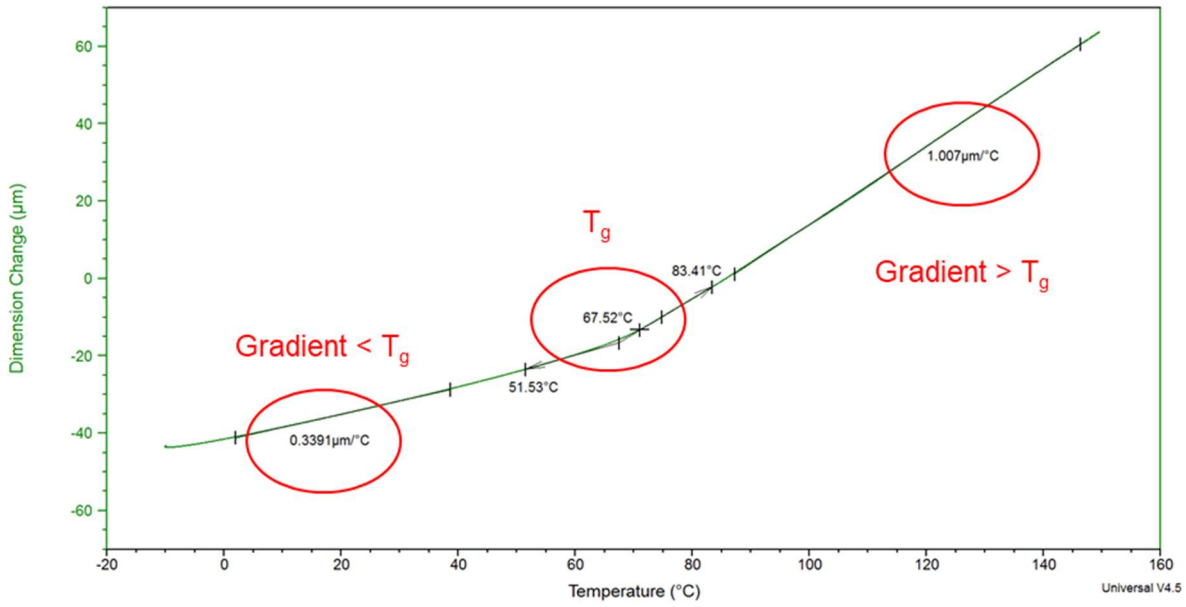

Figure 3.18 - Evaluation of gradients and Tg using TA Universal Analysis.

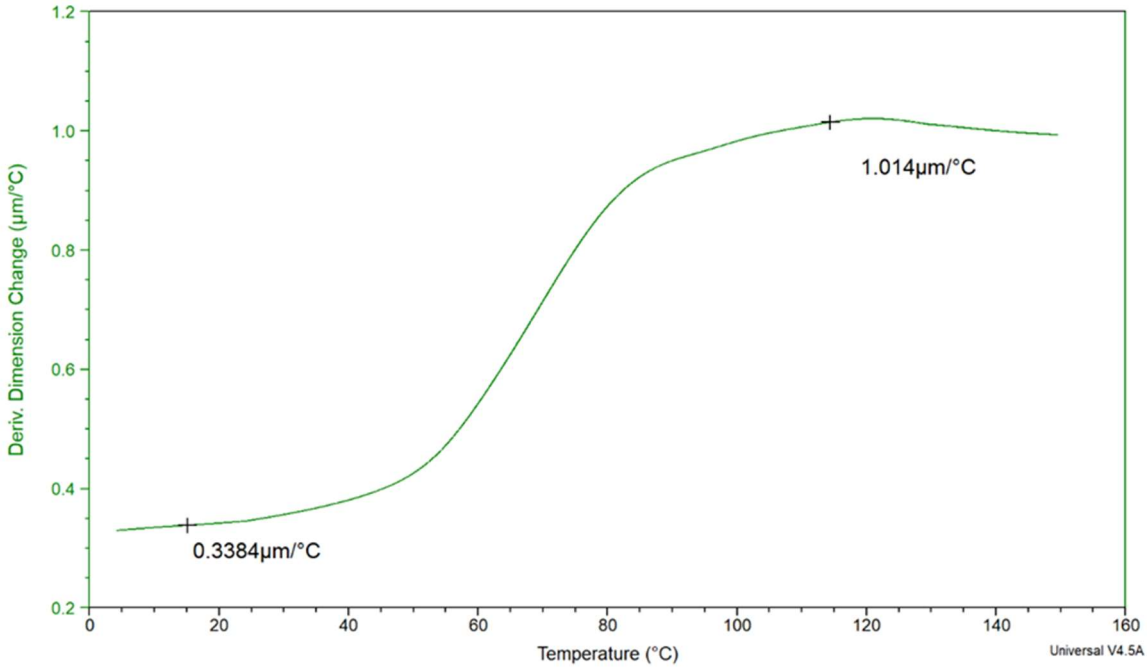

Figure 3.19 – Plot of gradient change using TA Universal Analysis.

3.2.3 Dynamic Mechanical Analysis (DMA)

Dynamic Mechanical Analysis, DMA, was carried out in accordance with ASTM standard D5023-07; '*Standard Test Method for Plastics: Dynamic Mechanical Properties: In Flexure (Three point Bending)*' [223]. The test, which required

rectangular shaped bars, is valid for frequencies ranging between 0.01 and 100 Hz and is equivalent to the standard ISO 6721, Part 5.

The glass transition temperature was assigned in agreement with standard E1640-13; '*Standard Test Method for Assignment of the Glass Transition Temperature by Dynamic Mechanical Analysis'* [224]. This test is intended for materials with an elastic modulus between 0.5 MPa and 100 GPa, is applicable to thermoplastics and thermosets and is similar to IEC 61006.

The analysis conducted was a 3-point bending test with rectangular shaped specimens supported at both ends whilst the centre underwent controlled oscillation. The test measured the epoxy polymer's viscoelastic properties under flexure. This was vital as the complex modulus alone would not fully describe the material's behaviour due to it displaying both viscous and elastic behaviour whilst in deformation. Throughout the test the loss modulus E'' and storage modulus E' were measured as functions of temperature, during a constant temperature ramp. TA Universal Analysis could then be used to calculate the tan delta. The effects of altering the hardener-to-epoxy ratio on these resulting properties could thus be studied.

A TA Q800 DMA fitted with the 3-point bending clamp was used to conduct the dynamic analysis as shown in Figure 3.20. The clamp loading nose and its supports possessed smooth semi-circular cross sections of radius 4 mm allowing for the required load to be exerted without creating any excessive indentation upon the specimens.

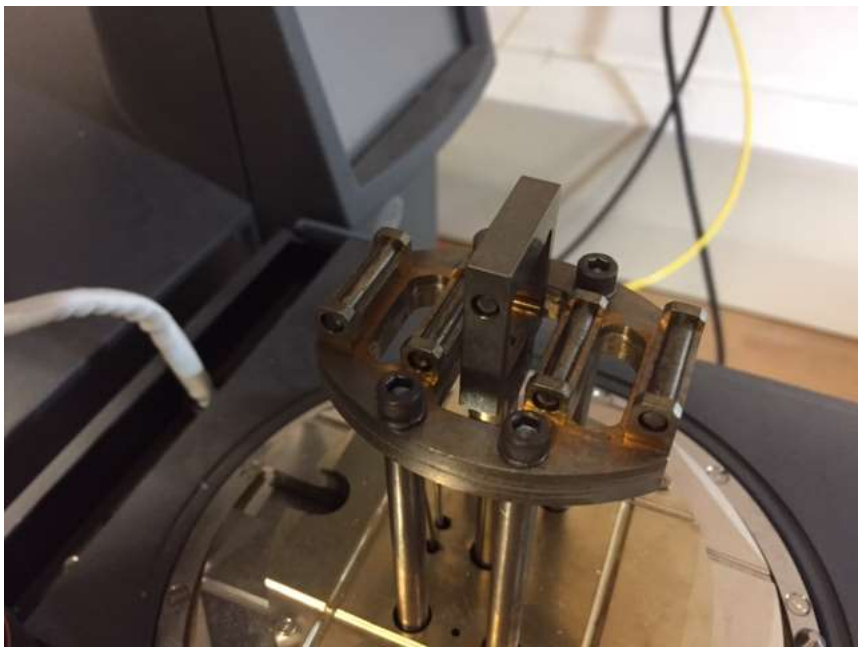

Figure 3.20 – DMA 3-Point Bending Clamp Setup.

The machine was highly sensitive, being able to measure modulus values with a precision of ±1%, over a frequency range of 0.01 to 200 Hz and could dynamically deform specimens from ± 0.5 to 10,000 μm. When possible, a tank of liquid nitrogen was attached to allow the DMA to gain sub-ambient temperatures. The furnace was thus capable of a temperature range from -150 to 600 °C and could provide heating rates from 0.1 to 20 °C/min. Unfortunately, during this project, the liquid nitrogen tank stopped functioning, preventing two of the ratios from being studied at sub-ambient temperatures (R ≈ 0.3 and R ≈ 2.92). Due to this difficulty, only the storage modulus values were studied for these particular ratios due to their T_g being relatively low, making accurate measurement of the other variables difficult.

The specimens used for testing were manufactured using the same silicon moulds and cure schedule as the TMA cube samples discussed in 3.2.2.2, typically at the same time. This produced 64 x 13 (+0.1 or -0.3) x 3 (+0.31 or – 0.26) mm^3 rectangular bars which were then sanded appropriately to remove any artefacts on the surface to produce samples like those shown in Figure 3.21. Each specimen was then placed

horizontally on the 3-point bending clamp, ensuring that the length was as perpendicular as possible to the supports, which were placed 50 mm apart. The support span-to-depth ratio (the length of the stand, divided by the depth resulting in a value of 50) changed per specimen, due to changes in the depth. The specimens tested all fell in the range 16 +2.65 or -1.5, which was within 16 (tolerance +4 or -2), as specified in ASTM standard D5023-07.

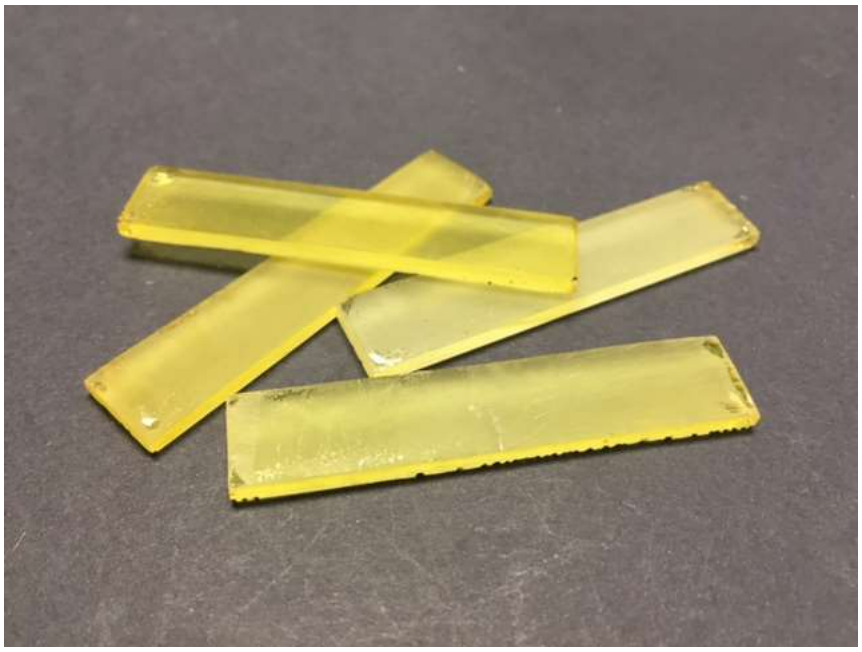

Figure 3.21 - DMA specimen bars with an amine-to-epoxy group ratio of R ≈ 1.25.

The displacement amplitude was programmed to 50 μm and the frequency at 0.1 N. The specimen was preloaded with a small force of 0.1 N.

The furnace was then closed, and the heating schedule was as follows:

i. Equilibrated at -10 °C;
ii. Held isothermally for 5 minutes;
iii. Temperature ramped at a rate of 2 °C per minute up to 150 °C;

Seven different ratios were studied using the sub-ambient capable schedule before the nitrogen tank stopped functioning. The two most extreme ratios of R ≈ 0.31 and R

≈ 2.92 were studied without liquid nitrogen cooling, thus the starting temperature was at ambient. This allowed for storage modulus comparisons with the other ratios measured, however reliable results for the T_g from the loss modulus and tan delta peaks were more difficult to obtain. A minimum of three specimens per ratio were tested.

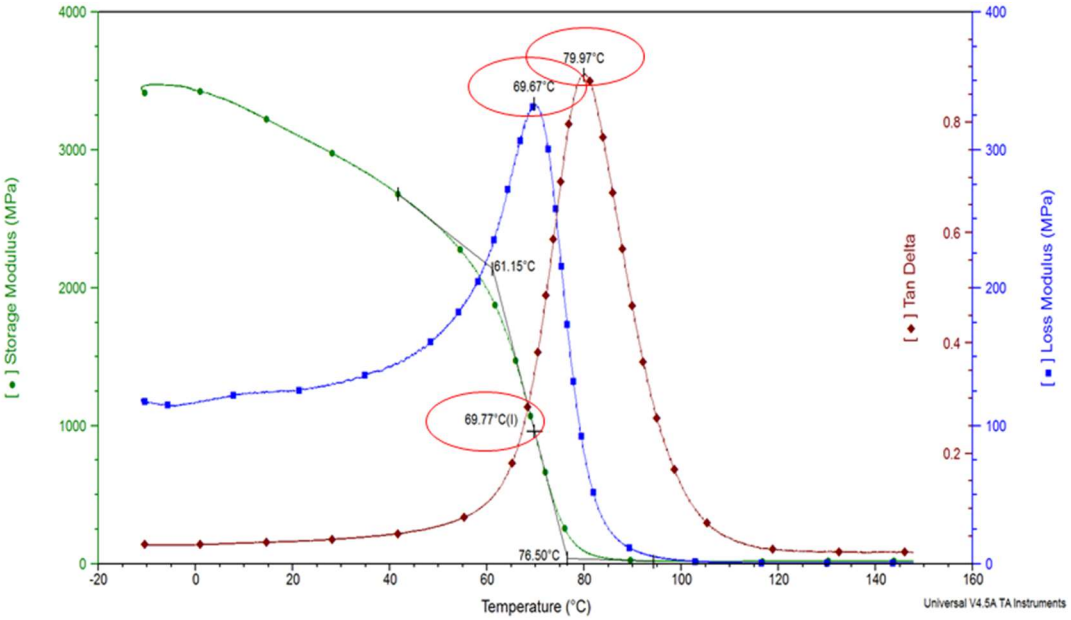

Figure 3.22 - Storage modulus, loss modulus and tan delta overlaid.

The data analysis was conducted using TA Universal Analysis, which allowed the storage modulus E', loss modulus E'' and tan delta values to be overlaid on the same plot as shown in Figure 3.22. This allowed for the different values of the T_g to be calculated accordingly, with the T_g assigned to the E' being calculated from the midpoint of the step change shown whilst the T_g assigned to the E'' and tan delta were the peaks of the respective plots.

3.3 Microbond Technique

The microbond technique is recognized as being one of the viable methods for studying the apparent adhesion that exists between the reinforcing glass fibre and the polymer matrix via measurement of the apparent interfacial shear strength (IFSS) [160]. This mechanically measurable value has been used in past literature to quantify the strength of the interface between several different fibre types and different polymer systems, including both thermosets and thermoplastics [14,15,153,179,225,226].

3.3.1 Instron Microbond Technique

The apparatus for the test can vary greatly, with different methods for specimen clamping and loading published in literature [149,154–156,158,167]. The configuration and development of the microbond test rig used for this thesis has been reported previously [149] and is shown in Figure 3.23.

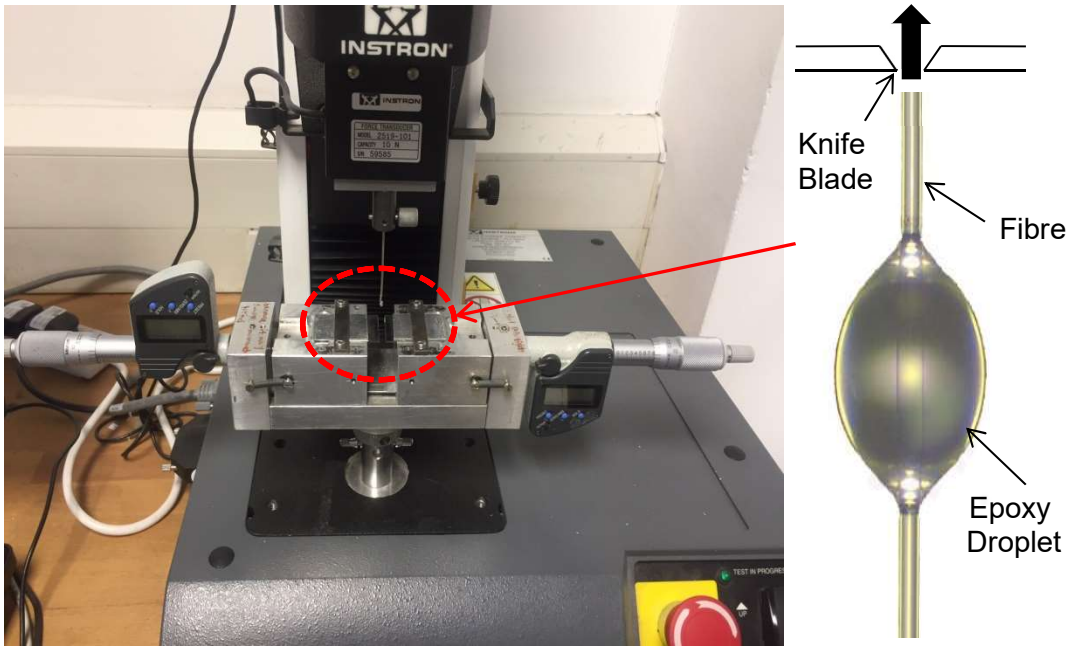

Figure 3.23 - Photo and schematic of Instron Microbond Setup.

The setup is based around an Instron 3342 universal testing machine equipped with a 10 N load cell to apply the load to the microbond samples.

3.3.1.1 Instron Microbond Sample Preparation

The microbond study was focussed on investigating the influence of varying several key variables on the resulting adhesion between the fibre and the polymer. Specifically, the influence of the hardener-to-epoxy ratio, the purity of the hardener used, and the silane surface coating applied to the fibre. The sample preparation process was consistent for each of these studies, with only the selected variable being changed.

The procedure began with approximately 20 cm long glass fibre bundles being taken from the inside of large rovings. The inside fibres were selected to ensure that they had been exposed to a minimum degree of mechanical contact. This was important since if the fibres were damaged this led to a greater number of fibre breakages prior to de-bonding during the test, rendering the results irrelevant for IFSS characterization. Single glass fibres were extracted from the bundle without touching the fibre surface where the epoxy droplet would be applied in order to minimise contamination. Individual fibres were then attached to a 20 mm gauge length card template, with tape initially being used to position the fibre on the central vertical axis to ensure it would hang vertically when tested. Loctite® super glue was then applied at a position as close to the edge as possible, in order to minimise potential small discrepancies in the gauge length value. The finished samples were then left for at least 24 hours at room temperature to ensure that the glue had fully cured. A schematic of a typical (Instron) mounted microbond sample before the addition of the minute droplets of epoxy is shown in Figure 3.24.

Although three different silane fibre coatings were studied in detail during this project, the procedure discussed for mounting the fibres for microbond testing was consistent for each fibre.

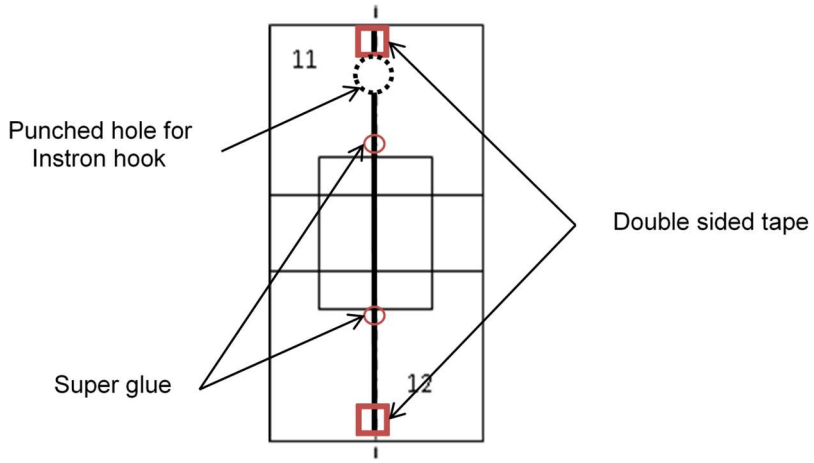

Figure 3.24 - Schematic of mounted fibre sample before addition of epoxy droplets.

Once the single fibres had been mounted successfully, the epoxy system was prepared. The procedure was the same as discussed in 3.2.1.1 with predetermined ratios having been calculated before measuring out the required amounts of resin and hardener. Approximately two grams of epoxy was measured into a small plastic container, with the predetermined mass of hardener then added via a pipette. Any remaining hardener within the pipette was then safely disposed of. The exact masses of both the epoxy and the hardener in the mixture were then noted so the corrected overall ratio could be recorded. The same procedure was also used for the study of the influence of the purity of the hardener on fibre-matrix adhesion. The mixture was then stirred to ensure it was as homogeneous as possible before being degassed under vacuum for approximately 15 minutes.

After removing the mixture from the degassing apparatus, it was ready to be applied to the mounted fibres. A small piece of 0.05 mm diameter steel wire was attached to a scalpel to create a tool capable of applying the epoxy to the fibre as shown in Figure 3.25.

Figure 3.25 - Adapted scalpel to apply droplets to mounted fibres.

Minute droplets of the resin mixture were then applied to the single fibres, with two sets being applied to each mounted fibre at the 5 mm gauge length marks shown on the card as shown in Figure 3.26. Droplets were applied to approximately 30 individual fibres before the samples were transferred to a convection oven to undergo the same curing schedule discussed in 3.2.1.1. The samples would then be left to cool overnight in the oven.

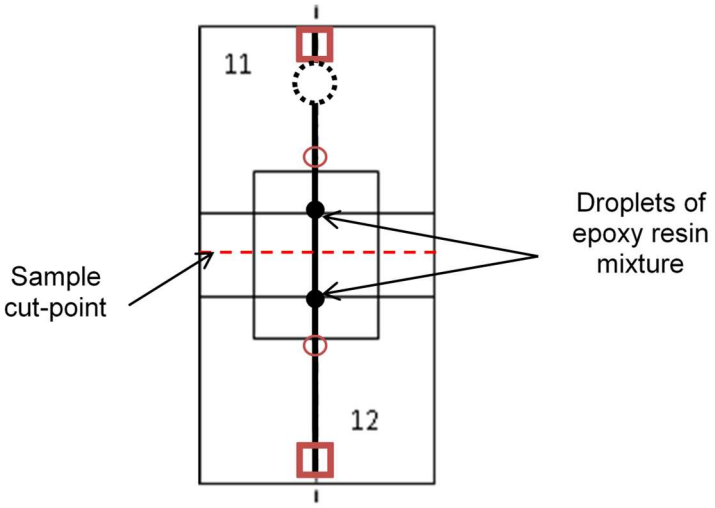

Figure 3.26 - Schematic of mounted fibre sample after addition of epoxy droplets.

It was discovered to be extremely difficult to apply only one droplet to the fibre for each sample without the droplet then being too large to successfully test. As a result, multiple droplets were typically applied to the fibre surface as shown in Figure 3.27, allowing for a selection of which droplet to test for each sample. This accounted for any droplets that were either deformed or damaged during the preparation process.

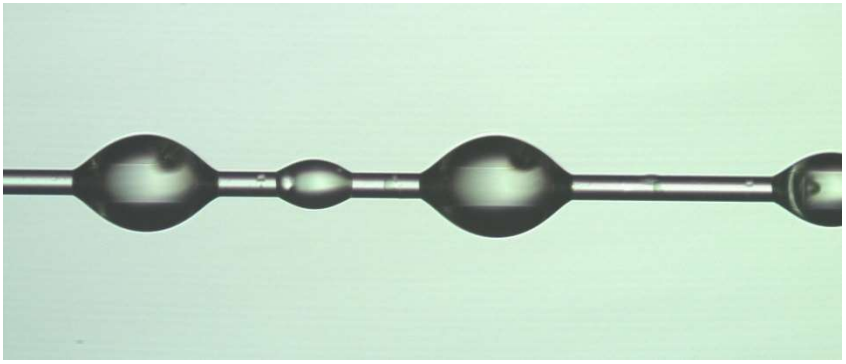

Figure 3.27 - Image of multiple droplets applied to a single fibre.

The time taken for the sample preparation process was carefully regulated, with the time from first contact between the hardener and the epoxy, to the samples being placed in the oven being kept to a minimum. As the curing process starts as soon as the components are mixed, the system could begin to cure to some small degree before going into the convection oven. The curing reaction is also an exothermic reaction, meaning that it produces heat as the reaction progresses. This produced heat then has the potential to accelerate the curing process further. This partial curing could negatively impact properties of the cured resin and thus potentially the stress transfer capability of the interface as well. The exothermic reaction was particularly noticeable for excess amine ratios, where a notable increase in temperature could be felt after degassing. This led to careful control being placed upon the exact amounts of epoxy and hardener being mixed, since larger amounts of both would lead to larger exothermic reactions and more potential for the mixture to partially cure before being placed in the oven.

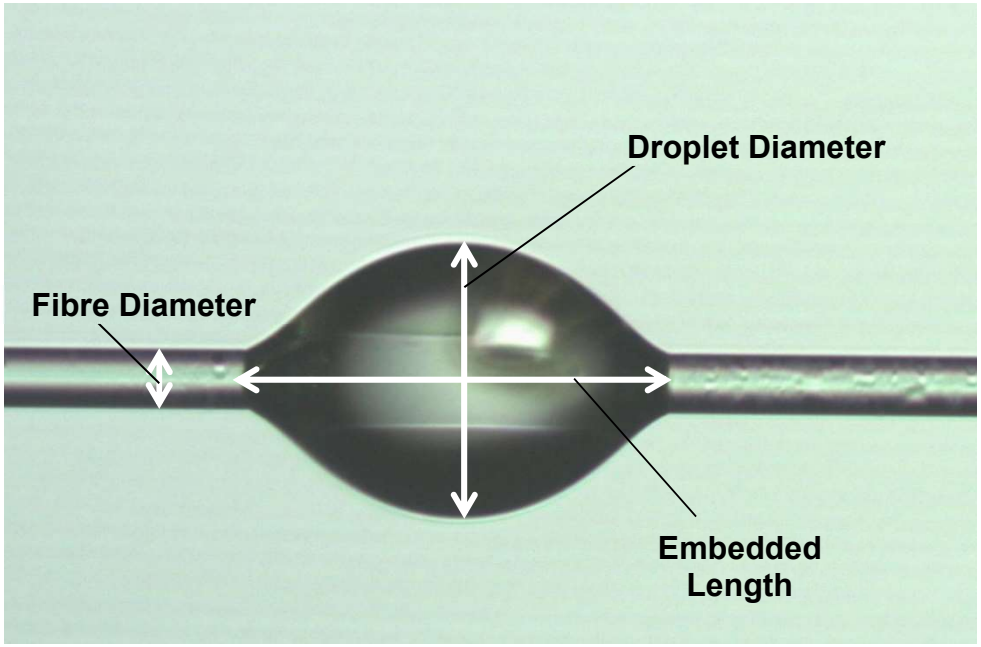

Figure 3.28 - Epoxy droplet at 200x magnification using optical microscopy.

Finally, once the curing process had completed, samples were examined under 200x magnification using a Nikon Epiphot inverted optical microscope. A suitable droplet was selected for each sample and a photo taken. This was further analysed using the image processing software package ImageJ to determine values for the fibre diameter, droplet diameter and droplet embedded length for each sample. An example is presented in Figure 3.28.

3.3.1.2 Instron Microbond Testing Procedure

The setup shown in Figure 3.23 was used to conduct the microbond testing. This was combined with a stereo microscope (45x magnification) connected with a DCM130 video camera to allow for the user to observe the microbond samples and the shear blades during the test as shown in Figure 3.29. Note a reflection can be seen overlapping the upper part of the sample during testing due to the background light reflecting off the knife blades of the setup.

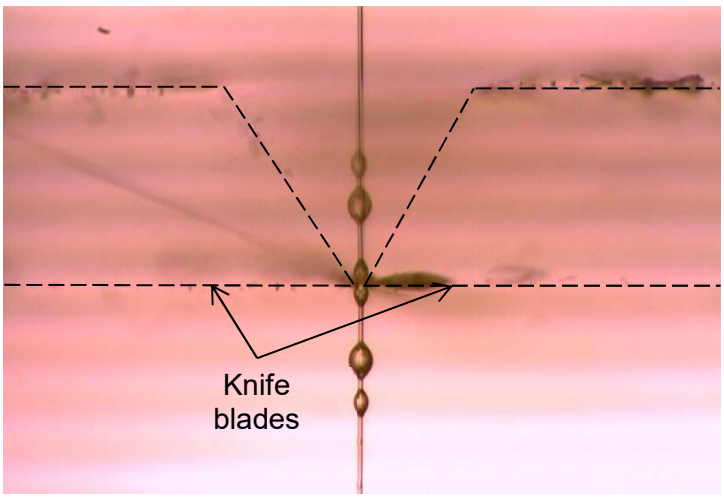

Figure 3.29 – View of sample during microbond test using 45x magnification microscope.

The loading rate was maintained at 0.1 mm/s throughout the entire study and all tests were performed at room temperature (22 ± 2 °C). Instron Bluehill 2 software was used to record the crosshead (fibre sample) displacement and the resultant applied load. An example of the load-displacement plot of a successful de-bond is presented in Figure 3.30 with the point of maximum load (F_{max}) highlighted.

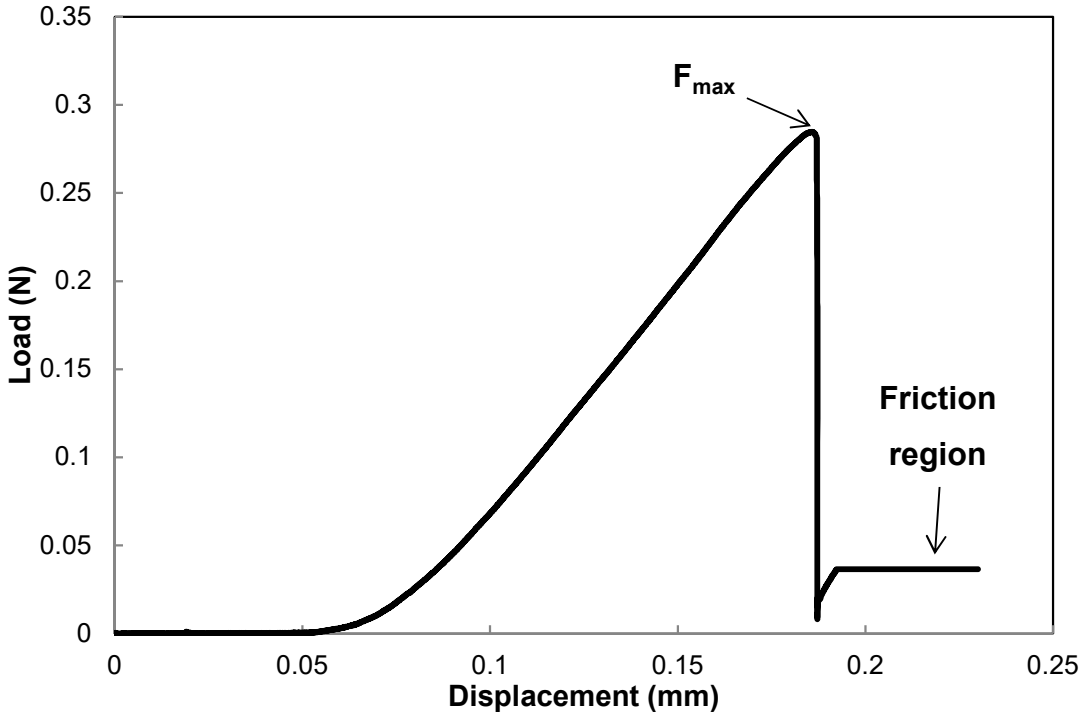

Figure 3.30 - Typical load/displacement curve of microbond test.

The load-displacement plot clearly shows the curve at the maximum load that is typical of a successfully de-bonded specimen. The friction force present after de-bonding occurs due to the tested droplet being dragged along the fibre after the test can also be seen.

Over the course of the study, three other types of load-displacement plot were encountered during testing. Figure 3.31 shows the plot for a sample where the fibre broke during testing before de-bonding occurred, with a notably sharper characteristic drop at the point of max load, with no friction force recorded afterwards. Results from these plots were not used for the IFSS analysis since the de-bonding load of the sample was never truly reached.

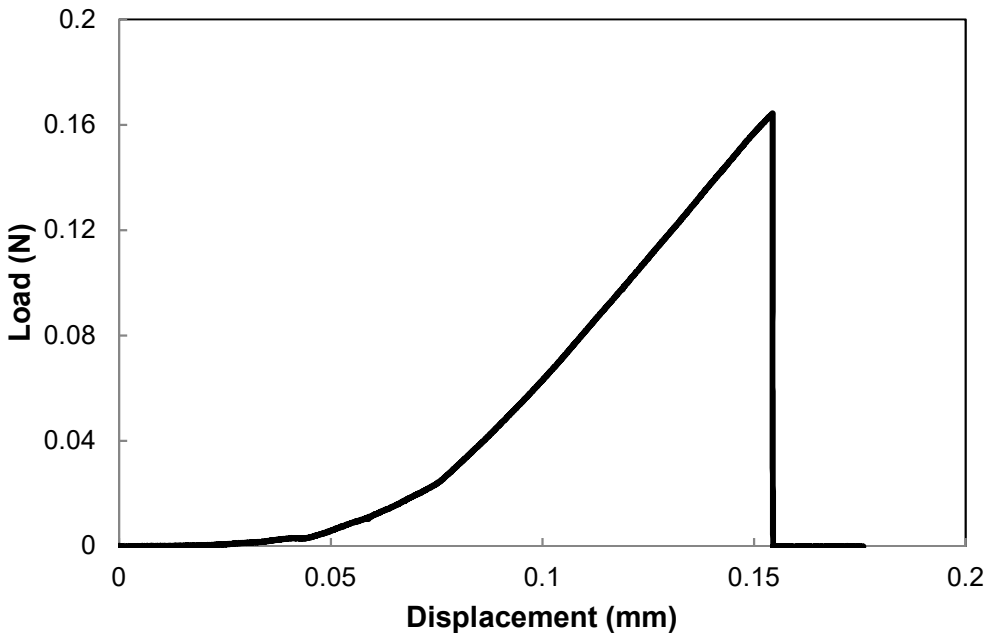

Figure 3.31 – Load/Displacement plot where fibre broke during testing.

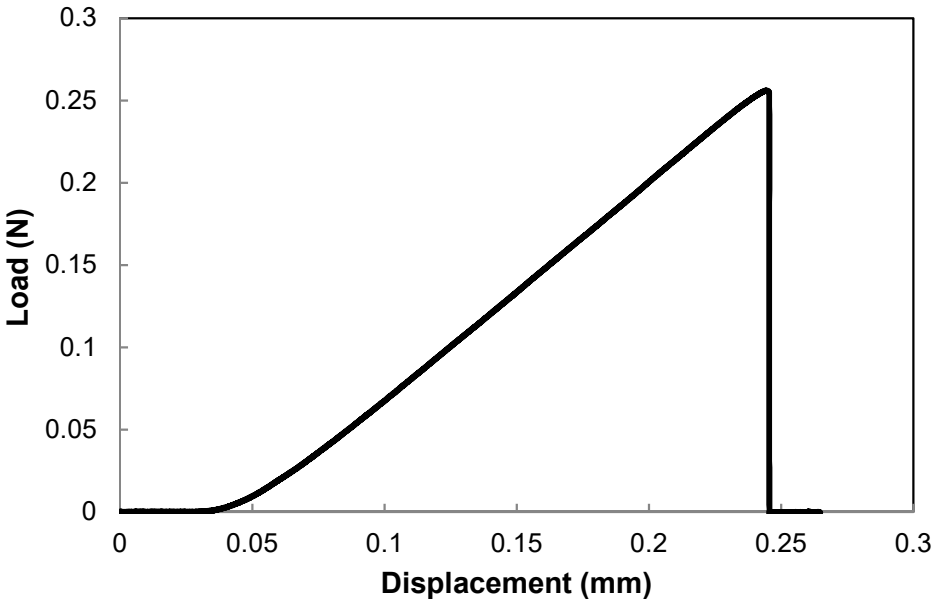

Figure 3.32 – Load/Displacement plot where fibre broke after de-bonding.

Figure 3.32 shows the plot for a sample where either the droplet has completely broken off the fibre during the test or the fibre has broken just after a successful de-bond, resulting in the curved drop similar to Figure 3.30 but without the friction force after the test. Data recovered from these plots could typically be included in the results since the maximum load recorded for de-bond was recorded; the fibre did not break before de-bonding occurred. However, further analysis of the sample was required, if possible, following testing in order to make a definite decision whether the droplet successfully de-bonded or not. Specifically, analysis of the load/displacement plots around F_{max} was conducted as well as studying the point of breakage of the sample under a microscope. If the gradient of the plot began to decrease before failure as shown in Figure 3.32 and the sample was shown to have broken at the exact contact point of the droplet with the knife blades, then it could be concluded that de-bonding did successfully occur.

The other load-displacement plot encountered is shown in Figure 3.33. This plot shows the successful de-bond of a droplet which as it slipped down the fibre, hit a droplet lower on the fibre, which then began the process of de-bonding also. This is

clear since the measured load does not drop down to approximately 0 N after the first de-bonding occurrence. If the test was left to run, the next droplet could then de-bond and so on. Data recovered from these plots could be used if the max load recorded was for the original de-bonded droplet, and not for the subsequent droplets.

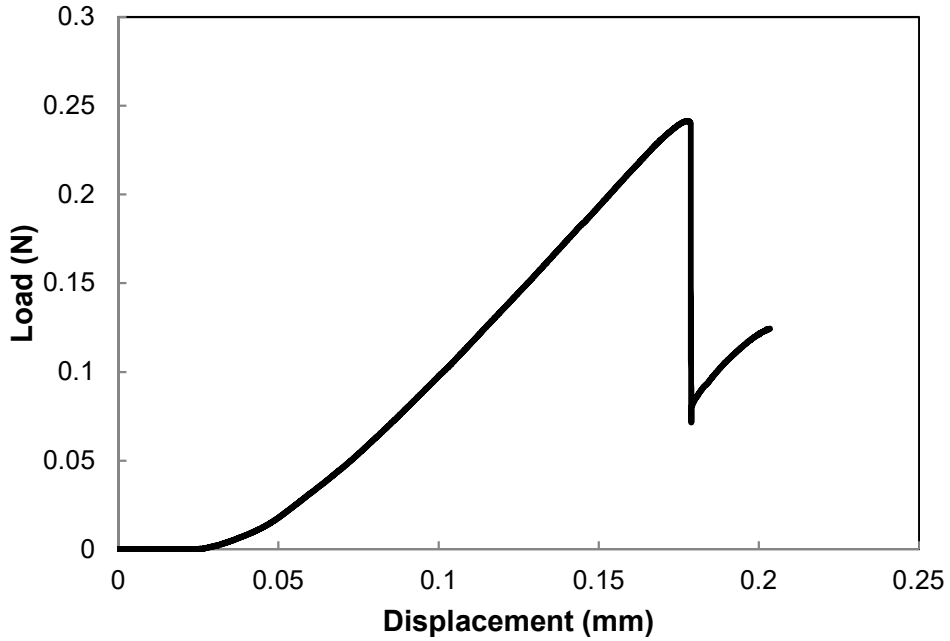

Figure 3.33 – Load/Displacement plot where de-bonded droplet slips into another droplet.

The load-displacement curve for each test was recorded in order to obtain a maximum force (F_{max}) at full interfacial de-bonding as shown in Figure 3.30. This value, along with the measured fibre diameter (D_f) and droplet embedded length (L_e), was used to calculate the apparent IFSS, τ_{app}, using Equation 3.8 which is based on the assumption that the shear stresses at the interface are constant throughout the droplet.

$$\tau_{app} = \frac{F_{max}}{\pi D_f L_e} \qquad 3.8$$

3.3.2 TMA Microbond Technique

In order to understand the influence of both testing temperature and the hardener-to-epoxy ratio on the strength of the GF - epoxy interface, it was necessary to adapt the technique used in subchapter 3.3.1 such that it could be completed within a temperature-controlled environment. This was achieved by using a technique previously reported in [14,15]. The TMA microbond technique uses a TA Q400 thermo-mechanical analyser, in combination with the cooling accessory MCA270 mounted with a film/fibre probe. A schematic and photo of the setup is shown in Figure 3.34 [15].

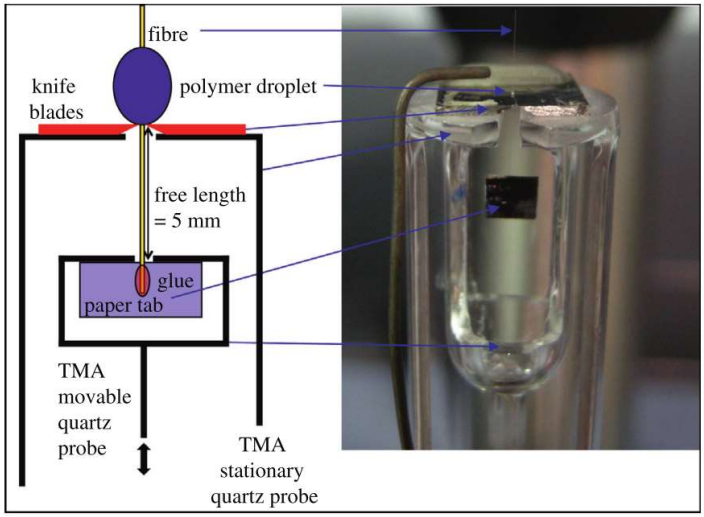

Figure 3.34 – Schematic and photo of TMA microbond setup taken from [14].

The droplet applied to the fibre sits on the shearing plate which itself sits on the stationary quartz platform. The movable probe, installed in the centre of the stationary platform, then rests on the paper tab of the sample. It is this probe which applies the load during the test. The entire microbond setup is then enclosed within the TMA temperature controlled programmable oven. Each sample was initially placed under a very small pre-load of 0.005 N, with the free fibre length between the tab and epoxy droplet maintained at a constant value of 5 mm to match the samples tested in 3.3.1. Fibres 1 and 3 as designated in Table 3.1 were used for this study.

The notable difference between the TMA and Instron microbond techniques relates to how each technique loads the sample. The technique described in 3.3.1.2 is carried out by measuring the load generated during the displacement of a droplet at a constant strain rate however the TMA is unable to operate in this mode. Instead, the TMA had to be configured to measure the sample displacement during a linear force ramp of 0.15 N/min [14].

The testing procedure proceeded as follows. The probe displacement was electronically zeroed and the microbond sample loaded into the shearing plate with the paper tab hanging freely below the movable probe. The movable probe was then carefully lowered onto the paper tab before the furnace was closed. The initial sample length and probe position was then recorded, and the furnace was programmed to equilibrate at the desired test temperature (ranging from -10 °C to 120 °C) with an additional three-minute isothermal segment to ensure a constant equilibrium temperature was achieved. The force ramp was then initiated at 0.15 N/min. As the test proceeded the probe displacement would increase and be recorded until a successful de-bond occurred. A typical result obtained from a TMA-microbond test is plotted as a force–displacement curve in Figure 3.35. The general form of the curve is clearly different from that obtained by the technique described in 3.3.1.2. Yet, it can be seen that the maximum value of force required to obtain a successful de-bond was still clearly obtainable. The major difference in the plots occurs after de-bonding. Due to the TMA continuing the force ramp after the successful de-bond, there is a rapid downward displacement of the de-bonded fibre [14]. As such, no observations can be made on the friction region that occurs after the de-bonding process.

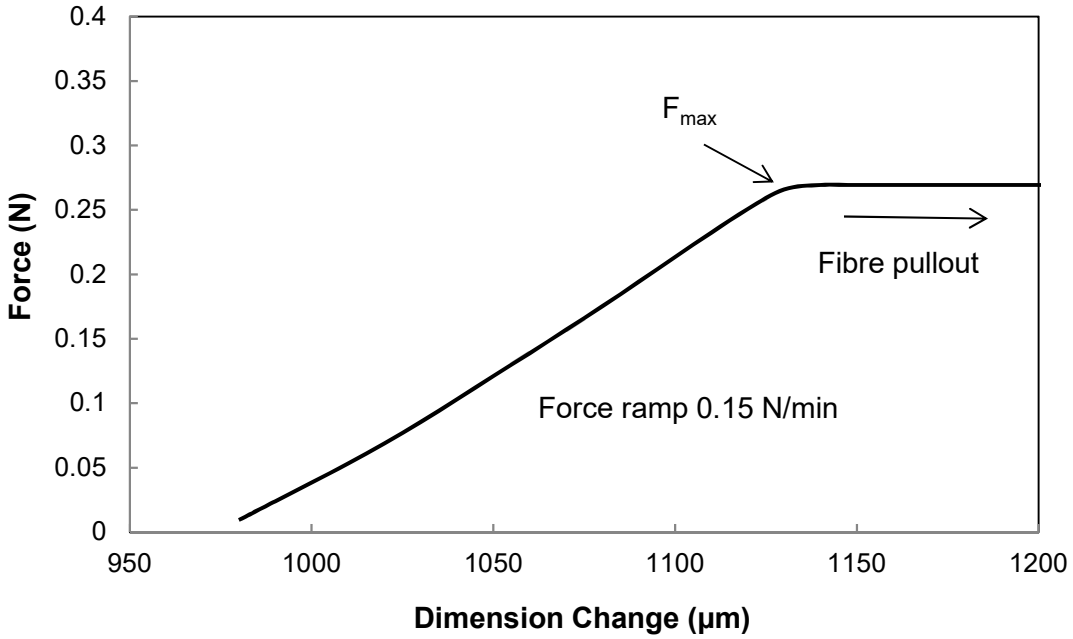

Figure 3.35 – Load/Displacement plot for TMA microbond test.

All tests were conducted under a dry nitrogen flow of 50 ml/min. For fibre 1 seven ratios were tested at the following temperatures: 20 °C, 50 °C, 90 °C and 120 °C respectively. The ratios R ≈ 0.53, R ≈ 1.0 and R ≈ 2.06 were exposed to three further temperatures (-10 °C, 70 °C, 80°C) due to them representing the stoichiometric value and the extreme values either side of stoichiometry. For fibre 3, the same three ratios were studied at the following temperatures: 20 °C, 50 °C, 70 °C, 90 °C and 120 °C respectively. Approximately 30 samples were studied per ratio per temperature.

3.4 Cure Shrinkage Analysis

Analysis of the behaviour of the interface during the microbond test made it clear that there was a need to study the formation of both the thermal residual stresses and chemical shrinkage residual stresses that form during the curing process [14,15]. Analysis of the thermal residual stresses was possible using the work conducted in 3.2, however this was not the case for the shrinkage stresses that form due to the chemical reaction during curing. To gain a better understanding of what could be occurring to the actual microbond samples under test, a technique was required for

analysing the shrinkage of an epoxy droplet embedded on a fibre during the curing process. As such, a novel technique was developed and then compared with other previously reported techniques used for analysing cure shrinkage [60,61,64].

3.4.1 Hot Stage Microscopy Technique

During analysis of past literature, it was discovered that no technique had been previously developed for studying microbond samples during the curing process to gauge the level of shrinkage that occurs.

This led to the creation of a new method using a Mettler Toledo FP90 hot-stage heating element combined with a microscope. The hot-stage setup allowed for a controlled temperature schedule to be programmed to match the standard cure schedule used in the preparation of microbond samples.

Samples would be prepared by suspending single glass fibres, taken from larger bundles of E-glass fibres coated with APS, above 1mm thick rectangular glass slide cover slips with a slow setting cement. The sample would then be left for 24 hours to allow for the cement to set. The procedure was extremely delicate since the glass fibre could not be allowed to touch the surface of the cover slip and had to be suspended as straight as possible relative to the cover slip to allow for easier analysis under the microscope. The level of cement used also had to be careful regulated to prevent it from coming in contact with the innards of the hot-stage heating element during the curing process.

Once the fibres had been successfully suspended, a minute droplet of epoxy was applied in a similar manner to that described in 3.3.1.1 with a schematic of a typical sample shown in Figure 3.36. The sample would then be placed in the hot-stage, ready for the curing process to start. As with the other work conducted in this project, the hardener-to-epoxy ratio was varied to gauge its effect on the resulting level of cure

shrinkage. Seven different ratios were studied with at least five samples tested per ratio.

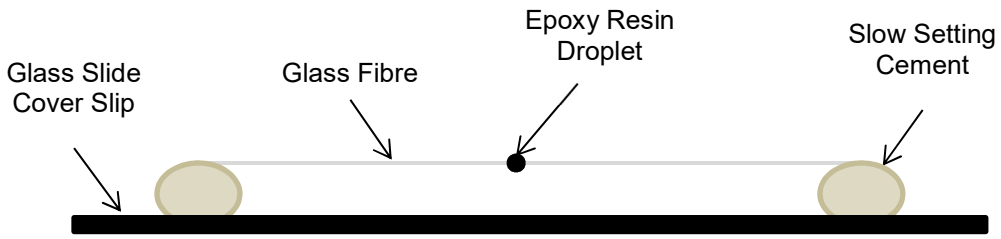

Figure 3.36 – Hot-stage microscopy sample schematic.

The temperature schedule selected for the test followed the similar curing schedule discussed in 3.2.1.1, except the there was no final isotherm at the end of the run as shown in Figure 3.37. This was selected due to time constraints regarding the test as well initial analysis suggesting that little additional shrinkage occurred over this period relative to the earlier heat ramps.

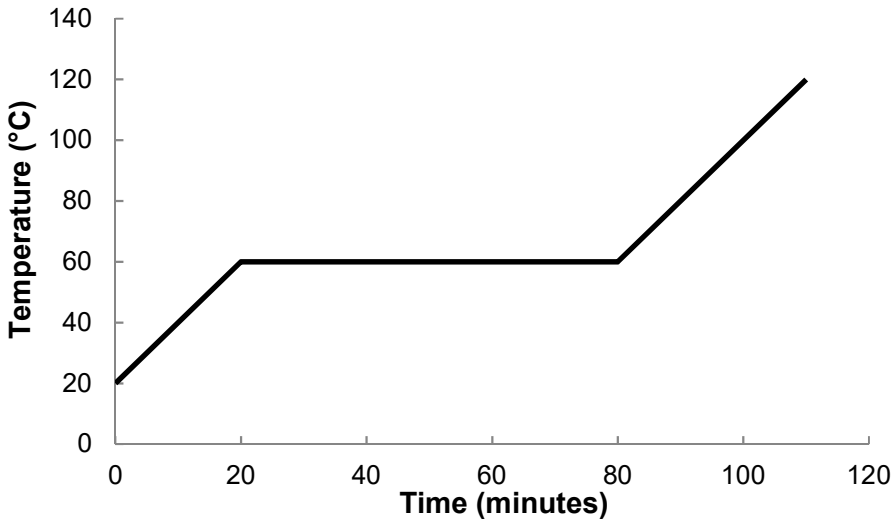

Figure 3.37 - Temperature schedule of hot-stage microscopy technique.

An Olympus BX51 microscope (200x magnification) was used to allow for the minute epoxy resin droplets and glass fibre to be focussed on without any distortion to the point of view. Images of samples were taken at one-minute intervals over the duration of the cure using a Nikon Coolpix P5100 digital camera, mounted to the head of the

microscope as shown in Figure 3.38. It was found that if left unchecked, the focus of the camera could drift during the curing process and as such the user was required to be present throughout the test to ensure that this was minimised.

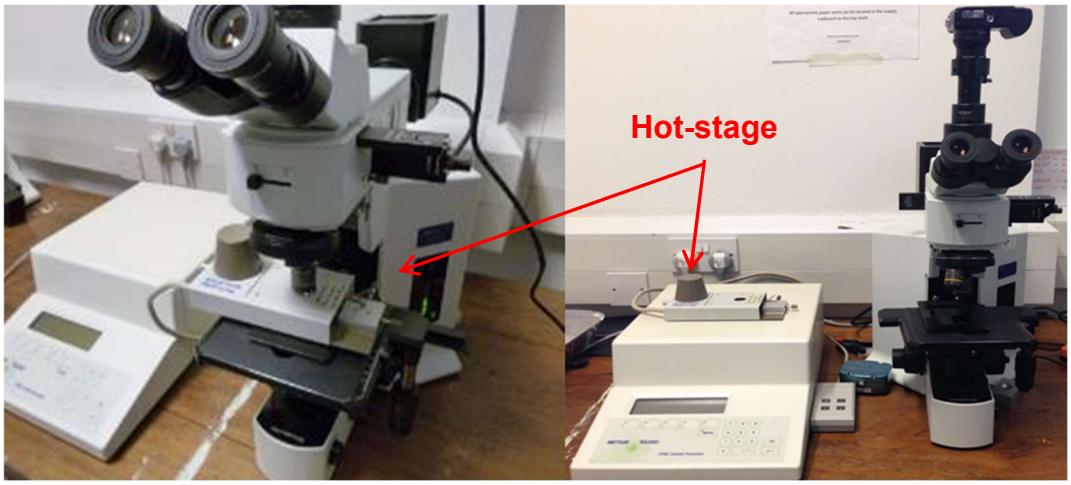

Figure 3.38 - Hot-stage and microscope setup.

Once the curing process had completed the images collected were analysed for each sample using the image processing software package ImageJ, an open source, freely available software package that allows for the distance within images to be measured. Calibration of the software was of key importance to ensure that all images were analysed to a consistent scale, hence why it was required that the user ensure that the level of magnification was maintained as close to constant as possible whilst the test was conducted. For each image the distances “a” and “b”, as shown in Figure 3.39, were measured and recorded.

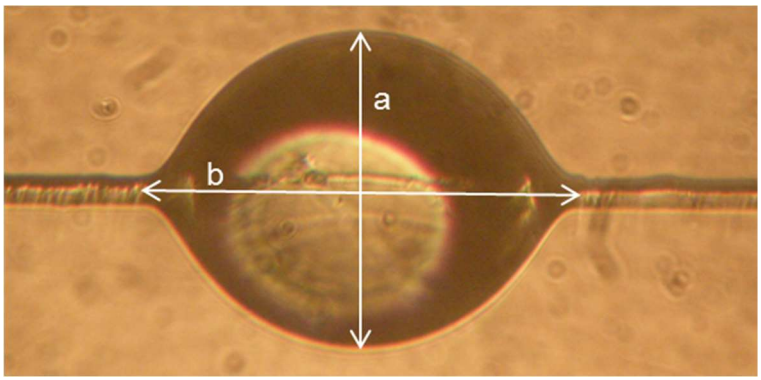

Figure 3.39 – Epoxy resin droplet under microscope with distances a and b.

The distance “a” was selected to be the major axis and “b” the minor axis. To allow for the volume of the droplet at each interval to be calculated several assumptions had to be made. First, it was assumed that the resin droplet remained symmetrical throughout the curing process, with any droplets developing deformities removed from the final result for each ratio. Typically, to calculate the volume of a spheroid three dimensions are required however since only two were known (dimensions a and b) it was assumed that the ideal model for the minute resin droplets embedded on the fibre was a prolate spheroid. The initial size of each droplet was difficult to maintain at a constant value thus the distances were normalised to give an overall percentage change. The volume of each was calculated using Equation 3.9.

$$Droplet\ Volume = \frac{4}{3}\pi\left(\frac{a}{2}\right)^2\left(\frac{b}{2}\right) \quad 3.9$$

The normalised volumetric change was then calculated as per the following equation:

$$\varepsilon_V = \frac{V_t - V_o}{V_o} \quad 3.10$$

Where V_o represents the initial volume of the sample whilst V_t represents the volume of the sample after a variable space of time t during the curing process.

3.4.2 TMA Cure Shrinkage Technique

The TMA Q400EM was used to determine the linear shrinkage of the different R values using a technique developed by Yu et al [64] and also adopted by Shah et al [60]. A schematic of the TMA shrinkage setup is shown in Figure 3.40.

Three different hardener-to-epoxy ratios were studied, with amine-to-epoxy group ratios of R ≈ 0.5, 1.0, and 2.0 respectively. The epoxy resin system was prepared in the same manner as in 3.4.1. After degassing, a small portion of resin was extracted and applied to a disposable square glass cover slip (10 mm x 10 mm square) using a

10 mL volume syringe. A second cover slip was then applied, sandwiching the epoxy resin between the two cover slips.

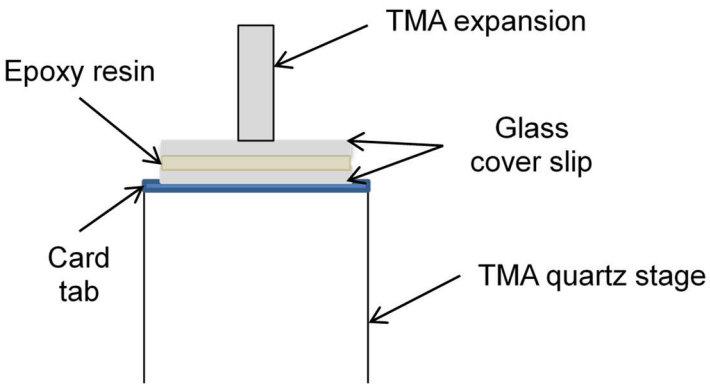

Figure 3.40 - TMA Cure Shrinkage Schematic.

The sample was then carefully transferred to the TMA to allow for the measurement of the initial thickness h_0. Once complete the sample was exposed to the same temperature profile used in 3.4.1. With the thickness of the glass cover slips known, any changes in the thickness of the sandwiched sample could be tracked and recorded by the TMA, with the level of shrinkage calculated using Equation 3.11.

$$\varepsilon_V = \left[1 + \frac{1}{3}\left(\frac{h - h_0}{h_0}\right)\right]^3 - 1 \qquad 3.11$$

Where h_0 represents the initial thickness and h represents the thickness at time t during the curing schedule. A low constant compressive load of 0.02N was applied to the samples throughout each test. The card shown in Figure 3.40 was applied in order to prevent any resin leakage from coming into contact with the stationary quartz platform of the TMA and curing during the test, since this could cause permanent damage to the platform.

3.4.3 Rheometry Technique

This technique was based on the methods used by Khoun et al [61] and D. Shah et al [60] to study cure shrinkage. It focused on the measurement of the gap variation

between the parallel plates of a rheometer as a sample of epoxy is cured. A controlled normal force was applied to maintain the contact between the two plates and the resin sample with the schematic of the setup shown in Figure 3.41. Ultimately the goal was to measure both the gel point and level of cure shrinkage (after gelation) which occurred as the chemistry of the matrix system was changed from the stoichiometric value to ratios possessing excess epoxy and hardener respectively. The same ratios as 3.4.2 were studied. This work was conducted by myself under the supervision of Mr Ananda Roy and Dr Walter Stanley at the University of Limerick, where the equipment was located.

Unlike the hot-stage technique, the rheometry technique required the sample to have gelled before accurate measurements could be taken, since the sample resin would potentially be pushed out from between the plates if a normal force was applied to the liquid resin. As such the procedure was split into two stages:

i. Pre-gelation;
ii. Post-gelation;

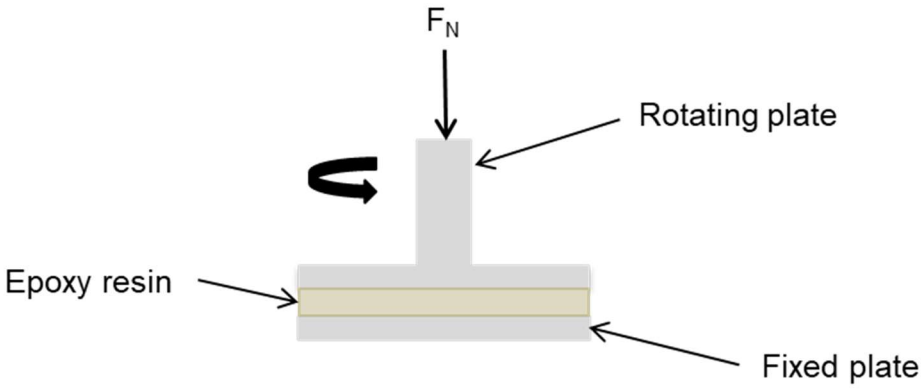

Figure 3.41 - Schematic of rheometer cure shrinkage setup.

The resin was prepared and mixed as was discussed in both 3.4.1 and 3.4.2 respectively before then being applied to the disposable 25 mm bottom plate of the rheometer. The plate included a drip channel to account for any spillage. Pre-gelation

involved the sample undergoing a single-frequency stress-controlled test conducted at a frequency of 0.2 Hz in oscillation mode with the gap between plates being maintained at 0.5 mm and the strain at 15%, with no normal force applied. The sample was then exposed to the same thermal schedule used in both 3.4.1 and 3.4.2 respectively.

Two options were available for defining when gelation had occurred, with the first being the cross-over point of the elastic modulus G' and viscous modulus G''. Although this represented a viable method, it required more user input in order to ensure the correct point had occurred before switching over to step two. Alternatively, the value of 500 Pa s for viscosity has also been used in literature to define the point when the second stage was initiated. It was this latter procedure that was used in the tests conducted within this study.

Once gelation had occurred the procedure moved to the second stage, which involved a single frequency stress-controlled test being conducted at 30Hz in oscillation mode. The stage involved a torque of 500 μNm and compressive force of 0.1 N being applied under isothermal conditions. The gap between the plates then began to vary due to shrinkage, allowing for it to be recorded by the rheometer. This change would then be used with Equation 3.11 to define the level of cure shrinkage.

3.5 Scanning Electron Microscopy (SEM)

A Hitachi SU6600 scanning electron microscope (SEM) was used to analyse the fracture surfaces of selected tested microbond samples for both the Instron and TMA techniques. Sample fibres, droplets included, were removed from the specimen card through use of a scalpel and affixed to a SEM stub using carbon tape. Typically, a minimum of 8 fibres could be applied to the stub before it was sputter gold coated to allow for imaging. Consistent beam settings were used for the highest resolution, to

allow for comparisons to made as well as gain the detailed images of the de-bonded surfaces:

- Accelerating voltage V_{acc} = 15.0 kV;
- Working distance = 10 mm.

3.6 Fourier Transform Infrared Spectroscopy and Raman Spectroscopy

Over the course of the project it became clear that there would be a need to analyse the changes in the chemical structure of the matrix system as the hardener-to-epoxy ratio was varied along with any potential changes due to exposure to elevated temperatures. Fourier transform infrared spectroscopy (FT-IR) and Raman spectroscopy represented two available methods for analysing the matrix by obtaining the molecular vibrations of the structure. This in turn allowed for qualitative and quantitative analysis.

Samples were prepared using the silicone moulds described in 3.2.2.1, taking the form of the DMA samples described in 3.2.3 for simplicity in handling the samples as well as trying to maintain as consistent a surface as possible. Seven different amine-to-epoxy group ratios were studied, again ranging from R ≈ 0.5 up to R ≈ 2.0, increasing incrementally in steps of 0.25. The same curing schedule as detailed in 3.2.1.1 was used. Five samples were prepared per ratio, with four being exposed to a post-curing schedule. Two samples were subjected to a post-curing temperature of 70 °C for two hours while the other two were subjected to a post-curing temperature of 120 °C for two hours.

FT-IR is a widely recognized technique used to obtain the infrared spectrum of emission or absorption of a material [227]. These spectra allow for the molecular structure of the material to be studied. For this study both mid-infrared FT-IR (mIR)

and near infrared FT-IR (nIR) were used. mIR has been widely used in past literature [228–230] to characterise epoxy resins due to its ability to provide both quantitative and qualitative data on the epoxy groups within the matrix. However, mIR can be quite restricted when it comes to analysing epoxy systems. This is due to the location and intensity of one of the epoxy ring absorptions used to quantify the number of unreacted epoxy groups [231]. Despite this, useful information can still be gathered using this technique, with the band at 915 cm^{-1} being assigned to epoxy groups as well as useful analysis of the quantity of hydroxyl groups present.

nIR represents a more useful technique for studying epoxies since it covers fewer, less overlapped bands, allowing for a better study of the curing reaction. The intensity of the bands in this region is much lower than in the mid-range, allowing for the use of thicker samples to get good quality data [231]. The bands for primary and secondary amines are also more defined and intense than for mIR [229,231–234]. Specifically, for this project nIR was used to quantity the number of epoxy groups and primary and secondary amines left within the matrix after curing for different R values.

mIR analysis was conducted using a 4100 Exoscan FT-IR setup with the diamond attenuated total internal reflectance (ATR) interface. The nIR spectra were recorded in transmission using an ABB MB160 with the following settings:

- Spectral resolution: 4 cm^{-1}
- Number of scans: 64
- Background: air
- Sensitivity of detector: B
- Type of detector: InAs

Raman spectroscopy represents another technique for sample identification and quantitation through studying molecular vibrations. A spectrum can be constructed, in

a manner similar to that used to analyse the mIR and nIR response, with the band positions corresponding to the energy levels of different functional group vibrations. Despite some similarities, infrared absorption and Raman scattering are governed by distinctly different selection rules, with infrared bands arising due to an interaction between light and the oscillating dipole moment of a vibrating molecule. Raman bands differ in that they are arise due to an oscillating induced dipole which forms due to the light waves interacting with the polarizability of a vibrating molecule [176,235–239]. The Raman spectra were acquired using a Kaiser RxN1 with a PhAT probe using the following settings:

- Exposure time: 10s
- Number of accumulations: 3
- Excitation wavelength: 785 nm

Both the nIR and Raman analysis were conducted under the supervision of Dr Florian Zehentbauer and Dr Alison Nordon, of the Centre for Process Analysis and Control Technology (CPACT), at the University of Strathclyde.

Chapter 4. The influence of matrix chemistry on the thermomechanical and mechanical properties of the matrix

4.1 Introduction

The aim of the research presented in this chapter was to develop a better understanding of the influence of the amine group: epoxy group ratio (R) over several thermomechanical properties of the matrix. The relevance of properties such as the glass transition temperature (T_g), linear coefficient of thermal expansion (LCTE) and storage modulus (E') to the performance of the final composite has been discussed in detail in the literature over the past number of decades. Now, as then, techniques such as differential scanning calorimetry (DSC), thermo-mechanical analysis (TMA) and dynamic mechanical analysis (DMA) provide effective and relatively simple methods for characterising these parameters. Using these tests, general trends for the variation of T_g, LCTE and E' with matrix chemistry have been reported in the literature [47,51,57,240]. Although these trends have become generally established, it is the case that these properties have never been thoroughly studied in conjunction with analysis of their potential influence on the formation of residual radial compressive stresses at the interface. Furthermore, the influence of the R value on the cure kinetics of this Araldite 506® resin system cannot be fully predicted based on what is known for other similar resin systems.

In this study, a full characterisation of the influence of the R value on the curing process of the resin, as well as several thermomechanical properties was necessary due to the inherent link between the properties of the matrix and the formation of residual radial compressive stresses at the interface. A constant curing schedule was

planned to be used for the preparation of matrix and interface test samples throughout the project; thus an in-depth understanding of how the chemistry of the matrix could influence the curing process was required. Little data has been produced in the past regarding how matrix chemistry may influence the magnitude of these residual stresses and the potential impact on the stress transfer capability of fibre-matrix interface. As such, a range of R values were studied to gain a better understanding of any changes that may occur. Infrared and Raman spectroscopy were used to further quantify the effect of changing the R value on the matrix at a molecular level. Two different purity hardeners were investigated to identify if there was any quantifiable benefit to working with a higher purity, more expensive curing agent. The chemical differences between the two are discussed in subchapter 3.1.

4.2 Cure Kinetics

Better understanding of the cure kinetics of an epoxy system has been acknowledged in the literature as being crucial for studying an epoxy system in depth [25,233,234,241–244]. The hardener type, the hardener concentration and the curing temperature schedule have all been shown to influence the curing process of epoxy resins. In particular the degree of cure has been shown to greatly influence the physical, thermomechanical and electrical properties of epoxy systems [233,244]. As such there was a need to study the cure kinetics for the Araldite 506®/TETA system.

4.2.1 Effect of heating rate

The procedure to study the influence of the heating rate on the cure kinetics of the epoxy resin system was described in subchapter 3.2.1. Samples were cured in the DSC at heating rates of 1, 2, 5 and 10 °C/min to study the curing behaviour of samples prepared at the stoichiometric ratio. Both purities of hardener were studied to gauge if there was any notable difference occurring during the thermoset reaction. This study

was conducted in collaboration with the undergraduate student Neng Qian as a part of her undergraduate project.

Figure 4.1 shows the superposition of the exothermic peaks produced by the four heating rates studied as a function of temperature for the epoxy system cured with standard purity TETA. As is shown in Figure 4.1, the exothermal peak produced by the thermoset reaction has a tendency of moving to higher temperatures and increase in height with the increase in heating rate. Figure 4.2 presents the same data as a function of time. It can be clearly seen that the curing reaction accelerated as the heating rate was increased.

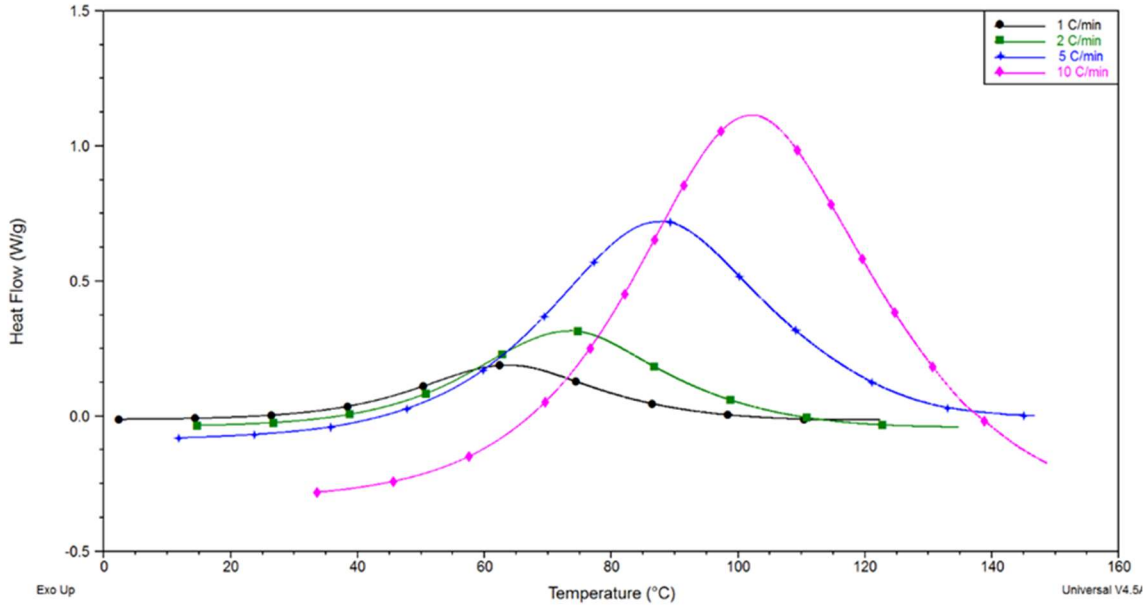

Figure 4.1 – Comparison of exothermic peaks produced by the four heating rates as a function of temperature (Standard TETA).

The onset temperature at 1 °C/min was shown to be adequate for starting the curing process of the amine-epoxy system yet the exothermal reaction accelerated at higher temperatures, allowing the curing process to be achieved faster. With the increase in heating rate the system is given a shorter period to react with the same level of heat compared to the lower heating rates. This agrees with the results discussed by

Sharma et al. [245] and Rosu et al. [44], the former of which suggested that the slower heating process allows for more efficient contact between epoxy and the curing agent i.e. more reaction before gelation and vitrification occurred. Thus, increasing the heating rate could potentially negatively impact certain properties related to the curing process of the epoxy system, as summarised in Table 4.1.

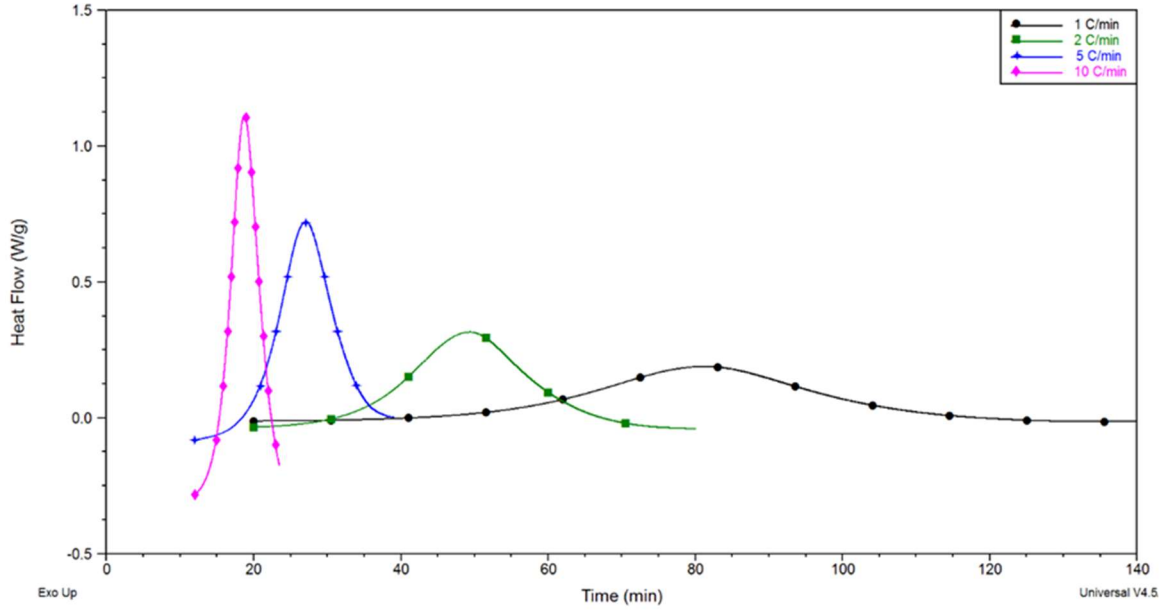

Figure 4.2 - Comparison of exothermic peaks produced by the four heating rates as a function of time (Standard TETA).

The values for peak temperature (T_p), onset temperature (T_{onset}), glass transition temperature (T_g) and reaction enthalpy (ΔH) are presented in Table 4.1 for the four heating rates tested.

Heating rate (°C/min)	T_{onset} (°C)	T_p (°C)	T_g (°C)	ΔH (J/g)
1	35.7	63.5	69.5	442.5
2	44.5	73.7	71.4	414.8
5	53.7	88.5	62.7	400.5
10	67.7	102.7	62.2	357.1

Table 4.1 – Heating rate properties (Standard TETA).

As discussed previously it can be seen that T_p was found to increase as the heating rate of the process was increased. In correlation with this increase in T_p the onset temperature was found to also increase with the heating rate, with the difference shown to be approximately 32 °C. Thus, if an epoxy were to be cured at a high heating rate then the temperature range would need to be extended to ensure the full curing of the polymer. The values for the reaction enthalpy trend support this hypothesis with the overall heat released during the reaction shown to decrease with increasing heating rate, due to the shortened exposure time preventing the curing reaction from occurring to the same degree as it would at lower heating rates.

The results shown in Table 4.1 were used to calculate the activation energy (E_a) of the thermoset reaction. The ASTM E698 kinetics approach [219] obtained from Ozawa's method was applied with the use of a Arrhenius plot to determine the E_a value for the system. The full method is described in subchapter 3.2.1.2. Figure 4.3 shows the Arrhenius plot created with a line of best fit plotted between the data points. The slope of this line was taken as the value for d log10 Φ⁄d (1/T) used in Equation 3.6 and then used to calculate the value for E_a. This was found to be 59.3 kJ/mol.

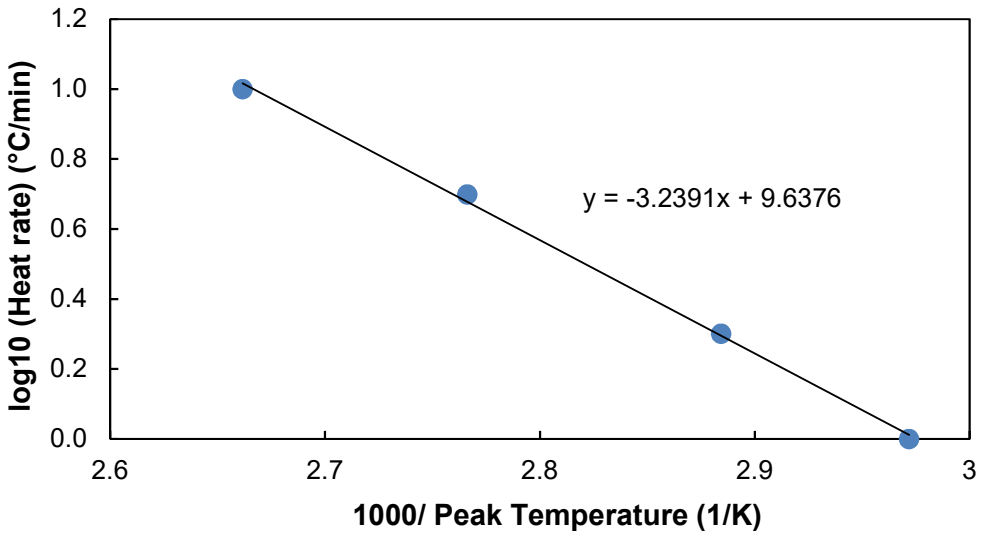

Figure 4.3 - Arrhenius plot (Standard TETA).

Interestingly it can be seen that the heating rate did have a notable influence on the T_g value measured for the cured epoxy during the second heat ramp, with a distinct transition shown between 2 to 5 °C/min. This would indicate that above 2 °C/min, the curing process of the polymer may have been negatively influenced. A possible explanation is that due to the shortened curing time of the process, the matrix is unable to form as full a crosslinked network as for lower heating rates. Since the matrix will reach gelation faster at higher heating rates, this will inhibit the mobility of the reaction groups, preventing them from reacting to the same degree as would be the case for lower heating rates. This would result in lower crosslink densities and the drop in T_g shown. Due to this result, a heating rate of 2 °C/min was used during the sample preparation for the rest of the project.

A similar investigation was carried out with a high technical grade hardener which consisted of, statistically, more ideal TETA molecules and less of the three other TETA ethyleneamines present in lower technical grade TETA used previously. Results are shown in Figure 4.4 and Figure 4.5. Figure 4.4 shows that, again, as the heating rate was increased, the exothermic peak increased in size and occurred at a higher temperature. Figure 4.5 shows that, like Figure 4.2, the exothermic peak occurred earlier as the heating rate was increased. The values for T_p, T_{onset}, T_g and ΔH for this high purity TETA system are presented in Table 4.2. Comparing the data in Table 4.1 and Table 4.2, correlating trends are shown for T_p, T_{onset} and ΔH respectively for the two purities.

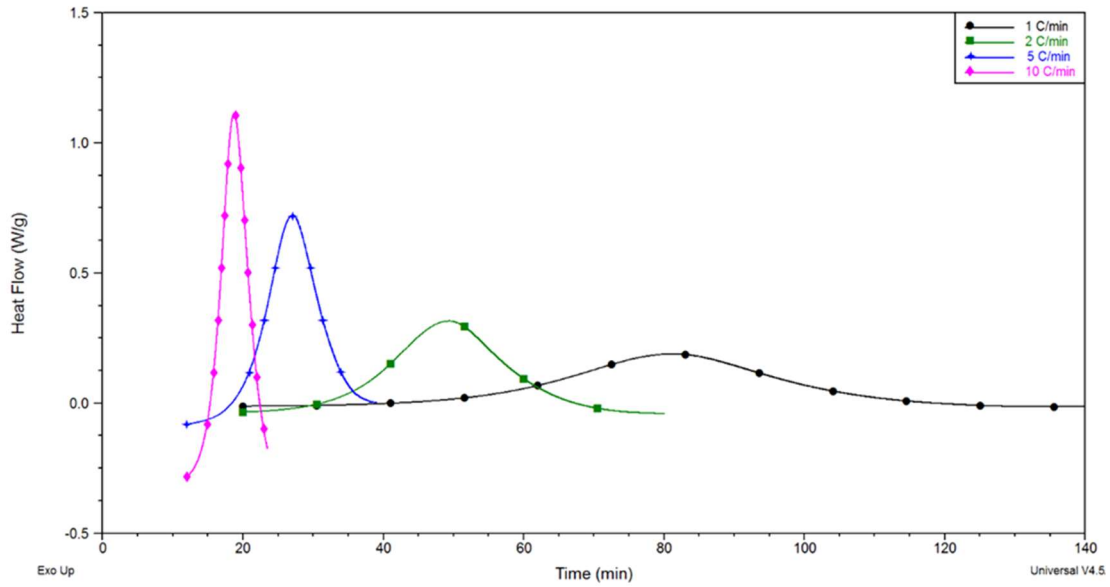

Figure 4.4 - Comparison of exothermic peaks produced by the four heating rates as a function of temperature (High Purity TETA).

Overall, there appears to be very little difference between the two purities regarding the curing reaction of the matrix other a clear difference between the T_g values of the cured polymer. Unlike the standard TETA the heating rate had no notable influence on the T_g value for the high purity TETA, with each rate producing a T_g value around 87 °C. Furthermore, these T_g values were shown to be higher for the high purity TETA across all heating rates, suggesting that the high purity TETA produced a more consistently developed crosslinked network regardless of the heating rate.

Heating rate (°C/min)	T_{onset} (°C)	T_p (°C)	T_g (°C)	ΔH (J/g)
1	36.5	63.65	86.7	439.2
2	47.0	75.03	87.7	413.0
5	55.7	88.09	87.5	397.1
10	67.7	102.39	87.6	350.7

Table 4.2 - Heating rate properties (High Purity TETA).

The values presented in Table 4.2 were used to find the E_a value for the high purity TETA system. The respective Arrhenius plot is shown in Figure 4.6.

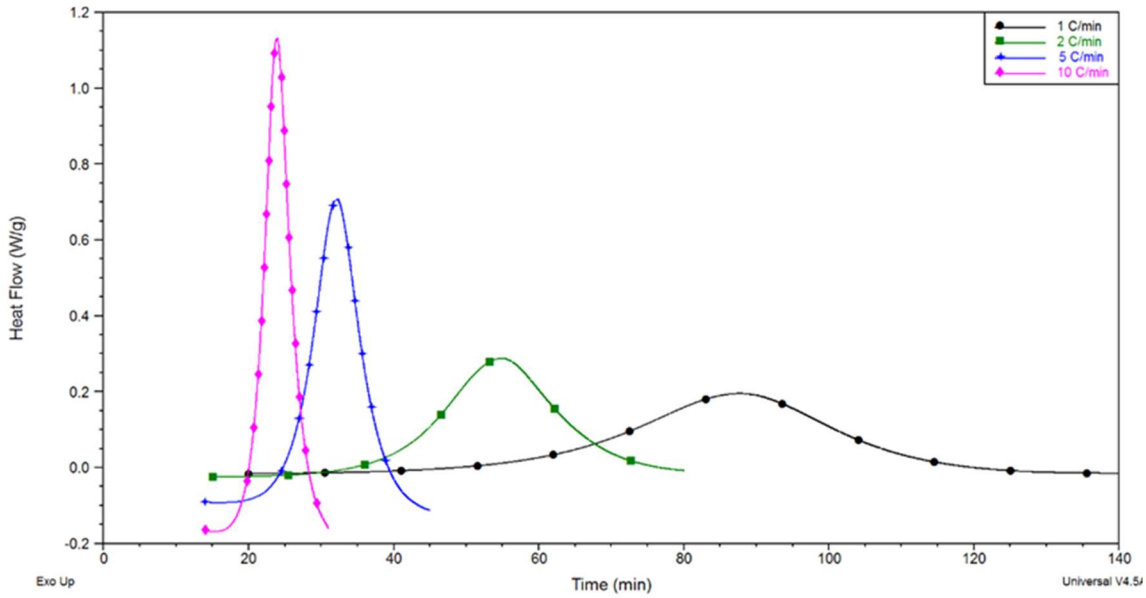

Figure 4.5 - Comparison of exothermic peaks produced by the four heating rates as a function of time (High Purity TETA).

Using Equation 3.6 and the gradient of the line shown in Figure 4.6, the value for E_a was found to be 58.6 kJ/mol. A direct comparison between the two plots is shown in Figure 4.7. Ultimately this does not represent a significant difference when compared to the notable difference between the values measured in this study and the 69.5 kJ/mol reported by Rosu et al. [44] for another DGEBA/TETA resin. This was likely due to the Araldite 506® resin being a modified low viscosity DGEBA resin.

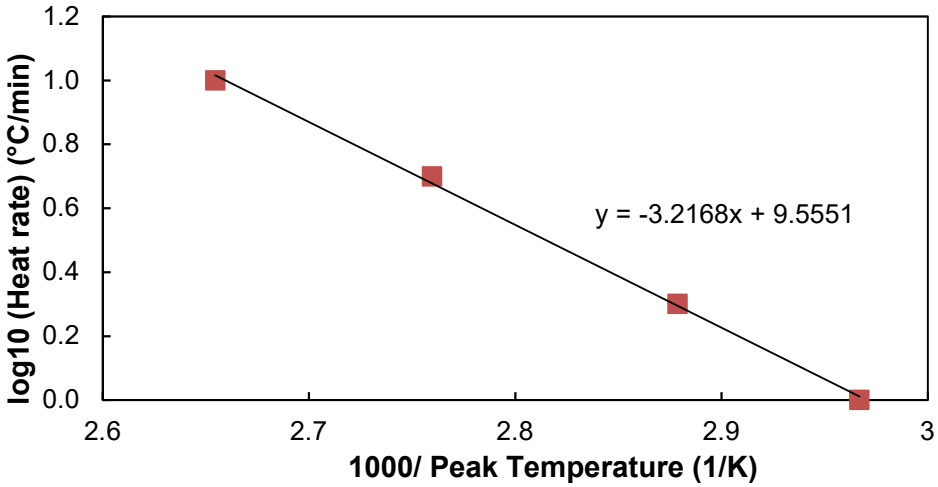

Figure 4.6 - Arrhenius plot (High Purity TETA).

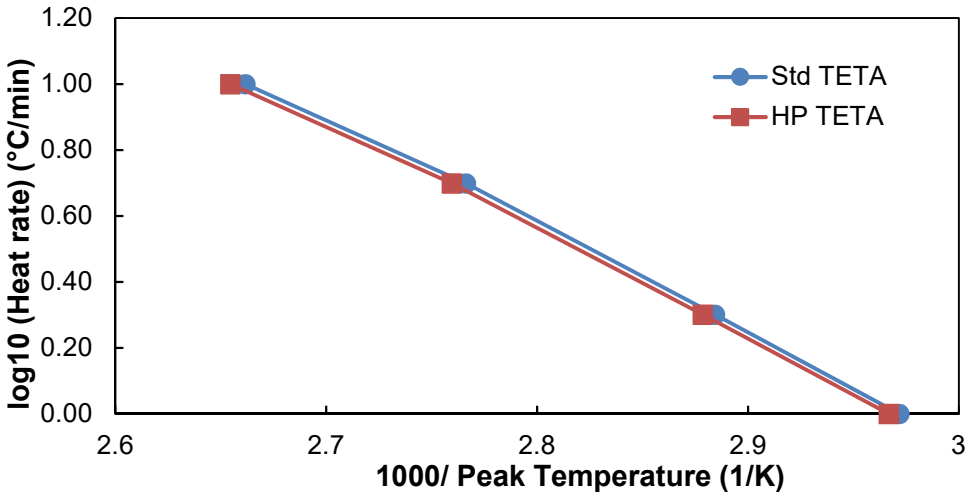

Figure 4.7 – Comparison of Arrhenius plots for standard and high purity TETA.

4.2.2 Degree of conversion

The influence of the hardener-to-epoxy ratio on the degree of conversion of the matrix will be discussed in this subchapter. The procedure used was discussed in detail in subchapter 3.2.1.3. Seven different R values were cured in the DSC to study whether the rate of cure conversion changed as the ratio was systematically varied. The temperature schedule used was the curing schedule used throughout this project. The objective was to identify whether off-stoichiometric ratios achieved 100% conversion using the curing schedule outlined previously, and the degree to which the speed of the reaction was influenced by the R value. Three samples were measured per ratio.

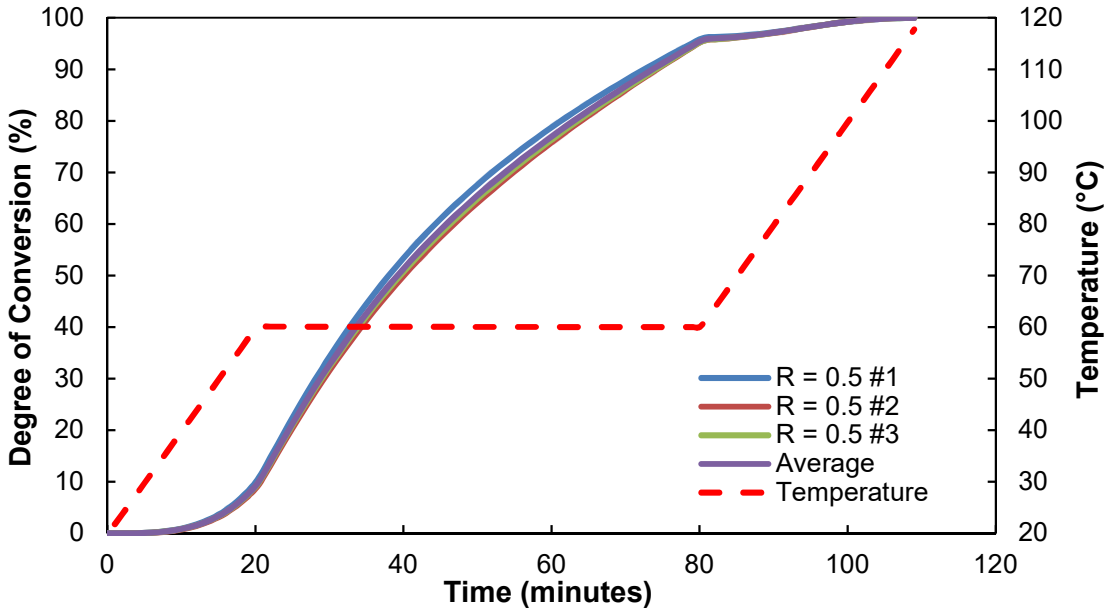

Figure 4.8 - Degree of conversion plot for R ≈ 0.5 samples with temperature schedule plotted.

Figure 4.8 shows the degree of conversion plot for the ratio R = 0.5, with the curing schedule used plotted for comparison. The plot suggests that the bulk of the curing process occurs during the isothermal section of the curing process, with a peak observed at ≈ 80 minutes, where the second heat ramp began. This was the case for each of the ratios studied.

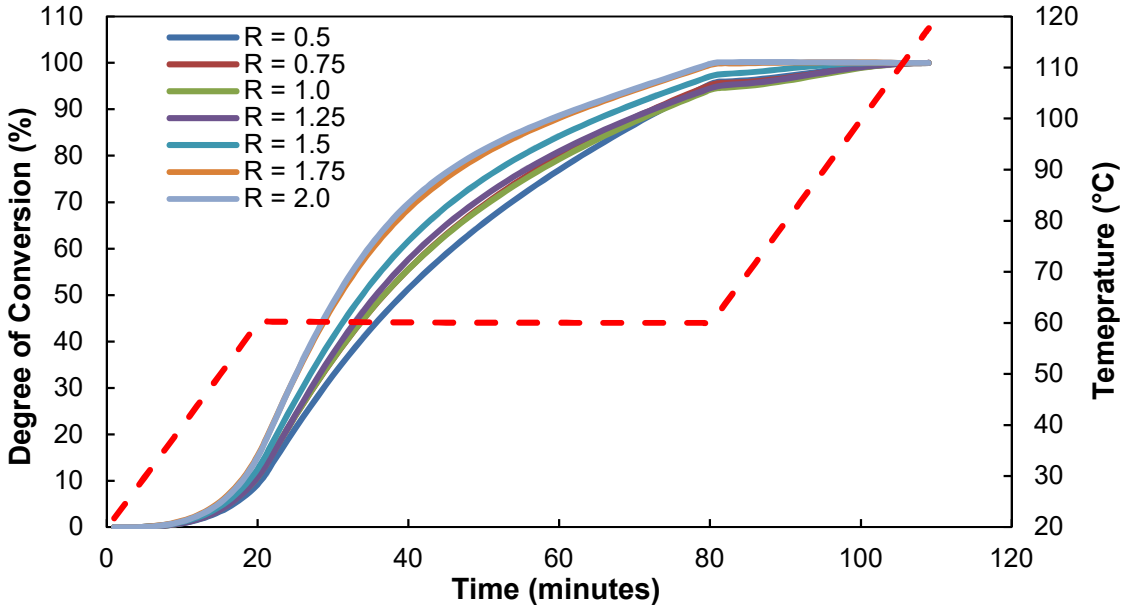

Figure 4.9 - Degree of conversion comparison plot samples with temperature schedule plotted.

Figure 4.9 shows a comparison plot for the different degrees of conversion measured as R was changed. Initially there appears little notable difference for ratios where R < 1. However, as the R value was increased above R > 1, the degree of conversion increased relative to time. This is shown particularly for ratios possessing a large excess of amine (R ≥ 1.75), with these ratios showing a distinct trend. Thus, it could be surmised that if amine continued to be added to the system then the reaction would ultimately progress faster. This is likely due to the exothermic reaction produced during the thermoset process increasing the temperature and reaction rate. This would be comparable to the results of increasing the heating rate shown in subchapter 4.2.1.

4.3 Glass Transition Temperature

The procedures used to measure the T_g of the amine cured epoxy system are described in sections 3.2.1.1, 3.2.2.3 and 3.2.3 respectively. Typically, a minimum of three cured samples were studied per ratio investigated.

Using the DSC technique, it was possible to plot two figures where the differences in T_g could easily be identified by the location of the step changes visible in the normalised heat flow versus temperature plots. Figure 4.10 provides the plots for ratios containing an excess of epoxy (R < 1) as well as the stoichiometric ratio. Figure 4.11 then provides the plots for ratios containing an excess amount of amine (R > 1) as well as the stoichiometric ratio again for comparison. In both plots it can be seen that as the R value deviated further from the stoichiometric value that the step change in these curves shifted to lower temperatures. For the more extreme ratios of R ≈ 0.31, R ≈ 2.92 and to a lesser extent R ≈ 0.52, it can be seen that the step change occurred at temperatures approaching room temperature.

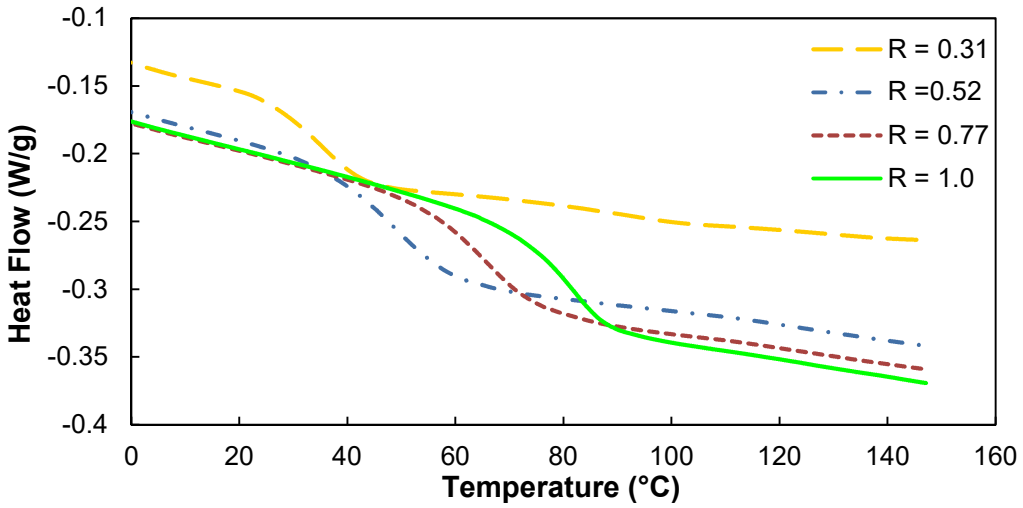

Figure 4.10 – Normalised heat flow versus temperature plot for R ≤ 1.

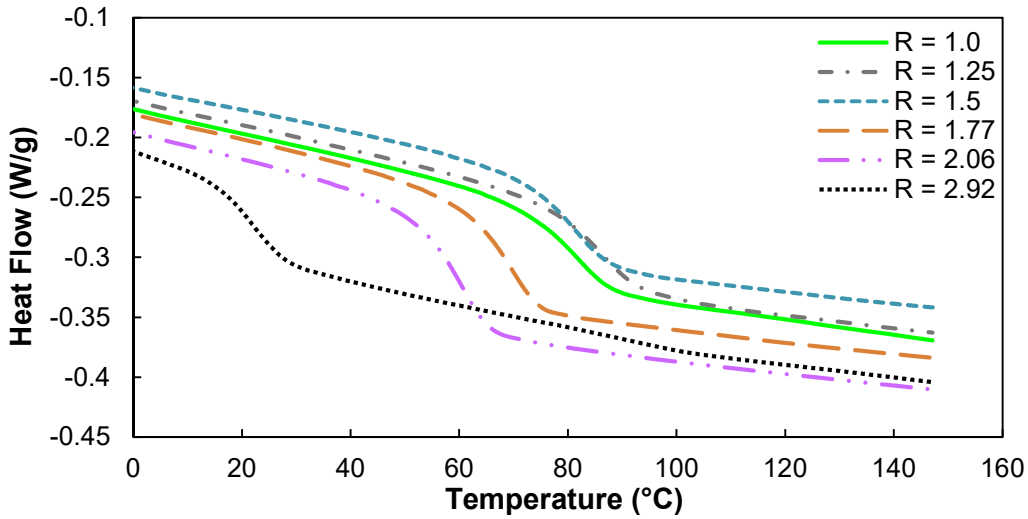

Figure 4.11 - Normalised heat flow versus temperature plot for R ≥ 1.

Values for the T_g were also obtained from the TMA analysis. Figure 4.12 shows a plot of TMA normalised dimension change versus temperature plots for ratios where R ≤ 1. Figure 4.13 provides a similar plot for ratios where R ≥ 1. In both cases, the gradient change corresponded to the T_g value. The results in both figures shows that as R deviated further from the stoichiometric value, that the gradient change occurred at lower temperatures, corresponding to lower values of T_g.

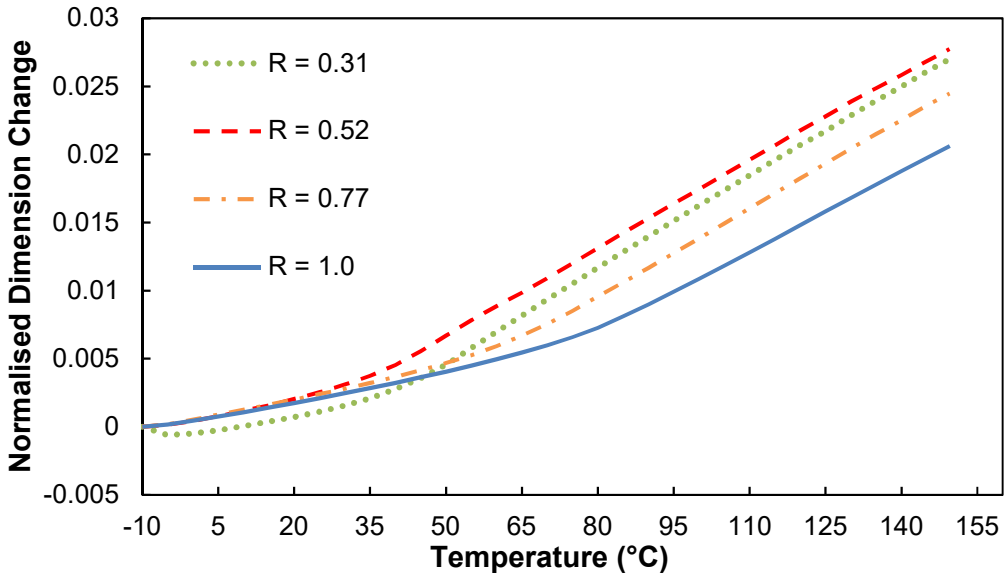

Figure 4.12 – Normalised dimension change versus temperature plot for R ≤ 1.

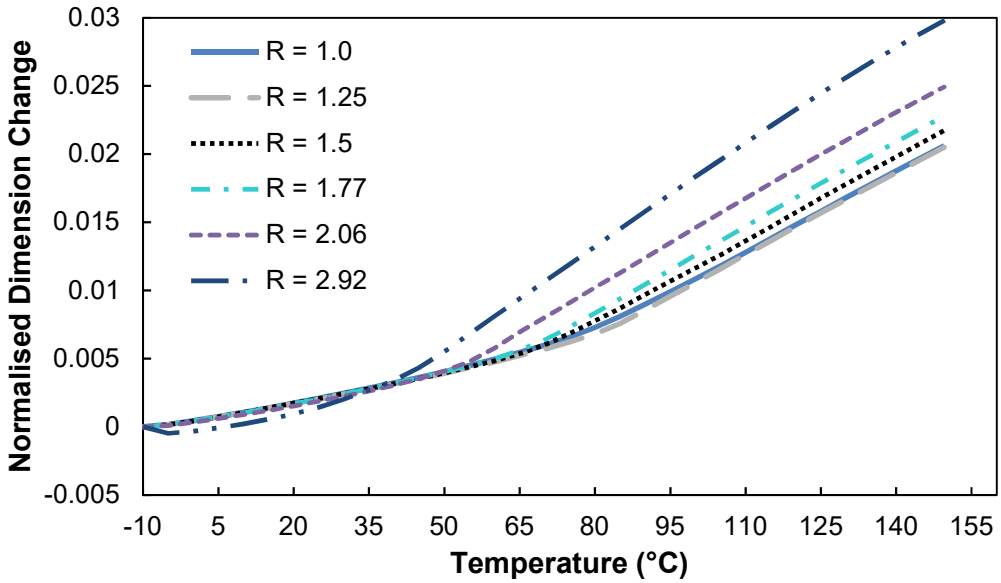

Figure 4.13 - Normalised dimension change versus temperature plot for R ≥ 1.

The T_g values of different mixture ratios were also evaluated by using DMA to study the change in the storage modulus (E') of the system with temperature. Figure 4.14 show a selection of plots for E' versus temperature for four of the R values tested.

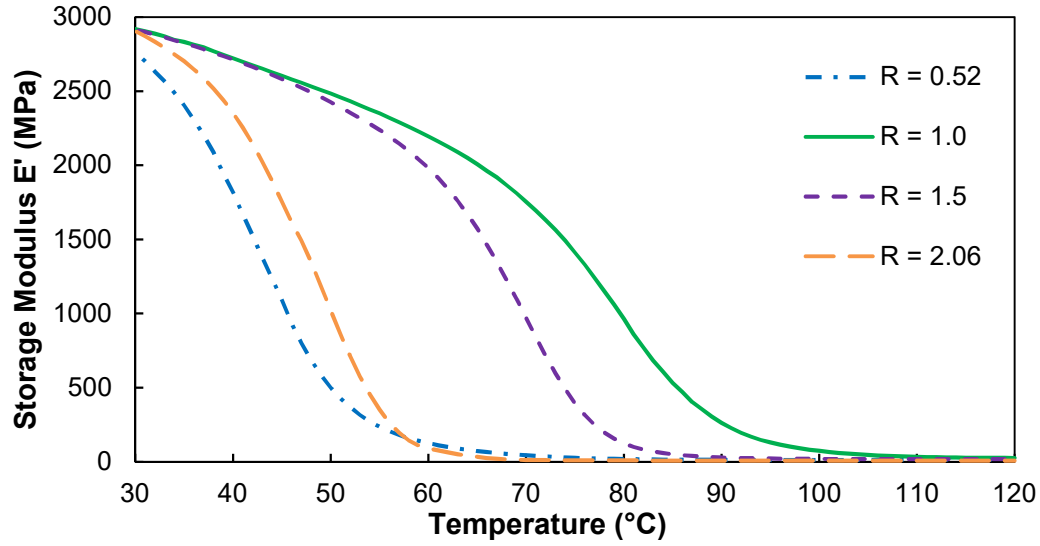

Figure 4.14 - Storage Modulus E' versus temperature for selected R values.

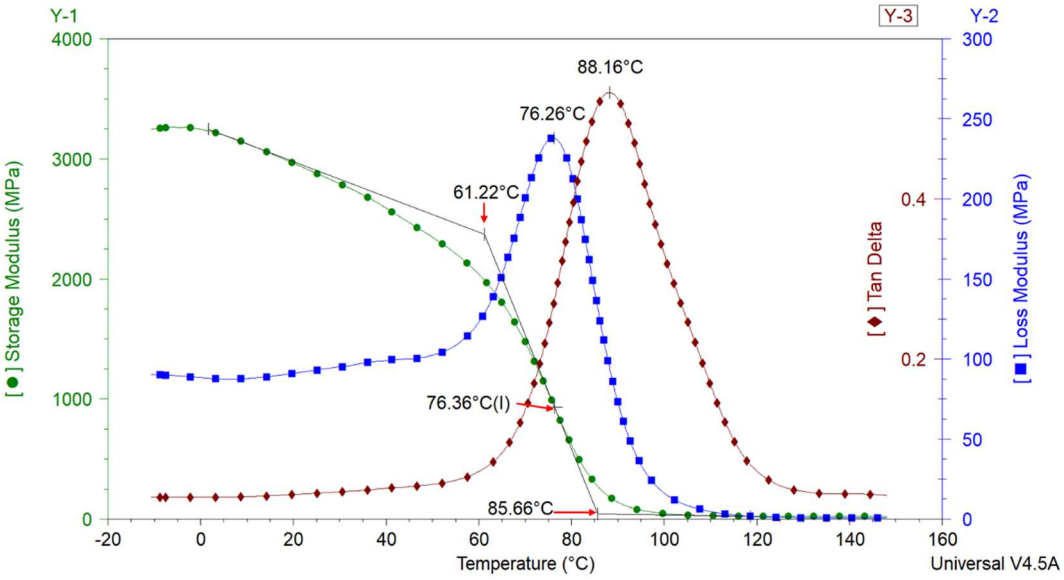

Figure 4.15 - Storage modulus, loss modulus and tan delta overlaid using TA Universal Analysis with glass transition range highlighted.

The gradient of each plot is shown to change at two points, signifying the beginning and end of the glass transition range, T_{gf} and T_{ge}, respectively. The midpoint of these two was taken as the value for the T_g. An example for R ≈ 1.0 is illustrated in Figure 4.15.

Again, it can be seen that the R value of the system has a major influence over the glass transition temperature, effectively shifting the value depending on how close R

is to 1. As the ratio deviates further from the stoichiometric value the plots are shown to shift to the left, effectively dropping the T_g value of the matrix.

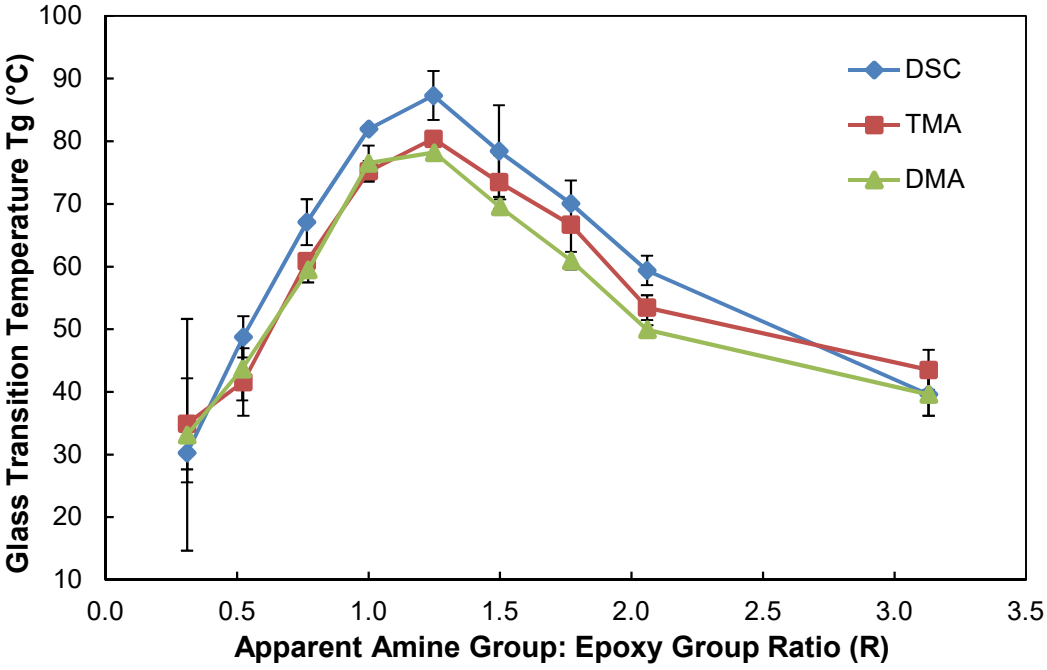

Figure 4.16 – Glass Transition Temperature T_g versus apparent amine-to-epoxy group ratio (R).

The T_g values collected using each technique were averaged for each ratio to identify whether any correlation existed between the techniques. Figure 4.16 shows that across all ratios tested, the three techniques exhibited a strong correlation. Specifically, it was observed that the T_g of the matrix was strongly dependent on the R value of the system for each technique used. It can be seen that the highest T_g values occurred slightly above the stoichiometric value ($R \approx 1.25$) for all techniques, with T_g values decreasing as the R value deviated from this value. This was potentially due to the presence of the butyl glycidyl ether within the Araldite 506® providing less reactive epoxy groups. In addition, it is acknowledged that as the matrix gels, some degree of the curing reaction will be unable to occur due the reactive epoxy and amine groups becoming locked in position by crosslinking. Hence the extra amine groups provided at $R \approx 1.25$ may lead to a greater degree of reaction occurring since the

amine groups are more readily available through the system, even as the matrix gels. The gradient of this decrease was shown to flatten for R values possessing a large excess of amine (R > 2.0) for all techniques. This would suggest that the gradient is non-linear with R, with T_g values for R > 4 likely to decrease below room temperature.

At ratios above the stoichiometric value a maximum in the value of the T_g has also been reported in tests using the Epon 828/ PACM-20 system [47,51,57]. It can be seen that T_g appears to be more influenced by ratios possessing excess epoxy relative to ratios possessing excess amine, with T_g approaching room temperature for R < 0.3. This suggests that the structure of the matrix is influenced more by the lack of amine due to the matrix being unable to form a full-crosslinked network during the curing process.

The influence of the R value on the T_g of the matrix may be explained by considering the resultant changes in the molecular structure of the matrix. For ratios containing excess epoxy (R < 1) the relative lack of amine in the polymer system hinders the formation of a fully crosslinked network. This would result in less restrained, bulky groups forming at the end of epoxidic chain, increasing polymer free volume and decreasing key thermomechanical properties of the matrix, such as T_g [52,58,246]. The sudden drastic drop in T_g shown at R < 0.5 may represent a critical point where there were not enough reactive amine groups in the matrix system to produce a strong crosslinked structure. For ratios with excess amine (R > 1), the curing reaction would be dominated by the primary amines, with reduced secondary amine bonding, resulting in a more branched polymer matrix structure. This would result in significant levels of unreacted secondary amines within the system. This abundance of unreacted molecules as well as the branched structure would increase the polymer free volume due to the poor packing ability of the amine molecule, again leading to the decrease in T_g observed [247,248].

The only notable discrepancies occur for the TMA and DMA techniques at the extreme R values, where the gradient for the plot for T_g value measured slightly higher than for the DSC technique. These discrepancies did not seemingly occur at any of the ratios closer to the stoichiometric value and the three techniques are in close agreement overall, suggesting these to be specific cases. It is interesting to note that these discrepancies only occurred for samples under mechanical load and not for the DSC samples, which were simply heated. Samples constructed for the extreme ratios of $R \approx 0.3$ and $R \approx 3.0$ were notably difficult to manufacture reliably, due to the higher viscosity of the resin trapping pockets of air within the sample during curing. This deteriorated the surface quality of the sample, potentially explaining the differences shown due to errors introduced into the measurement technique. This variability is shown in the larger error bars for the DMA and TMA techniques at $R \approx 0.3$ relative to the DSC method. Due to these difficulties it would be recommended that DSC be the primary technique for measuring the T_g of an epoxy thermoset when the influence of the R value is being investigated for a wide variety of ratios.

Figure 4.17 shows a comparison between the T_g values recorded using the DMA with those recorded in past literature [47,51,57] for non-TETA epoxy systems. Despite this, correlation between the systems can be seen. However, the results recorded for Araldite 506® are notably lower than those measured for the Epon 828 epoxy resins. This appears to be consistent across the multiple test techniques and was likely due to the nature of the Araldite 506® resin used. As discussed in subchapter 3.1, Araldite 506® is a modified DGEBA resin, possessing up to 25% butyl glycidyl ether. This gives the resin its low viscosity but may also result in the T_g value dropping when compared to unmodified DGEBA resins. This would also explain the large difference between the results presented and those reported by Garcia et al. [49] for another DGEBA/ TETA resin system using both DSC and DMA measurements. It is interesting

however to note that there appears a clear correlation between the data presented in this thesis and that presented by Vanlandingham [51], with the variation of T_g with the R value appearing comparable for the two different resin systems. Both exhibit a peak at an R value above the stoichiometric ratio, with T_g decreasing the further the ratio deviates from this value. This is also shown to be the case for the Garcia data [49].

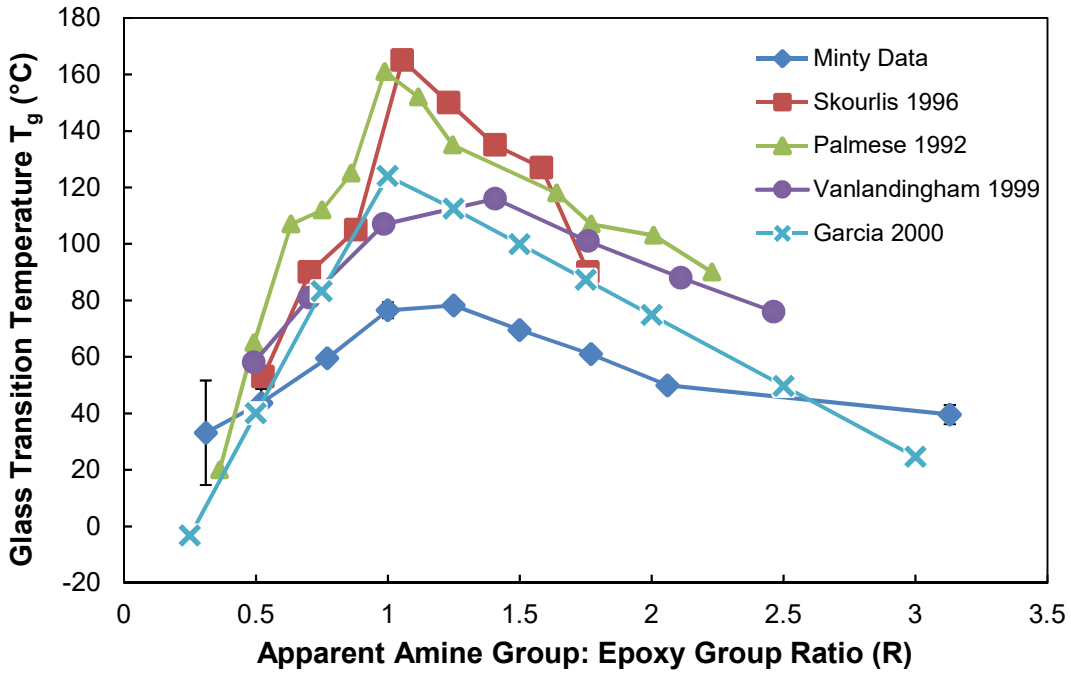

Figure 4.17 - Comparison of DMA Glass Transition Temperature T_g plots.

Following the analysis of cured epoxy samples within the DSC it was decided to study the influence of the R value on the T_g of samples cured within the DSC. This would allow for analysis of the cure kinetics to be studied with varying matrix chemistry as discussed in subchapter 4.2 as well as further investigation of the T_g value. Samples were prepared as detailed in subchapter 3.2.1 and cured in the DSC, with the process recorded and the T_g measured during a second heat ramp. A comparison between the T_g values for these samples cured within DSC and those discussed previously is presented in Figure 4.18.

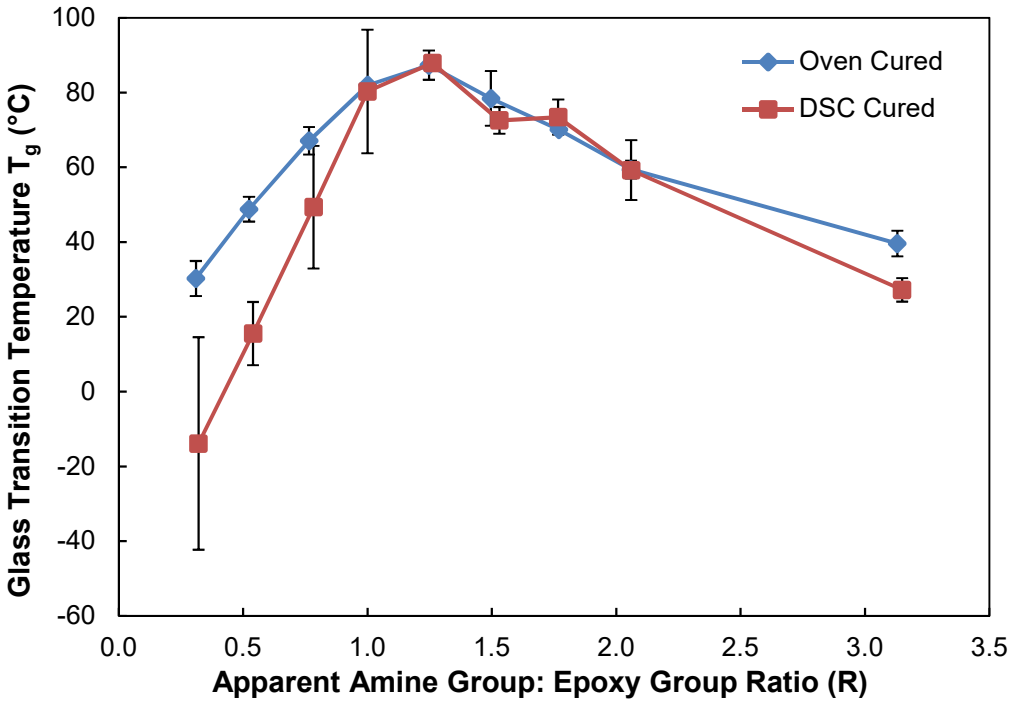

Figure 4.18 - Comparison of DSC T_g plots for cured and curing samples.

There is a clear correlation between the data sets, with the general trend of a maximum T_g obtained around the stoichiometric value before decreasing as the ratio deviated further from this value. It can be seen that the T_g of DSC cured samples occurred at R ≈ 1.25. Interestingly it can be seen that for R ≥ 1.0, the two data sets correlate very well with each other with only a slight difference shown to occur for R > 3. However, for R < 1 the T_g values appear notably smaller for the DSC cured samples in comparison to those cured in the oven. This potentially suggests that the resin system did not achieve as full a cure during the first heat cycle within the DSC compared to the curing process in the oven due to the differences in cure schedule. This would result in a lower crosslink density and the lower T_g value shown. The effect is shown to increase the further the ratio deviates from the stoichiometric ratio with the difference shown to be approximately 40 °C at R ≈ 0.3.

After considering the differences in cure kinetics shown in section 4.2 it was decided to study the TETA purity to quantify whether it would continue to influence the T_g value

whilst varying the R value. The initial results shown in section 4.2 suggest this may be the case. Samples were prepared using the same process as described previously and then cured in the DSC, allowing the exothermic process to be recorded. A comparison of the two data sets is presented in Figure 4.19.

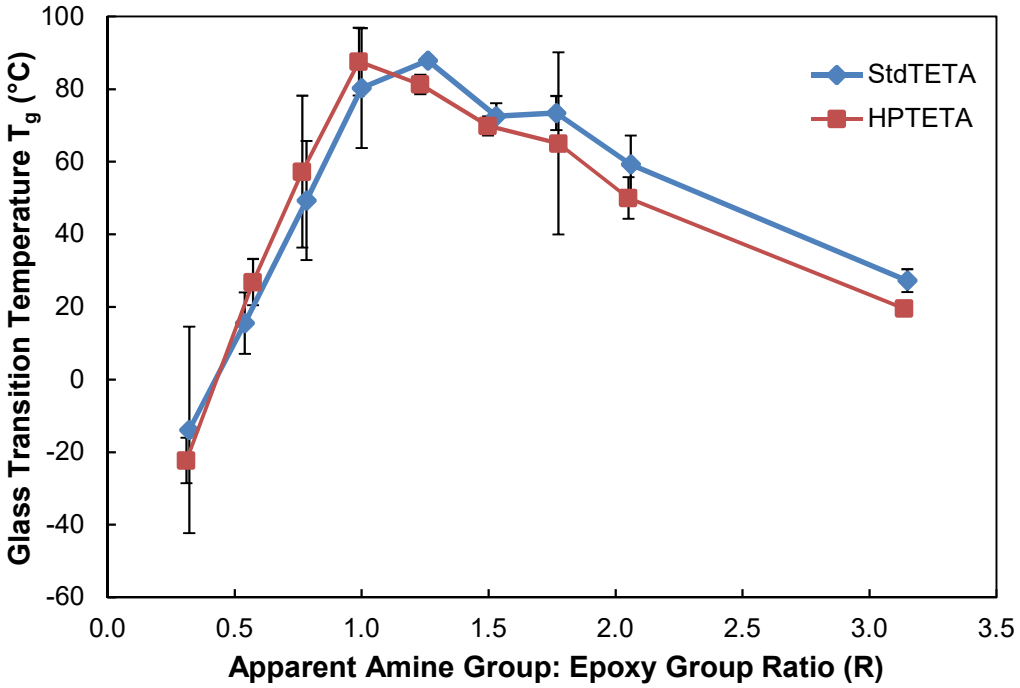

Figure 4.19 - Comparison of different purity TETA T_g plots.

It can be seen that the two data sets correlate well with each other. The higher purity hardener appears to achieve its highest T_g at the stoichiometric ratio, whereas the standard TETA achieves its highest value at R ≈ 1.25. Overall the two values appear comparable in size with 87.6 °C for the higher purity TETA and 87.9 °C for the standard TETA respectively. Interestingly there appears little difference between the two for ratios where R < 1. This is interesting since it would be expected that the higher purity TETA might yield higher T_g values due to the lesser amount of impurities in its mixture. These impurities, listed in subchapter 3.1, were shown to possess a lesser functionality than the standard TETA molecule and thus would be expected to provide less reactive amine groups to the overall system, yet there appears to be no

significant effect other than perhaps the superior performance at R = 1. It is also noticeable that the T_g values for ratios where R > 1 for the higher purity TETA were smaller than those for the standard TETA. This was unexpected since it was thought that the impurities discussed within the standard TETA would negatively impact the crosslink density of the system further as the level of excess amine was increased.

4.4 Storage Modulus

Another property of importance to the stress transfer capability of the interface is the modulus of the polymer matrix. This has been shown to be influenced by both testing temperature and matrix chemistry for other epoxy polymer systems [47,51,246]. Consequently, it was necessary to study the Araldite 506® system with varying levels of TETA hardener to compare whether comparisons could be made and to allow for the data to be used in later residual stress theory calculations. Dynamic mechanical analysis (DMA) was carried out using the technique described in section 3.2.3.

Figure 4.20 and Figure 4.21 show the results recorded for the storage modulus (E'), loss modulus (E'') and tan delta value as the testing temperature was increased. Figure 4.20 clearly shows the very large drop in modulus as the epoxy resin is heated above T_g. This value can be comparable to the peak of the loss modulus plot shown in Figure 4.20. The tan delta was graphed, and its maximum is also clearly evident in Figure 4.21.

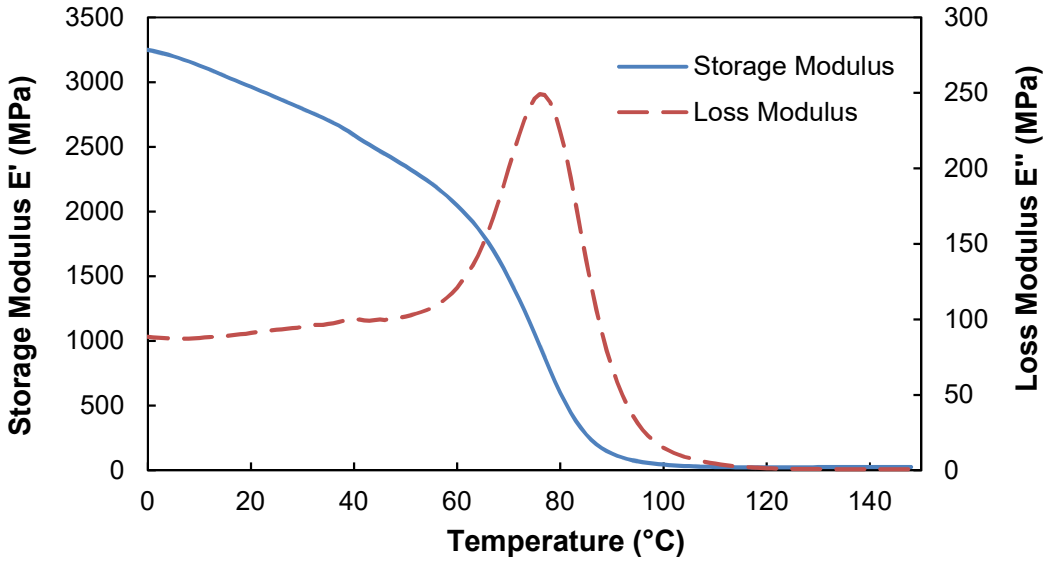

Figure 4.20 – Influence of testing temperature on storage and loss moduli.

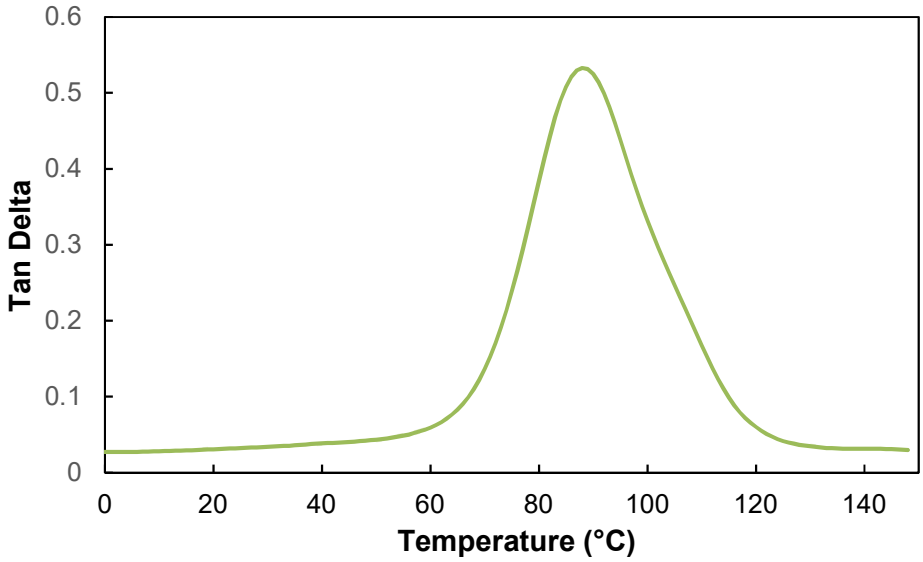

Figure 4.21 – Influence of testing temperature on tan delta.

Figure 4.22 and Figure 4.23 show the storage modulus plotted against temperature for ratios where R ≤ 1.0 and R ≥ 1.0 respectively. Both show how the DMA storage modulus of the matrix was influenced by testing temperature as well as the R value of the system.

It can be seen that the magnitudes of the E' and T_g reached a peak at the stoichiometric ratio, with R ≈ 1.25 appearing the most comparable. Initially the ratios

of R ≈ 0.77 and R ≈ 1.5 possess comparable E' values at low temperatures yet as the temperature rises the values for E' begin to decrease. Overall the plot shows that as the R value deviates further from the stoichiometric value, the large decline in E' will occur at lower temperatures. This would make sense since the gradient change in E' represents the glass transition phase of the matrix, which was shown to be influenced by the R value in subchapter 4.3. Figure 4.24 and Figure 4.25 shows the magnitude of E' plotted against the ratio R at a constant delta T value of ± 20 °C relative to T_g. Due to the low T_g of R ≈ 0.3 and R ≈ 3.0 and the lack of the cooling system for the DMA for these samples, this data could not be plotted for Figure 4.24 since data 20 °C below T_g could not be collected.

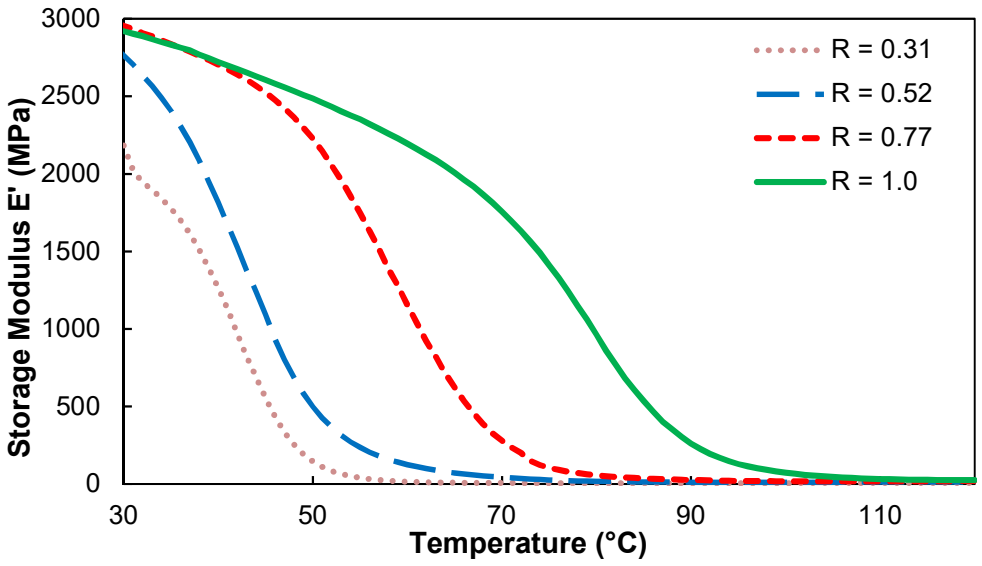

Figure 4.22 - Storage Modulus E' versus temperature plot for R ≤ 1.

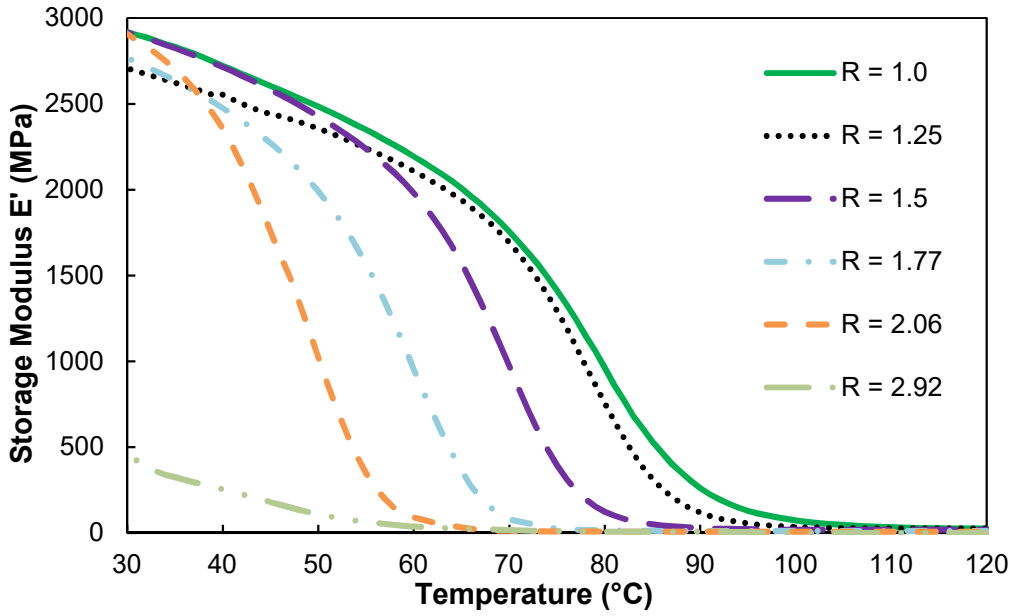

Figure 4.23 - Storage Modulus E' versus temperature plot for R ≥ 1.

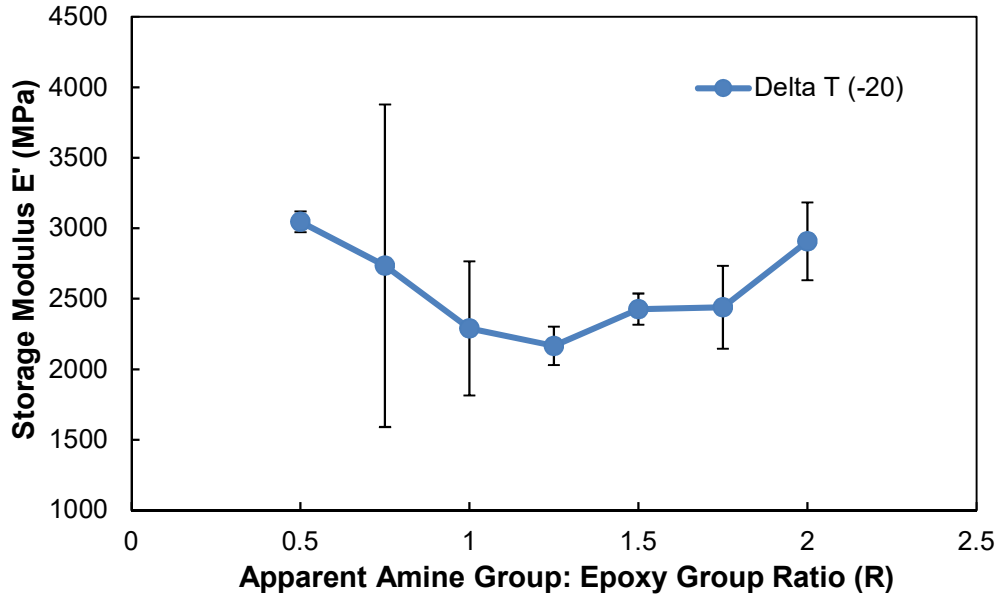

Figure 4.24 - Influence of amine group: epoxy group ratio on storage modulus at $\Delta T = T_g - 20$ °C.

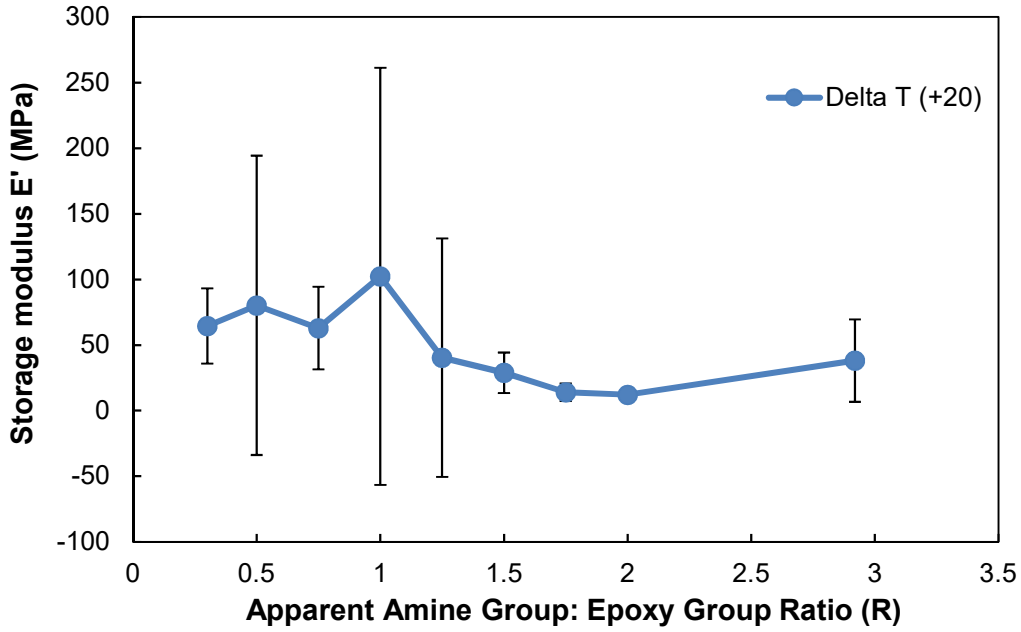

Figure 4.25 - Influence of amine group: epoxy group ratio on storage modulus at $\Delta T = T_g + 20$ °C.

Figure 4.24 shows that at a fixed delta T below T_g the storage modulus E' decreases in magnitude the closer the R value is to $R \approx 1.25$. This is the ratio that possesses the largest T_g value and thus the highest temperature at which E' was plotted relative to the other ratios. However, the results shown in Figure 4.25 appear to show no clear relationship when plotted at a fixed ΔT above T_g. A maximum is observed at $R \approx 1.0$, however due to the size of the error bars it is difficult to make any clear conclusions. It is interesting to note that for ratios where $R > 1.5$, the level of variation shown in the results is lower than that when $R < 1.5$. Overall the significant size of the error bars for the results above T_g would suggest that the accuracy of the DMA 3-point bending test decreases due to the polymer transitioning from a glass to a gel.

4.5 Linear Coefficient of Thermal Expansion

The influence of matrix chemistry on the linear coefficient of thermal expansion (LCTE) value of an epoxy matrix has been reported by Palmese [57]. However, this was for a different epoxy and hardener system and had never previously been

correlated with the stress transfer capability of the fibre-matrix interface. TMA expansion analysis was conducted using the technique described in subchapter 3.2.2.3.

Figure 4.12 shows the average normalised dimension change for the different R values tested. As the R value deviated from the stoichiometric value, more dimension change occurred for the sample. The variation of the LCTE value as the temperature was increased was plotted for the different ratios as shown in Figure 4.26 and Figure 4.27. It can be seen that as R deviated further from the stoichiometric value, the values for LCTE below T_g increased more rapidly.

Due to the gradient of the dimension change, plots possessing a transition point at the T_g value two different LCTE values (above and below T_g) could be calculated for each ratio. As such two different plots could be constructed as shown by Figure 4.28 and Figure 4.29.

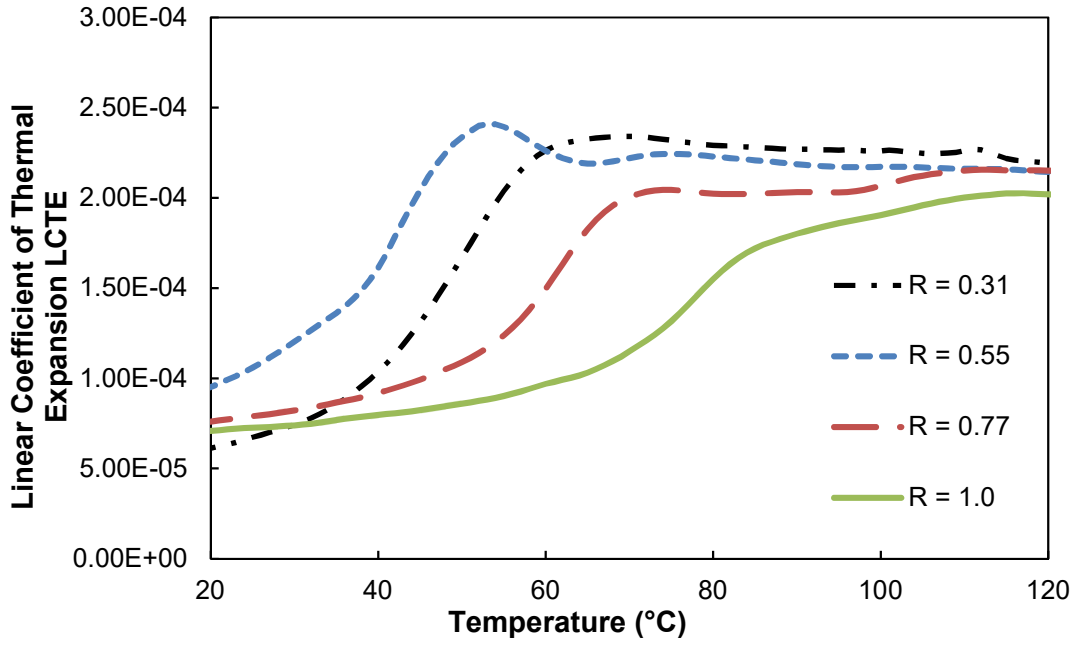

Figure 4.26 - Variation of linear coefficient of thermal expansion with temperature for ratios where R ≤ 1.0.

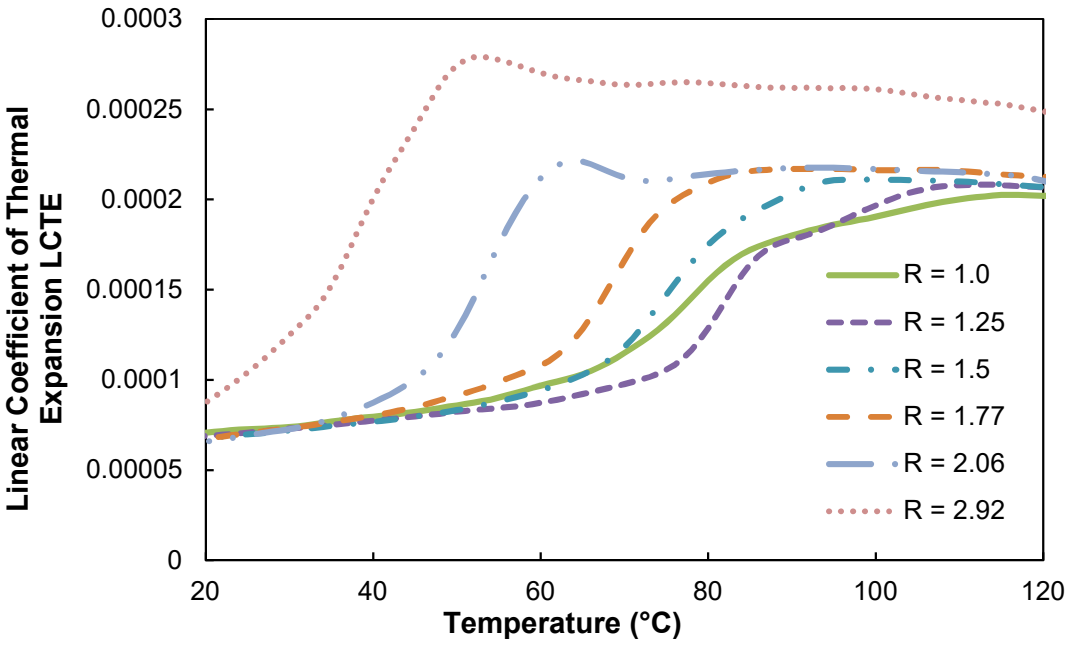

Figure 4.27 - Variation of linear coefficient of thermal expansion with temperature for ratios where R ≥ 1.0.

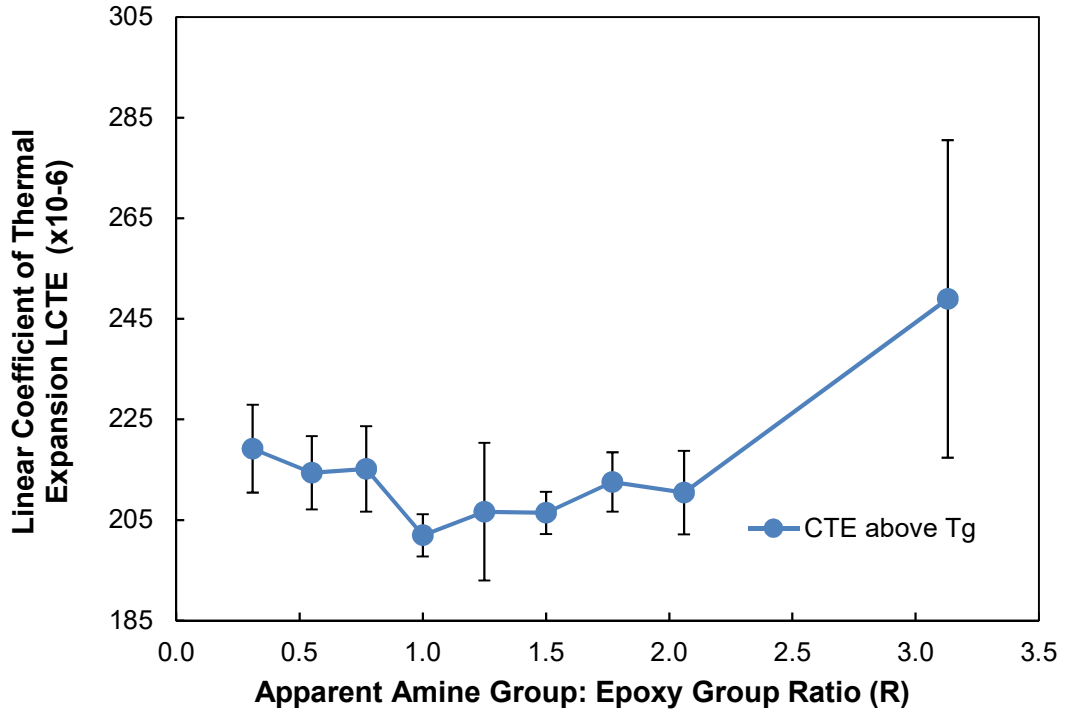

Figure 4.28 - Linear coefficient of thermal expansion above the glass transition temperature T_g.

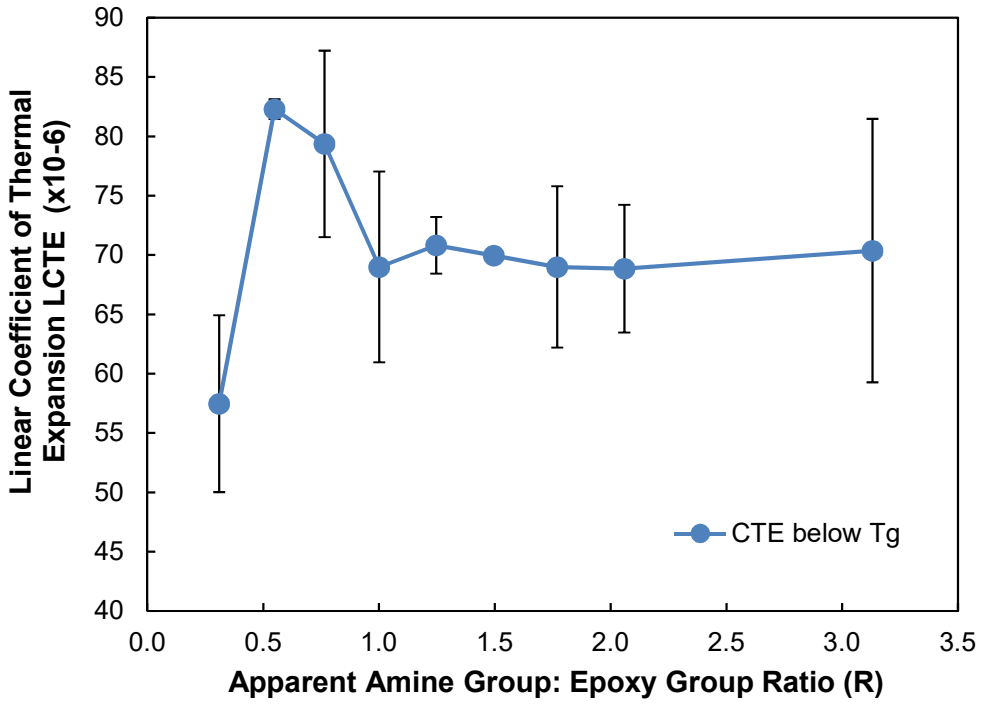

Figure 4.29 - Linear Coefficient of thermal expansion below the glass transition temperature T_g.

The results presented in Figure 4.28 correlate well with those shown in past literature [57], with the value for LCTE increasing the further R deviated from the stoichiometric value. Figure 4.29 shows that, at temperatures below T_g, the value of LCTE generally increased for ratios possessing excess epoxy. The trend shown would indicate that the value would continue to increase as the ratio was decreased, however the LCTE value for R ≈ 0.3 appears as a point of discrepancy. This is potentially due to the T_g of the matrix approaching the initial starting temperature of the TMA experiment.

Figure 4.30 - Before and after comparison for TMA samples with a ratio of R ≈ 3.12.

An interesting observation taken from the TMA expansion technique was that a notable change in colour occurred between samples that had been tested and samples that had not. Samples that had undergone testing and been exposed to elevated temperatures were distinctly more “opaque” compared to untested samples, as shown in Figure 4.30. Such a difference was also noticed when comparing ratios close to the stoichiometric value to ratios possessing a large excess of epoxy or amine groups. This is consistent with the matrix possessing a higher crosslink density, leading samples being more opaque [249]. As such this would suggest that the samples were undergoing some level of post-curing treatment during the test and thus tests could not be repeated using the same samples due to the material having changed. In addition, the decrease of transmitted light in any sample is associated, typically, with the onset of phase separation. This phase separation will occur due to an increasing incompatibility between the polymer chains and the modifier present within the resin [250]. In this case the phase separation occurring would be due to the butyl glycidyl ether modifier applied to the resin to lower its viscosity. Typically, this would occur during curing, however, it appears to continue if the system is post-cured at high temperature.

4.6 Fourier Transform Infrared Spectroscopy

Due to one of the main variables being studied involving changing the hardener-to-epoxy ratio of the matrix system, it was decided to study whether the differences at the molecular level could be studied and quantified. Fourier transform infrared spectroscopy (FT-IR) is a relatively simple technique for producing both qualitative and quantitative data on the molecular structure of epoxy polymers [229,231,232,251]. A combination of near-infrared (nIR) and mid-infrared (mIR) spectroscopy measurements will be presented in this subchapter.

Both qualitative and quantitative information can be obtained using mIR, although its use in epoxy systems is restricted because of the location and intensity of the epoxy ring absorptions, with only two characteristic absorptions observed in the range between 4000 cm^{-1} and 400 cm^{-1} [231]. The first one is located at 915 cm^{-1} and is attributed to the C-O deformation of the epoxy group. The second band is located at approximately 3050 cm^{-1} and is attributed to the C-H tension of the methylene group of the epoxy ring [231]. This band is not as useful as the first band due to its lower intensity and location close to the strong O-H absorptions [231].

Compared to mIR, nIR is much more useful for epoxies. nIR spectrum allows for the user to monitor the overtones of the strong vibrations in mIR and combination bands. Within this range there are fewer and less overlapped bands [231]. This has led to it being used by several authors for monitoring the curing reaction of epoxies [33,228,229,252]. The intensity of the bands in the nIR spectrum is considerably lower than those found in the mid-range, allowing for the use of thicker samples to get good quality data [231]. As with mIR, nIR possesses two absorptions related to the epoxy group: the first is located at 4530 cm^{-1} and is attributed to a combination band of the second overtone of the epoxy ring stretching with the fundamental C-H stretching at 2725 cm^{-1}. This band is suitable for quantitative analysis [231]. The second band is located at 6070 cm^{-1} and corresponds to the first overtone of terminal CH_2 stretching mode. This band is not suitable for epoxies possessing aromatic rings within its structure due to band interference [231].

Both techniques are described in detail in subchapter 3.6. Tested samples took the form of the DMA bending bars detailed in subchapter 3.2.3, due to the ease of manufacture and consistency possible. Samples were cured using the standard cure schedule detailed in Chapter 3. Selected samples were then exposed to a post-cure of either 70 °C or 120 °C for two hours. This was to gauge whether any further

changes would occur with further heating to the polymer after curing, such as etherification. The same samples used for mIR were then used for the nIR and Raman respectively.

4.6.1 Mid-Infrared Spectroscopy

mIR was the first analysis conducted to confirm that the number of unreacted epoxy groups within the matrix system would increase as the R value was decreased, as theory would suggest. The reactive amine groups could not be easily quantified using mIR due to the vibrations coinciding with the strong bands produced by the hydroxyl groups [231].

Figure 4.31 shows a comparison plot between the different R values focussing on the epoxy peak at ≈ 915 cm^{-1} for samples cured using the standard cure schedule with no post-cure. This corresponds to the C-O deformation of the epoxy group [231]. It can be seen that a large downwards peak occurs for the R ≈ 0.5 ratio, signifying an excess of unreacted epoxy groups. The magnitude of this peak is shown to decrease dramatically, with each peak approximately the same size for the other ratios. This is surprising: a more notable peak would have been expected for the R ≈ 0.75 ratio, since it would have still contained unreacted epoxy groups. One difficulty encountered regarding the mIR technique which may explain this is that the accuracy of the method is heavily dependent on the contact achieved between the sample and the ATR crystal. With each sample there was some variation in the sample surface, particularly as R deviated from the stoichiometric value. The opaqueness of the sample may also influence the absorbance results received, with the infrared beam struggling to pass through more opaque samples. This may explain why the absorbance values for R ≈ 1 are overall notably smaller for the peaks shown than the other ratios tested.

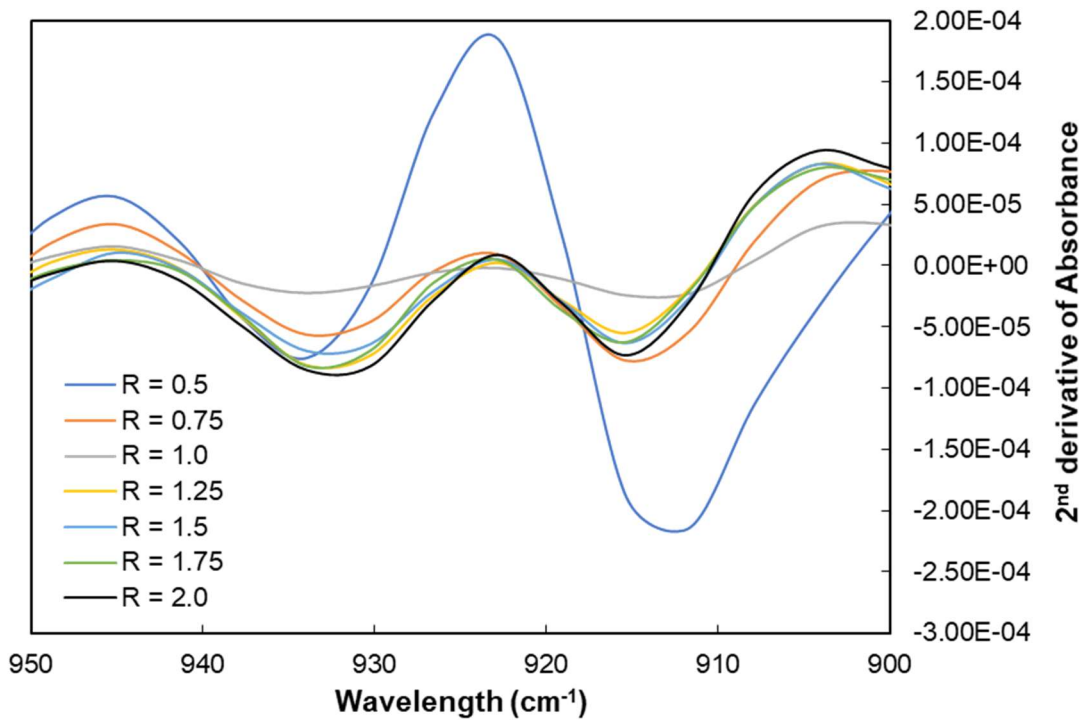

Figure 4.31 - mIR 2nd derivation of absorbance plot focussing on the epoxy peak (≈ 915 cm^{-1}) for samples with no post-cure.

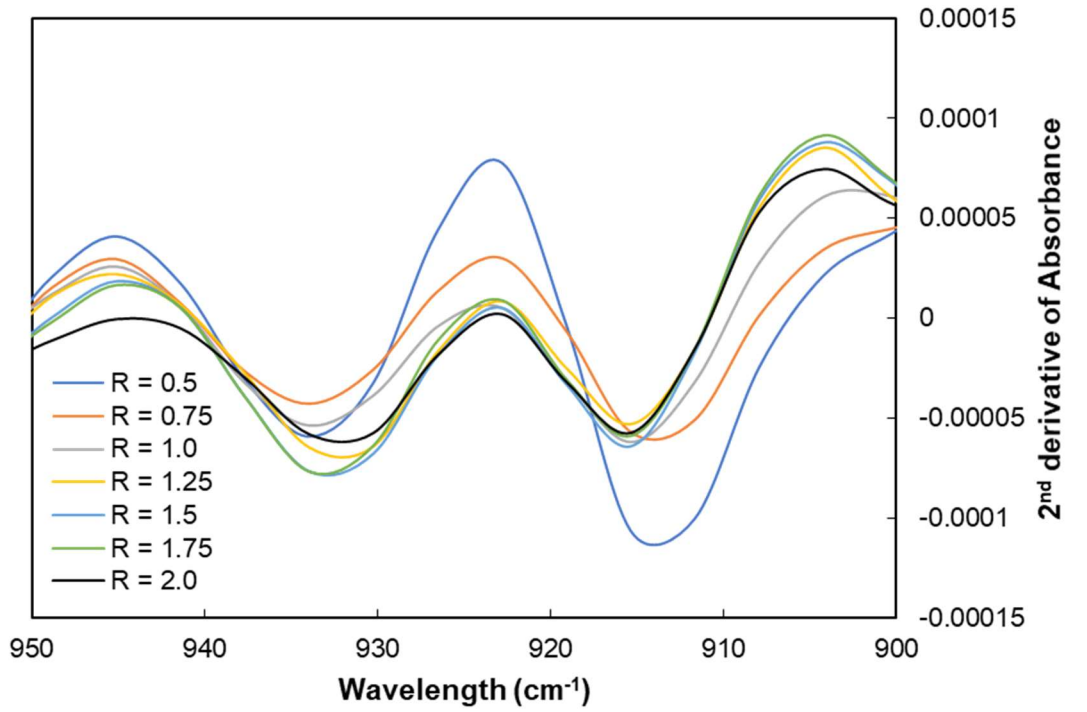

Figure 4.32 - mIR 2nd derivation of absorbance plot focussing on the epoxy peak (≈ 915 cm^{-1}) for samples post-cured at 70 °C.

Figure 4.32 and Figure 4.33 show similar 2nd derivate plots for samples which were exposed to a post-curing treatment at either 70 °C or 120 °C for two hours respectively. It can be seen that as the samples were post-cured, the peak assigned to the epoxy group for R ≈ 0.5 decreased in size. Increasing the post-cure temperature reduced this peak further. Due to the lack of amine groups in the reacted R ≈ 0.5 ratio it would be unlikely that any further curing reaction would be occurring with post-curing. However, it has been noted in the past that epoxy systems will undergo etherification for ratios where R < 1 and are heated to elevated temperatures [51,242,243,252,253]. Swier et al [254] have noted that at the stoichiometric ratio or when amine is present in excess, the etherification reaction is generally insignificant in comparison the normal curing reactions occurring. Moreover, etherification is usually much slower than the amine–epoxy reactions but it does become significant in epoxy-rich systems when the primary amine is sufficiently depleted. This would explain the decrease in the peak size shown, and potentially impact the material properties of the matrix by increasing the crosslink density [51].

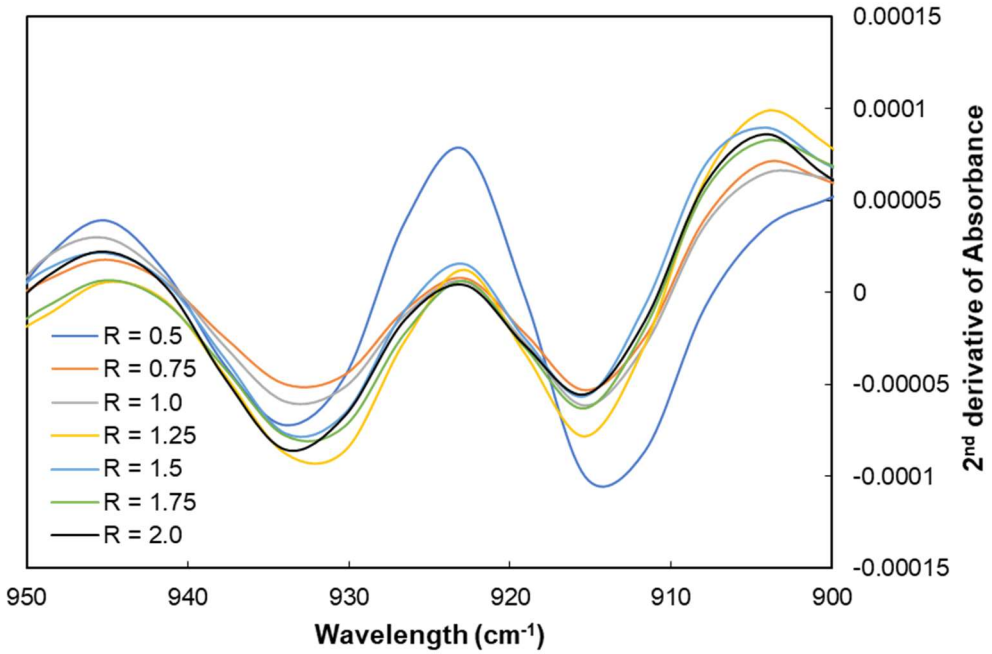

Figure 4.33 - mIR 2nd derivation of absorbance plot focussing on the epoxy peak (≈ 915 cm^{-1}) for samples post-cured at 120 °C.

4.6.2 Near-Infrared Spectroscopy

Following the initial results produced using mIR it was decided to also conduct nIR on the same samples. The primary benefit of the nIR technique was that it allowed for the quantification of both the primary and secondary amine groups as well as the epoxy groups.

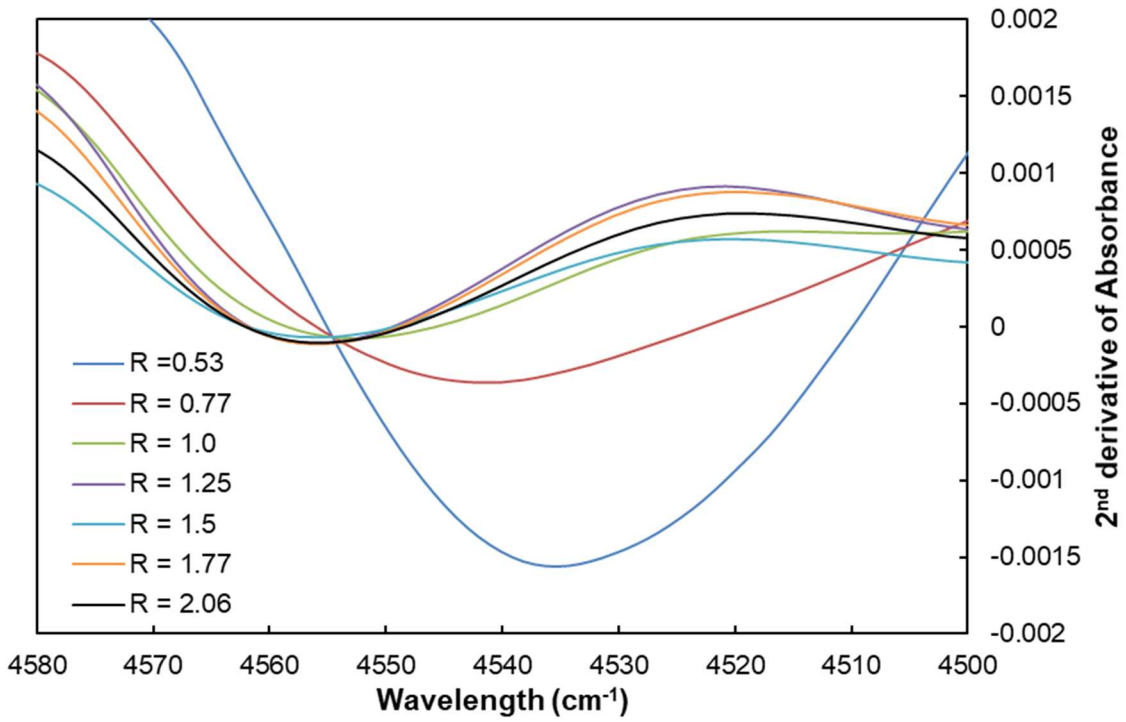

Figure 4.34 - nIR 2nd derivation of absorbance plot focussing on the epoxy peak (≈ 4530 cm^{-1}) for samples with no post-cure.

Figure 4.34 shows the 2nd derivation plot for the different ratios focussing on the epoxy group peak (≈ 4530 cm^{-1}) for samples which did not undergo any post-curing. It can be seen that a distinct downward peak, representing excess epoxy groups within the matrix, existed for the ratios R ≈ 0.53 and R ≈ 0.77 respectively. It is notable that the peak for R ≈ 0.77 appears more distinct that that recorded using mIR in Figure 4.31 suggesting that the nIR technique is more sensitive. Interestingly a shift occurs when R ≥ 1, with the corresponding peaks shown to shift to 4560 cm^{-1}. A similar transition appears to have begun for R ≈ 0.77 when compared to the peak shown for R ≈ 0.53.

This suggests that the shift may be linked to the changing chemical structure of matrix, thus the nature of the vibrations changes as the epoxy groups bond with the reactive amines present within the system.

Comparing Figure 4.35 and Figure 4.36, which show the results for the post-cured samples, it can be seen that the epoxy group peak for R ≈ 0.53 decreases in magnitude significantly, agreeing with the findings for mIR. After the 120 °C post-cure the peak for R ≈ 0.77 also decreases, again suggesting the possibility of etherification occurring.

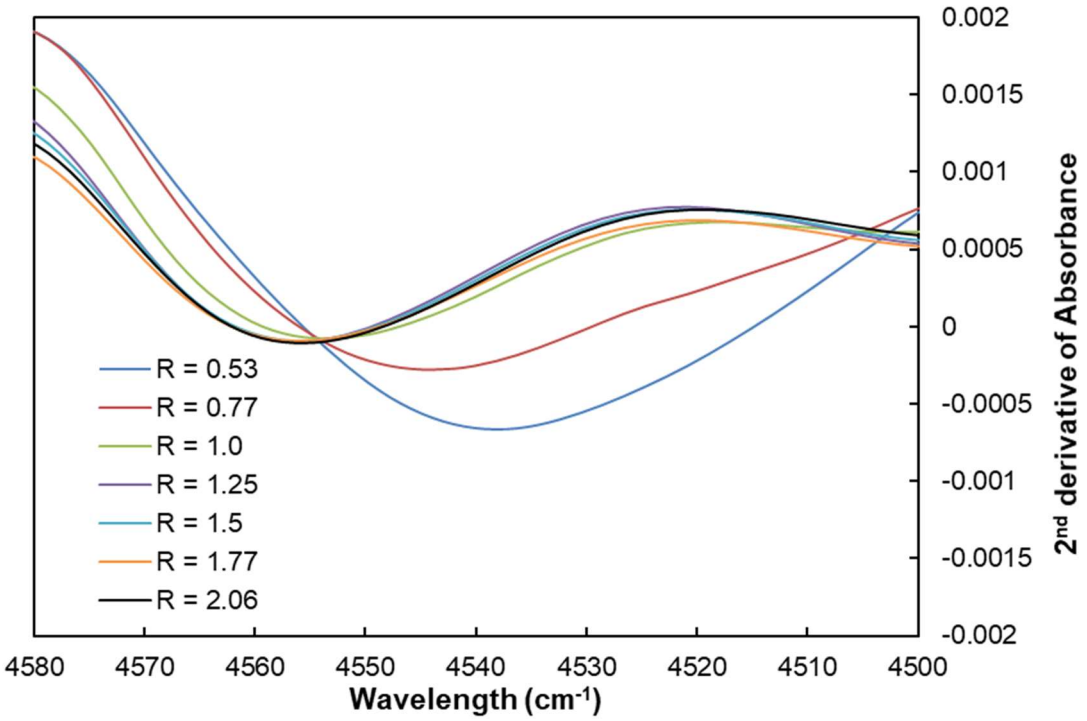

Figure 4.35 - nIR 2nd derivation of absorbance plot focussing on the epoxy peak (≈ 4530 cm^{-1}) for samples post-cured at 70 °C.

However, the peak shown for Figure 4.36 is larger than that shown in Figure 4.35, despite the post-curing temperature having been raised. This may be an anomaly due to the onset phase separation discussed in subchapter 4.5. nIR measurements are very sensitive to the degree of transmitted light being able to pass through, thus the results may have been influenced by this. In addition, the geometry of each sample is

different to a small degree, which led to difficulties mounting some of the samples. This may have led to the anomaly shown.

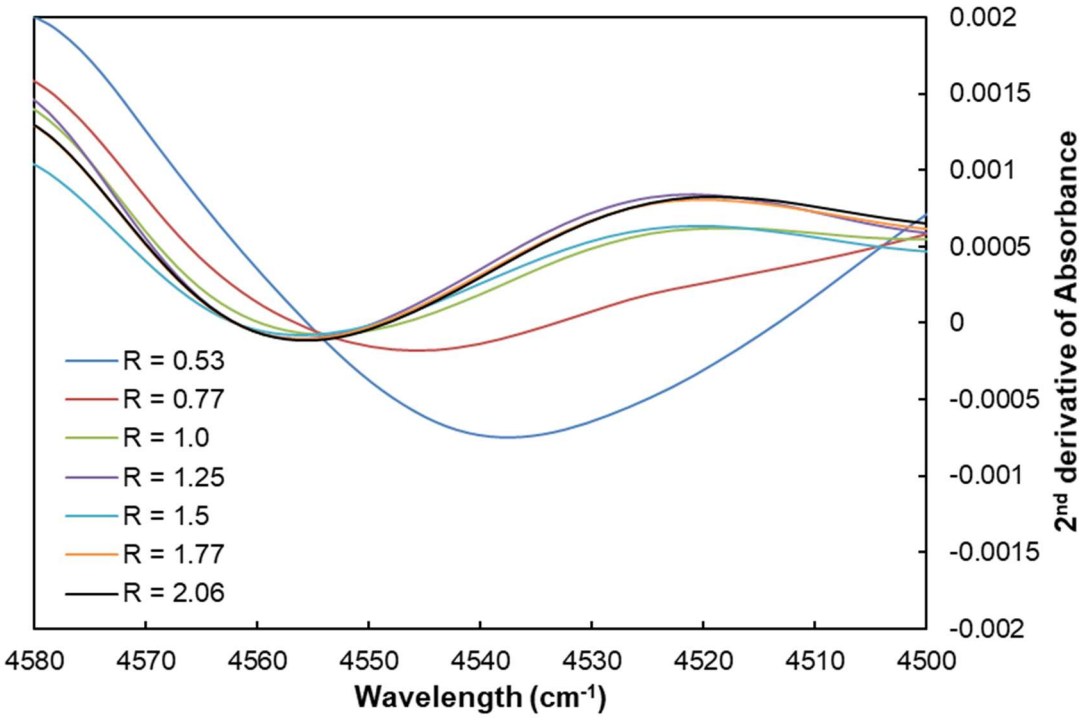

Figure 4.36 - nIR 2nd derivation of absorbance plot focussing on the epoxy peak (≈ 4530 cm^{-1}) for samples post-cured at 120 °C.

Figure 4.37 shows the 2nd derivation plot for the different ratios, focussing on the primary amine peak (≈ 4930 cm^{-1}). This plot shows that as more hardener was added to the system (R > 1) the level of unreacted amine groups within the matrix increased. Interestingly it can be seen that there appears to be no remaining primary groups for R ≈ 1.25, despite the ratio being above stoichiometry. This would suggest that the epoxy groups will typically react first with all the remaining primary amines within the system before then reacting with the secondary amines present.

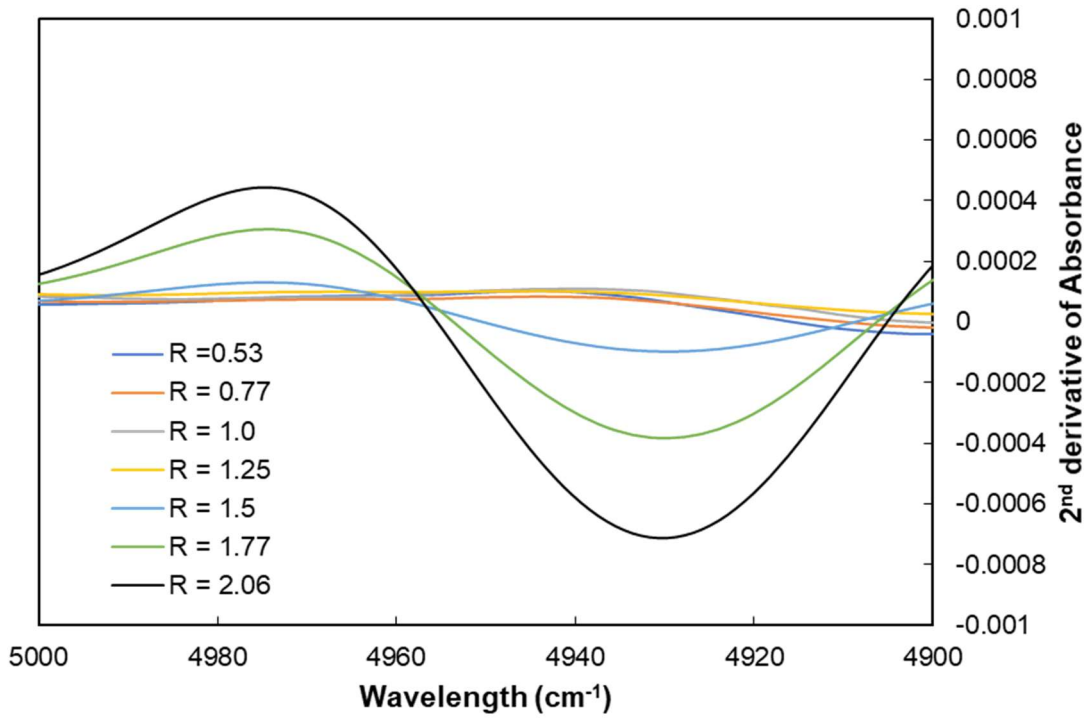

Figure 4.37 - nIR 2nd derivation of absorbance plot focussing on the primary amine peak (≈ 4930 cm^{-1}) with no post-cure.

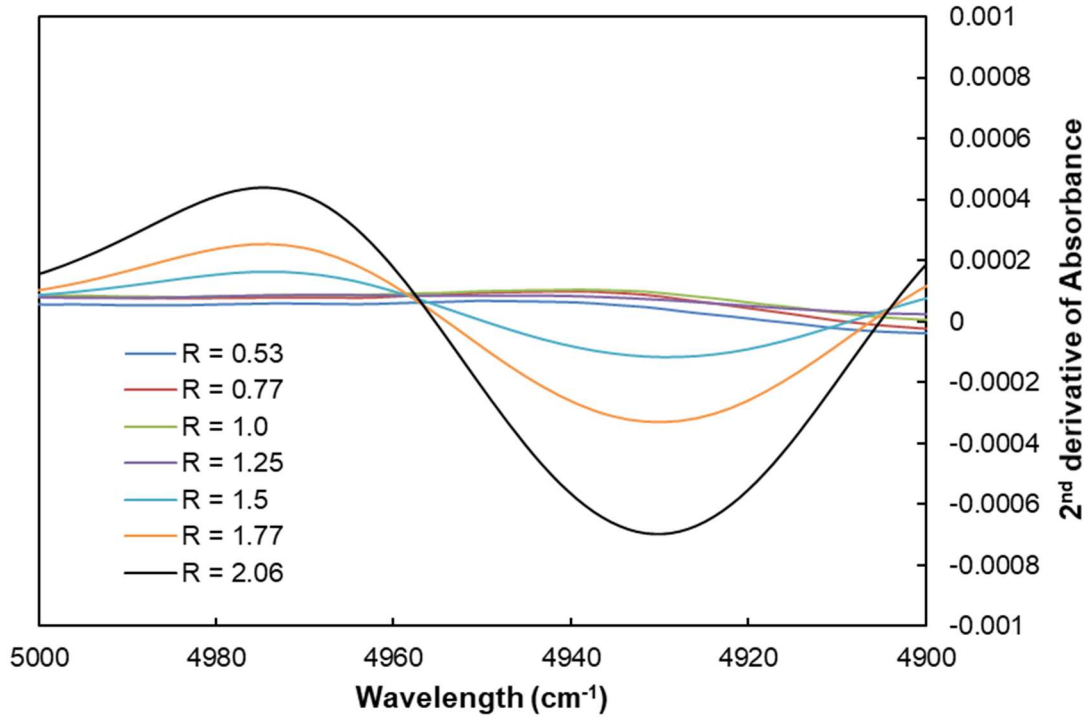

Figure 4.38 - nIR 2nd derivation of absorbance plot focussing on the primary amine peak (≈ 4930 cm^{-1}) post-cured at 70 °C.

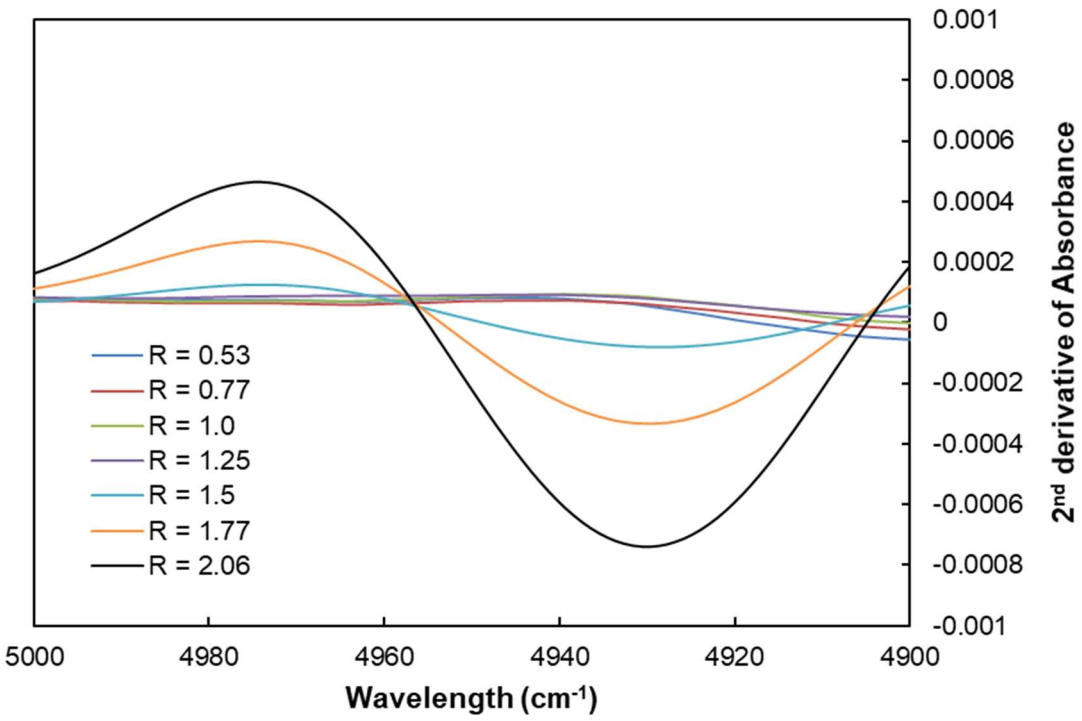

Figure 4.39 - nIR 2nd derivation of absorbance plot focussing on the primary amine peak (≈ 4930 cm^{-1}) post-cured at 120 °C.

Again, comparing the post-cured samples shown in Figure 4.38 and Figure 4.39, the magnitude of the primary amine peaks decreases for the 70 °C samples, suggesting further reaction has occurred. The results for the 120 °C are less clear, with the peak for R ≈ 2.06 shown to remain approximately the same as the non-post-cured samples whilst the peak for R ≈ 1.5 is shown to decrease.

The hypothesis of excess amine ratios containing a large degree of unreacted secondary amines within the structure is confirmed by Figure 4.40 which shows the 2^{nd} derivation plot focussing on the secondary amine peak (≈ 6460 cm^{-1}). A downward peak is shown to exist for ratios where R > 1 and increases in size as more hardener was added to the system.

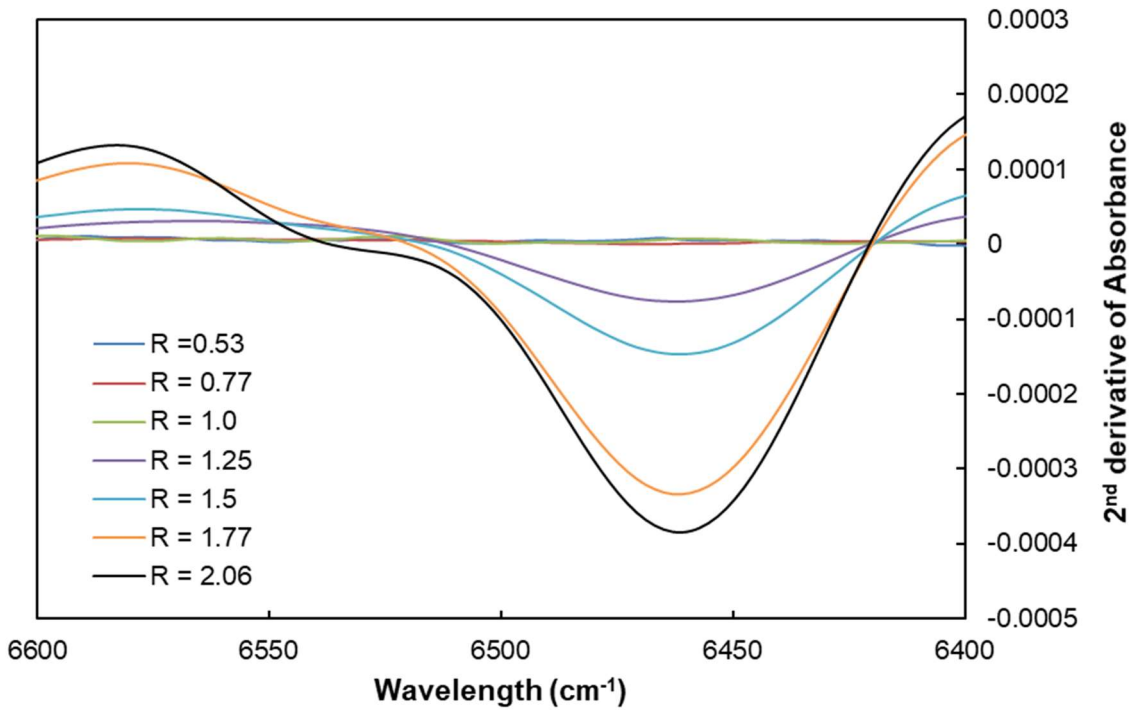

Figure 4.40 - nIR 2nd derivation of absorbance plot focussing on the secondary amine peak (≈ 6460 cm^{-1}) with no post-cure.

Compared to Figure 4.37, it can be seen for R ≈ 1.25 that some level of secondary amine groups remains in the system, whilst all primary amine groups have reacted. As R >> 1 the peak representing the secondary amines within the system is shown to increase to larger values than that shown for the primary amine peak. However, at R ≈ 2.06 it can be seen that the secondary amine peak is smaller than the primary amine peak, suggesting that epoxy groups are still reacting with some level of the secondary amine groups. This ratio represents the first ratio measured where, in theory, there would be statistically enough primary amine groups within the system to react entirely with the epoxy groups, with no secondary reaction then occurring. Yet Figure 4.40 shows this not to be the case. Thus, although the reaction appears to be dominated by the primary amine groups, some level of reacting with the secondary amine groups will continue to occur.

Figure 4.41 and Figure 4.42 similarly show the peaks for the secondary amine groups for the post-cured samples. It is interesting to note that there appears to be an increase in the magnitude of the peak when the post-cure temperature is raised from no post-cure, to 70 °C and then to 120 °C for R ≥ 1.77, suggesting that potentially more primary amines have reacted. The relation is less clear for 1.0 < R ≤ 1.5 where we can see both an increase and decrease depending on the temperature.

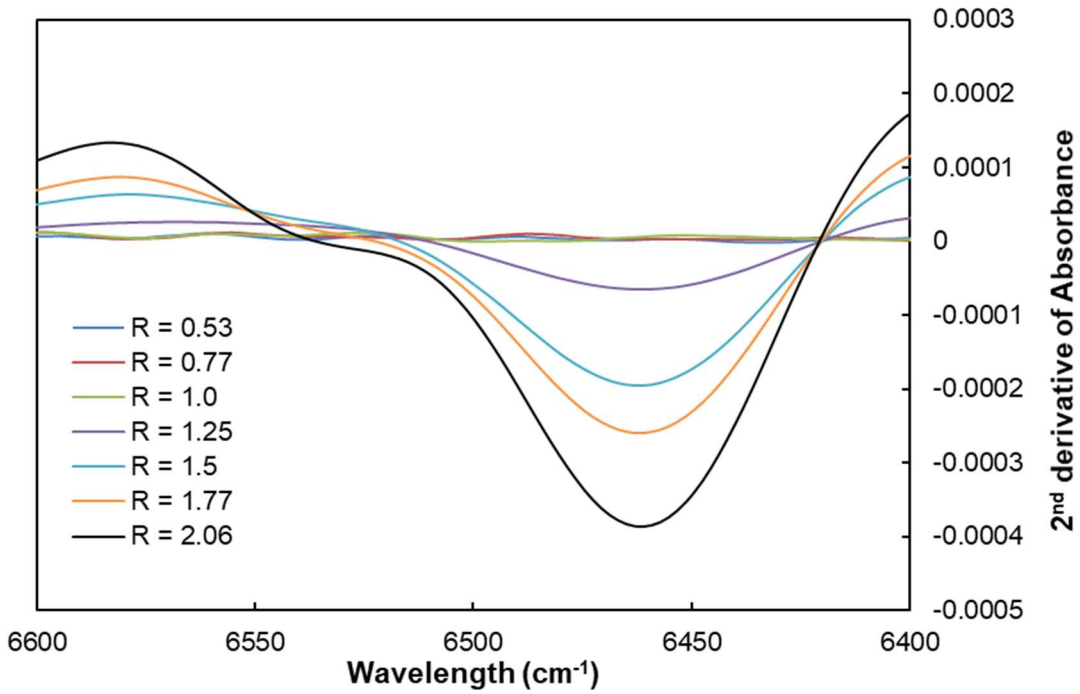

Figure 4.41 - nIR 2nd derivation of absorbance plot focussing on the secondary amine peak (≈ 6460 cm^{-1}) post-cured at 70 °C.

Finally, Figure 4.43 shows the 2nd derivation plot focussing on the peak produced by the hydroxyl (O - H) groups within the system (≈ 7010 cm^{-1}). Interestingly It can be seen that the larger peaks occur for the ratios where 1.0 ≤ R ≤ 1.25, with the largest peak occurring for R ≈ 1.25. The results appear to correlate with the plot for T_g shown in Figure 4.16, with performance optimised at R ≈ 1.25 before then decreasing as R deviated from stoichiometry. Looking at Figure 4.44 and Figure 4.45 it appears that the level of OH groups remains relatively constant despite the post-curing process. Notably for the post-cured samples at 70 °C, the peak for R ≈ 1.25 reduces in

magnitude such that it is lower than R ≈ 1.0, however it then returns to approximately the same size at 120 °C. It is difficult to ascertain whether this is due specifically to the post-curing process or minute differences in the samples.

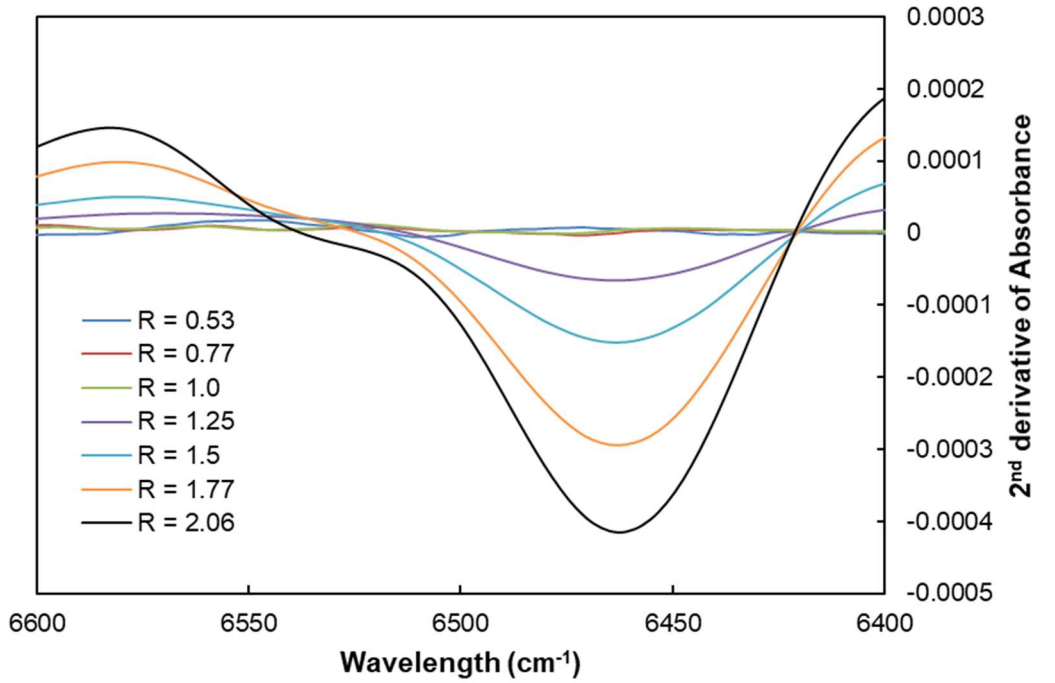

Figure 4.42 - nIR 2nd derivation of absorbance plot focussing on the secondary amine peak (≈ 6460 cm^{-1}) post-cured at 120 °C.

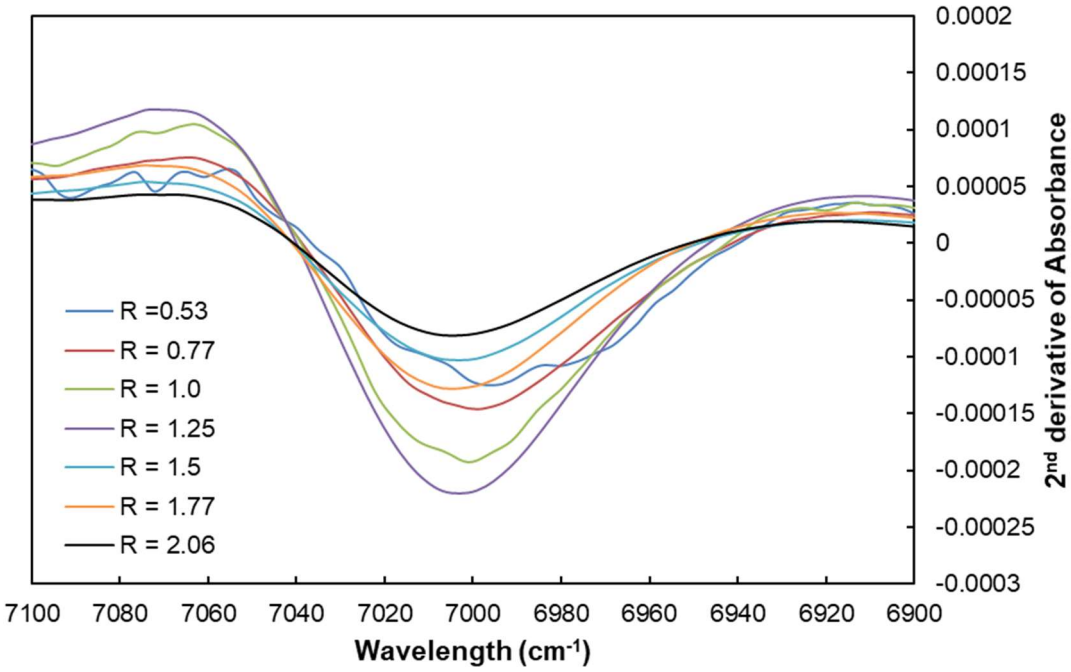

Figure 4.43 - nIR 2nd derivation of absorbance plot focussing on the O – H peak (≈ 7010 cm^{-1}) with no post-cure.

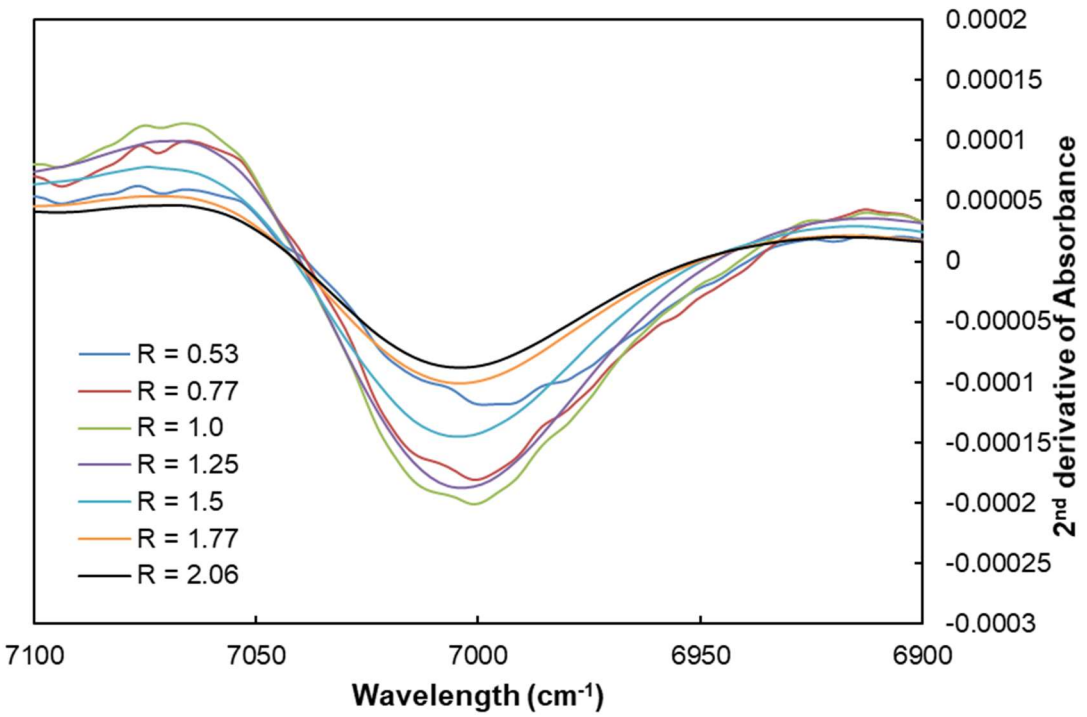

Figure 4.44 - nIR 2nd derivation of absorbance plot focussing on the O – H peak (≈ 7010 cm^{-1}) post-cured at 70 °C.

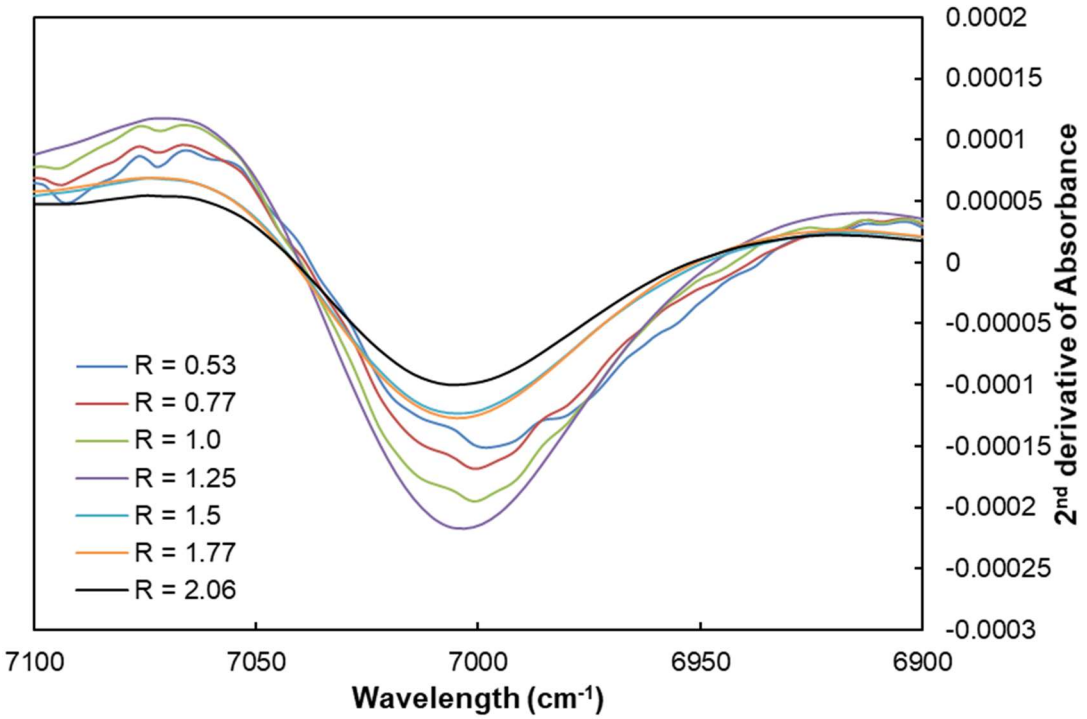

Figure 4.45 - nIR 2nd derivation of absorbance plot focussing on the O – H peak (≈ 7010 cm^{-1}) post-cured at 120 °C.

4.7 Raman Spectroscopy

In combination with the FT-IR analysis it was decided to also conduct Raman spectroscopy to check whether the techniques agreed with each other. Raman represents another technique for gathering qualitative and quantitative data through analysing the molecular vibrations of the material being studied [229,238,241].

Overall the Raman spectroscopy data appeared less informative than that gathered using FT-IR. Figure 4.46 shows the 2nd derivation plot focussing on the epoxy group peak. Past literature has agreed that the peak assigned to the epoxy group typically occurs between 1230 and 1280 cm^{-1} [238,241,255]. It can be seen in Figure 4.46 that a distinct peak cannot be identified across all the ratios, with potentially a similar transition shown in the mIR data occurring for the Raman data. However, if the peak for R ≈ 0.53 at 1259 cm^{-1} and the peak for R ≈ 0.77 at 1257 cm^{-1} indeed represent the epoxy group then it can be seen that the level of unreacted epoxy groups decreases as more hardener was added to the system. A similar peak does not occur for any of the other ratios (R ≥ 1). This would agree with the nIR and mIR data, however the Raman technique itself appeared less accurate and more influenced by background noise. The peaks appeared much more difficult to accurately compare and attribute to specific functional groups. The test also appeared more influenced by minute differences in the samples studied, with samples of the same ratio sometimes showing large discrepancies. A potential point of future research would be to cure the different ratios whilst subject to Raman spectroscopy analysis to allow direct comparisons to be made. This would remove the potential errors introduced by the sample bars used in this thesis.

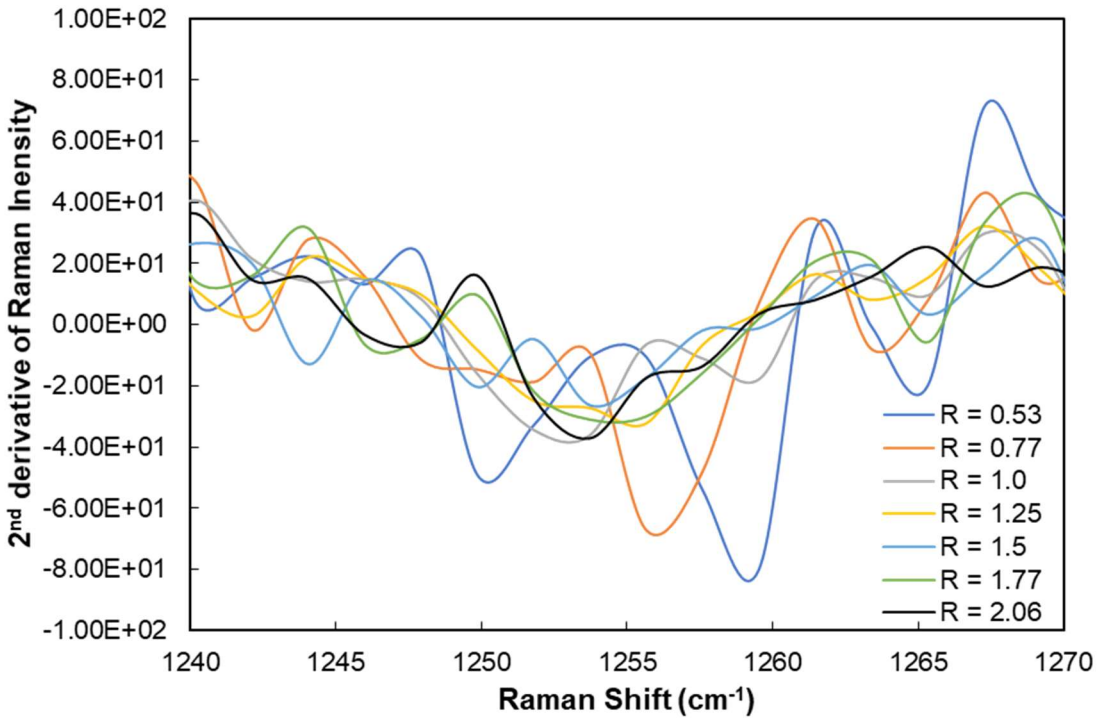

Figure 4.46 - Raman 2nd derivation of Raman Intensity plot focussing on the epoxy group peak (≈ 1255-1260 cm^{-1}).

4.8 Summary and conclusions

In conclusion it was shown that the amine-to-epoxy group ratio (R) had a major influence on all the thermomechanical properties of the matrix studied. The cure kinetics of the Araldite 506® TETA system were analysed by DSC with the heating rate of the curing process shown to distinctly influence the thermoset reaction that occurs. Although higher heating rates led to a faster completion of the reaction, it was found that T_g was greater for rates below 5 °C/min and thus a heating rate of 2 °C/min would be used throughout the remainder of the project. The R value was shown to influence the LCTE value of the matrix, especially above T_g. Above T_g, the magnitude was shown to reach a maximum at the stoichiometric ratio due to this ratio inducing the highest crosslink density. As the ratio was deviated from stoichiometric the matrix crosslink density decreased, leading to an increase in LCTE [57]. Below T_g, the R

value appears to have less influence, with only excess epoxy ratios (R > 1) appearing to possess larger LCTE values.

The chemistry of the matrix system also greatly influences the final value for T_g, for both purities of hardener investigated. The maximum T_g value was recorded at a ratio slightly above the stoichiometric point (R ≈ 1.25), with good correlation between each of the measurement techniques used. Some correlation was shown with past results in the literature despite the differences in resin. The high purity TETA was shown to possess greater values of T_g measured for ratios around the stoichiometric point when compared to the standard purity TETA. However, the values for T_g and activation energy (E_a) were notably lower than published values for other DGEBA/ TETA systems. It was concluded that this was due to the modified nature of the Araldite 506® resin.

Finally, the chemistry of the matrix was shown to have some influence over the storage modulus (E') of the matrix. Ultimately the stoichiometric ratio possessed the largest magnitude of E' however many of the other ratios close to R ≈ 1.0 possessed comparable values at lower temperatures. It was not until the ratio deviated sufficiently from R ≈ 1.0 that E' was significantly impacted due to the significant drop in the T_g of the matrix.

FT-IR and Raman spectroscopy were used to quantify the influence of the amine-to-epoxy group ratio on the potential molecular structure of the final matrix. It was shown that systems mixed with excess epoxy did indeed possess excess epoxy groups remaining within the matrix and that these could undergo an etherification reaction if exposed to elevated temperatures. For ratios where R > 1, primary amines were shown to dominate the thermoset reaction, with more secondary amine groups remaining in the system after curing. If R >> 1 then it was also found that primary

amine groups could also be found in the matrix after reaction. Both would result in reduced crosslink density of the matrix which could explain the decrease in thermomechanical properties observed for off-stoichiometric ratio polymers.

Chapter 5. The influence of matrix chemistry on the GF – Epoxy interface

5.1 Introduction

In this chapter the effect of changing the hardener-to-epoxy ratio on the stress transfer capability of the interface is investigated. Other variables related to chemistry that could potentially influence interfacial strength are also discussed. Although tailoring the stress transfer capability is widely recognized as being vital to optimising the performance of the final composite, it is routinely reduced to a discussion about optimizing the 'adhesion' between the fibre and the matrix. Adhesion represents a simplified term which encompasses the multiple complex mechanisms that exist at the interface and contribute to its strength. One accepted mechanically measurable value for quantifying fibre-matrix adhesion is the apparent interfacial shear strength (IFSS). It was noted in the literature review (2.3.3) that there was a significant body of opinion that chemistry must, in some way, play an active role in the stress transfer capability of the interface. As such chemistry would also have to play an active role in defining the contribution of the residual stresses located at the interface. Hence, investigation of variables related to the chemistry of the system, such as the chemistry of the matrix and fibre sizing, was required in relation to interfacial performance. This would allow for discussion of the potential influence of chemistry on the formation of the residual stresses formed at the interface. In subchapter 5.2 the influence of the amine group: epoxy group ratio (R) on the IFSS value is discussed. Subchapter 5.3 presents the results for how the IFSS value could be influenced by the combination of matrix chemistry and the chemistry of the silane coating on the fibre. After the potential differences discussed in subchapter 4.3 regarding the thermomechanical properties of the matrix it was deemed necessary to also study the influence of the

hardener purity on the stress transfer capability of the interface for different silane sized fibres. This discussion is presented in subchapter 5.4. The thermomechanical data collected in Chapter 4 is then used in subchapter 5.5 to discuss the contribution of residual stresses due to thermal shrinkage to the stress transfer capability of the interface.

Microbond tests were performed to determine the IFSS between the glass fibres and the epoxy matrix. The error bars in all plots represent 95 % confidence intervals.

5.2 The influence of matrix chemistry on stress transfer capability of interface

In past discussions about the interface the focus has been primarily on the chemistry of the fibre coating and the necessity to maximise the level of chemical bonding between the fibre and the polymer matrix to optimize the level of ‘adhesion’ between the two [6,9–13]. It is known that glass fibre sizings often utilise chemicals containing unreacted amine and epoxy groups to facilitate good adhesion between the glass fibre and epoxy matrix [2]. In practice however, the level of sizing applied to a coated fibre is very difficult to maintain and thus may vary along the length of the fibre [2,256]. This sizing has the potential to influence the R value at the interface and may lead to variations in the formation and performance of the fibre-matrix interface. Despite this, the influence of the R value on the stress transfer capability of the interface has not been studied in detail in previous literature. As such it was decided to simulate the potential variation of sizing along the fibre by studying different hardener-to-epoxy ratios applied as minute droplets to single glass fibres to better understand the effect on the stress transfer capability of the fibre-matrix interface.

The microbond test technique was used to measure the IFSS of minute epoxy droplets with various matrix chemistries and is described in detail in subchapter 3.3. Eight different ratios ranging from R ≈ 0.3 up to R ≈ 3.1 were applied to single fibres of fibre 1 and studied. After testing, samples were re-examined using either microscopy or scanning electron microscopy as shown in Figure 5.1. This was conducted in order to analyse the point of de-bond as well as to calculate the corrected de-bonded length of the droplet (L_C). This calculation involved subtracting the length of the remaining meniscus (L_m) from the original length value as shown in Equation 5.1. Without this correction it was found that the relative level of scatter present in the peak load versus embedded area plots was significantly larger. In addition to this the values calculated for IFSS were shown to increase when the embedded length was corrected, due to the true embedded length value being smaller for the droplet than was originally input into the calculation.

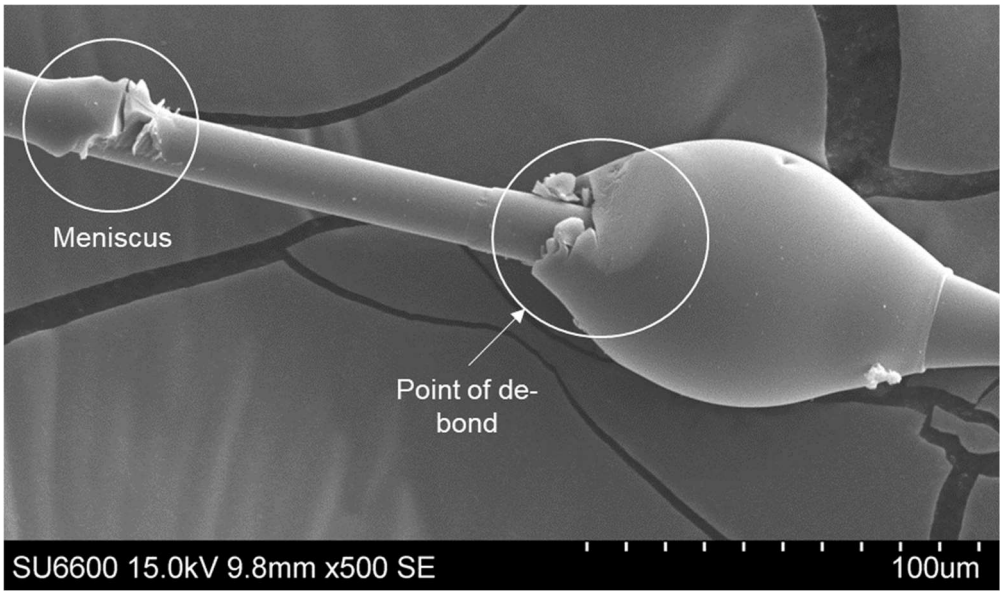

Figure 5.1 - SEM Image of a de-bonded droplet with a ratio of R ≈ 1.0.

$$L_C = L_e - L_m \quad (5.1)$$

The results recorded for peak load versus embedded area plots for R ≈ 0.3, R ≈ 1.0 and R ≈ 3.1 are compared in Figure 5.2 and Figure 5.3. These represent the

comparison between the stoichiometric ratio and the most extreme ratios measured either side of it. It can be seen that the magnitude of the peak loads for R ≈ 1.0 were significantly larger than those measured for R ≈ 0.3 and R ≈ 3.1 for droplets of comparable embedded area. This is reflected in the magnitude of IFSS recorded for each ratio.

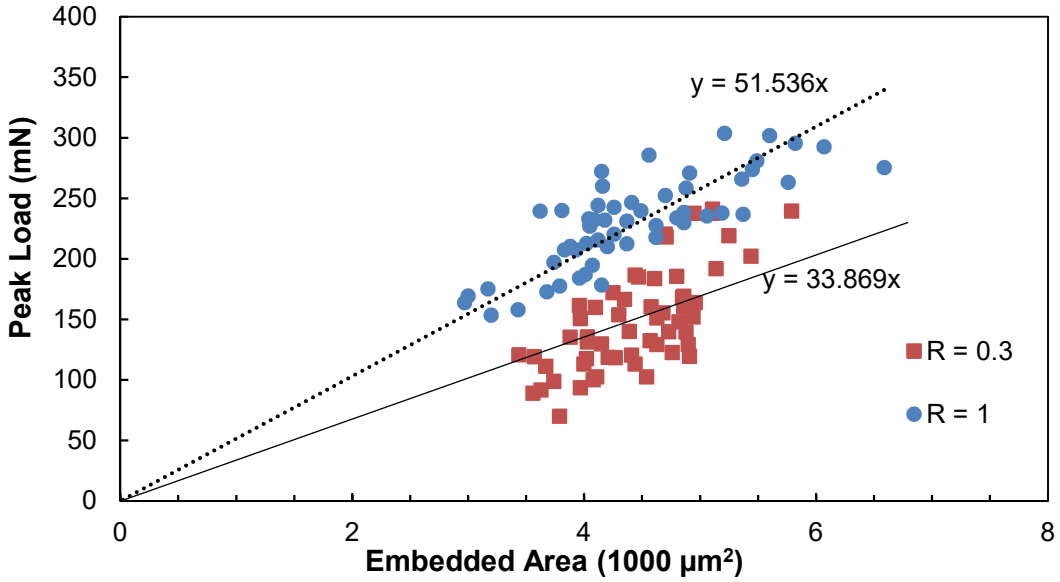

Figure 5.2 - Comparison of peak load versus embedded area plots for R ≈ 0.3 and R ≈ 1.0.

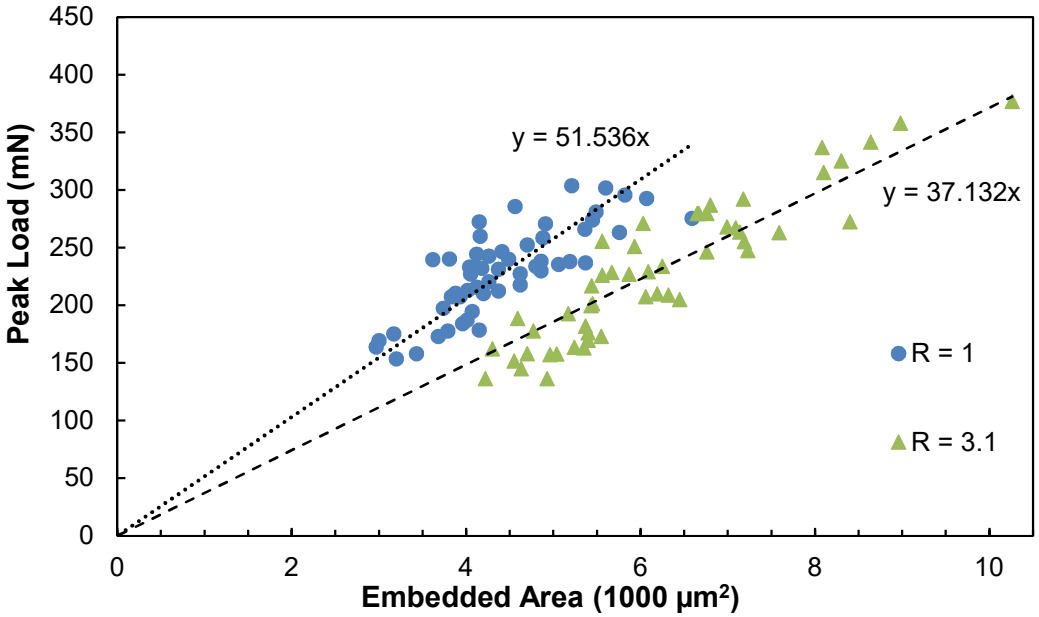

Figure 5.3 - Comparison of peak load versus embedded area plots for R ≈ 1.0 and R ≈ 3.1.

The final results are presented in Figure 5.4 with each data point representing the average IFSS value measured from the 50-60 individual samples tested per ratio shown in the peak load versus embedded area plots.

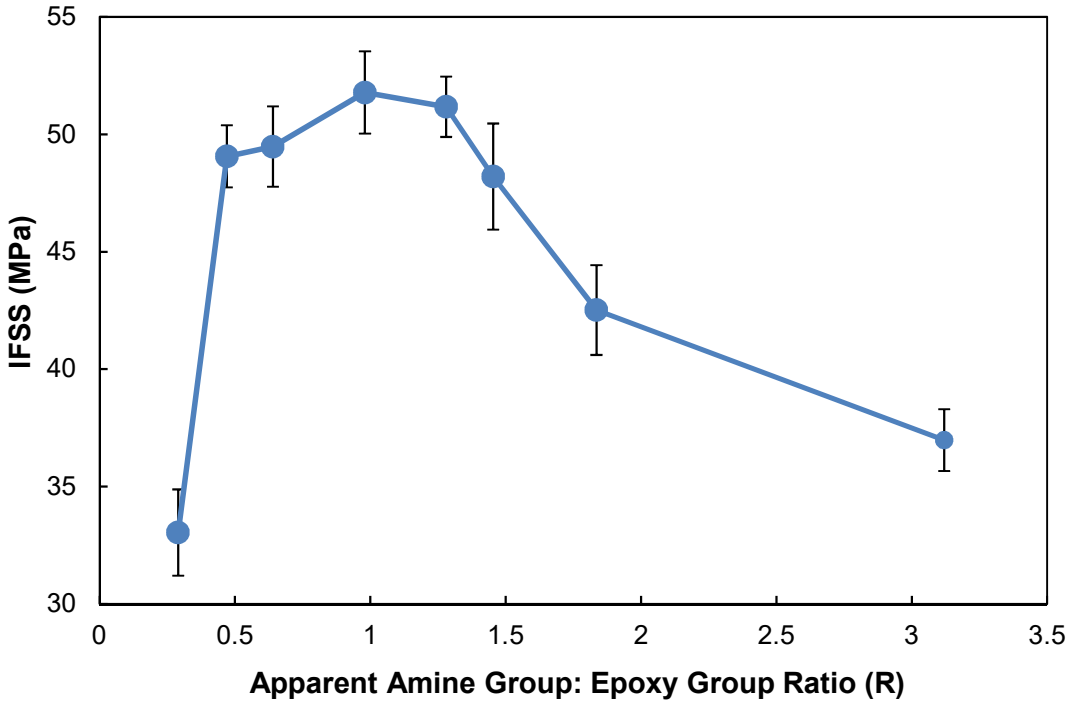

Figure 5.4 - IFSS versus R value for fibre 1.

It can be seen that the IFSS value was maximum (~ 52 MPa) at the stoichiometric value, before decreasing as the R value deviated from this value. Changing the R value around the stoichiometric value ($0.5 < R < 1.5$) shows only a slight decrease in the IFSS value (~ 3 MPa). However, it appears that once the R value deviates further from the stoichiometric value, for instance $R < 0.5$, that the stress transfer capability of the interface appears to decrease greatly with a drop in IFSS of ≈ 16 MPa shown between $R \approx 0.5$ and $R \approx 0.3$.

It can be seen that the gradient of decline for IFSS when $R > 1.8$ is smaller in magnitude than that between $1.28 < R < 1.8$. Going from $R \approx 1.8$ to $R \approx 3.1$ the IFSS is shown to drop by approximately 6 MPa whilst between $1.28 < R < 1.8$ the IFSS is

shown to drop by approximately 9 MPa. Judging by the trend shown, it would be expected that the IFSS would continue to decrease as more amine was added to the system. A decrease in IFSS would also be expected for ratios where R < 0.3 yet for excess epoxy ratios the rate of the decline in IFSS with changing R value appears much greater, with the IFSS value dropping from ≈ 49 MPa to ≈ 33 MPa over an R change of only ≈ 0.17. The final IFSS value for R ≈ 0.3 appears smaller than the value shown at R ≈ 3.1, suggesting that the lack of amine within the system has a greater effect on the decrease in IFSS. The effect is shown by plotting the IFSS against 1/R as shown in Figure 5.5. It can be seen that there is a significant difference between the plots for R ≈ 1.8 and the 1/R plot for R ≈ 0.47, which is notably higher. This emphasises the magnitude of the gradient of drop shown in Figure 5.4 for R < 0.5 relative to the lesser gradient shown for R > 1.25. Otherwise the two plots appear comparable.

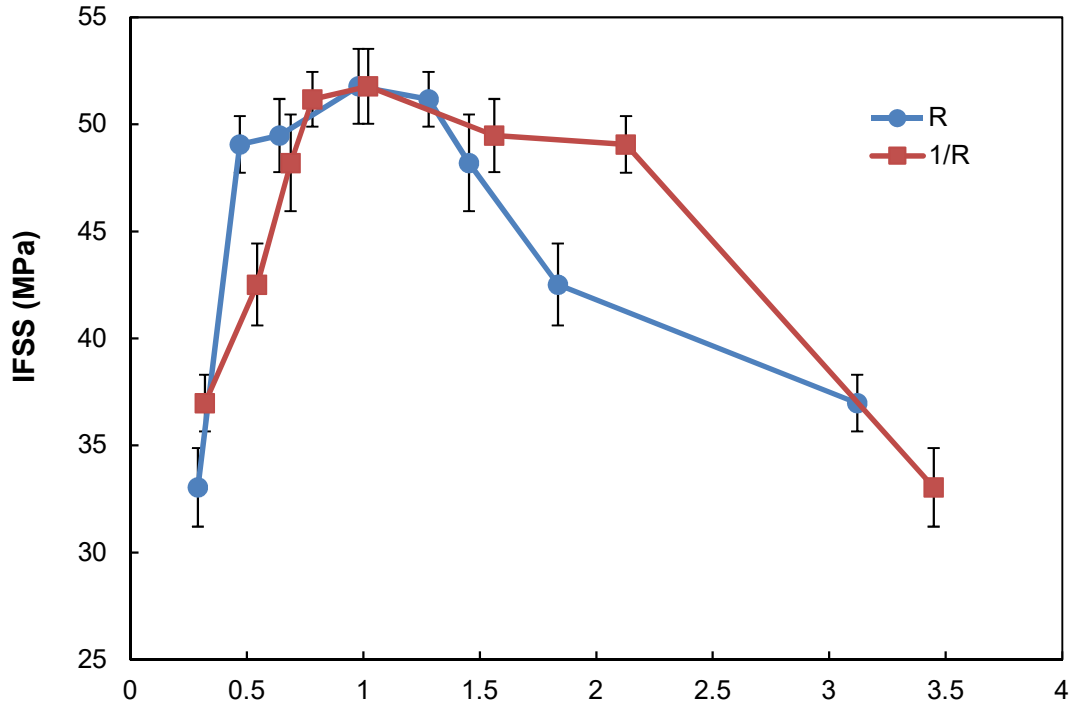

Figure 5.5 – Comparison of plots for IFSS versus R and 1/R.

The dependence of IFSS with the R value shown in Figure 5.4 may be explained to some degree by chemical bonding [11,51,56]. For ratios possessing excess epoxy (R < 1), due to the lack of both primary and secondary amine within the polymer system, it would be expected that a larger quantity of reactive epoxy groups would be statistically available to bond with the amine groups provided by the silane. This could result in the creation of more covalent bonds across the interface, in theory forming a stronger link and thus a larger IFSS value. However, the lack of amine would also result in negative attributes to occur that would decrease the IFSS value. At the interface although the reactive epoxy groups would be more likely to bond with the silane they would also be less likely to bond with any other amine present due to the lesser amount present in the system. There would be potential for epoxy molecules to bond to the silane and yet not be bonded across the interface due to them not being part of the crosslinked network. In addition to this the polymer would be unable to form a fully crosslinked network due to the lack of amine. This would result in less restrained, bulky groups forming at the end of epoxy chain, causing an increase in polymer free volume and a decrease in key thermomechanical properties associated with the matrix such as T_g [52,58,246]. The sudden drastic drop shown at R < 0.5 may represent a critical point where there were not enough amine groups present to bond with enough of the epoxy groups within the system to produce a crosslinked structure. This increases the potential for non-bonded, unreacted epoxy molecules to exist within the matrix structure and at the interface. This would decrease the mechanical properties of the bulk matrix and as a result the mechanical properties of the interphase formed between the fibre and matrix would also decrease. The lack of amine groups would also account for the significant levels of unreacted epoxy groups discussed in subchapter 4.6.

For ratios with excess amine (R > 1), the epoxy groups would statistically be less likely to bond with the amine groups provided by the APS silane due to the abundance of available primary amines already present within the matrix system. Thus, fewer bonds might be expected to form across the interface. For these ratios the curing reaction would also be dominated by the primary amines, with little secondary amine bonding, resulting in less branched polymer matrix structures. These structures would also occasionally consist of rings constructed from partially reacted tri-amine molecules and the epoxide chain [257]. This would agree with the significant levels of unreacted secondary amines remaining in the system shown in subchapter 4.6. This abundance of unreacted molecules along with the less branched structure would again lead to an increase in the polymer free volume due to the poor packing ability of the amine molecule. Hence key thermomechanical properties of the polymer would decrease similarly to the situation described previously [247,248].

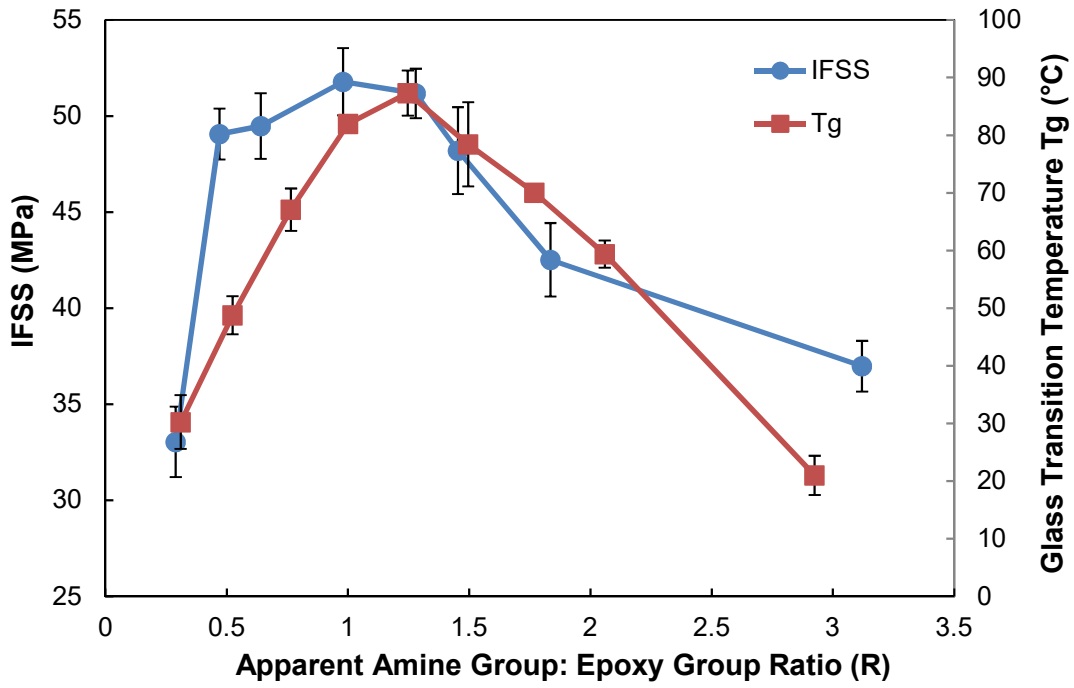

Figure 5.6 – Comparison between IFSS and glass transition temperature T_g plot.

To expand on this hypothesis, Figure 5.6 shows a direct comparison between the IFSS values and the respective T_g values discussed for each R value in Chapter 4. It can be seen that the two data sets show a clear degree of correlation. Both plots show a distinct peak value before then decreasing as the R value deviates from this optimum value. It can be seen that for ratios possessing excess amine ($R > 1.25$) that the decrease in IFSS shown does correlate with a drop in the T_g of the matrix material. Yet it can be seen that the peak shown for T_g does not coincide exactly with the peak in IFSS, occurring at $R \approx 1.25$ rather than at stoichiometry ($R = 1$). It can also be seen that the decrease in T_g shown for $0.5 < R < 0.1$ does not coincide with a comparable drop in IFSS, which appears to maintain a value of ≈ 49 MPa until $R < 0.5$. However, once $R < 0.5$ the drop in IFSS is shown to coincide with the T_g of the polymer approaching ambient. This would suggest that the T_g may influence the stress transfer capability of the interface differently for ratios possessing different levels of either excess amine or excess epoxy. Judging by the clear correlation between the plots for $1.25 > R > 2$, it appears that the T_g may have more influence in defining the strength of the interface in this region than for the other ratios, with the correlation shown to decrease once $R > 2.5$. Once R approaches extreme excess epoxy values, such as at $R \approx 0.3$ the drop in T_g to near room temperature may appear to play a larger role in influencing the adhesion mechanisms.

The correlation between IFSS and T_g shown in Figure 5.6 is expanded upon in Figure 5.7 where the IFSS values are plotted versus the T_g values of the respective R values. Here the correlation can be seen much more clearly, with the peak IFSS values shown to coincide with the peak T_g values respectively. The extreme ratios tested are also shown to possess both the lowest IFSS and T_g values. Yet this plot does highlight the large IFSS value shown for $R \approx 0.5$ in relation to its T_g value, with it appearing higher than the trendline would predict. Again, this would suggest that although the T_g may

be influencing the adhesion mechanisms present to some degree for 0.5 < R < 1, it does not necessarily have a major influence until R < 0.5. One particular adhesion mechanism where this would be relevant would be the formation and magnitude of residual stresses located at the fibre-matrix interface.

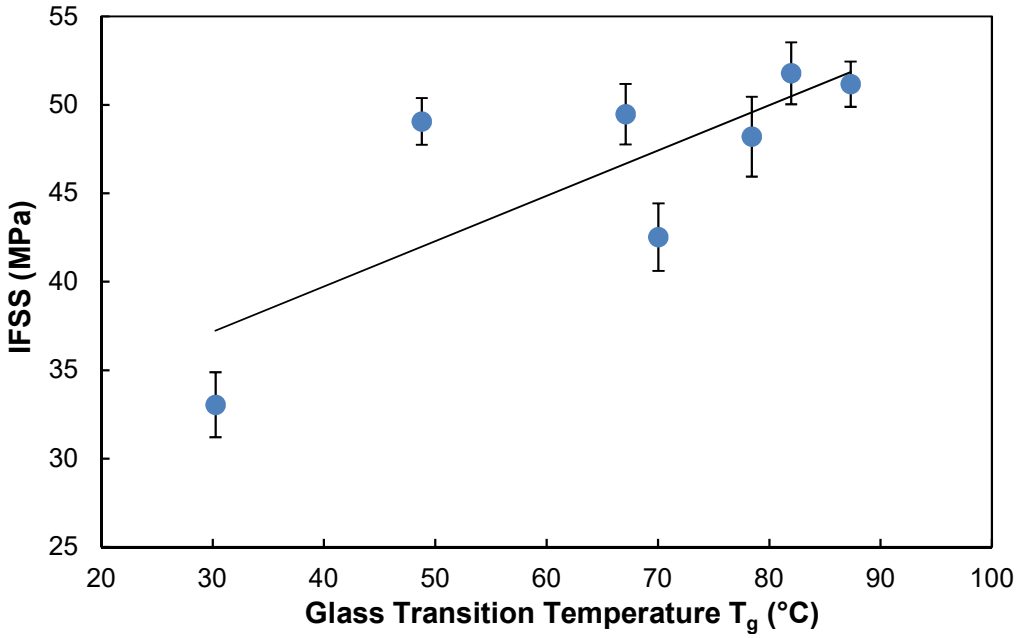

Figure 5.7 - IFSS versus glass transition temperature T_g plot.

In conclusion, it has been shown that the R value of the matrix system can clearly influence the stress transfer capability of the interface. Changes to the R value of the matrix (0.5 < R < 1.75) may result in small variations in the level of adhesion with minimum impact on the stress transfer capability of the interface. However, if the variation from the stoichiometric value is large enough then there may be potential for a significant impact on the performance of the final composite material. This is particularly the case for excess epoxy ratios where the IFSS value was shown to drop off drastically between R ≈ 0.5 and R ≈ 0.3.

5.3 The influence of fibre silane coating on stress transfer capability of interface

It was discussed in the literature review that a large volume of research has been conducted into studying the influence of chemical sizings on the properties of a glass fibre/ epoxy interface [5,10,24,79,94,99,100,108,258,259] as well as a number of other fibre types and matrix systems. With the work in subchapter 5.2 showing that changes to matrix chemistry at the interface could greatly influence its stress transfer capability it was decided to study whether the influence of different silane coatings on the measured IFSS was larger than that of changing the matrix chemistry.

The microbond test technique used to measure the IFSS of epoxy droplets with various fibre surface chemistry is consistent with that used previously in subchapter 5.2. Four different coated fibres were studied with three of them coated with silanes as designated in Table 3.1. The epoxy droplets were prepared and applied in the same manner as was discussed in subchapter 5.2. This work was conducted in collaboration with the undergraduate student David Bryce.

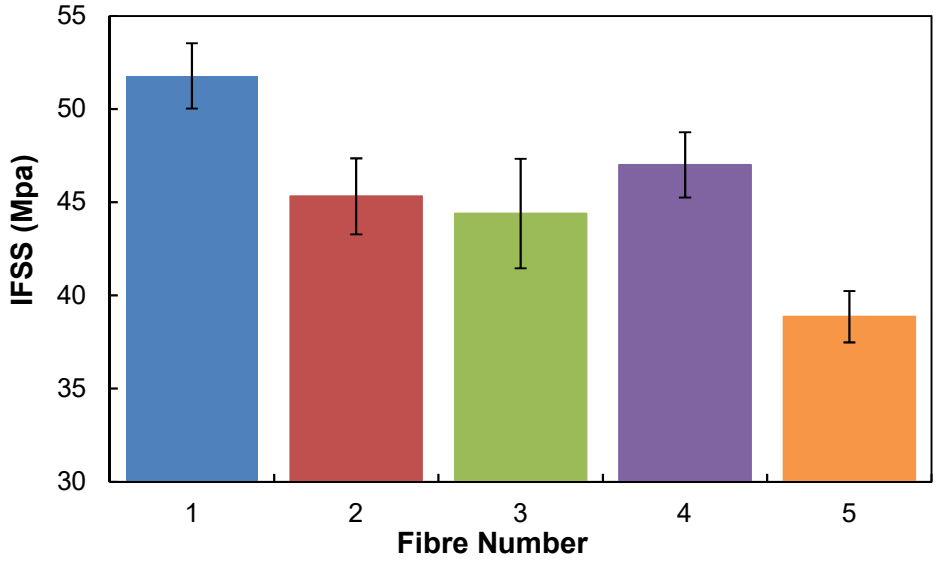

Figure 5.8 - IFSS comparison between different coated fibres at R = 1.0.

Figure 5.8 presents a comparison between the four different fibres at R = 1 tested as well as comparing it with the value shown in subchapter 5.2 for fibre 1. It can clearly be seen that Fibre 5, the water sized fibre, possessed the lowest value for IFSS. This could be expected due to the lack of any primary chemical coating on the surface of the fibre. This would reduce the probability of any primary chemical bonding from occurring across the interface other than at points where the epoxy groups had bonded to the OH groups located on the fibre surface. As a result, the only other intermolecular forces at work would likely be weak forces such as London dispersion and polar forces or acid base interactions, which are very susceptible to water ingress [5]. Thus, the IFSS would be expected to be lower than for fibres coated in silanes. Indeed, the apparent difference in IFSS is still relatively small considering the level of effort that has been put into maximising the output of silanes to promote bonding between the fibre and polymer. Otherwise the IFSS values appear comparable for the coated fibres, with fibre 1 shown to possess the largest IFSS value at the stoichiometric ratio. The difference shown between fibres 1 and 2 was notable since both were E-glass fibres coated with APS however the results showed a difference of ~ 6 MPa between the two. This would suggest that there may be minor differences between the two, possibly due to loss on ignition (LOI) taking place after the sizing application during the manufacturing of the fibre.

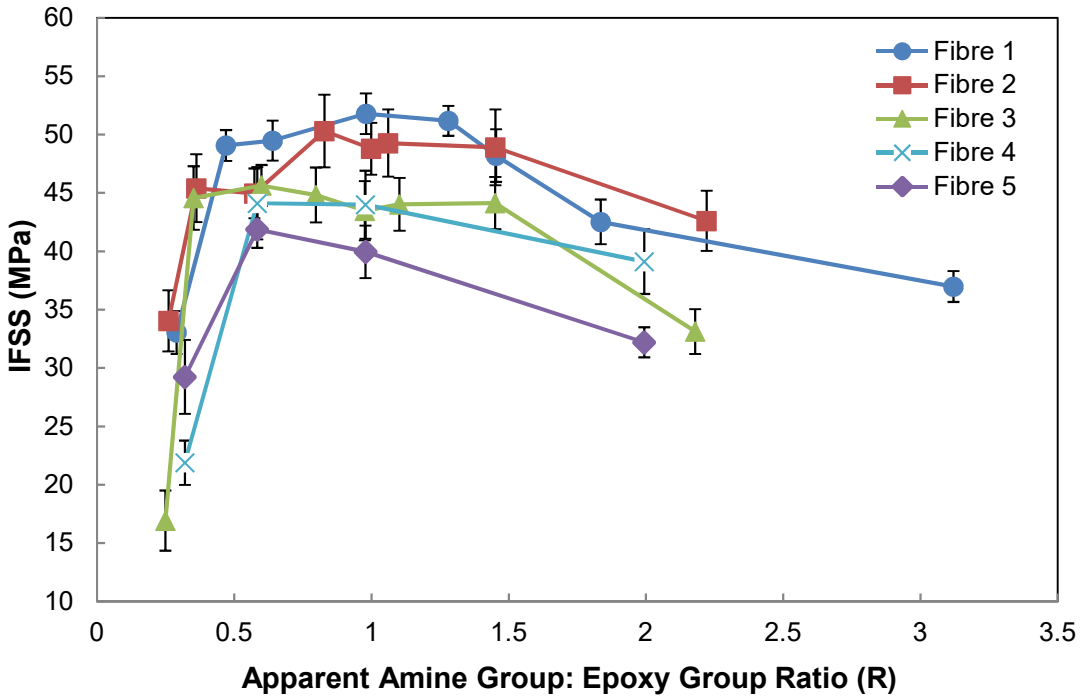

Figure 5.9 - IFSS comparison between fibres 1 – 5 with changing R values.

Expanding on this hypothesis, Figure 5.9 shows a plot comparing the influence of matrix chemistry on the IFSS values measured for fibres 1 through 5. It can be seen that a degree of correlation does exist between all five data sets with each highlighting that the IFSS value could be greatly influenced by the chemistry of the epoxy system. Interestingly the point of maximum IFSS occurs at different ratios for each fibre. Fibres 4 and 5 were shown to possess lower magnitude IFSS values on average versus the other fibres tested, with the decrease in IFSS as R > 1.5 shown to occur for each of the fibres tested. For fibres 1 through 3 the value for IFSS was shown to decrease greatly once R < 0.5, particularly for fibre 3 which was sized with an epoxy silane. This would coincide with the distinct drop in the T_g of the matrix discussed previously in subchapter 4.3.

Following on from the discussion in subchapter 5.2, the extra epoxy groups provided by the silane coating would in theory decrease the effective R value at the interface. This would mean there were more epoxy groups available for fibre 3 relative to the

other two fibres, effectively shifting the actual R value of the data points to the left and potentially accounting for the larger drop in IFSS (at R ≈ 0.3) shown for fibre 3. Since fibres 1 and 2 are coated with APS, the coating would be providing more amine groups to the system, effectively leading to a more crosslinked structure when R < 1. The extra epoxy groups provided by the coating of fibre 3 would do the opposite. The result would be a negative impact on the properties of the interface and may explain why the drop in IFSS is distinctly larger for fibre 3 than for the other fibres when R < 0.5.

It is interesting to observe that for ratios where R > 1.0 the opposite would be expected to occur, yet this does not seem to be the case for fibre 3. As was touched upon in subchapter 5.2, it would be expected for ratios where R > 1 that the epoxy groups within the matrix would be statistically less likely to bond with the amine groups provided by an APS silane. This would be due to the abundance of available primary amines already present within the matrix system. Yet GPS silane provides further epoxy groups and as such when R > 1 it would increase the statistical chance of amine groups bonding with the epoxy groups of the silane across the interface. According to chemical bonding theory this would lead to a stronger interface and the IFSS values for fibre 3 being greater than that of fibres 1 and 2 once R > 1. However, Figure 5.9 shows this not to be the case, with fibre 3 consistently possessing lower magnitude IFSS values for each ratio tested.

Overall the different magnitudes for IFSS would suggest that there may be minute differences between the two fibres although the overall trend of the data is comparable. Taking the two sets of data and then combining them presents the data shown in Figure 5.10 plotted along with the T_g data as shown in Figure 5.6. It can be seen that with the combined data, there is even more correlation shown to occur

between the magnitude of the IFSS value measured and the T_g of the matrix.

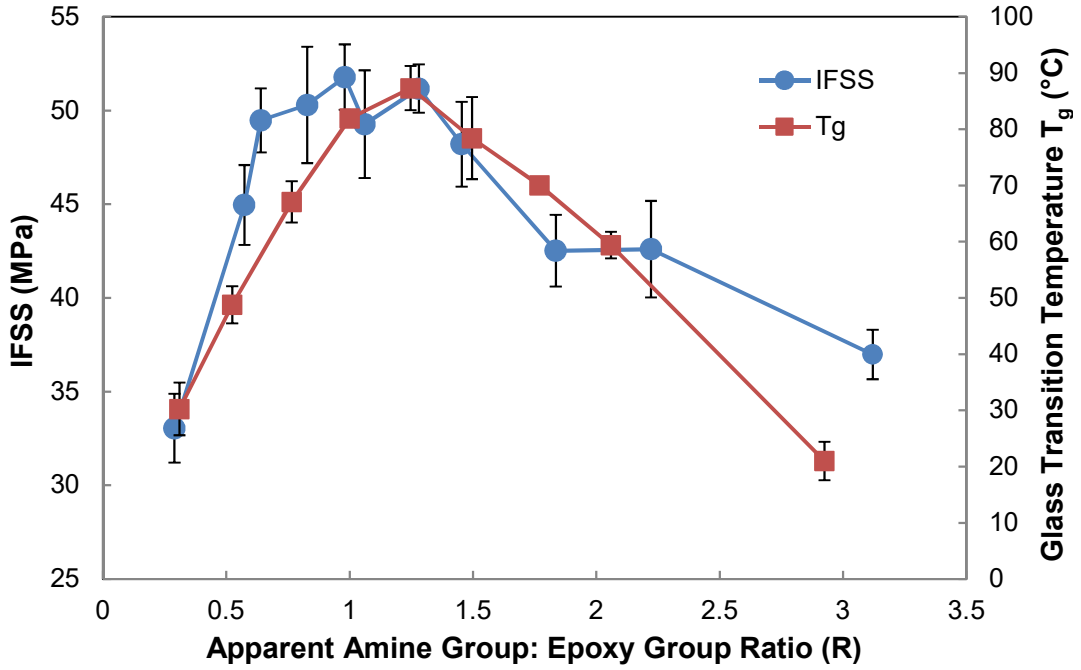

Figure 5.10 - IFSS versus Tg for combined data from fibres 1 and 2.

Meanwhile, in Figure 5.9, fibre 3 showed a maximum IFSS value at a ratio (R ≈ 0.6) which would not fit with typical chemical bonding theory. This was unexpected given the epoxy silane coating of the fibre. It was initially hypothesised that fibre 3 would exhibit superior performance at the stoichiometric ratio or ratios measured slightly above (1 < R < 1.25) due to the increased statistical chance of bonds forming across the interface. The extra amine groups in an R > 1 system would also be expected to balance out the extra epoxy groups provided by the epoxy silane, effectively pushing the local interfacial R value closer to R = 1. However, this was shown to not be the case with the IFSS value at R ≈ 0.6 appearing slightly above the values recorded at R ≈ 0.8 and R ≈ 1.0 with the overall values for IFSS being comparable between R ≈ 0.35 up to R ≈ 1.5. The IFSS value for fibre 3 was also shown to decrease at a greater rate relative to fibres 1 and 2 when R > 1.5. This would suggest that although the epoxy-silane coating should increase the statistical chance of bonds forming across the interface for excess amine ratios (R > 1), this does not seem to offset the negative

impact that the excess amine groups have on the mechanical properties of the matrix. In relation to this it also appears that a significant abundance of reactive epoxy groups within the system does not appear to affect the stress transfer capability of the interface for fibre 3 until R < 0.3, whereupon it decreases more relative to the other fibres studied.

The plots for fibres 4 and 5 show much the same trend as the other tested fibres, despite the lack of coating on the latter and the methacryl coating on the former. Both show a peak IFSS value at R ≈ 0.6 although the maximum shown for fibre 4 is much more comparable to the measured value at the stoichiometric ratio. As was expected the water sized fibre (fibre 5) was generally shown to possess smaller IFSS values for the ratios tested. However, interestingly at R ≈ 0.3 it possessed a larger IFSS value than fibres 3 and 4.

Despite the differences between fibres, the overall influence of matrix chemistry on the measured IFSS appears comparable to the results discussed in subchapter 5.2 for each of the different silanes tested, with the IFSS value shown to vary greatly depending on the R value. This would suggest that the influence of matrix chemistry on the stress transfer capability of the interface is greater than that of the fibre surface chemistry. Thus, it can be hypothesised that the number of chemical bonds forming across the interface may not be ultimately dictating the level of apparent IFSS. In fact, it may be the level of silane applied at the fibre surface and how it varies along the length of the fibre that is dictating the level of apparent IFSS. This varying level of silane is then potentially influencing key thermomechanical properties by changing the local R value along the interface which are then responsible for influencing the stress transfer capability of the interface. Therefore, chemistry would still clearly be playing an active role, however it would be specifically the influence of the matrix properties, not the number of interfacial chemical bonds, which is contributing most to

the stress transfer capability of the interface. A point of future work would be to investigate the exposed fibre surface chemistry in-detail to measure the amine/epoxy group content on the different sized fibres studied. This would aid in understanding the degree to which the fibre surface coating could influence the local matrix stoichiometry at the interface.

5.4 The influence of hardener purity on stress transfer capability of interface

Due to the differences discussed in Chapter 4 in relation to hardener purity it was decided to study whether the increase in T_g for $R \leq 1$ using the high purity TETA equated to an increase in the stress transfer capability of the interface for these ratios. The test technique and sample preparation technique were as used in subchapters 5.2 and 5.3 with the only difference being that higher purity TETA was instead used as the hardener. The data points shown represent the average IFSS value measured across the 60 samples tested, as was the case in subchapters 5.2 and 5.3.

Figure 5.11 shows a comparison between the IFSS results recorded for the standard purity TETA and those recorded for the higher purity TETA. A degree of correlation can be seen between the two data sets, with the large drop in IFSS for ratios where $R < 0.5$ being clear in both. Despite this it can be seen that although the high purity TETA was measured as having higher T_g values, it generated lower IFSS values relative to the standard purity TETA used in subchapter 5.2. It might have been expected that the high purity TETA would have performed better due to the higher concentration of reactive amine groups within the structure as well as the higher T_g values discussed previously. Despite this, the influence of R on the measured IFSS value is shown for both purities of hardener. Hence, this would suggest that the IFSS

is more influenced by the R value of the matrix system than the purity of the hardener itself.

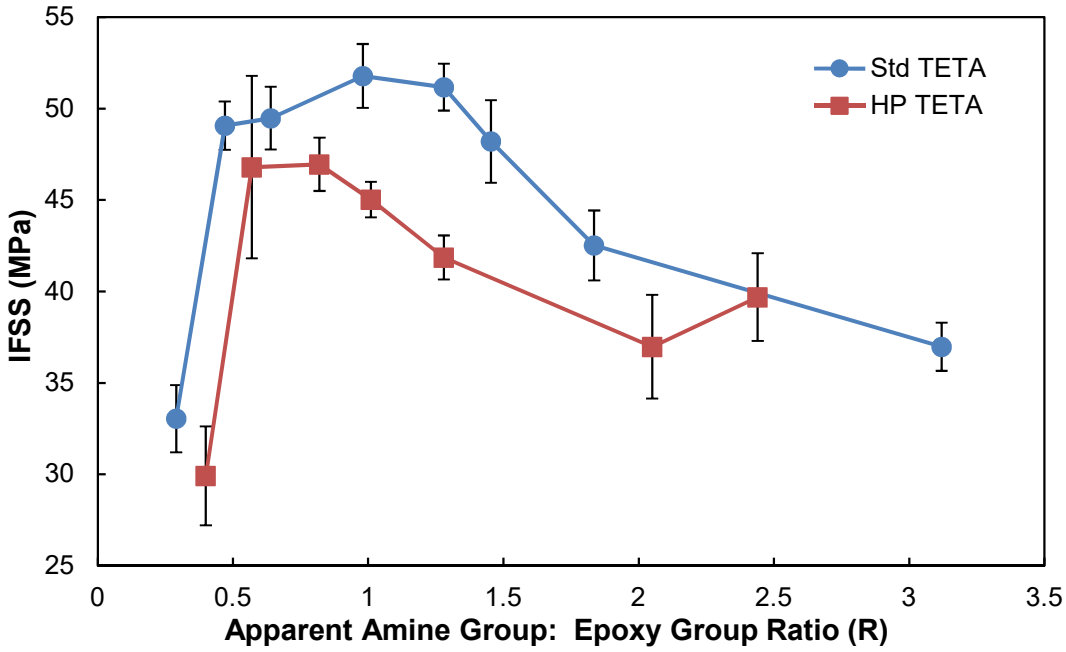

Figure 5.11 - IFSS comparison between two different hardener purities.

Figure 5.12 shows a comparison between the IFSS values measured and the T_g values discussed in subchapter 4.3. Again, like Figure 5.6 a correlation between the two datasets can be seen, although not to the same degree. The peak value for T_g appear to occur around the stoichiometric ratio whilst the peak IFSS value occurs R ≈ 0.8. Overall the same trend shown in Figure 5.6 for the standard TETA is generally shown to occur.

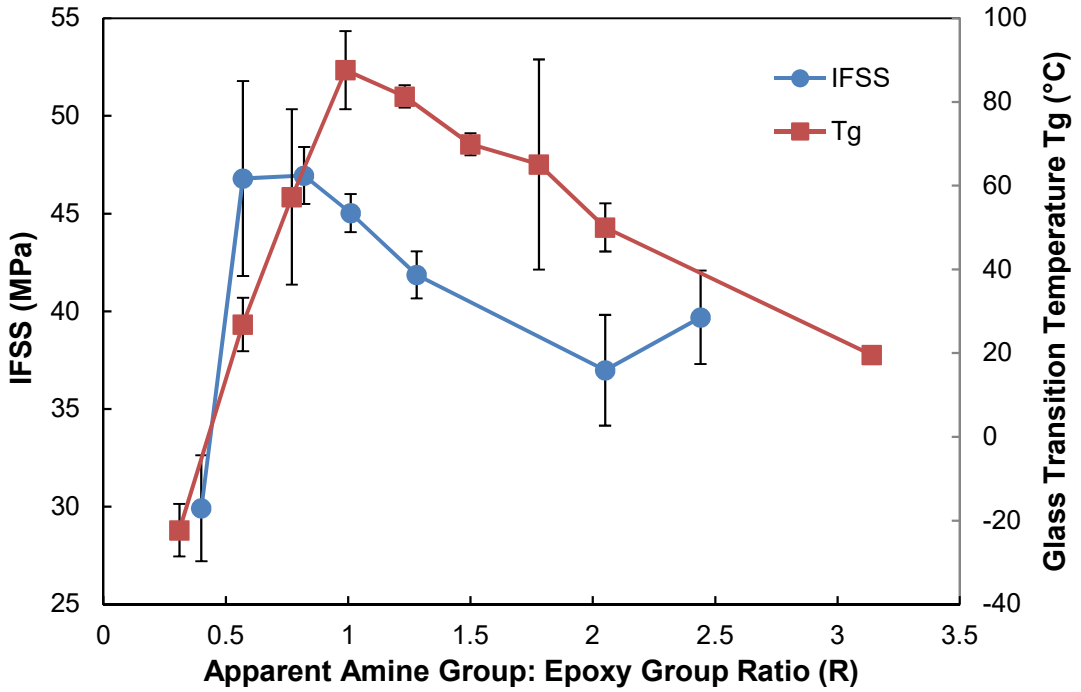

Figure 5.12 - Combined IFSS and glass transition temperature Tg plot using high purity TETA.

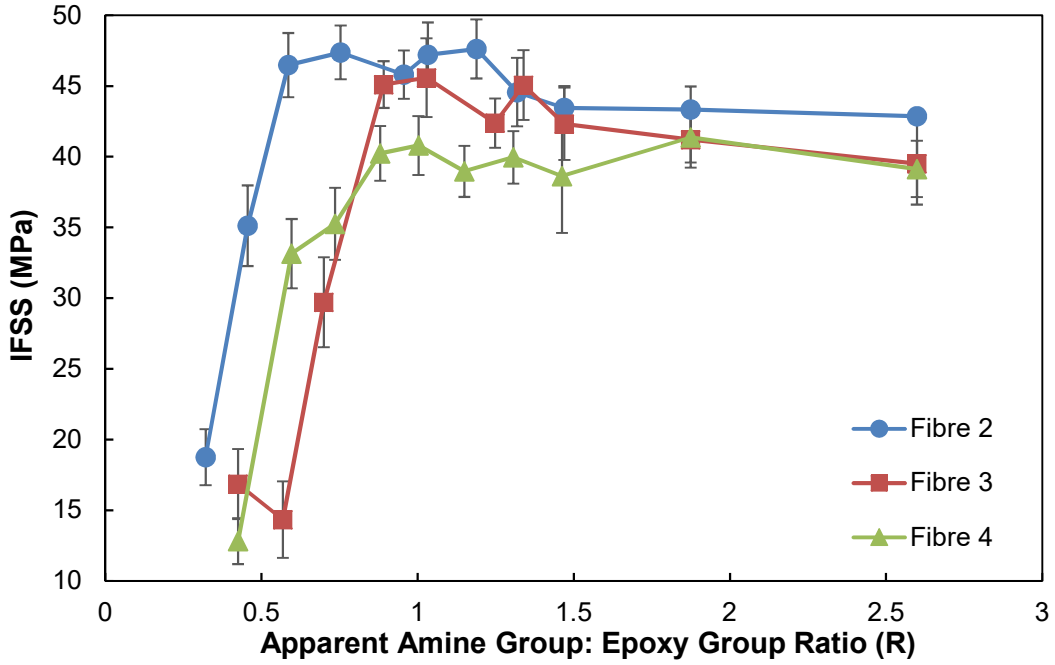

Figure 5.13 - IFSS comparison between fibres 2 – 4 with changing R values using high purity TETA collected.

Given the influence of fibre surface chemistry discussed in subchapter 5.3 and the results shown in Figure 5.11 it was decided to investigate whether the chemical purity

of the hardener could influence values for IFSS differently for different silanes. This work was conducted in collaboration with the undergraduate student Molly Stewart. Figure 5.13 presents a comparison between the different coated fibres studied.

It can be seen that the overall influence of the R value on the measured IFSS appears to correlate with that shown using the standard purity TETA in Figure 5.9. Unlike the results for the standard TETA, there appeared to be much less evidence of a "maximum" in IFSS value for the different fibres tested using the high purity TETA. Instead, broader peaks were shown to occur across a range of R values for each fibre, with the APS fibre shown to be the most consistent over the widest range of ratios. The data presented in Figure 5.13 also seems to present more evidence for the influence of the silane type on the measured IFSS. The difference due to the silanes appears to be more distinct than that found using the standard TETA in Figure 5.9. This was particularly the case for excess epoxy ratios for each of the different silanes tested, with the large decrease in IFSS occurring at different R values. The amine silane of fibre 2 was shown to be superior over the full range of R values studied, with higher IFSS values occurring between $R \approx 0.6$ and $R \approx 1.2$. The rate of IFSS decline as the R value deviated from stoichiometry for fibre 2 was also shown to be smaller than that for the other silanes. This would suggest that a stronger link is formed between fibre 2 and the matrix due to the larger stress transfer capability of the interface.

The results shown would suggest that the extra amine groups provided by the APS of fibre 2 may ensure a greater level of crosslinking within the matrix network at the interface, effectively increasing the R value at the interface. The extra epoxy groups provided by the GPS of fibre 3 would thus be expected to do the opposite, effectively decreasing the R value at the interface and potentially weakening its stress transfer capability as was shown. This would explain why at $R < 0.6$, fibre 2 is able to maintain

a larger IFSS value at a lower R value relative to fibres 3 and 4. It would also explain why fibre 4 appears between fibres 2 and 3 at these low ratios since the MPS would not influence the matrix chemistry to the same degree as either the APS or GPS.

Although the two plots in Figure 5.9 and Figure 5.13 do show some correlation, there are also some distinct differences. Overall the magnitude of the IFSS values shown in Figure 5.13 are smaller when compared to those shown in Figure 5.9 for each fibre. Interestingly the results in Figure 5.13 also show that the optimized IFSS occurred nearer to the stoichiometric ratio for each fibre when compared to the results shown in Figure 5.9. The drop in IFSS at R < 0.6 also appeared significantly greater for fibre 2 in Figure 5.13 (≈ 28 MPa) than in Figure 5.9 (≈ 12 MPa). This is interesting since the values shown for the T_g in subchapter 4.3 appeared comparable between the two TETA purities and yet there is a significant difference present at this ratio.

Overall, from the IFSS results presented, it can be concluded that changing the matrix R value has a larger influence on the stress transfer capability of the interface than the hardener purity or chemistry of the applied silane coating. This agrees with the conclusions of subchapters 5.2 and 5.3 respectively. Despite the differences in chemistry the overall trend for IFSS with R was shown to be consistent for both hardener purities, with a clear correlation again shown between the IFSS value and the T_g of the matrix. The IFSS values for mixtures using the higher purity TETA were shown to be consistently smaller for all silanes studied. This was unexpected due to the larger T_g values shown for the higher purity TETA in subchapter 4.3.

5.5 Thermal residual stress contribution to interface stress transfer capability

It was seen in the literature review that a number of authors [14–20,85] have commented on the potential role of shrinkage stresses contributing to the stress transfer capability of the interface. In particular, it has been suggested that residual radial compressive stresses at the interface may contribute significantly to the IFSS. Thermal radial compressive stresses can build up at the interface during the cooling process due to differences in the thermal expansion coefficients of the matrix polymer and the reinforcement fibre. Polymerising thermoset matrices also undergo a volume change known as cure shrinkage. Due to the increase of the glass transition temperature (T_g) as a thermoset matrix reacts it is possible for some level of this cure shrinkage to be 'frozen' into the system, creating additional residual stresses at the interface [15,21]. If the IFSS testing temperature is raised above the matrix T_g then these residual stresses can potentially relax away, decreasing IFSS. This was shown to occur by Thomason et al [15]. Nevertheless there is still a significant body of opinion that holds that, even if residual stresses formed at the interface do contribute to the stress transfer capability, chemistry and chemical reactions must still play a direct role in determining the IFSS [21–25].

The results presented in Chapter 4 and subchapters 5.2 - 5.4 showed that the chemistry of the matrix system has a major influence on several of the key properties discussed above, such as the IFSS, T_g, matrix modulus and LCTE. Given this fact it was considered necessary to study how the matrix chemistry and residual stresses may be interrelated to influence the stress transfer capability of the interface. Several models have previously been proposed [16–20] to quantify the magnitude of the thermal residual stresses (σ_R) at the interface due to differences in the coefficients of

expansion of the matrix and fibre. Nairn [16] proposed a model to calculate the σ_R that accounted for the effects of differences in the axial and transverse fibre properties:

$$\sigma_R = A_1(1 - \frac{b^2}{r^2}) \quad 5.2$$

where A_1 is the result of the calculation shown in Equation 5.3.

$$A_1 = \begin{bmatrix} X_{11} & X_{12} \\ X_{21} & X_{22} \end{bmatrix} \begin{bmatrix} A_1 \\ A_3 \end{bmatrix} = \begin{bmatrix} (\alpha_m - \alpha_{fT})\Delta T \\ (\alpha_m - \alpha_{fL})\Delta T \end{bmatrix} \quad 5.3$$

Where b is a function of the fibre volume fraction (V_f), r is the radius of the fibre, α is the linear coefficient of thermal expansion, ΔT represents the difference between the stress-free temperature (T_s) and the testing temperature (T_t) and f, m, L and T are subscripts for the fibre, matrix, longitudinal and transverse respectively. From the result of the model in Equation 5.3 we can see that thermal residual stresses are directly influenced by changes in ΔT. For thermosetting systems, the stress-free temperature is accepted as being the glass transition temperature T_g and hence the results for T_g presented in subchapter 4.3 indicate that the level of residual stress should vary with the chemistry of the system as well as the testing temperature. Other key variables such as the matrix modulus and linear expansion coefficient of the matrix were also clearly shown to be dependent on both temperature and matrix chemistry as discussed in subchapters 4.4 and 4.5 respectively. Glass fibre properties are also temperature dependent, but to a much lesser degree, and can be considered constant for the temperature range explored in this study, with α_f = 6.0 x10^{-6} °C^{-1} used throughout this study along with a Young's modulus value (E_f) of 78.7 GPa [15].

$$\tau_R = \mu_s \sigma_R \quad 5.4$$

Using Equation 5.3 and the above data, the magnitude of the interfacial radial thermal residual compressive stresses at room temperature were calculated for different

ratios. These values were then used in Equation 5.4 with a coefficient of static friction of $\mu_s = 0.6$ [15,144] to obtain the residual stress contribution to the interfacial stress transfer capability (τ_R). The results are plotted in Figure 5.14. Due to difficulties encountered gathering the E' data for ratios R ≈ 0.3 and R ≈ 3.0 the data points could not be plotted for the residual stress model at 20 °C. This was due to the starting temperature of the model being 20 °C, with the DMA only capable of measuring the E' values for these ratios at a temperature of 30 °C and above. As such a comparable plot is shown in Figure 5.15 where the model was used to calculate the residual stress contribution at 35 °C to allow for the inclusion of the two extreme ratios.

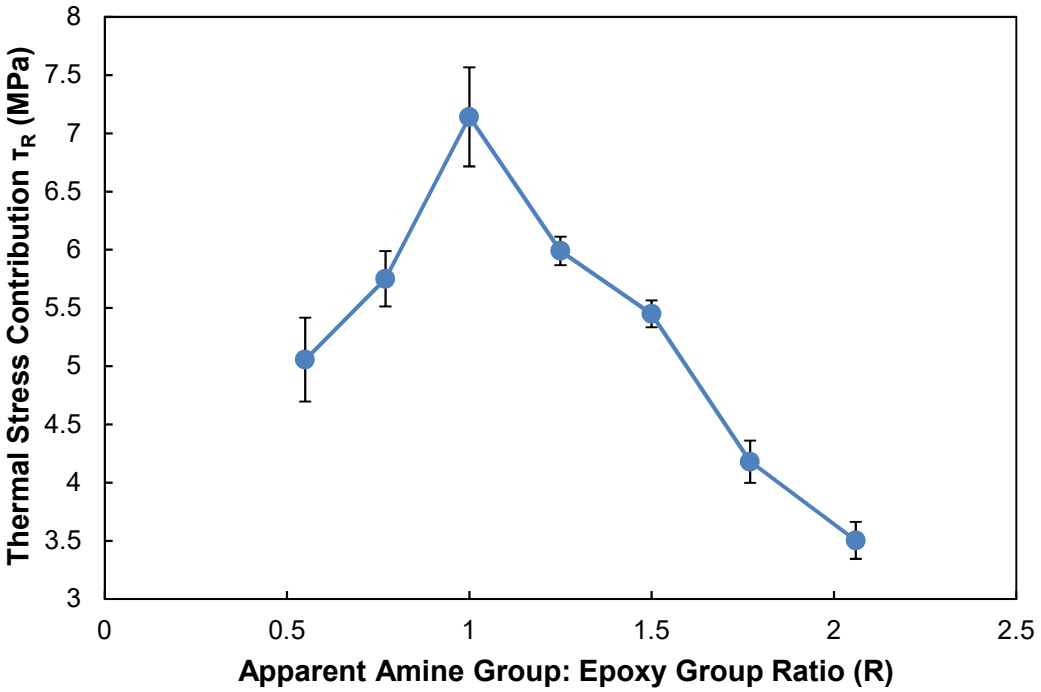

Figure 5.14 - Interfacial thermal residual stress contribution τ_R versus R value at 20 °C.

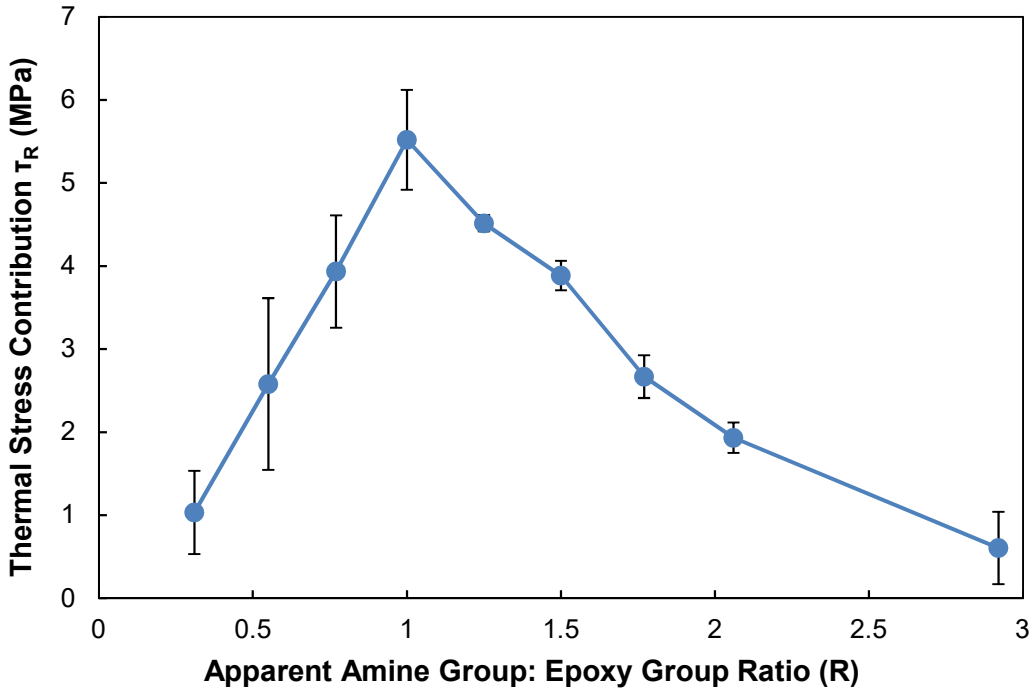

Figure 5.15 - Interfacial thermal residual stress contribution τ_R versus R value at 35 °C.

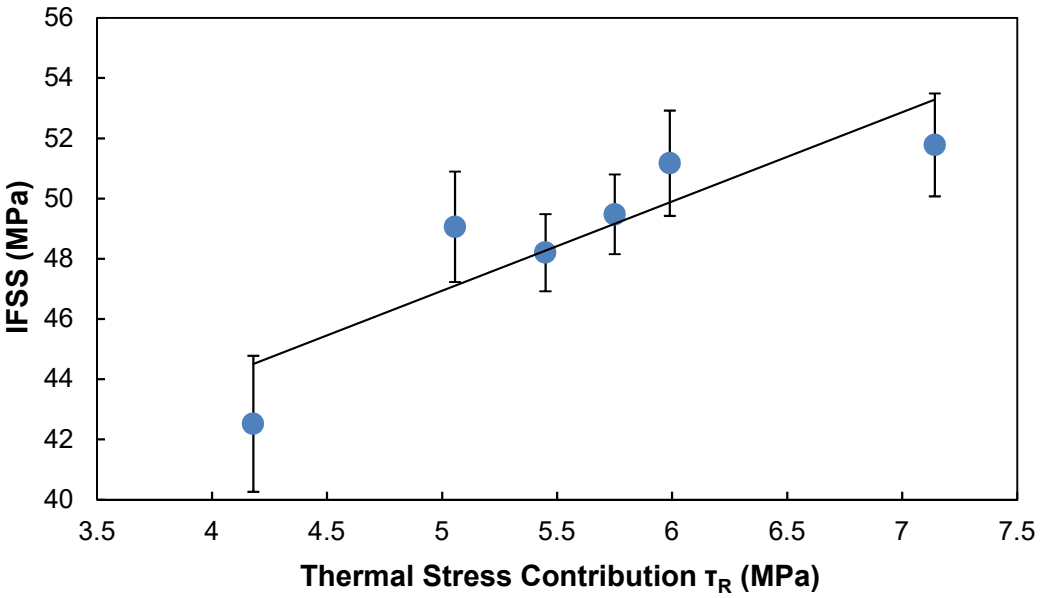

Figure 5.16 - IFSS versus interfacial thermal residual stress contribution τ_R at 20 °C.

It can be seen that as hardener was added to the epoxy system, the thermal stress contribution value changed, with a peak occurring at the stoichiometric point. Notably as the ratio deviated further from the stoichiometric value this contribution value was

shown to decrease in a manner similar to that shown for the IFSS value in Figure 5.4. This correlation is expanded upon in Figure 5.16, where the IFSS value is plotted against the respective thermal residual stress contribution. We can see that, similar to Figure 5.7, as the level of thermal residual stress at the interface was increased, the IFSS also increased.

However, despite the clear correlation shown in Figure 5.16, we can see that this contribution by the thermal residual stresses still only represents about 10% -13% of the final IFSS value. Therefore, the changes in IFSS shown in Figure 5.4 must be attributed to the decrease in size of multiple adhesion mechanisms at the interface, one of which will be the contribution of thermal residual stresses. As previously discussed, the lack of amine at low R values may prevent the formation of a strong crosslinked structure, thus resulting in a notable drop in performance for multiple thermomechanical properties associated with the strength of the interface.

Another potential contributing factor may be the variation in residual stresses formed during the curing process due to the chemical curing reaction. These stresses are known as cure shrinkage stresses. Cure shrinkage is known to occur during the thermoset reaction process, however residual stress only builds up for the cure shrinkage after gelation due to the polymer structure becoming increasingly rigid, resulting in the stresses being unable to relax away [15,21,22,65,260]. Thus, there is potential for different levels of residual stress due to cure shrinkage forming during the curing process. It has been suggested in the past that residual cure shrinkage stresses may contribute significantly more than residual thermal stresses [15,21] and thus any changes in cure shrinkage stresses may significantly impact the stress transfer capability of the interface. This topic is further explored in Chapters 6 and 7.

5.6 Summary and conclusions

In conclusion, it was shown in this chapter that the chemistry of the matrix has a major influence over the stress transfer capability of the interface. This was shown to be the case for each different silane coated fibre tested as well as for a different purity hardener. Thus, it was hypothesised that the chemistry of the matrix may have more influence in defining the level of adhesion between the fibre and the polymer than the chemistry of the fibre coating applied. However, the chemistry of the fibre coating was shown to also influence the IFSS values measured, specifically the maximum value achievable and the R value at which it would occur. Hence it could be concluded that chemistry overall does play a key role in defining the stress transfer capability of the interface in adhesion mechanisms other than just chemical bonding at the fibre surface.

Interestingly it was found that, despite the higher values for the glass transition temperature shown in Chapter 4, the higher purity TETA possessed lower IFSS values for each ratio tested when compared to the standard purity TETA until R > 1.5. Above this ratio, the higher purity TETA was found to give significantly larger IFSS values, suggesting that the impurities in standard TETA may inhibit adhesion if present in too great a quantity. A clear correlation was established between the IFSS value measured and the measured T_g value of the polymer matrix, suggesting a potential link between the two. This link was expanded upon by studying the formation of thermal residual stresses at the interface and how they could be interrelated to the stress transfer capability of the interface and matrix chemistry respectively. It was shown how the decrease in IFSS with deviating R value could be correlated to a decrease in the contribution of the thermal residual stresses formed at the interface. This suggests that thermal residual stresses can contribute significantly to the stress

transfer capability of the interface. However, this contribution still only represents around 10% -13% of the total IFSS value measured and thus other mechanisms, such as cure shrinkage stresses, must make a significant contribution.

Chapter 6. The influence of matrix chemistry and temperature on the GF – Epoxy interface

6.1 Introduction

Having investigated and discussed the influence that the matrix chemistry exerts over both the thermomechanical properties of the interface as well as the IFSS value, this chapter looks to further expand upon this work by introducing testing temperature as a variable. With the correlation discussed in Chapter 5 between the IFSS and the thermal residual stresses formed during curing, it was logical to study whether these stresses would relax away at higher testing temperatures. In theory this would then result in a drop in IFSS. The influence of testing temperature on the strength of the interface has been discussed previously by Thomason et al [14,84] for both thermosetting and thermoplastic systems, however this did not account for the importance of matrix chemistry discussed in Chapter 4 and Chapter 5. Subchapter 6.2 will discuss the influence that both the matrix chemistry and testing temperature have on the IFSS value of APS coated fibres, with comparisons made with the results presented in Chapter 5. Subchapter 6.3 will then further expand upon this by discussing the results for a GPS coated fibre (fibre 3), analysing whether surface chemistry would impact IFSS values with increasing temperature. Finally, subchapter 6.4 will compare the results presented in subchapters 6.2 and 6.3 with the residual stress model results discussed in subchapter 5.5. Analysis will be conducted into whether residual stresses formed at the interface due to a combination of chemical cure shrinkage and thermal shrinkage can contribute significantly to the stress transfer capability of the interface.

Microbond tests were performed within the furnace chamber of a thermomechanical analyser to determine the IFSS between the glass fibres and the epoxy matrix. The error bars in all plots represent 95 % confidence intervals.

6.2 The influence of temperature on IFSS with different R values

Previous studies [14,84] have shown how the stress transfer capability of the interface could be significantly influenced by the testing temperature. This was attributed to the existence of the residual stresses at the interface. However, as discussed previously, there is still a significant body of opinion that chemistry in some manner must be involved in defining the stress transfer capability of the interface. This potential link between IFSS, chemistry and residual stresses was initially explored in Chapters 4 and 5. The results presented in Chapter 5 highlighted the importance of matrix chemistry in defining the strength of the interface whilst the results presented in Chapter 4 highlighted the potential link between the R value and key thermomechanical properties linked to the residual stresses formed at the interface due to thermal shrinkage. As such, it was decided that the work presented by Thomason et al. [14,84] could be expanded upon to include the influence of changing the R value. This would allow for a better understanding of the link between matrix chemistry, the contribution of residual stresses and the stress transfer capability of the interface.

The microbond technique was adapted to allow for testing whilst in a temperature-controlled environment as discussed in subchapter 3.3.2. Epoxy resin matrices with eight different R values, systematically ranging from R ≈ 0.3 up to R ≈ 2.0, were applied as droplets to single fibres of APS coated fibre 1. Up to seven different temperatures were studied, with R ≈ 0.5, 1.0 and 2.0 being tested at each temperature

respectively. The four primary temperatures studied were 20 °C, 50 °C, 90 °C and 120 °C. The IFSS values plotted represent the average of the individual samples. After testing, samples were re-examined to identify which droplets had been tested and for analysis of any remaining meniscus as was discussed in Chapter 5.

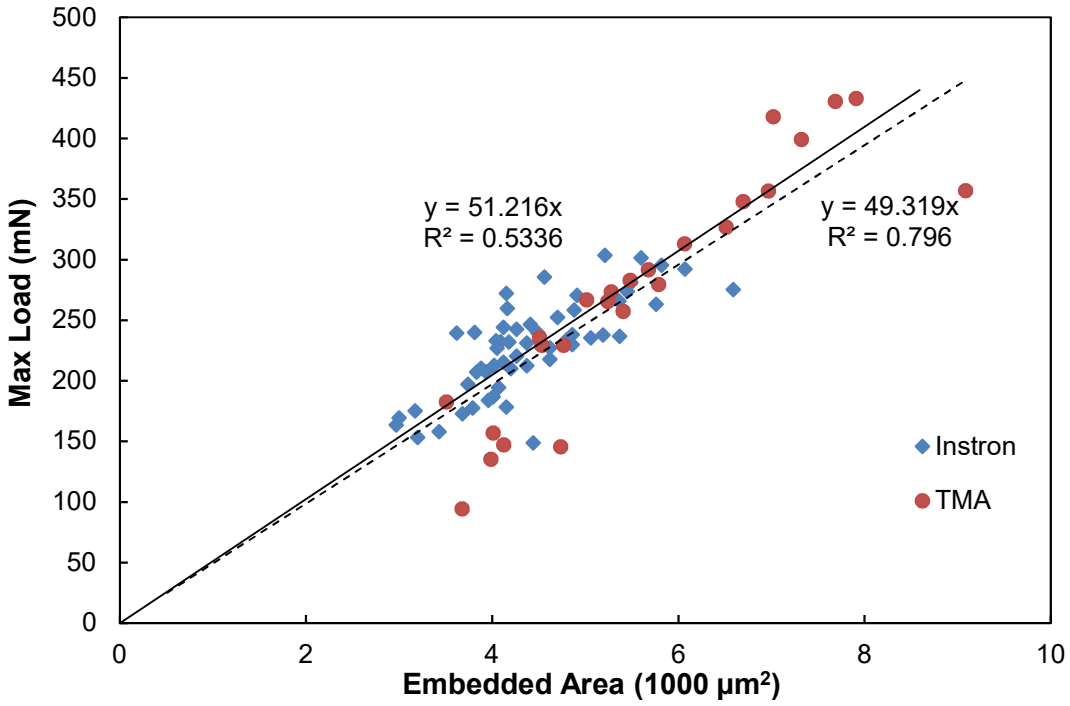

Figure 6.1 - Comparison between force/displacement plots collected using the TMA microbond technique and data collected using the Instron microbond technique, R ≈ 1.0 and testing temperature = 20 °C.

Figure 6.1 - Figure 6.4 each display peak load versus embedded area plots for the samples tested using fibre 1. Figure 6.1 shows a comparison between the TMA microbond results taken at 20 °C and the previous data collected using the Instron microbond technique in Chapter 5 for R ≈ 1.0. Overall the data collected using the TMA technique is shown to correlate well with the data collected using normal microbond testing with the trendline gradients predicting an IFSS value of 51.2 MPa for the Instron versus 49.3 MPa for the TMA. Interestingly, the R^2 value for the TMA data is shown to be significantly higher than that for the Instron microbond data. This would suggest that there is less data scatter when using the fixed blade setup

compared to the adjustable setup. Following this discovery, a more thorough investigation between the two blade setup types was carried out and is covered in more detail in Appendix A.

Figure 6.2 shows a comparison between the different testing temperatures for R ≈ 1.0. We can see that as the testing temperature was increased, the peak load of the microbond samples decreased, with a notable drop once the temperature was raised above the matrix T_g value of 82 °C.

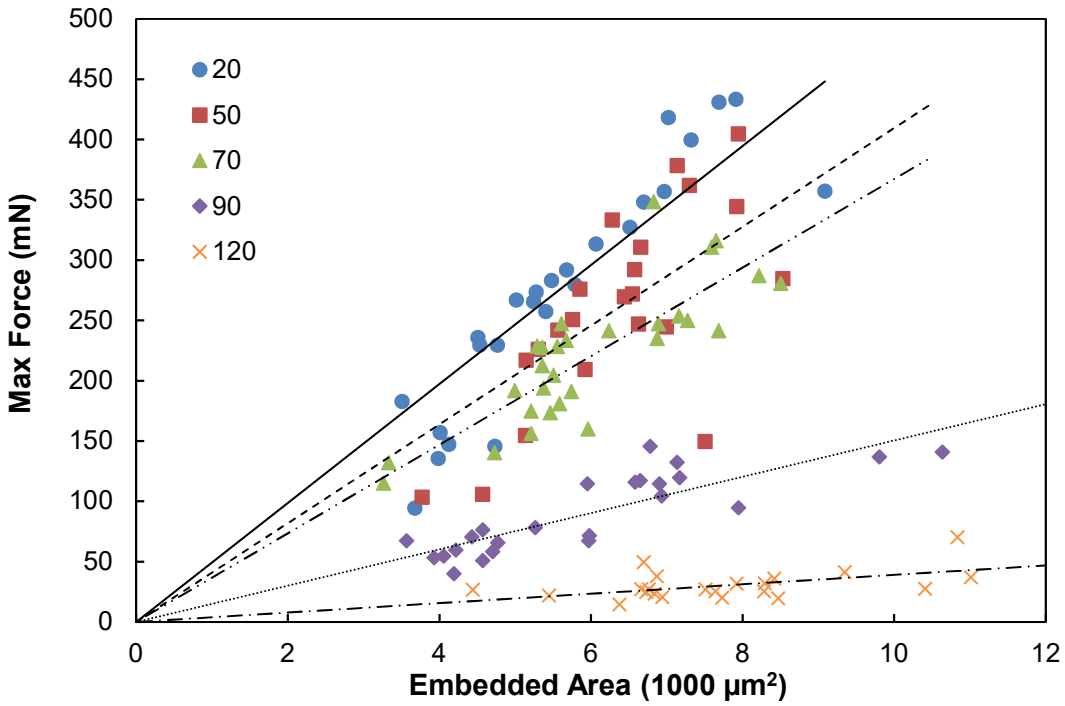

Figure 6.2 - Comparison between force/displacement plots for R ≈ 1.0 at different testing temperatures.

Figure 6.3 and Figure 6.4 show plots where the testing temperature was maintained at constant values of 50 °C and 120 °C respectively whilst the R value of the matrix system was systematically changed. At 120 °C the effect of changing the matrix chemistry appears greater than at 50 °C. The data for the three ratios is shown to be quite distinct at 120 °C with clear differences in max load shown, whereas at 50 °C the max load values measured for the different ratios appear more comparable across

the measured embedded areas. This suggests that the influence of the matrix chemistry on the magnitude of the IFSS may be greater when the testing temperature reaches a value above T_g. In addition, the plot shown in Figure 6.4 does appear to show signs of correlation with Figure 6.2, with both possessing a notable decrease in the max force as the variable was changed past a certain value. In the case of Figure 6.2 the transition occurs as the temperature was increased from 70 °C up to 90 °C. For Figure 6.4 the transition occurs when the R value decreased for R ≈ 2.1 to R ≈ 1.0.

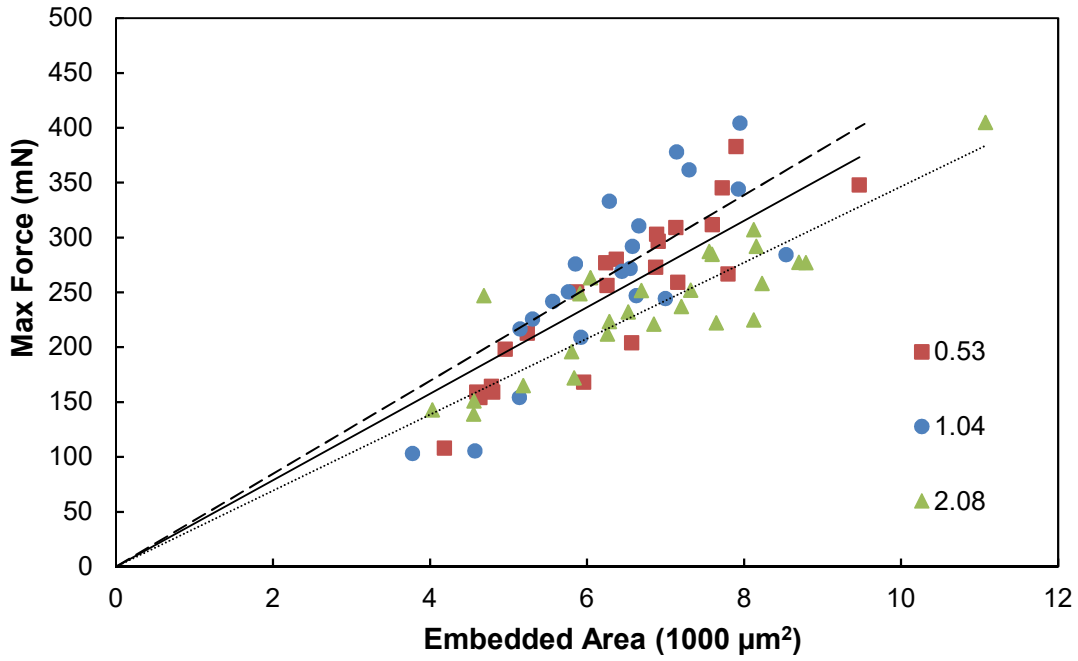

Figure 6.3 - Comparison between force/displacement plots for different R values at a testing temperature 50 °C.

Figure 6.5 presents a comparison between the IFSS values measured using the TMA microbond technique at 20 °C and the values measured using the Instron technique discussed in Chapter 5. It can clearly be seen that despite the differences in how the test is carried out there is a distinct level of correlation between the two sets of data. Both show a maximum occurring near R ≈ 1.0, with values for IFSS then dropping off the further the ratio deviated from the stoichiometric value.

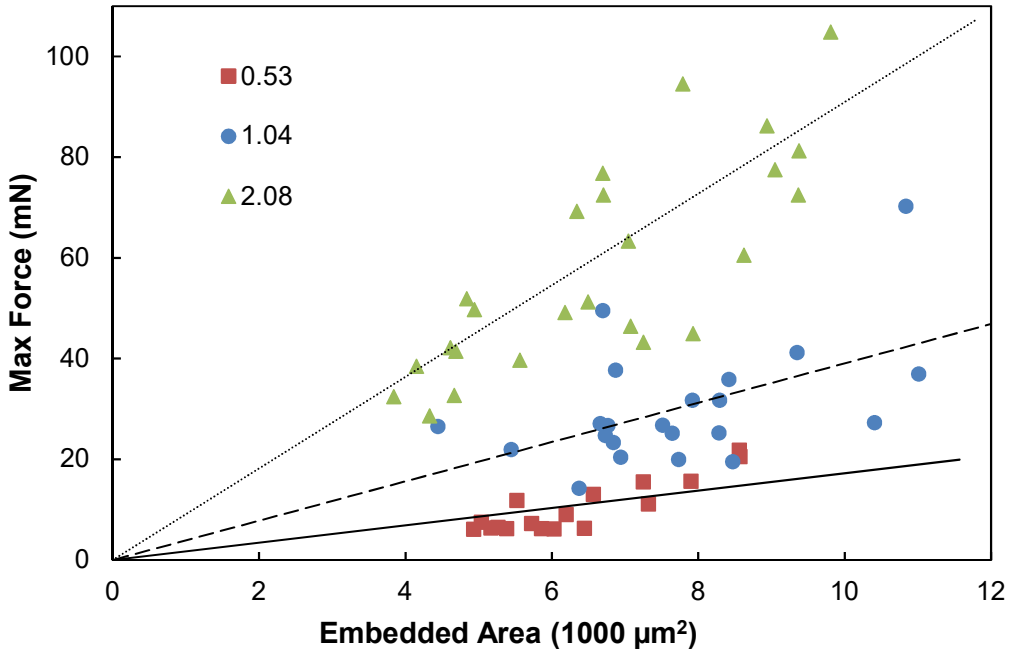

Figure 6.4 - Comparison between force/displacement plots for R values at a testing temperature 120 °C.

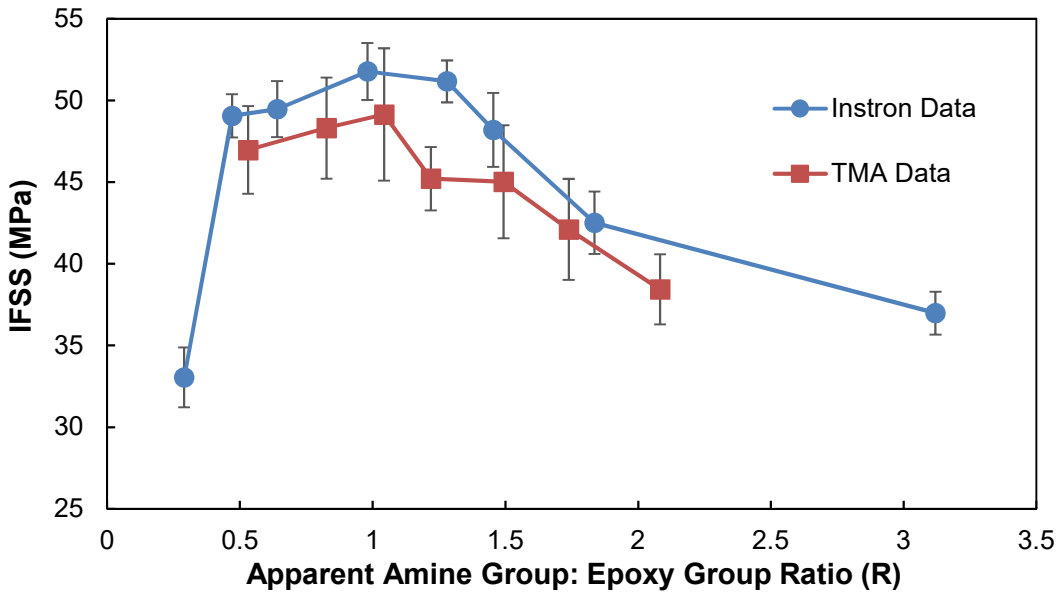

Figure 6.5 - Comparison plot of IFSS values recorded using the Instron and TMA microbond techniques for fibre 1 samples.

Figure 6.6 and Figure 6.7 present the data for IFSS values versus the testing temperature. Specifically, Figure 6.6 presents a comparison between the seven different ratios across the four primary temperatures studied. Figure 6.7 then presents

a more focussed set of data, concentrating on the ratios R ≈ 0.5, R ≈ 1.0 and R ≈ 2.0 tested at three further temperatures of -10 °C, 70 °C and 80 °C respectively. Figure 6.6 shows that the IFSS possessed an inverse dependence with the testing temperature as well as a dependence on the R value of the matrix system like that discussed in Chapter 5. The results indicated that the IFSS value decreased as the testing temperature was increased for all ratios, with R values close to the stoichiometric value initially exhibiting the largest IFSS values for temperatures ≤ 70 °C. It was hypothesised that this drop in IFSS could be correlated with the influence of matrix chemistry on the T_g of the matrix discussed in Chapter 4 and its resulting effect on the contribution of thermal residual stresses.

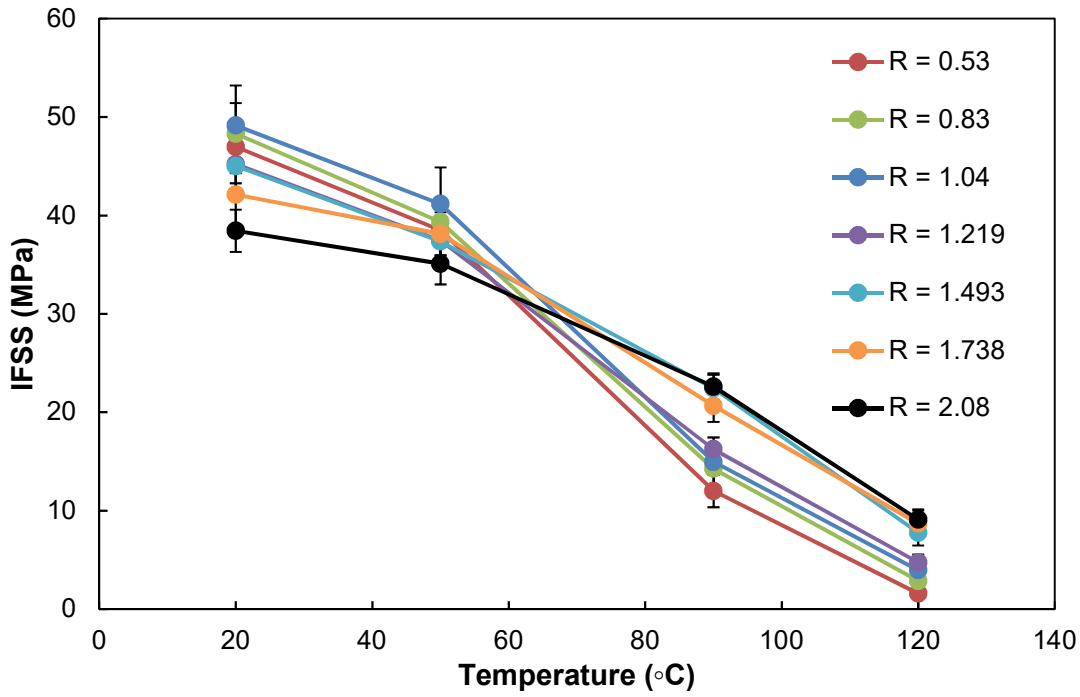

Figure 6.6 - Plot of IFSS versus Testing Temperature for Ratios R = 0.53 to R = 2.08 for four primary temperatures studied for all R values (20 °C, 50 °C, 90 °C and 120 °C) for fibre 1 samples.

However, Figure 6.6 also showed that once the testing temperature increased ≥ 70 °C, that the ratios which had excess amine (R > 1) possessed larger IFSS values than the other ratios (R ≤ 1). This is in direct contrast to ≤ 70 °C where the R > 1 ratios

possessed smaller values for IFSS. This would suggest that between 50 °C and 90 °C there exists a critical point where the value for IFSS changed relative to the R value. Hence two further temperatures were selected within this region, 70 °C and 80 °C to be studied for three of the ratios as shown in Figure 6.7. In addition to this the temperature of –10 °C was also studied to analyse whether the IFSS would continue to increase as the temperature was lowered further.

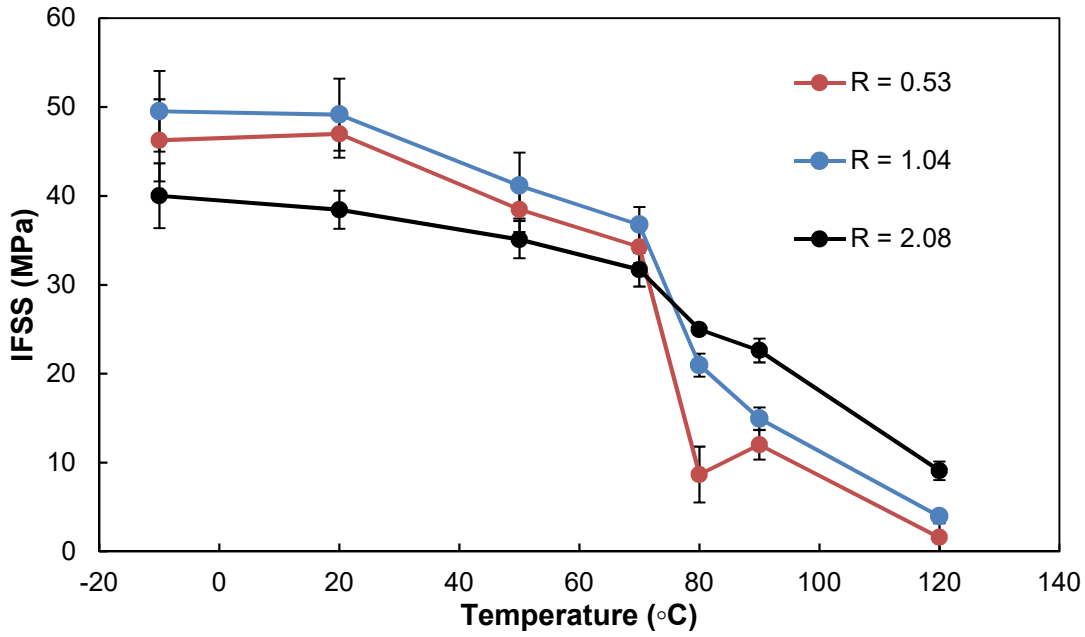

Figure 6.7 - Plot of IFSS versus Testing Temperature for Ratios R = 0.53, R = 1.04 and R = 2.08 for all temperatures tested for fibre 1 samples.

A similar trend to that shown in Figure 6.6 is present in Figure 6.7, with R ≈ 2.0 possessing a larger IFSS value once the temperature > 80 °C. Interestingly this would be below the T_g for the stoichiometric value shown in Chapter 4 but significantly higher than that shown for the other two extreme ratios. This would suggest that although T_g may have an influence in the decrease of IFSS to some degree, it may not be what is governing the transition shown at this point as previously hypothesised. The temperature dependent decrease in IFSS for R ≈ 2.0 is shown to still appear less affected by the increase in temperature than the other two ratios, which appear to

both possess a drop off point at 80 °C in terms of IFSS. The larger drop in IFSS for R ≈ 0.5 could be expected due to the larger deterioration in thermomechanical properties shown in Chapter 4, although the IFSS value at 80 °C still appears notably low. It is in fact lower than that recorded at 90 °C, suggesting that it may be an anomaly or that a phenomenon is specifically occurring in excess epoxy ratios at 80 °C which is not present for ratios where R ≥ 1.0. Interestingly it can be seen that at – 10 °C, the IFSS values for R ≈ 1.0 and R ≈ 2.0 reach a maximum value, with a slight decrease shown for R ≈ 0.5. The results for R ≈ 1.0 and R ≈ 2.0 would tend to agree with the residual stress interface contribution hypothesis. Overall judging by the trend shown it looks as though the IFSS value is likely to reach a plateau if the testing temperature is dropped lower.

The data presented in Figure 6.6 and Figure 6.7 may be replotted as a function of the R value, rather than temperature, to better illustrate some of the relationships that occur. This is shown in Figure 6.8 for each of the temperatures tested.

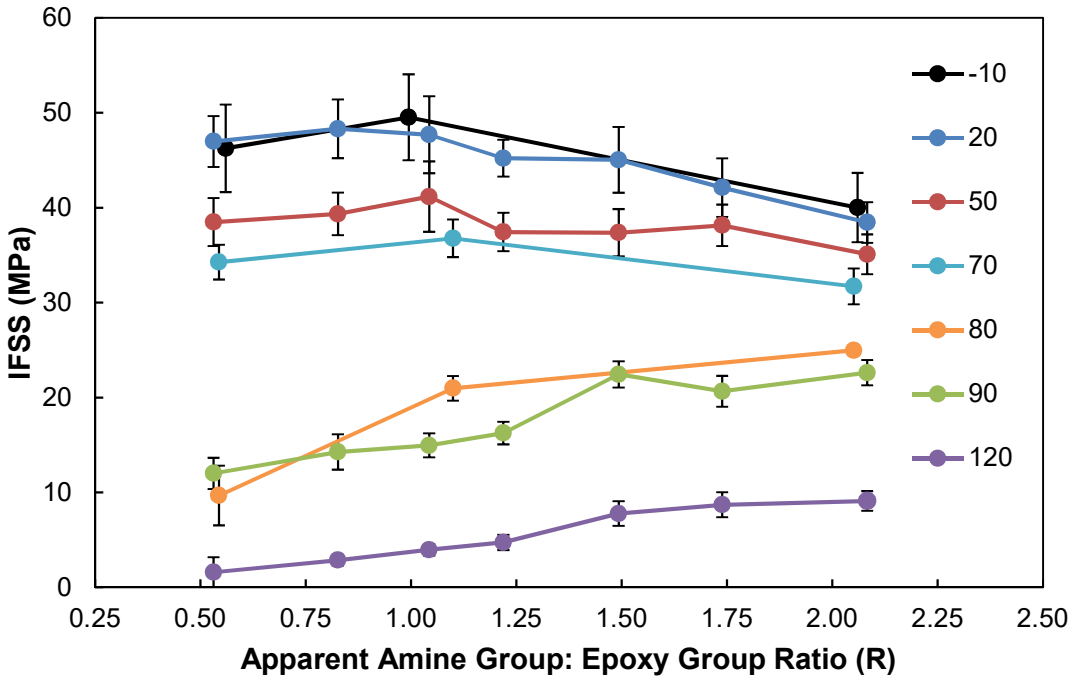

Figure 6.8 - Plot of IFSS versus the apparent Amine Group: Epoxy Group Ratio (R) for all temperatures studied for fibre 1 samples.

The distinct transition present between 70 °C and 80 °C appears much clearer in this plot, with each temperature ≥ 80 °C shown to achieve a maximum IFSS value at the highest R value. For temperatures ≤ 70 °C the maximum IFSS is achieved near the stoichiometric ratio, following the general trend found in Chapters 4 and 5. However, the trends shown in Figure 6.8 would suggest that there exists a critical testing temperature whereupon the matrix chemistry would possess no significant influence on the IFSS value. This is hinted at due to the nature of the trends for 70 °C and 80 °C, with a potential flat point existing between the two. This would likely occur closer to 70 °C due to the lines for 50 °C and 70 °C already appearing to have begun to level out relative to the other plots. This point is interesting since it would again seem to suggest that the T_g of the polymer may not play as active a role in defining the strength of the interface at this point. It appears in Figure 6.7 that the temperature dependent drop in IFSS occurs at approximately the same temperature, independent of the R value. This is in stark contrast to the changes in T_g that were shown to occur with different R values discussed in Chapter 4, thus suggesting that the drop in IFSS shown is not caused by T_g. This scenario is quite difficult to accept given all the previously assembled evidence regarding the potential link between the T_g and the stress transfer capability of the interface. Be that the case then there must exist a separate explanation which addresses the interesting trends shown in Figure 6.7. One potential explanation focuses on the applicability of taking the DSC measured T_g value for each ratio and assigning them to be that of the minute droplets tested. It could be quite possible that the T_g of these droplets is in fact different from the results discussed in Chapter 4 due to some previously unknown scaling issue. The difficulty of analysing single fibre tests and then applying their results to larger scale scenarios has previously been a point of some discussion by Piggott [150].

Using the T_g data collected in Chapter 4, it is possible to investigate this hypothesis further by constructing a plot where the IFSS is plotted against ΔT, the difference between the testing temperature (T_t) and the T_g for each ratio. This plot is shown in Figure 6.9 for three of the ratios studied. Interestingly it can be seen that the IFSS transition for R ≈ 1.0 coincides with ΔT ≈ 0, suggesting a possible connection as the polymer transitions from a glass to a rubber. However, this is shown to not be the case for the other two ratios. The plot highlights how for R ≈ 0.5 and R ≈ 2.0 that most of the values measured during the study for IFSS occur at ΔT values > 0, where the polymer in theory would be in a rubbery state. Thus, the adhesion mechanisms at work would be functioning for a rubber, not a glass. In addition, the ratio R ≈ 2.0 appears less influenced by the temperature passing across T_g relative to the other ratios. This would suggest that the adhesion mechanisms potentially at work for excess amine ratios differ for excess epoxy and stoichiometric ratios.

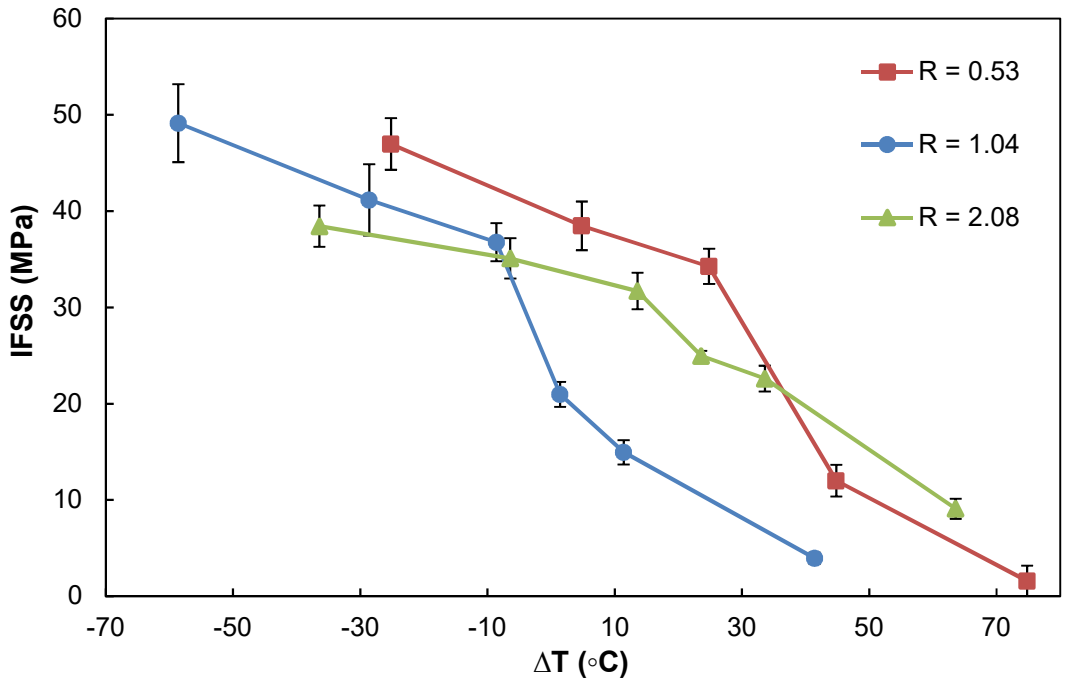

Figure 6.9 - Plot of IFSS versus ΔT, where ΔT = T_t – T_g for APS fibres.

A potential hypothesis is that at these higher temperatures, due to the polymer now being a rubber, the nature of the de-bonding process is being influenced by the R value. D'Almeida et al. have discussed [52–54] how epoxy matrices containing excess amine can possess greater deformation capacity than those at lower R values. Thus, at these higher temperatures, the higher R value matrices may be superior at maintaining the stress transfer capability at the interface whilst under load. Zhao et al. [261] also observed that higher crosslink densities negatively impact the shear failure behaviour in amorphous polymers. This would agree with what is shown in Figures 7 and 10 and explain why excess amine ratios exhibit superior performance to those ratios where R ≈ 1 However, ratios where R < 1 would also possess smaller crosslink density values [57], and thus would be expected to benefit in the same manner; yet they do not. As such it could be hypothesized that although this mechanism may be contributing to the stress transfer capability of the interface its contribution is less than other mechanisms.

Overall, the large shifts in IFSS between 70 °C and 80 °C would suggest that a notable change occurs in terms of the adhesion mechanisms governing the stress transfer capability of the interface. When the temperature is ≤ 70 °C, it appears that the mechanisms at work remain consistent in terms of contribution, with the stoichiometric ratio maintaining optimized performance. Once ≥ 80 °C, the contribution of these adhesion mechanisms appears to potentially change with any excess amine within the system beginning to aid the stress transfer capability of the interface rather than hinder it. One viable explanation for the increase in IFSS with R may be due to an increase in the level of hydrogen bonding active between molecules at the fibre/matrix interface. This would be due to the extra degree of reactive hydrogens present as the result of the excess amine. At temperatures ≥ 80 °C other adhesion mechanisms, such as residual stresses, may have potentially relaxed away to the point where the

hydrogen bonding would provide a significant contribution to the remaining strength of the interface.

In conclusion, the results presented here further highlight the clear influence that the R value of the matrix system has on the stress transfer capability of the interface. Although chemical bonding may be a contributor, chemistry appears more important when it refers to the level of amine groups versus epoxy groups within the polymer system. The decrease in IFSS with increasing temperature for all ratios was taken as support that residual stresses at the interface do contribute significantly to its strength. However, a notable part of this research refers to how the stress transfer capability of the interface is influenced by the transition of the polymer from a glass state to a rubbery state. This topic has not been studied in detail in the literature, and the results presented in Figure 6.6 - Figure 6.9 would suggest that the adhesion mechanisms change accordingly. Excess amine ratios clearly appear less influenced by this transition of states, with mechanisms such as residual stress relaxing away and others such as hydrogen bonding potentially contributing more.

6.3 The influence of fibre silane coating on IFSS with different R values and temperature

A conclusion from the literature review was that glass fibre sizings have long been viewed as being one of the crucial linchpins in influencing the stress transfer capability of the interface. Specifically a large amount of research has been invested into studying chemical coupling agents, such as silanes, to ensure a bond will form between the inorganic glass fibre and the organic thermoset polymer [24,98,108,258,262,263]. As such the discussion has focussed heavily on the importance of chemistry and chemical bonding between the fibre, sizing and polymer. However, the research presented in Chapter 5 of this thesis suggested that although

the chemistry of silane did play a role in defining the ultimate IFSS measured, it did not appear to be the main mechanism dictating the strength of the interface. In fact, the results highlighted the clear importance of the R value in the matrix system in defining the stress transfer capability of the interface. Close to the fibre surface the R value may be influenced by the chemistry of the sizing applied to the fibre, ultimately leading to local changes in thermomechanical properties of the matrix and thus in the strength of the interface. With the results discussed in Chapter 5 and the initial results gathered using TMA microbond for an aminosilane sized fibre it was felt necessary to conduct a study using an epoxy silane sized fibre (fibre 3) to see if, again, the chemistry of the silane only played a small role. Samples were prepared as described in subchapter 6.2 with up to six different temperatures studied. Given the results shown in subchapter 6.2 and time constraints it was decided to only study three different R values: $R \approx 0.55$, $R \approx 1.01$ and $R \approx 2.05$ respectively. It was accepted that the span of these ratios would be wide enough to encompass any major changes occurring as the ratio changes from possessing excess epoxy groups to excess amine groups.

Figure 6.10 shows an IFSS versus testing temperature plot for fibre 3 which was coated with GPS. Correlation between this plot and that shown in Figure 6.6 for fibre 2 samples can clearly be seen regarding the significant decrease in IFSS with temperature. At 20 °C the IFSS is shown to be a maximum value at the stoichiometric ratio. $R \approx 0.55$ provides the next largest IFSS value whilst $R \approx 2.05$ provides the smallest IFSS value. This correlates with the data shown in Figure 6.6 where IFSS is optimized at the stoichiometric ratio, with excess epoxy ratios initially possessing larger IFSS values than excess amine ratios whilst at 20 °C. The IFSS values for each ratio are then shown to decrease as the testing temperature was increased, with the excess amine ratio again possessing larger IFSS values once the temperature was

raised above 70 °C. This data would tend to agree with the hypothesis presented in Chapter 5, that chemistry of the fibre coating ultimately does not seem to have the same degree of influence over the IFSS values as the chemistry of the matrix system.

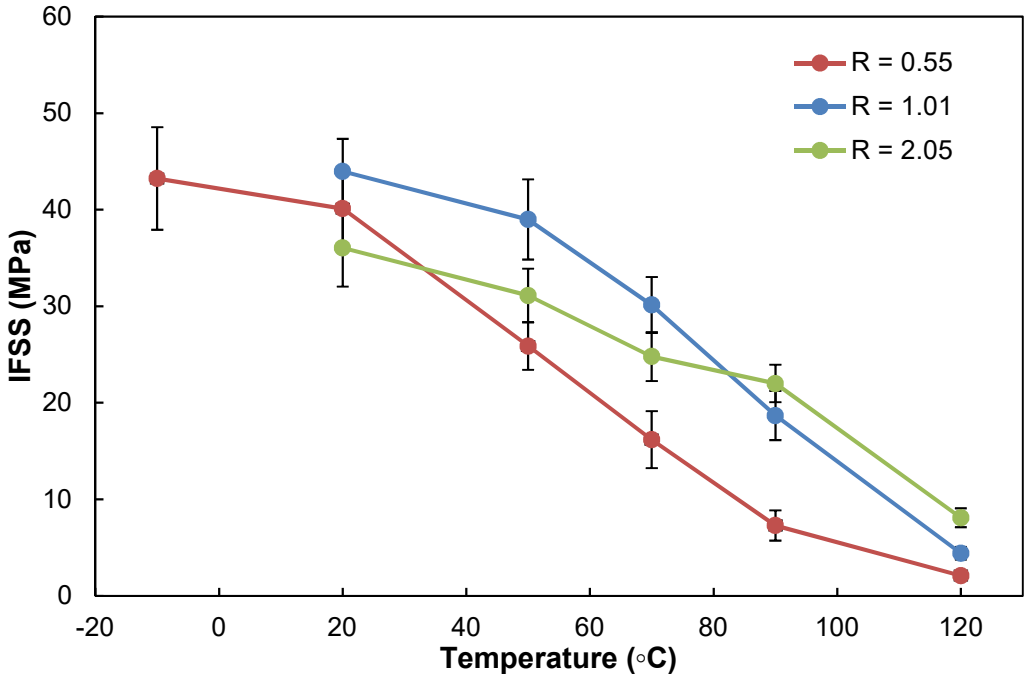

Figure 6.10 - Plot of IFSS versus Testing Temperature for Ratios R = 0.55, R =1.01 and R = 2.08 for fibre 3 samples.

The data trends shown with increasing temperature appear consistent between the two different silanes tested, with the notable difference being the actual IFSS values measured at each temperature for each of the ratios. The results would also again suggest that the decrease in IFSS with temperature is partially due to the relaxation of residual stresses which had formed at the interface during curing. Both Figure 6.6 and Figure 6.10 exhibit a similar decline in IFSS with temperature that would coincide with the modulus of the matrix decreasing. Thus, the overall trend can be seen to not be significantly influenced by the chemistry of the silane but by the R value of the system. It is then the resulting influence on the residual stresses that are present at the interface due to the R value that are influencing the stress transfer capability.

Figure 6.11 presents the data in Figure 6.10 shown instead as a function of the R value, as was the case with Figure 6.6 and Figure 6.8. The trend of IFSS increasing with R once the temperature increases > 70 °C can again be seen quite distinctly when compared to the lower temperatures. Interestingly the plot differs from Figure 6.8 in that it does not suggest the existence of a temperature where IFSS is unaffected by the R value. Instead it appears for the fibre 3 samples that the drop between 70 °C and 90 °C is significantly smaller.

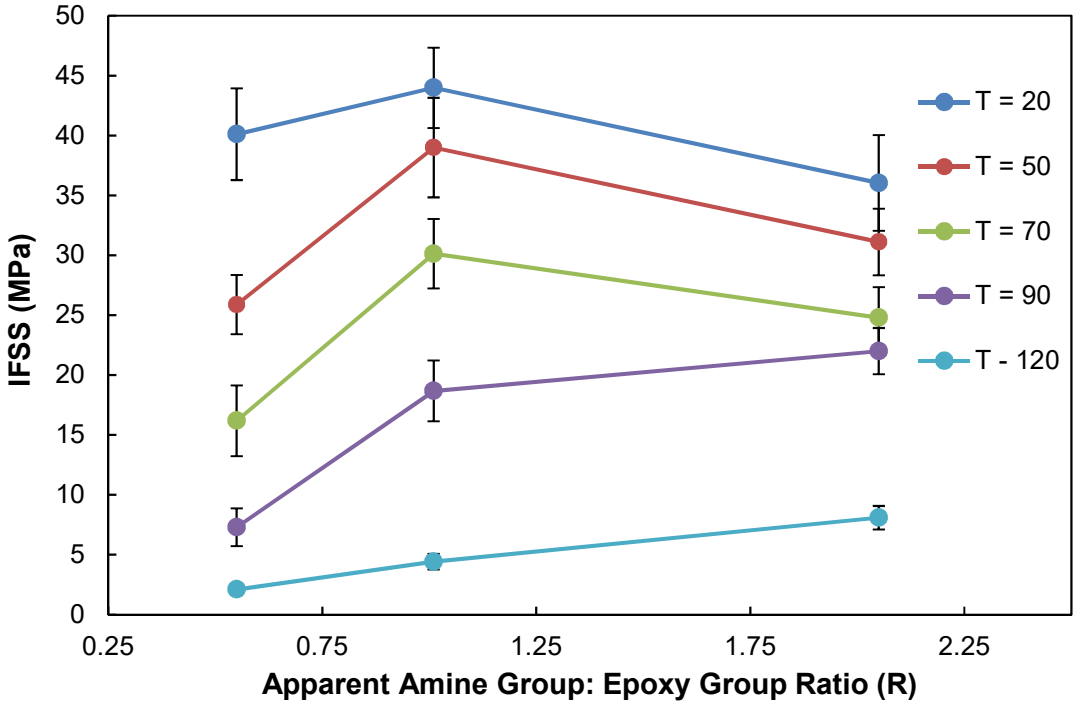

Figure 6.11 - Plot of IFSS versus the apparent Amine Group: Epoxy Group Ratio (R) for all temperatures studied for fibre 3 samples.

As was the case in Chapter 5, the values presented in Figure 6.6 and Figure 6.10 show that the IFSS values measured for each ratio are smaller for fibre 3 than for fibre 2. This difference only disappears once the temperature is raised all the way up to 120 °C, where values for both fibres are closer for the amine-rich ratio R ≈ 2.0. This would reinforce the hypothesis that adhesion mechanisms such as hydrogen bonding are dominant at this temperature in providing the strength of the interface. Despite the

different silane coatings of the fibres, at R ≈ 2.0 there would be a significant amount of unreacted amine groups within the matrix system that would provide a large degree of reactive hydrogens into the system. This would result in an increase in hydrogen bonding and may account for why the stress transfer capability of the interface remains above 5 MPa for some ratios.

One distinct difference that can be seen when comparing Figure 6.6 and Figure 6.10 relates to the decrease in IFSS for the different ratios measured with increasing temperature. A comparison between the different silanes is shown in Figure 6.12

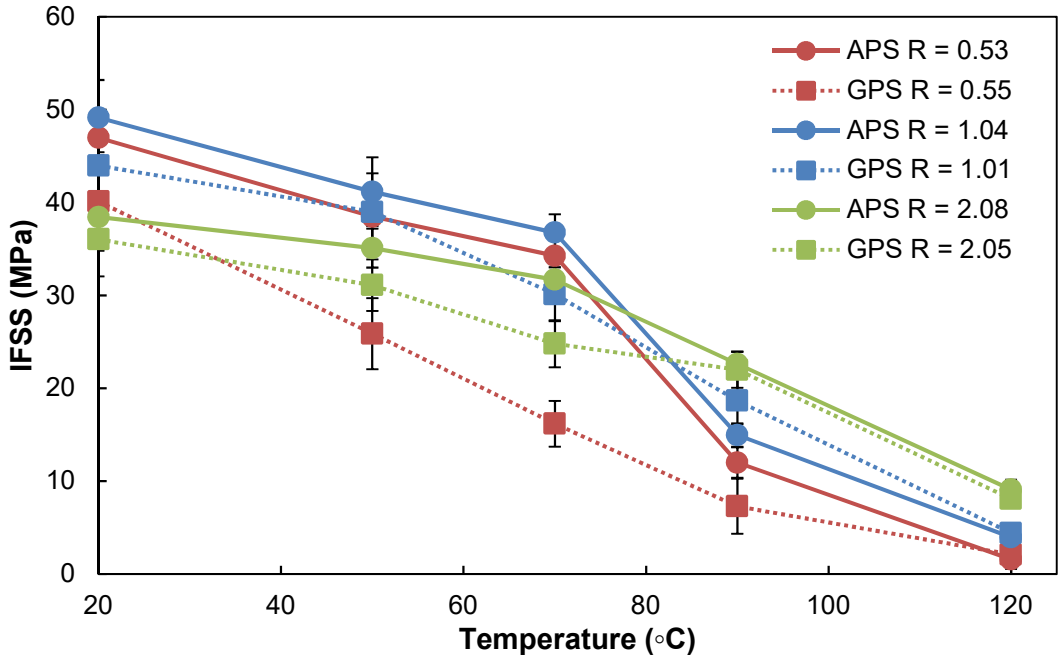

Figure 6.12 - Plot comparing results for R ≈ 0.5, R ≈ 1.0 and R ≈ 2.0 for both silanes studied.

For the GPS sized fibres (fibre 3) it can be seen that IFSS values for R ≈ 0.5 and R ≈ 1.0 tend to decrease in a more linear manner when compared to the APS fibres. The APS samples are shown to possess a significant transition point at ≈ 70 °C when R ≈ 0.5 and R ≈ 1.0 where the IFSS value drops by ≈ 20 MPa. This does not seem to exist for the GPS samples. In addition to this the difference between silanes for the R ≈ 0.5 ratio is quite distinct, with the GPS samples possessing significantly smaller IFSS

values up until 120 °C. For R ≈ 2.0, the IFSS values between the APS and GPS samples appear very comparable, with the overall trend with temperature shown to be very similar. Again, GPS samples appear to have consistently lower IFSS values at the R value until the temperature increases above 70 °C. The trend of smaller IFSS values would agree with the data discussed in Chapter 5 when the different fibre coatings were compared, with the IFSS values of the GPS fibres dropping away at a higher ratio value than the other silanes. The data shown in this subchapter would thus again suggest that the extra epoxy groups provided by the GPS coating are effectively lowering the relative R value of the system. This would negatively impact several of the key thermomechanical properties of the interface as discussed in Chapter 4 and result in a corresponding drop in the IFSS value. The extra amine groups provided by the APS silane would do the opposite for excess epoxy ratios (R < 1) hence explaining the larger IFSS values measured for R ≈ 0.5 and the more comparable values for the two measured ratios.

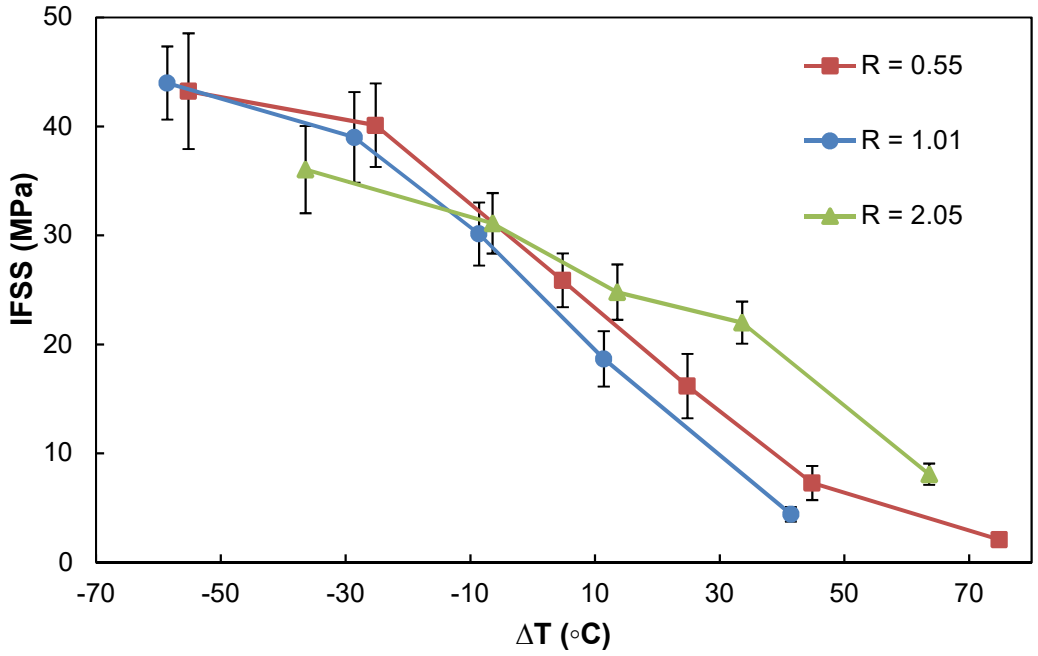

Figure 6.13 - Plot of IFSS versus ΔT, where $\Delta T = T_t - T_g$ for GPS fibres.

As was the case in subchapter 6.2, it was possible to re-plot the IFSS data as a function of ΔT to understand the influence of T_g. The plot is shown in Figure 6.13. Interestingly the data for R ≈ 0.5 and R ≈ 1.0 appears to correlate significantly better for the GPS fibres than for the APS fibres shown in Figure 6.9. It can be seen in Figure 6.9 that the data for R ≈ 0.5 seems to correlate more with the data for R ≈ 2.0. Thus, there does appear to be a notable difference between using the two different silanes. However, the main influence over IFSS appears to be the chemistry of the matrix system, with the general trend of decreasing IFSS with increasing temperature shown to occur for both silanes. This would follow the hypothesis that chemistry is indeed important to the strength of the interface, but that it is dictated more by the R value than chemical bonding due to fibre coatings.

6.4 Contribution of total potential residual stress

On reviewing the results shown in Figure 6.6 - Figure 6.13, it can be seen that the IFSS showed a significant inverse dependence on the testing temperature for both the APS and GPS fibres. With that in mind it would suggest that the deterioration in IFSS was due to factors other than a decrease in chemical bonding at the interface. One potential explanation is the existence of residual radial compressive stresses that may contribute significantly to the stress transfer capability of the fibre-matrix interface [14,21,84] as originally discussed in Chapter 5.

Taking the thermal residual stress data discussed in Chapter 5 and combining it with the TMA microbond data presented allows us to compare the IFSS value for each ratio versus the residual stress contribution to the interfacial stress transfer capability (τ_R) for the APS coated fibres. The calculations were completed using a MATLAB program originally developed by Dr Liu Yang [67]. Figure 6.14 shows the comparison for the stoichiometric value (R ≈ 1.0) whilst Figure 6.15 and Figure 6.16 show

comparable plots for ratios of R ≈ 0.53 and R ≈ 2.06 respectively. It can be seen that for each R value there is some level of correlation between the IFSS decrease with temperature and the relaxation of the residual stresses due to thermal shrinkage as the testing temperature was raised. However, it is also clear that the residual stresses due to thermal shrinkage could only be making a small contribution to the overall IFSS values observed in the system.

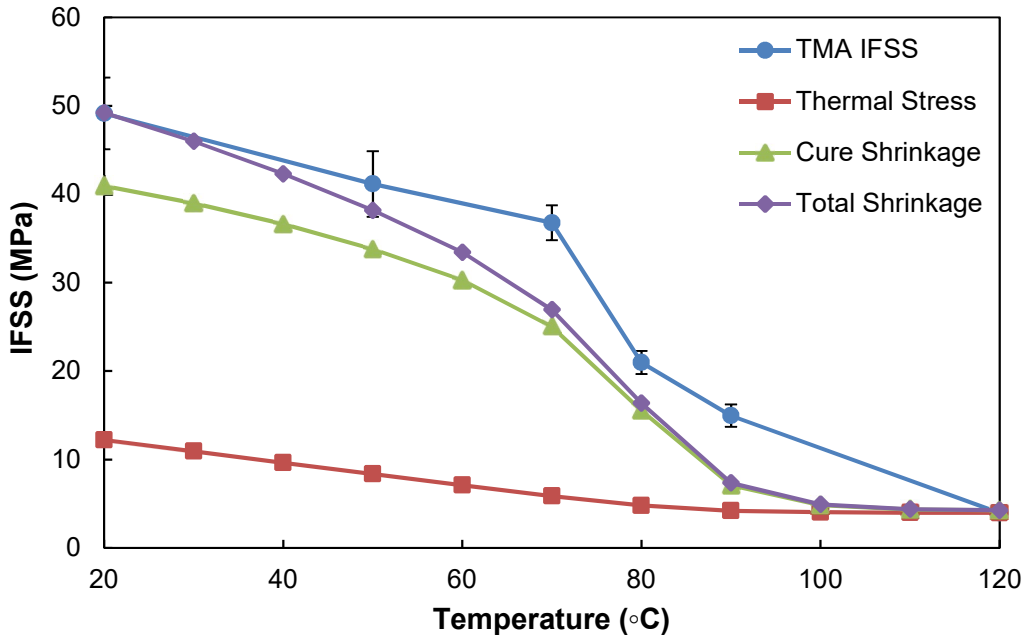

Figure 6.14 - Comparison of glass fibre epoxy IFSS with calculated residual radial stresses for an amine-to-epoxy group ratio of R ≈ 1.0 (the stoichiometric value) for APS coated fibre.

One significant difference between thermosetting and thermoplastic systems is that thermosets will undergo chemical shrinkage during the curing process due to the polymerization reaction. This cure shrinkage can result in significant volumetric changes, applying a large degree of strain to the system. Di Landro and Pegoraro have previously discussed that cure shrinkage may actually provide the bulk of the residual stresses when compared to thermal shrinkage stresses [22] in thermoset systems. However, any cure shrinkage that occurs before the gel point of the system can potentially relax away. This can be attributed to the low molecular weight and

liquid nature of the matrix in this state. Gelation is defined as the liquid–solid transition of an epoxy resin that occurs when the average molecular weight approaches infinity. One can reasonably assume that any strain induced by cure shrinkage will require more time to relax away as the system approaches the gel point. Thus, presumably once the gel point is exceeded then any further cure shrinkage related residual strain will be locked into the epoxy network. As the system is cooled back through T_g the matrix modulus will increase and consequently the residual stress from the cure shrinkage strain will increase in proportion to the matrix modulus. This hypothesis fits with the relationships observed in Figure 6.6 and Figure 6.10 where the increase in temperature would lead towards this stress potentially relaxing away. Applying this hypothesis, using the modulus data from Chapter 4 and applying an isothermal volumetric cure shrinkage value of -6% [12,19,31,32] produces the additional stress curves shown in Figure 6.14 - Figure 6.16.

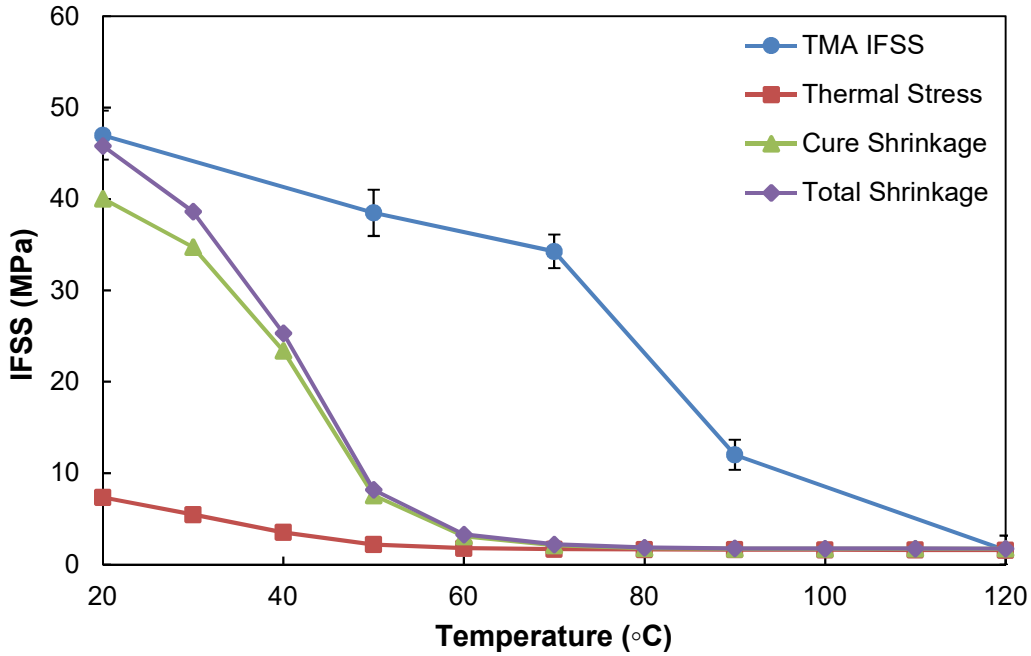

Figure 6.15 - Comparison of glass fibre epoxy IFSS with calculated residual radial stresses for an amine-to-epoxy group ratio of R ≈ 0.53 for APS coated fibre.

The residual stress contribution due to cure shrinkage appears to be significantly larger than that provided by the thermal shrinkage for each ratio. This is in agreement with the results discussed by both Thomason [84] and Jakobsen [21].

Similar plots may be constructed using the TMA generated IFSS data for the GPS coated fibres discussed in subchapter 6.3 as shown in Figure 6.17 - Figure 6.19. Again, good correlation can be seen in Figure 6.17 between the measured TMA IFSS values and the model for R ≈ 1.0. Interestingly the correlation for R ≈ 0.55 shown in Figure 6.18 appears slightly improved than that shown for the APS fibres. However, the same overall issues discussed for the APS fibre for R ≈ 0.5 and R ≈ 2.0 appear to occur for the GPS fibre plots also.

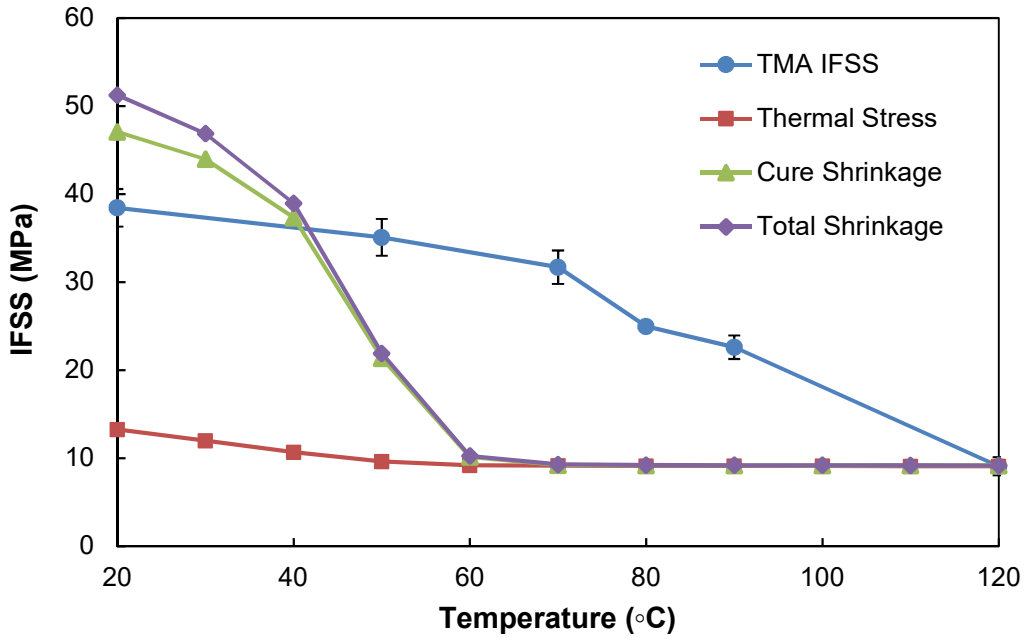

Figure 6.16 - Comparison of glass fibre epoxy IFSS with calculated residual radial stresses for an amine-to-epoxy group ratio of R ≈ 2.06 for APS coated fibre.

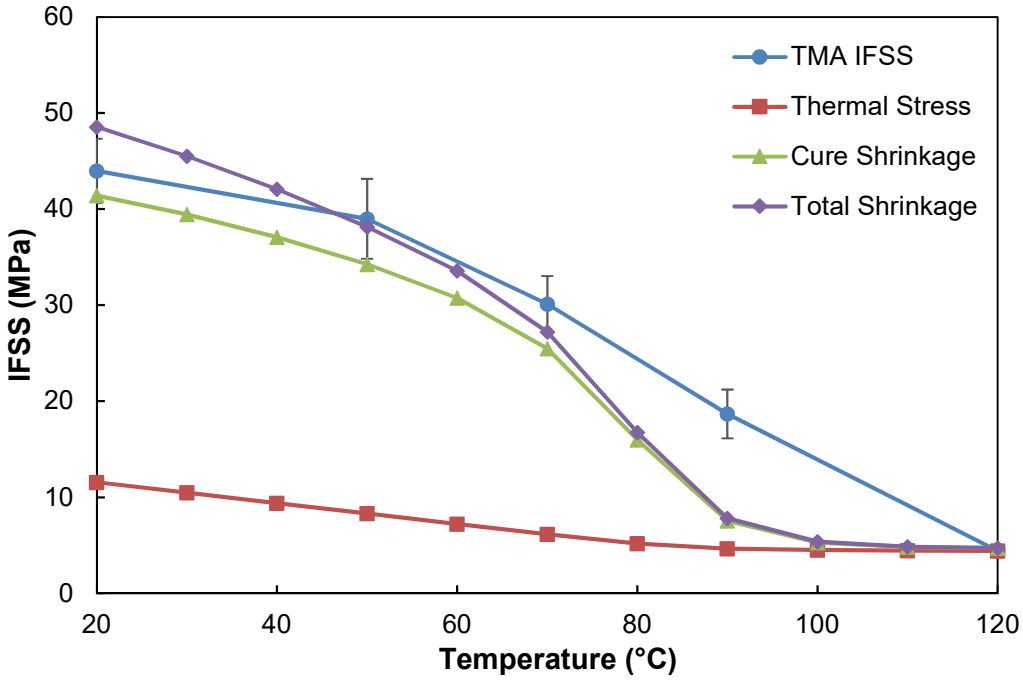

Figure 6.17 - Comparison of glass fibre epoxy IFSS with calculated residual radial stresses for an amine-to-epoxy group ratio of R ≈ 1.0 (the stoichiometric value) for GPS coated fibre.

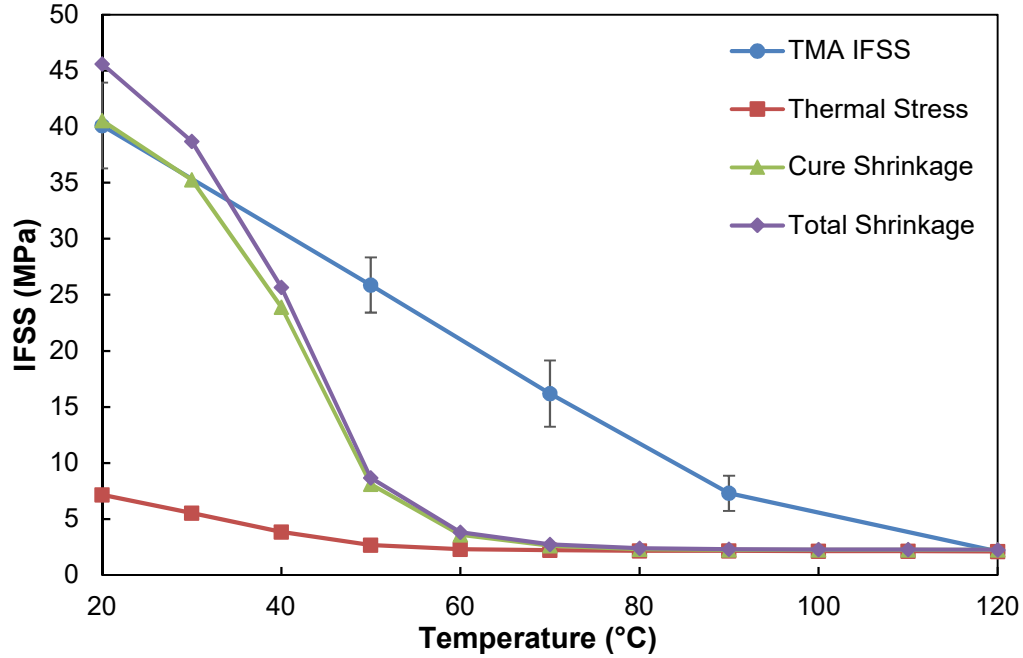

Figure 6.18 - Comparison of glass fibre epoxy IFSS with calculated residual radial stresses for an amine-to-epoxy group ratio of R ≈ 0.55 for GPS coated fibre.

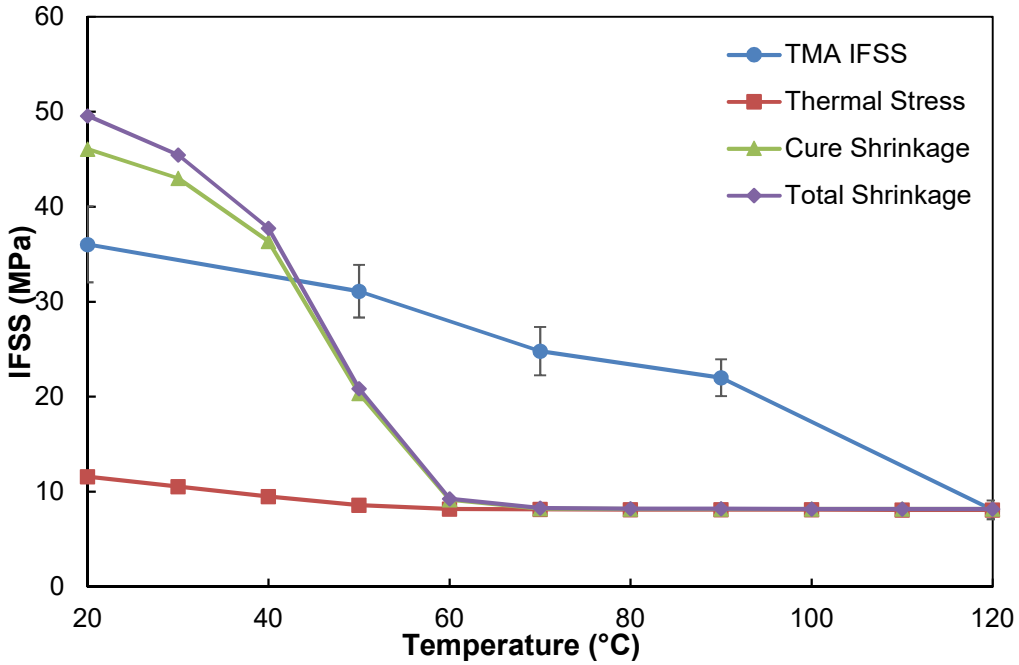

Figure 6.19 - Comparison of glass fibre epoxy IFSS with calculated residual radial stresses for an amine-to-epoxy group ratio of R ≈ 2.05 for GPS coated fibre.

Figure 6.14 - Figure 6.19 show that the residual radial compressive stresses at the interface could indeed be contributing significantly to the stress transfer capability of the interface at room temperature. The sum of the thermal and cure shrinkage contributions produces a value comparable in magnitude to that measured using the microbond technique. This was particularly the case for ratios close to the stoichiometric value, where good correlation was shown as in Figure 6.14 and Figure 6.17.

However, it appears that the decrease of IFSS at temperatures > T_g cannot be due to the residual stresses at the interface relaxing away alone, particularly in the case for the extreme ratios studied. Specifically, at 120 °C there is still a distinct level of adhesion shown to remain between the fibre and matrix, at a point where it would have been expected that all the residual stresses would have relaxed away. This would fit with the hypothesis discussed in subchapter 6.2 that hydrogen bonding could

be a larger contributor to the strength of the interface at the higher ratios and temperatures.

Analysing Figure 6.14 - Figure 6.19, whilst the assumptions for the model appear acceptable for the stoichiometric ratio (R ≈ 1.0), the model appears to be less accurate once the ratios tend to extreme levels of excess epoxy or amine. For R ≈ 0.5 the residual stresses appear to relax away before the IFSS begins to decrease, whilst for R ≈ 2.0 the model predicts a distinctly larger IFSS value at room temperature than was measured and again falls away before the IFSS decreases. This was shown to occur for both silanes, however the effect described for R ≈ 0.5 appeared less prominent for the GPS fibre. Unless there is something fundamentally missing in our understanding of the T_g of a microdroplet then both cases would suggest that the model may be an over simplification for the complex mechanisms at work when the R value is not near stoichiometry. Whilst it is clear that residual stresses do contribute to the stress transfer capability of the interface, other mechanisms must contribute more for ratios off-stoichiometry.

One assumption made for the models which may explain the extra contribution shown for R ≈ 2.0 is the use of a constant value, and 100 %, of cure shrinkage in the model calculations. This does not account for the fact that a large percentage of the cure shrinkage related strain would have relaxed away before the resin reached gelation. Thus, the degree of shrinkage frozen into the matrix structure would be influenced by the gel point of the system, as well as the degree of shrinkage that occurred. The level of cure shrinkage in epoxy matrices has been shown to change with different curing schedules [25,60,61] and with the influence of different R values on cure kinetics [243,257]. It can be hypothesized that a similar relationship may exist between matrix chemistry, cure shrinkage, residual interfacial stress and interfacial stress transfer capability.

6.5 Summary and conclusions

The results presented in this chapter show that the R value, testing temperature and fibre silane coating can each influence the stress transfer capability of the interface in a glass fibre reinforced epoxy composite. The IFSS was shown to possess an inversely dependent relationship with the testing temperature and was found to change for each R value studied. Below the matrix T_g values measured in Chapter 4, the highest IFSS value was shown to occur at the stoichiometric value, with IFSS decreasing as the ratio deviated further from this value for both types of silane coated fibres. However, as the IFSS testing temperature was increased a transition in IFSS was observed when the testing temperature exceeded 70 °C for the APS coated fibres. The GPS coated fibre data differed in that the observed decrease in IFSS with increasing temperature appeared much more linear with increases in temperature.

Whilst interfacial performance continued to decrease overall after this point, the optimum relative IFSS value was shown to improve linearly when more amine was added to the epoxy system. This was the case even when the testing temperature was raised further to 120 °C. It was shown that there was some correlation between the deterioration in IFSS and the potential relaxation of the “frozen in” residual stresses at the interface as the temperature was increased. This was shown particularly for R values close to the stoichiometric value. It was also observed that at temperatures well above T_g a small value of IFSS still existed, despite the residual stresses probably having relaxed away completely. It was hypothesized that a combination of increased level of hydrogen bonding and variation in shear failure behaviour of the matrix due to the differing crosslink densities was potentially responsible for this remaining strength.

Despite the correlation shown between residual stress and IFSS, assumptions made by the model appeared to be oversimplifications once the matrix R value deviated significantly from the stoichiometric value. The potential contribution of cure shrinkage stresses to the interface was shown to be large enough that more research was required to address some of the unknowns and assumptions. Specifically, more work regarding the link between cure shrinkage, matrix chemistry and the gel point of the polymer was required to ascertain the potential total contribution of the residual stresses at the interface to its stress transfer capability.

Chapter 7. The influence of matrix chemistry on the cure shrinkage of polymer matrix

7.1 Introduction

Having analysed and discussed the potential contribution of residual stresses to the interface using thermomechanical analysis in Chapter 6, it was shown that the bulk of the contribution would be provided by cure shrinkage as shown in Figure 6.14 and Figure 6.17. This conclusion agreed with that made by Jakobsen et al. [21] and Thomason et al. [15]. However, it was also shown that the model used was less accurate once the R value began to deviate significantly from the stoichiometric value. In particular, the contribution of the residual stresses was shown to relax away for off-stoichiometric values before the IFSS began to significantly decrease. Consequently, it was clear that an investigation was required to better understand the link between the R value and the resulting chemical shrinkage of the polymer. To achieve this a number of different techniques were used, including a novel technique designed to allow for the measurement of the shrinkage of an epoxy microdroplet on a single fibre during curing. Subchapter 7.2 introduces this novel technique and reviews the results obtained. The phenomenon of microdroplet deformation is also introduced and discussed. Subchapter 7.3 provides the results of another previously reported shrinkage characterisation technique designed to use the TMA [60,64]. Subchapter 7.4 discusses results obtained on cure shrinkage using a modified version of the rheometry technique reported in past literature. Analysis of the influence of the matrix chemistry on the gel point of the matrix system is also discussed. Finally, subchapter 7.5 re-examines the residual stress plots initially discussed in Chapter 6 with the updated measured cure shrinkage values.

7.2 Hot Stage Microscopy

7.2.1 Technique Results

It was established in Chapter 6 that the residual radial compressive stresses at the interface could potentially contribute significantly to its stress transfer capability. The bulk of this contribution was, in theory, provided by the chemical cure shrinkage stresses that form during the curing process. However, the simplified model used in Chapter 6 made use of a constant value for cure shrinkage. This appeared to be an oversimplification of the model, with its ability to match the measured IFSS values appearing to decrease the further the R value deviated from the stoichiometric value. It was previously shown in Chapter 4 that stresses formed due to thermal shrinkage could be significantly influenced by matrix chemistry. As such it was hypothesised that matrix chemistry would have a similar influence over the stresses formed due to cure shrinkage. Thus, this relationship had to be studied in detail to establish whether this was indeed the case.

Since the bulk of the interface research conducted within this thesis involved microdroplets of epoxy resin, it was required that a technique be designed to allow for analysis of the shrinkage of such microdroplets during curing. No such technique had been previously discussed in the literature, with cure shrinkage techniques primarily requiring larger samples of resin to study. Thus, in collaboration with Dr Liu Yang, a novel technique was designed using a hot-stage microscope to monitor the curing process. The setup and technique used is discussed in further detail in subchapter 3.4.1. This investigation built on the initial studies conducted by Daniel Simpson for his undergraduate thesis.

Seven different R values were selected for the study, with the values systematically ranging from R ≈ 0.5 to R ≈ 2.0 in blocks of 0.25. The samples were prepared as

discussed in subchapter 3.4.1 and cured in the hot-stage using a modified version of the curing schedule used throughout this thesis. At least five samples per ratio were studied using this temperature program. Two further samples per ratio were studied using the full curing schedule discussed in 3.3.1.1. Photos were taken at one-minute intervals throughout the cure to track the change in microdroplet dimensions. The samples were then left to cool for 24 hours before then being photographed once more. These photos were then analysed using the image processing software Image J and a normalised volumetric change plotted.

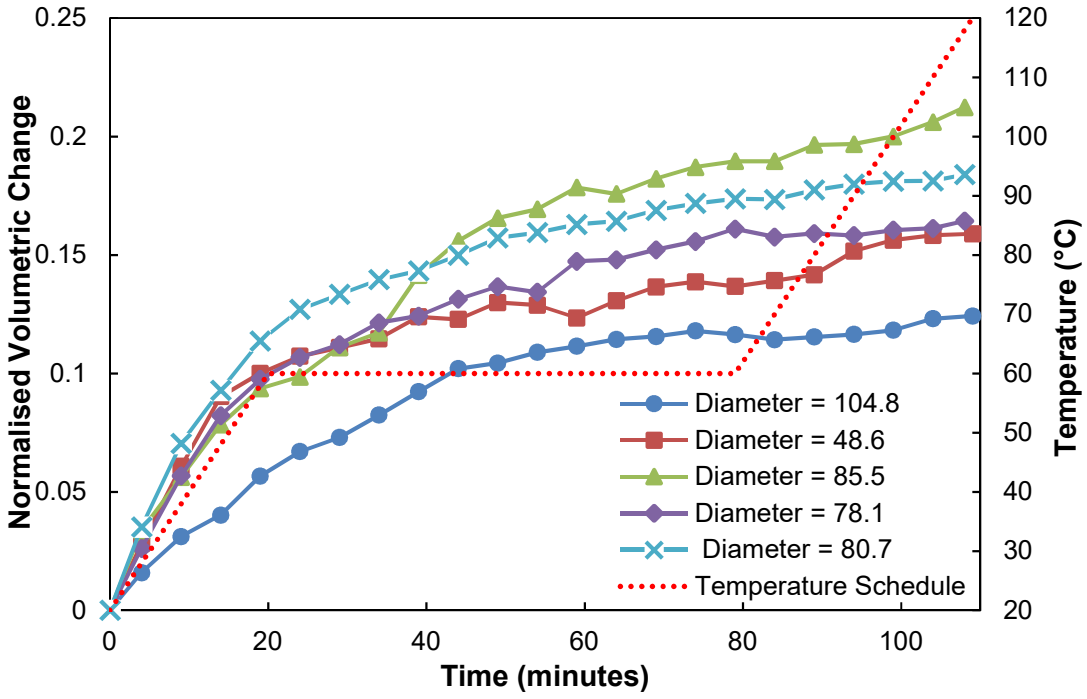

Figure 7.1 - Normalised volumetric change versus time plot for R ≈ 1.0 samples for modified cure schedule.

Figure 7.1 and Figure 7.2 shows the results recorded for the R ≈ 1.0 samples exposed to both the modified and full cure schedules. The initial measured diameters of the droplets are listed for reference. It can be seen in Figure 7.1 that a good degree of correlation has been achieved between the five different tests, with the main portion of shrinkage occurring during the first 10 minutes. This takes place during the initial heat ramp up to 60 °C. It can be seen that the level of shrinkage that occurs appears

to be independent of the initial droplet diameter, with the 48.6 µm droplet shown to experience comparable shrinkage to droplets > 75 µm. This is a positive sign since it suggests the test is not impeded by varying droplet dimensions, a variable which is typically very difficult to control.

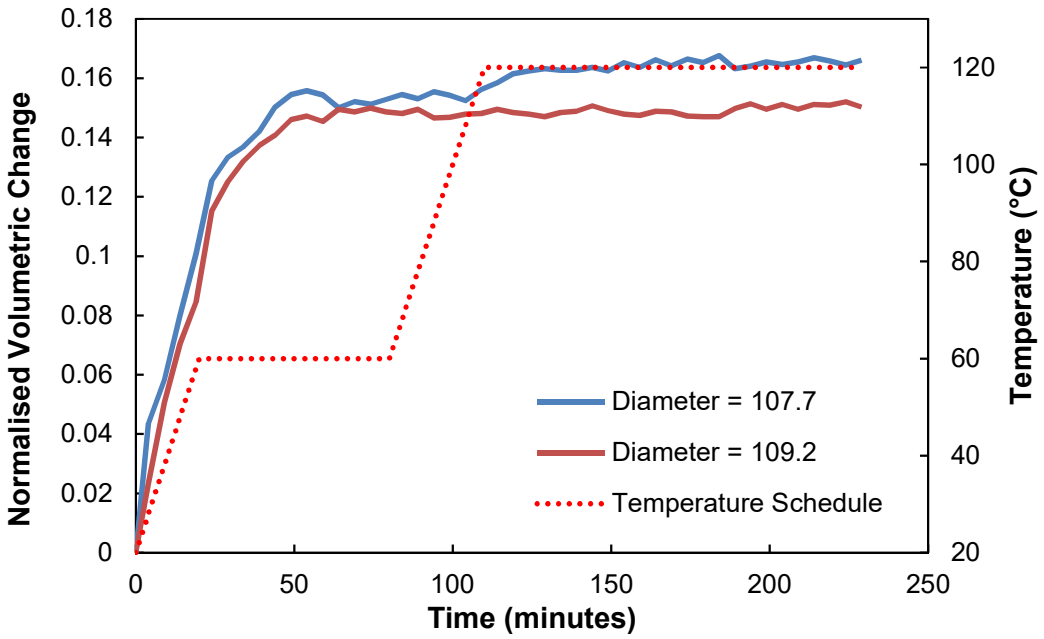

Figure 7.2 - Normalised volumetric change versus time plot for R ≈ 1.0 samples for full cure schedule.

Figure 7.2 further highlights that most of the cure shrinkage occurs early on during the curing process before then reaching a constant value. Specifically, it was shown that after around 50 minutes, virtually all the cure shrinkage had occurred for the R ≈ 1.0 samples. This would represent a point where the sample was under isothermal conditions at 60 °C during the curing process. This means that the further isothermal at 120 °C appears to cause no significant shrinkage of the microdroplet samples relative to the initial phases.

By taking the average of the different plots shown in Figure 7.1, along with those for the other ratios a comparison plot can be constructed as shown in Figure 7.3. The corresponding temperature during the curing process is also plotted. The data from

Figure 7.3 was also used to construct Figure 7.4 to show the influence of the R value over the level of shrinkage more distinctly. For comparison with Figure 7.3, Daniel Simpson's results are presented in Figure 7.5.

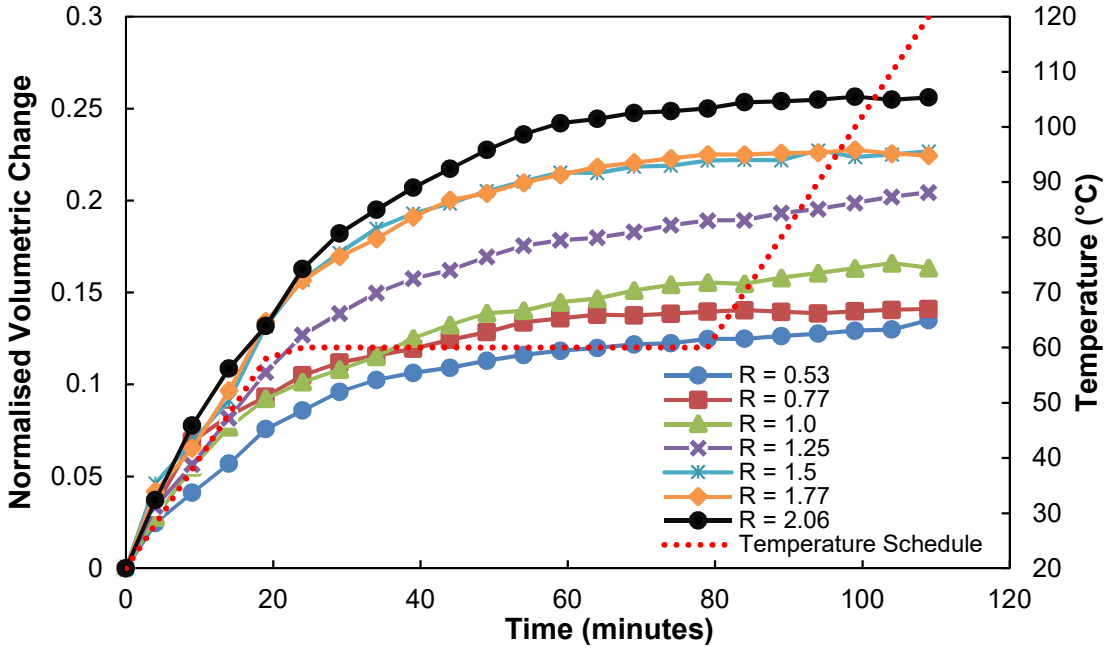

Figure 7.3 - Normalised volumetric change versus time comparison plot for all R values studied collected by Minty.

The results shown in Figure 7.3, Figure 7.4 and Figure 7.5 emphasise the influence the R value exerts over the level of chemical cure shrinkage that will occur. Both figures show good correlation despite the different users, which highlights the consistency of the technique. One difference between the users was that Daniel Simpson took a photo of the sample every five minutes compared to the one photo per minute approach I took. That along with the potential variation in camera focus, due to different users, likely accounts for the larger degree of noise shown in Figure 7.5.

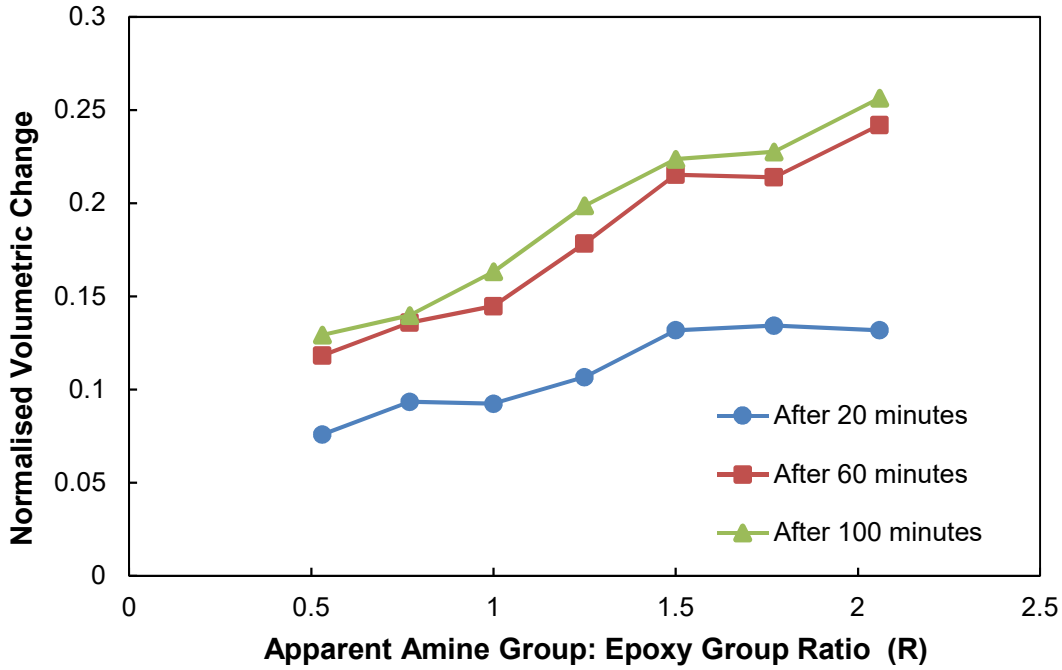

Figure 7.4 - Normalised volumetric change versus R value comparison plot after specific time periods collected by Minty.

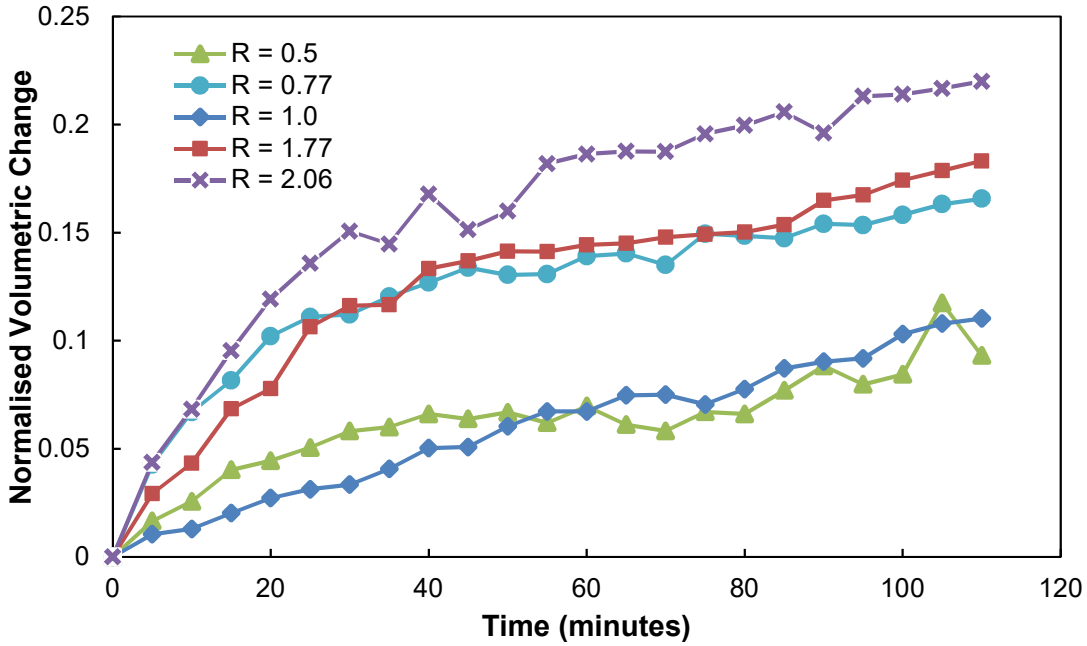

Figure 7.5 - Normalised volumetric change versus time comparison plot collected by Simpson.

Overall the plots show that as the R value of the matrix system was increased the corresponding level of shrinkage also increased. The overall difference is shown to be of significant size, with the smallest shrinkage value measured as ≈ 13% for R ≈

0.5 whilst the largest is ≈ 26% for R ≈ 2.0 in Figure 7.3. As with Figure 7.1, it appears that the greatest amount of shrinkage occurs during the initial heat ramp up to 60 °C, with the second ramp up to 120 °C seemingly not having any significant affect.

However the values measured using the hot-stage technique appear significantly larger than those reported in the literature [60,61,63,64,84] for other techniques. One general difference between the hot-stage method and other cure shrinkage measurement methods is that the hot-stage allows for measurement as soon as the curing process begins. Other techniques such as the TMA and rheometry techniques are reliant on the polymer having gelled before proceeding to measure any further shrinkage. This distinction is important, since any cure shrinkage measured prior to gel point for each ratio would likely have relaxed away, thus not contributing to the residual stresses. Hence, although the values shown in Figure 7.3 and Figure 7.5 are larger than expected, potentially a great degree of this measured cure shrinkage will have relaxed away. For a true representation of the data to be shown the gel point of each R value would need to be known; thus this topic was studied in subchapter 7.3. In addition, the technique assumes that all shrinkage shown is due to the chemical reaction, and not loss of material due to volatilisation. With the modified nature of the Araldite506® resin, this could be a point of future investigation also.

7.2.2 Droplet Deformation Study

A benefit of the hot-stage microscopy study was that it allowed for real-time direct observation of an epoxy microdroplet during its curing process. Over the course of the different microbond tests discussed in this thesis, a phenomenon was found within the minute droplets used for testing. This phenomenon had not been previously reported in the literature until recently by Thomason et al. [257]. It was discovered that during the curing process deformations could occur in the minute epoxy droplet, ranging from smaller surface craters to relatively large holes. These deformations

were difficult to identify using optical microscopy unless one was specifically searching for them and were only initially discovered when analysing tested samples using SEM.

These deformations were found to occur whilst using both the standard purity TETA and the higher purity TETA as well as for a second DGEBA epoxy system (D.E.R 332). This would suggest that the cause for these deformations was related to how an epoxy system reacts whilst undergoing a specific curing schedule. Thus, the hot-stage technique allowed for an approximate point in time to be found whereupon a deformation may be expected to occur.

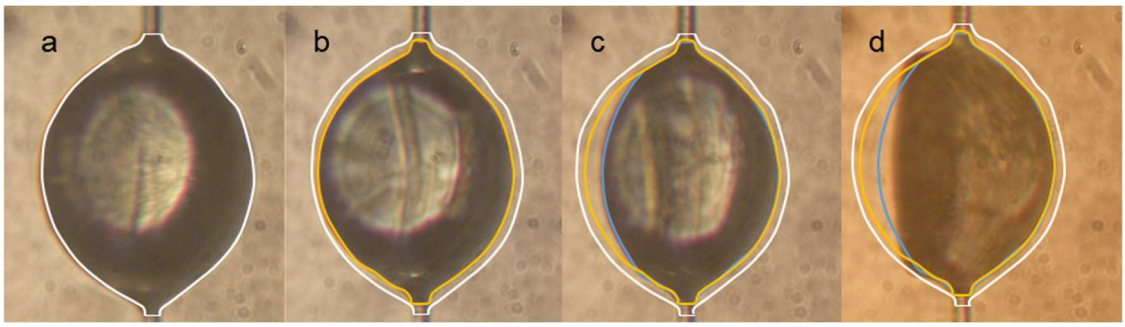

Figure 7.6 - Level of cure shrinkage and droplet deformation shown using hot-stage microscopy technique after approximates times: a) 0 mins, b) 20 mins, c) 80 mins and d) 110 mins.

An example of optical observation of a droplet that has deformed whilst curing in the hot-stage is presented in Figure 7.6. The initial outline of the droplet is shown in white, with a second outline showing the level of cure shrinkage that occurred before the droplet began to deform. These outlines help emphasise the magnitude of deformation that can potentially occur, with almost half of the droplet having collapsed in on itself.

An interesting aspect of this phenomenon was that the quantity of deformations appeared to increase as more amine was added to the system. Figure 7.7 [257] presents the data collected by myself (Operator 1) and David Bryce (Operator 2) with the percentage of tested droplets with deformations quantified. It can clearly be seen

that ratios possessing a large excess of epoxy (R < 1) were shown to possess few deformations whilst ratios where there was a large degree of excess amine (R > 1) were shown to possess deformations in a minimum of 60% of samples tested. As such, it appeared that for the higher ratios studied, most samples tested contained some degree of flaw. SEM micrographs of many of the different deformations are shown in Figure 7.8 and Figure 7.9 respectively.

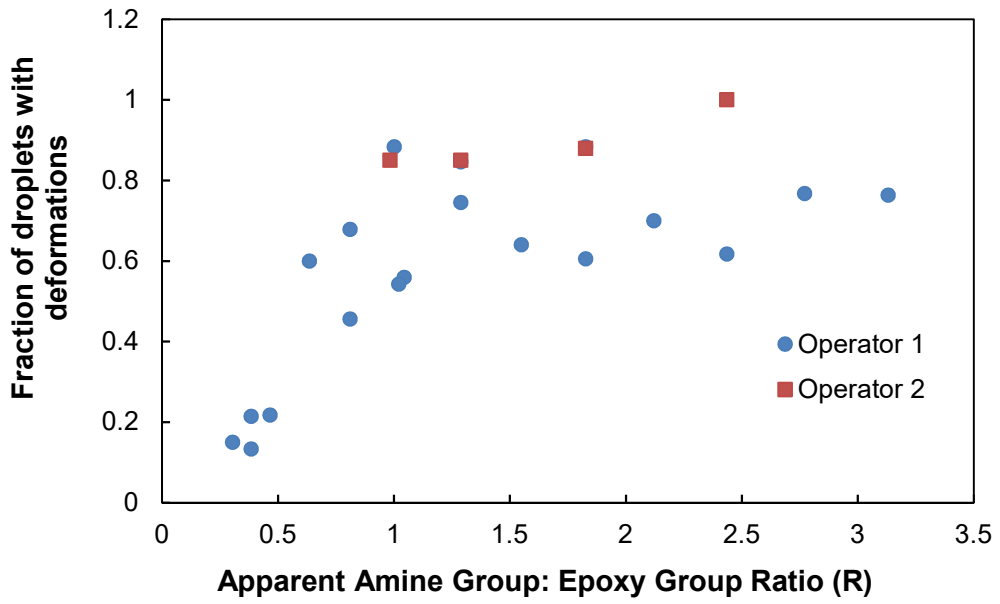

Figure 7.7 - Observation of droplet deformations versus amine group: epoxy group ratio (R).

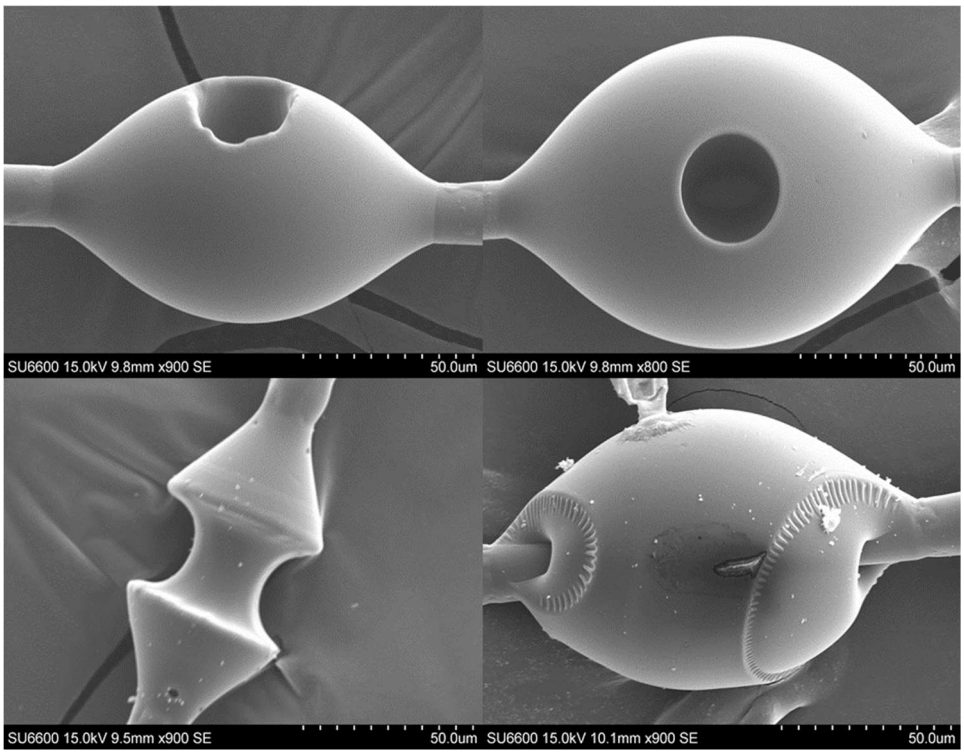

Figure 7.8 - SEM micrographs showing various deformations of cured microbond samples #1.

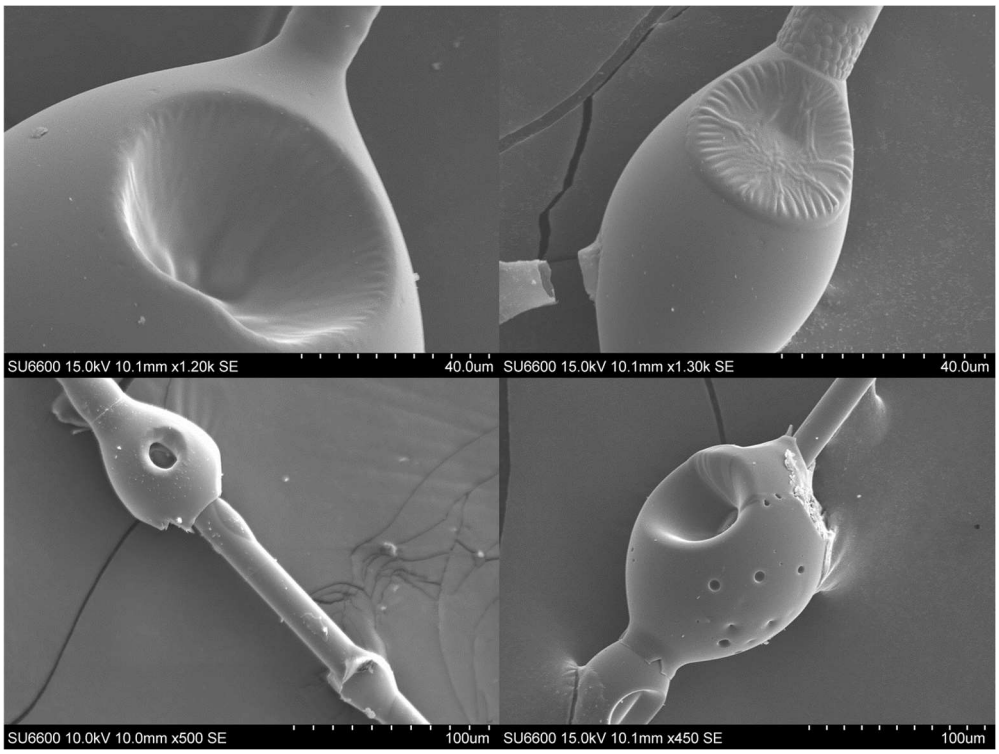

Figure 7.9 - SEM micrographs showing various deformations of cured microbond samples #2.

It can be seen in both figures that the level of deformation can vary quite dramatically, ranging from small craters within the droplet surface or a distinct pattern forming to the creation of large craters, sometimes exposing the surface of the fibre. It is not uncommon for some droplets to possess multiple flaws.

Yet despite this, analysis carried out by both operators suggested that these deformations had no adverse impact on the IFSS values measured, since many of the samples tested contained flaws, as illustrated in Figure 7.10. This would seem counter-intuitive given the large volume of research carried out on modelling the microbond test using finite element analysis (FEA) [171,172,186], which suggests that these deformations should act as stress concentrations, weakening the droplet, particularly where the flaw extends all the way down to the fibre surface. However, the IFSS analysis in Figure 7.10 surprisingly suggests that the IFSS between the droplet and the fibre is not significantly influenced by these deformations, even though they may decrease the interfacial contact area of the samples.

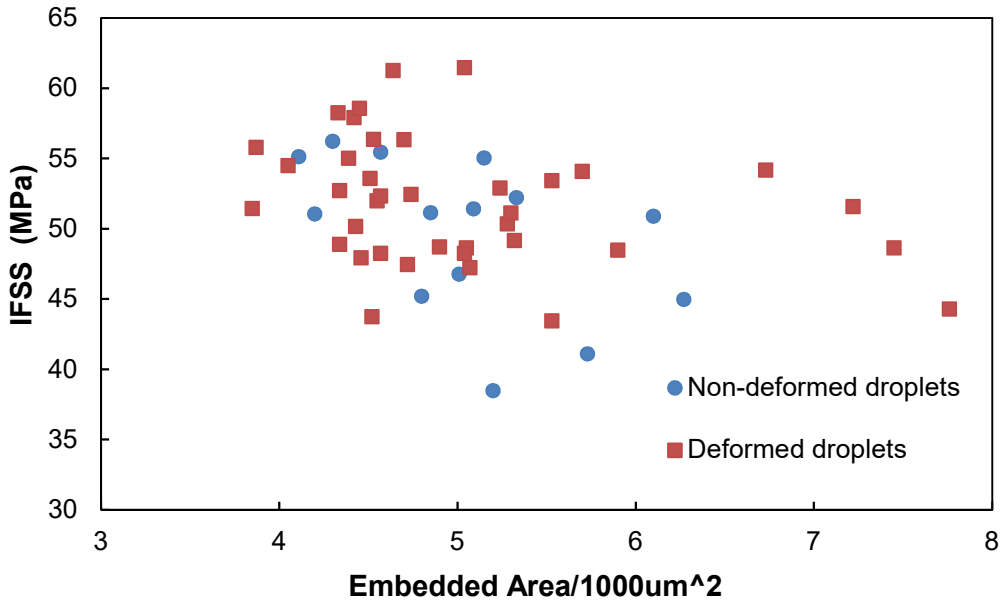

Figure 7.10 – Comparison IFSS Plot of samples with/without deformations at R ≈ 1.28.

One aspect that appeared consistent across all the different ratios regarding deformities was the point at which they would occur. From direct observations of curing droplets using the hot-stage microscopy technique we found that the deformations are the result of a build-up of residual cure-shrinkage stress in the droplet during the initial isothermal stage of the curing process detailed in subchapter 3.4.1, where the samples are held at 60 °C. This residual stress would become "frozen" in as the T_g of the reacting droplet rose above the isothermal cure temperature. However, once the second heat ramp up to 120 °C began the droplet would be placed back into the rubbery state and some degree of the residual stress would be expected to relax away. It is this relaxation which then leads to the formation of these deformations. This link is suggested further by Figure 7.3 since higher R values undergo more cure shrinkage, coinciding with the increased level of deformities shown in Figure 7.7. These discussion points were touched upon in the paper by Thomason et al. [257]. The level of deformation shown in some of the samples in Figure 7.8 and Figure 7.9 certainly suggest a significant level of residual stress can form within a droplet due to cure shrinkage.

7.3 Rheometry

With the completion of the hot-stage microscopy study it became clear that more information regarding the gel point of the system was required. Specifically, whether the gel point would be influenced by the R value and at what point in time each mixture would gel during the cure schedule. This would allow for the level of cure shrinkage after gelation to be established and then used for the residual stress model discussed in Chapter 6. Rheometry is one of the more established techniques for studying cure shrinkage [60,61,251], however the rheometry equipment required for this study was not present at the University of Strathclyde. Consequently, this work was conducted

under the supervision of Dr Walter Stanley and Mr Ananda Roy at the Irish Composites Centre at the University of Limerick.

The techniques used to study the gel point and cure shrinkage are described in detail in subchapter 3.4.3. Due to time constraints, only three R values were studied – R ≈ 0.5, R ≈ 1.0 and R ≈ 2.0. Despite this, a better understanding how excess epoxy groups or excess amine groups may influence the gel point of the overall system was established. Results for the cure shrinkage showed potential for measurement using the rheometry technique however more work was required to ensure the accuracy of the method. 95% confidence values were used for data analysis.

7.3.1 Gel point

The initial set of tests were focussed on finding the gel point of the Araldite 506® epoxy system at the stoichiometric ratio. The primary technique used to define the gel point during these tests was the cross-over point of G' and G'' as shown in Figure 7.11.

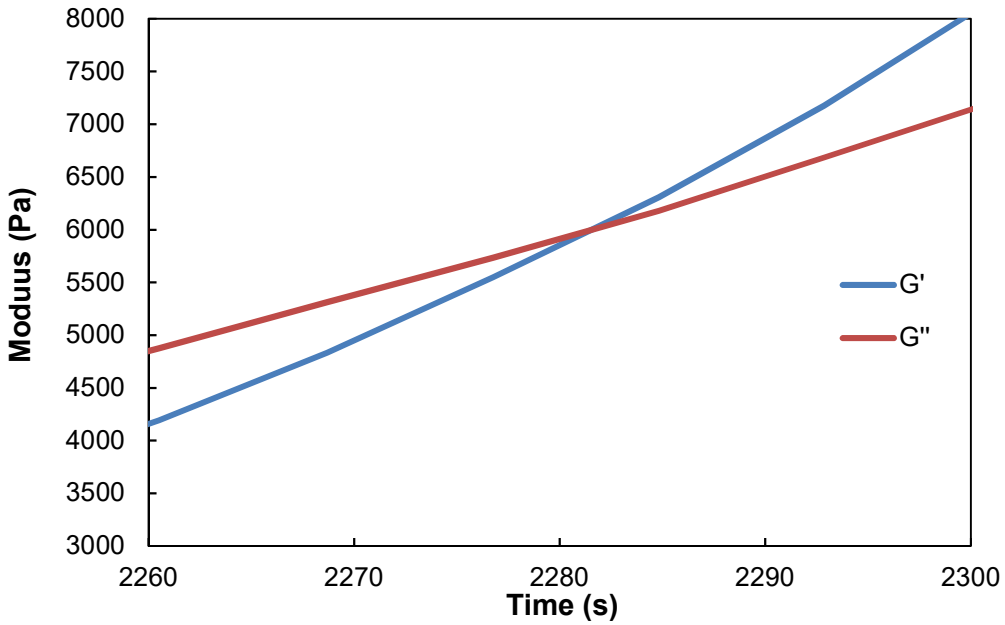

Figure 7.11 - Crossover point of G' and G'' used as one technique to define the gel point of the sample (R ≈ 1.0).

Three samples per ratio were studied for R ≈ 0.5 and R ≈ 1.0 however due to time constraints only two samples were tested for R ≈ 2.0. The average value as then taken for the gel point of each specific R value. The results are presented in Table 7.1.

Ratio	R ≈ 0.5	R ≈ 1.0	R ≈ 2.0
Average Gel Point (s)	3060.2	2252.2	1982.2
Standard Deviation	157.1	36.9	108.4
Confidence	390.3	91.7	974

Table 7.1 - Average gel point values according to moduli crossover point.

Another technique for calculating the gel point of each ratio involved extrapolating the viscosity data for each sample and assigning a time to which the viscosity began to increase exponentially. An example of such a plot is provided in Figure 7.12.

The data using this technique is then provided in Table 7.2. Comparing the two sets of data in the two tables, we can see that the values correlate well with each other. This suggests that either technique is acceptable for calculating the gel point of the matrix system.

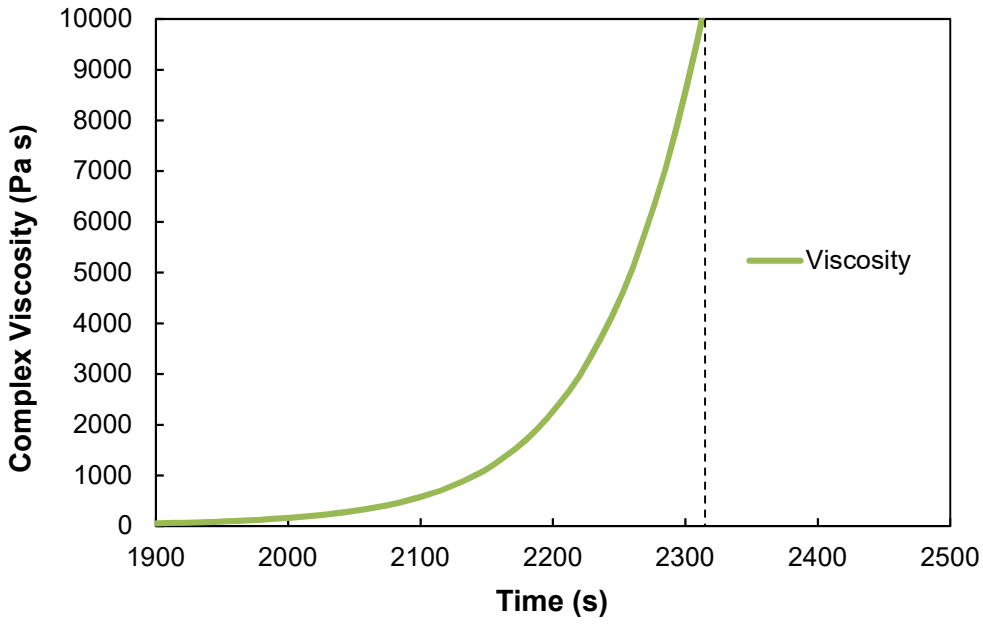

Figure 7.12 – Extrapolation of viscosity plot for gel point of sample (R ≈ 1.0).

Ratio	R ≈ 0.5	R ≈ 1.0	R ≈ 2.0
Average Gel Point (s)	3313	2306.5	2018.4
Standard Deviation	120.6	12.6	125.6
Confidence	299.7	31.2	1128.1

Table 7.2 - Average gel point values according to viscosity extrapolation.

Overall it can be seen that the R value did have a significant influence over the gel point of the system as shown in Figure 7.13. As the R value was increased the gel point of the matrix system was shown decrease, with R ≈ 2.0 shown to gel after ≈ 33 minutes. This compares to ≈ 51 minutes for R ≈ 0.5, highlighting the significant difference between the two extreme values. The difference between R ≈ 0.5 and R ≈ 1.0 appears notably larger than that shown between R ≈ 1.0 and R ≈ 2.0. This phenomenon confirms that adding extra amine groups to the reacting system will lead to the reaction speeding up. This would correlate with the DSC cure conversion data discussed in subchapter 4.2.2. The faster reaction will then produce more exothermic heat catalysing it further and leading to the resin gelling faster. It appears that having excess epoxy groups has a greater effect in slowing the gel point than having excess amine groups does in speeding it up.

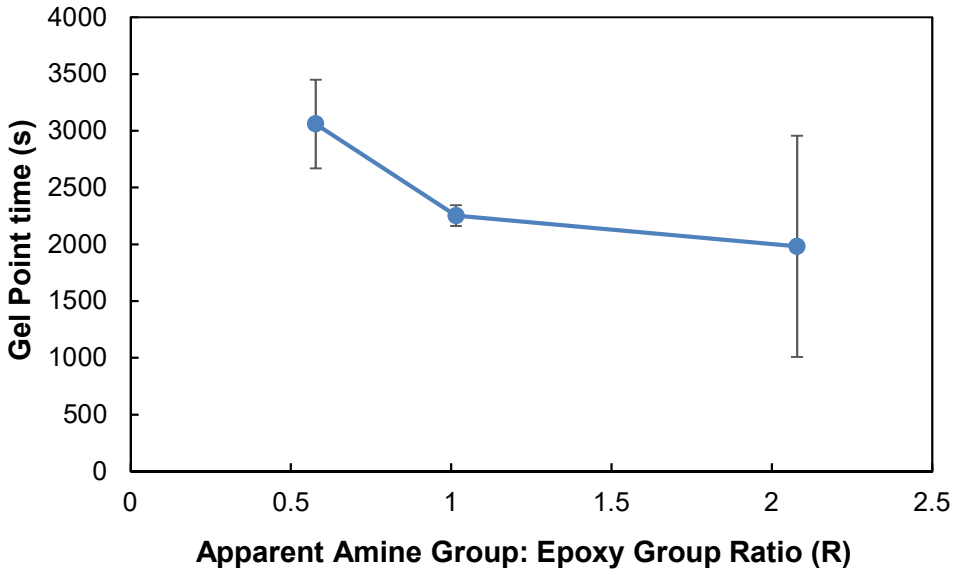

Figure 7.13 - Plot of gel point versus apparent R value.

Interestingly for each of the ratios the gel point was shown to occur during the 60 °C isothermal stage of the curing process. According to Figure 7.3 this would suggest that a large degree of the initial shrinkage shown would not be frozen into the system and will have relaxed away. Thus, the hypothesis discussed in subchapter 7.2.1 that the fraction of the shrinkage values which result in interfacial residual stress may be smaller than those recorded in Figure 7.3 proved correct. Applying the gel point data to the hot-stage microscopy data of Figure 7.3 allows a plot to be constructed which shows the actual level of cure shrinkage that will have been frozen into the system during the curing process. Figure 7.14 shows that the cure shrinkage values potentially frozen into the system are notably smaller than those initially shown in Figure 7.3. However, once the gel point was accounted for, we can see that the values we measured for shrinkage vary between around 2% up to 6%, matching values discussed in past literature [21,60,61,64,65,260]. This seems to confirm that the hot-stage microscopy technique is indeed a viable method for studying cure shrinkage.

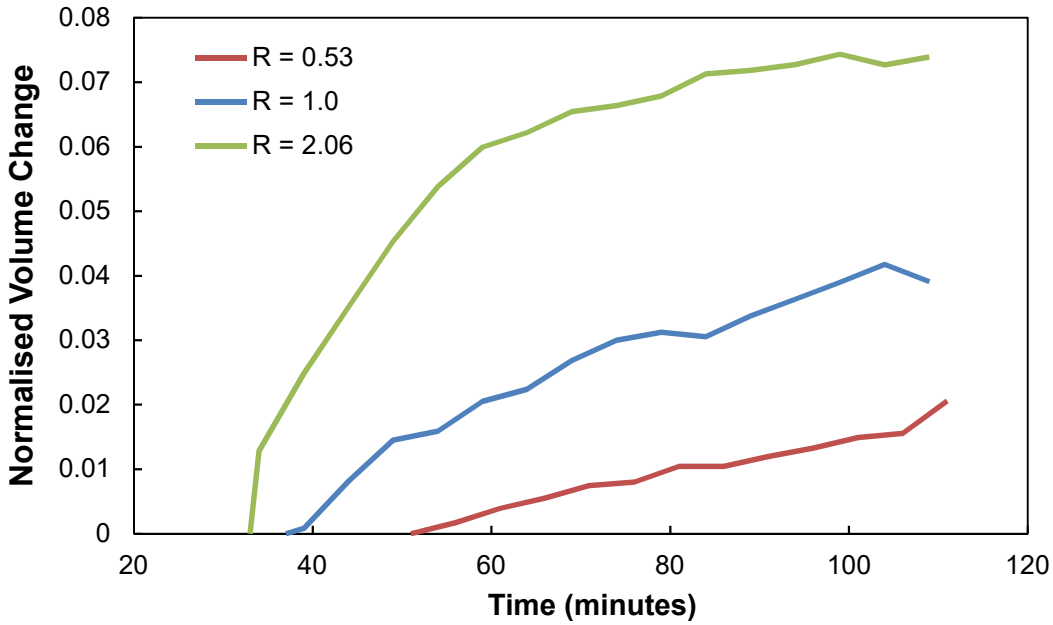

Figure 7.14 - Adjusted cure shrinkage results measured using hot-stage microscopy taking account for gel point.

7.3.2 Cure Shrinkage

It was noted in the literature review that one of the more established techniques for studying cure shrinkage was rheometry [60,61,251]. Given the need to find the gel point, this method appeared to be an appropriate candidate to compare with the results from the hot-stage technique. The challenge in using the rheometry method focussed on applying the standard microdroplet cure schedule used in subchapter 7.2. All previous published studies [60,61,251] had primarily focussed on isothermal curing, not a ramp-isothermal-ramp schedule as was the case with this research. Due to scheduling issues only two samples were studied.

As part of the method, the sample was initially unloaded as described in subchapter 3.4.3 during the initial phases of the curing process to allow for the system to gel. Once the measured viscosity reached a value of 500 Pa s, a load was applied to the sample to allow for measurement of any shrinkage. In theory this should have produced results comparable to that shown in Figure 7.14 however the transition point of 500 Pa s was found to be inconsistent when defining a clear gel point for the different R values. As a result, it was found that some samples could undergo a large degree of compression, with some resin being pushed out from between the plates due to it having not sufficiently gelled. This can be seen in Figure 7.15 where each sample initially undergoes a large decrease in the gap between the rheometer plates, before then levelling off to some degree.

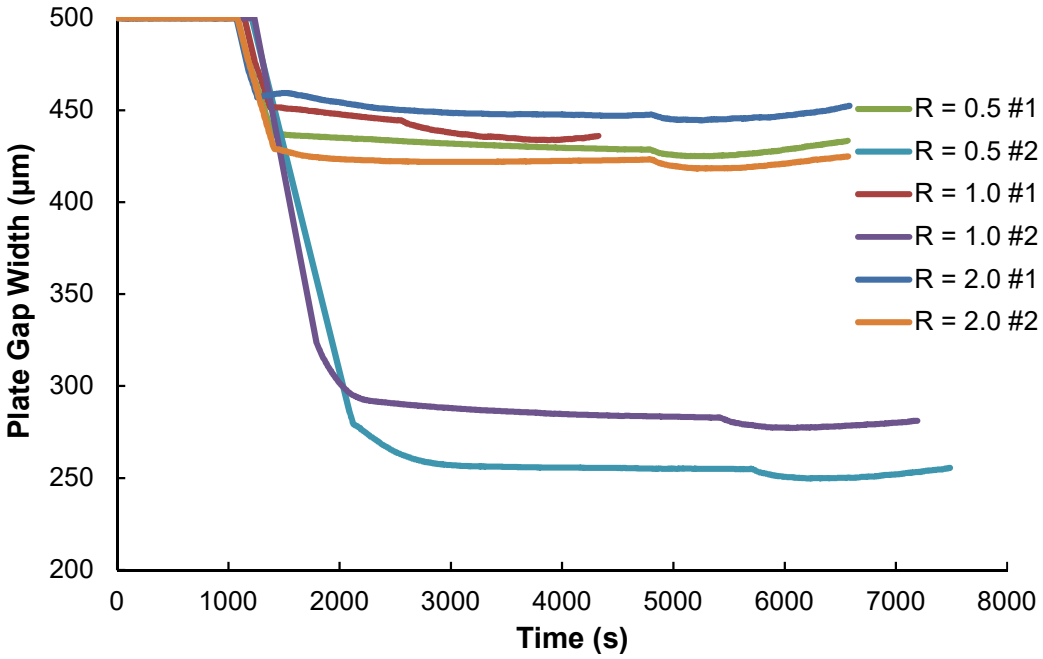

Figure 7.15 - Plot of rheometer plate gap width versus time into curing schedule.

It appears that this phenomenon applies to each of the R values studied with samples for R ≈ 1.0 and R ≈ 2.0 undergoing the largest change. Although this clearly hinders the measurement of the cure shrinkage, it can be seen in the plot that shrinkage does indeed occur once the system has gelled. The samples are shown to undergo a degree of cure shrinkage of a magnitude similar to that in Figure 7.14. Unlike Figure 7.14 there is a notable bump downwards for each ratio where the temperature began to ramp up to 120 °C. The difficulty with the data is that the initial starting point for each sample was shown to vary greatly, thus affecting the overall calculation for cure shrinkage. This makes it difficult to discern whether the shrinkage measured is accurate or not.

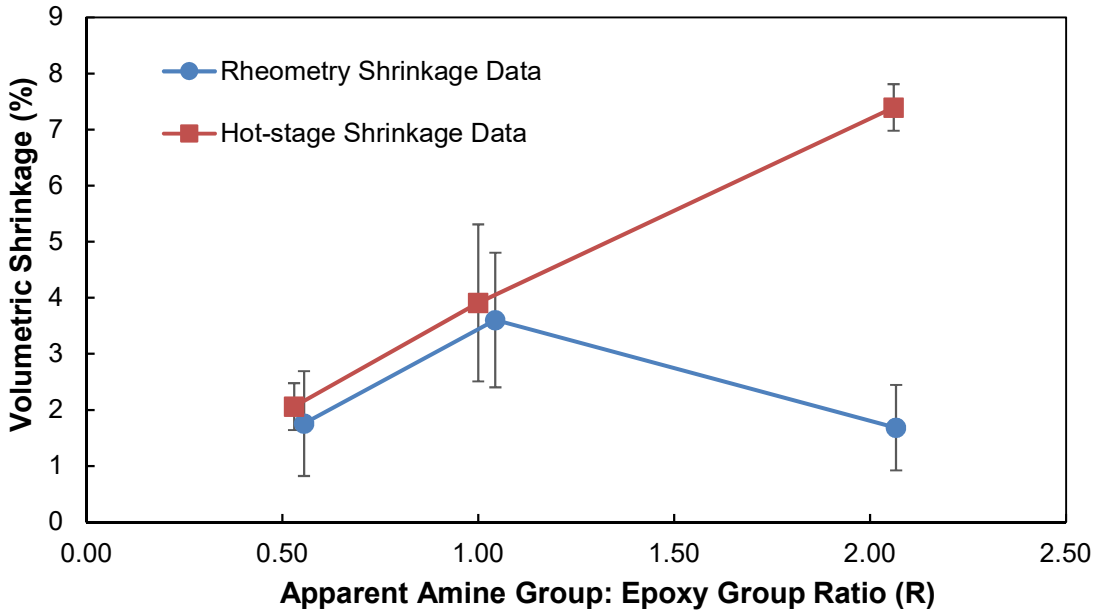

Figure 7.16 – Comparison of cure shrinkage results measured using the rheometer and hot-stage techniques.

Using the data presented in Figure 7.15 and Equation 3.11, Figure 7.16 can be plotted showing the comparison between the hot-stage and rheometer data. The values for cure shrinkage measured using the rheometer were significantly smaller than that for hot-stage technique. However, once the gel point was accounted for as shown in Figure 7.14 the values become greatly comparable, with the values for R ≈ 0.5 and R ≈ 1.0 appearing consistent between the methods. Interestingly the primary difference is that the cure shrinkage for R ≈ 2.0 is significantly smaller when measured using the rheometer method. This would suggest that the rheometer method is not as accurate for ratios where R > 1.0. It may be that the faster gel point of the higher ratios is leading to difficulties in accurately measuring the level of shrinkage from the initial stages after the gel point. This hypothesis would be supported by the fact that the results for other two ratios studied compare very favourably. However due to the variation in initial gap sizes discussed, it is difficult to fully confirm whether this is the case without future experiments.

Overall it appears that the rheometer technique is another potentially viable method for studying cure shrinkage during curing conditions as well as allowing for analysis of the gel point for different R values. The values produced for cure shrinkage appear comparable, to a degree, with those shown for the hot-stage despite the difficulties in applying the cure schedule. The true level of shrinkage that may have occurred was hard to fully evaluate due to the large initial drop in the gap between rheometer plates, which varied for each sample. It was concluded that in future the viscosity value of 500 Pa s was not a viable transition point for the experiment. Instead, it is recommended that the user identify the point where G' and G'' cross during the experiment before then manually instructing the software to begin the loading phase. This would ensure that the material would have gelled before loading, ensuring that any further gap changes measured was due to the chemical cure shrinkage reaction. This would negate the variation that was shown between the different samples.

7.4 TMA Shrinkage Technique

Following the completion of the hot-stage and rheometry studies, the final technique chosen to study cure shrinkage involved adapting the TMA expansion method used in Chapter 4. This allowed for the contraction of the gap between a sandwiched epoxy sample to be measured during the curing process. The technique and sample preparation are described in more detail in section 3.4.2.

Although this technique initially appeared relatively simple compared to hot-stage microscopy it was found to be especially sensitive during testing. It was noted in the literature that although the initial developer of the technique had managed to measure shrinkage successfully [64], a more recent study comparing techniques had been unable to replicate the results [60]. In addition to this, for comparisons to be made with the hot-stage method the same cure schedule had to be used, as opposed to the

isothermal schedule used in previous studies. Ultimately the results gained from this method proved inconclusive when compared to the two other techniques.

As was discussed by Shah et al. [60], it was notably difficult to apply a fixed volume of the epoxy resin system to the glass slips and then ensure an even coating. This was due to the extremely small volume of material that was being studied. The manner in which this was originally done by Yu et al. [64] was never described in sufficient detail, thus the technique was adjusted. For ease of consistency, sample sizes were measured by the mass of material applied to the glass slip using a syringe.

The results recorded and then analysed using TA Universal Analysis proved difficult to fully understand due to the many seemingly uncontrollable variables. The first related to spillage out of the sandwiched sample, due to the probe applying a small load during the initial stages of the cure. This was similar to the issue in the rheometry technique, where the consequence of having the compressive load applied before the sample had fully gelled was clearly visible. For the TMA method this could also result in significant changes in dimension which did not reflect the actual shrinkage occurring. In addition to this, the contribution of the two glass cover slips would also be included within the results of the test, making it hard to fully quantify the shrinkage of the resin that had occurred. For reference, the thickness of the cover slips was said to vary between 0.08 - 0.12 mm whilst the thickness of the resin applied within the cover slips averaged at 28.9 μm. This is slightly larger than the 20 μm that was used by Yu et al. [64].

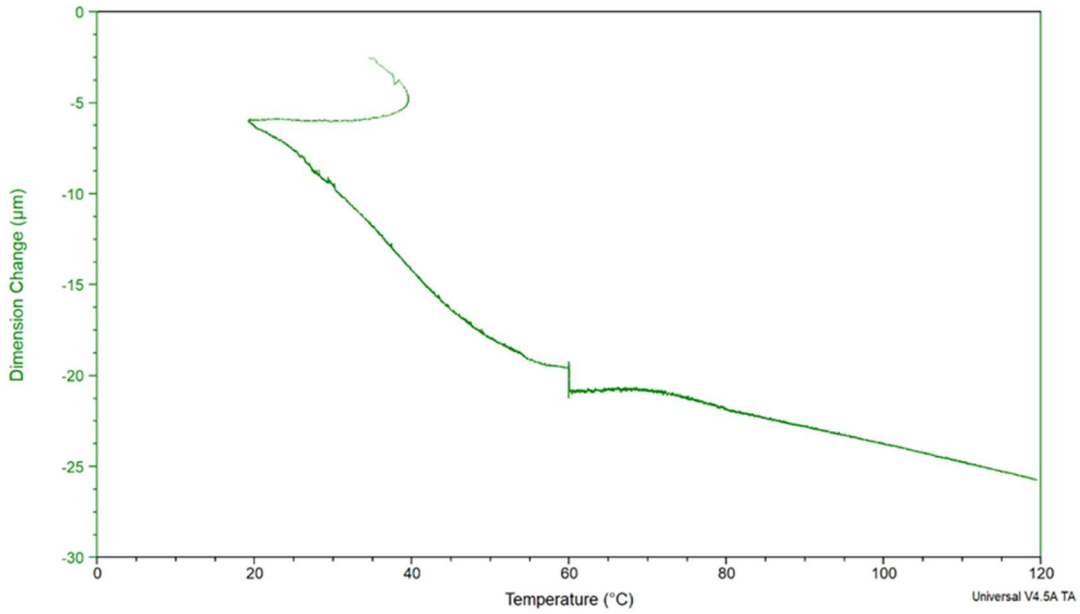

Figure 7.17 - Dimension change versus temperature plot for TMA shrinkage technique.

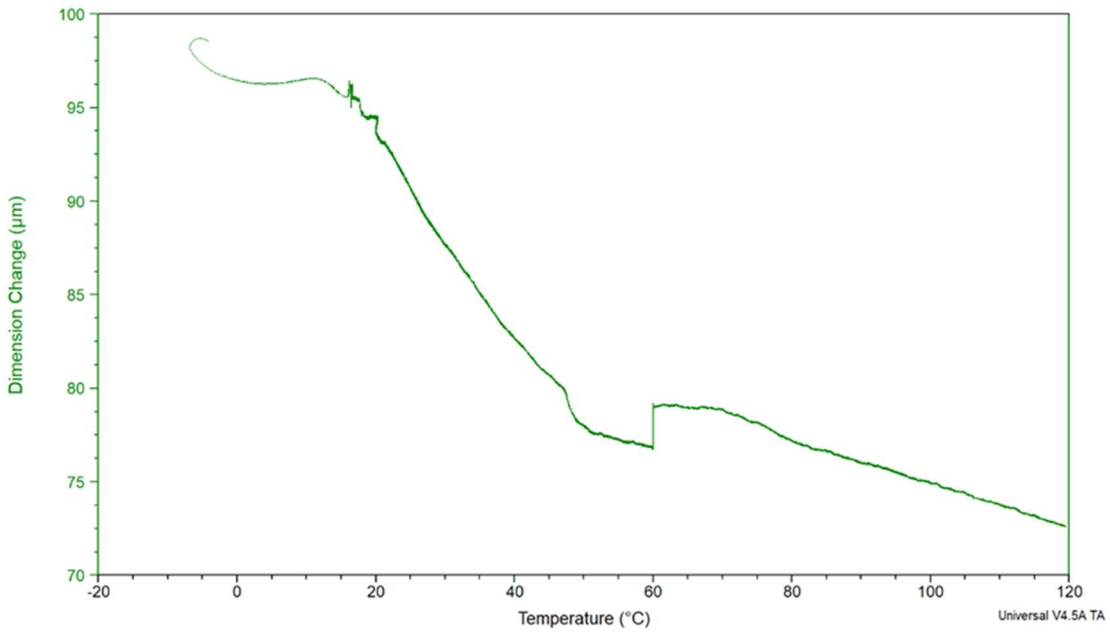

Figure 7.18 - Dimension change versus temperature plot for TMA shrinkage technique with expansion phenomenon.

The results also showed a particular phenomenon that was difficult to explain. Figure 7.17 shows a plot from TA Universal Analysis where the sample was exposed to the same cure schedule as used in subchapter 7.2. It can be seen that there appears to be shrinkage occurring as the temperature was increased, with the initial shrinkage

during the ramp to 60 °C being larger than that for 120 °C. This would concur with what was shown in the hot-stage and rheometry techniques. Yet once the temperature reached the isotherm at 60 °C, the dimension change appears to linearly decrease slightly. However, this slight linear decrease in dimension change shown at 60 °C in Figure 7.17 did not occur consistently from test to test, with the change occasionally being measured as an expansion. This phenomenon is shown in Figure 7.18.

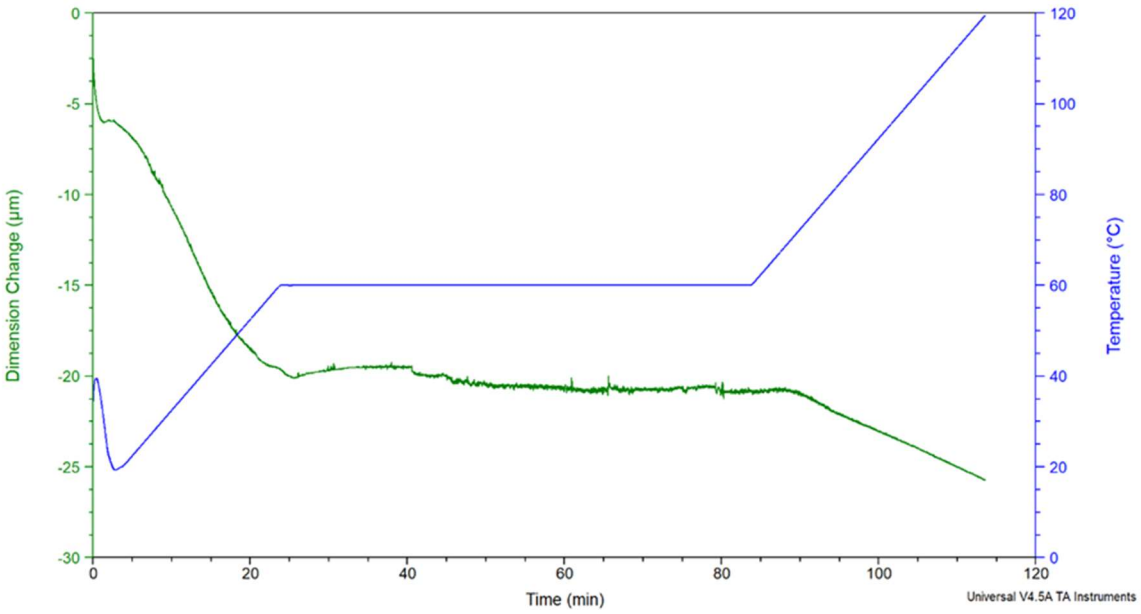

Figure 7.19 - Data from Figure 7.17 plotted as a function of time.

Taking the data shown in Figure 7.17 and Figure 7.18 and plotting them as a function of time supports the hypothesis that, in principle, the technique should be able to study cure shrinkage of a polymer during curing. Figure 7.19 and Figure 7.20 show that shrinkage occurs during the heat ramp up to 60 °C before then remaining consistent during the isothermal part of the curing process for both plots. The difference is that in Figure 7.19 there is a slight decrease whilst in Figure 7.20 there is a slight increase resulting in the different jumps shown in Figure 7.17 and Figure 7.18 respectively. This pattern of plot does appear to be comparable to those shown by Yu et al. [64].

Yet the manner in which the level shrinkage flattens out during the isothermal stage appears distinctly different from that shown in the hot-stage and rheometry results.

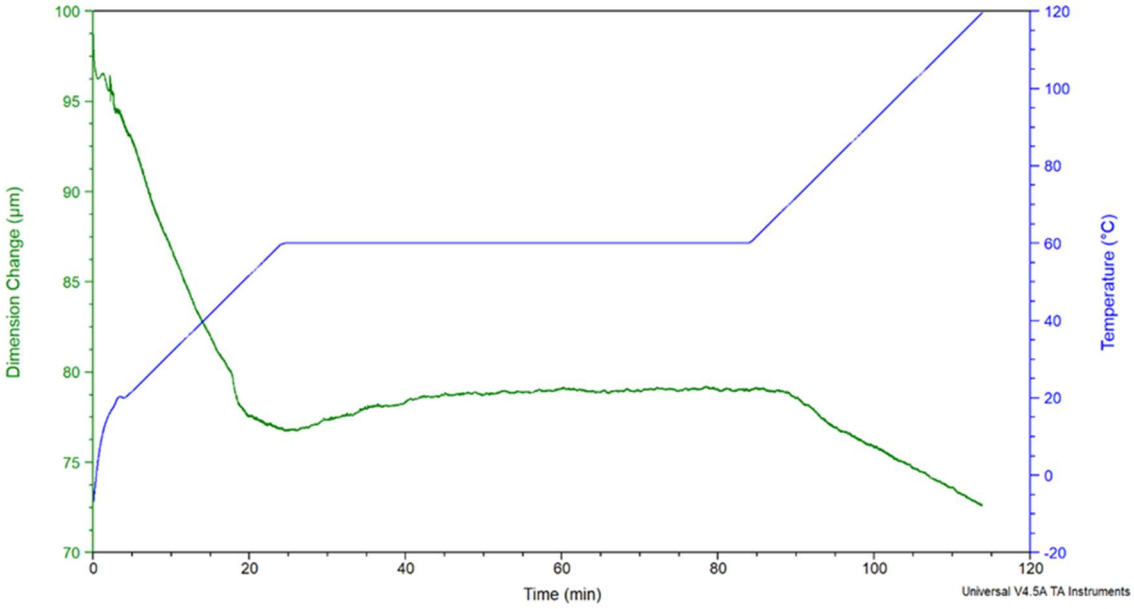

Figure 7.20 - Data from Figure 7.18 plotted as a function of time.

In addition to this, by analysing the dimension change values measured using the TMA and comparing to the averaged initial thickness of 28.9 µm of resin it can be seen that, according to the TMA, a significant portion of it would have shrunk (> 20 µm) on a consistent basis. Based on the work done with the other techniques this occurrence would appear unlikely unless a significant level of the resin was being pushed out of the sample during the test due to it having not gelled sufficiently.

Thus, with these variables, it proved very difficult to ascertain whether an accurate value for shrinkage of the polymer was being measured. As such it would be recommended that this technique not be used for further studies of cure shrinkage due to the number of unknowns regarding its accuracy.

7.5 Updated contribution of total residual stress to IFSS

The results shown in subchapters 7.2 and 7.3 showed that the level of cure shrinkage could be influenced by the R value of the epoxy system. As a result, the initial models presented in Chapter 6 needed to be adjusted accordingly to take account of this varying shrinkage value. The adjusted plots for R ≈ 0.5, R ≈ 1.0 and R ≈ 2.0 are presented in Figure 7.21, Figure 7.22 and Figure 7.23 respectively. The same coefficient of static friction value of 0.6 has been used.

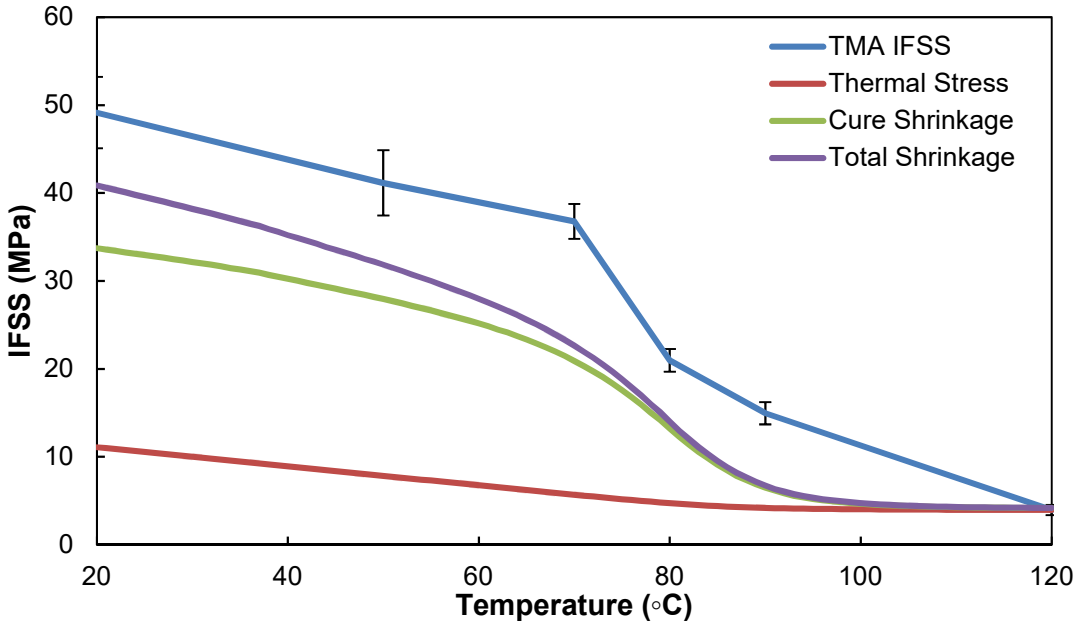

Figure 7.21 – Updated plot for contribution of residual stresses plot to IFSS for R ≈ 1.0.

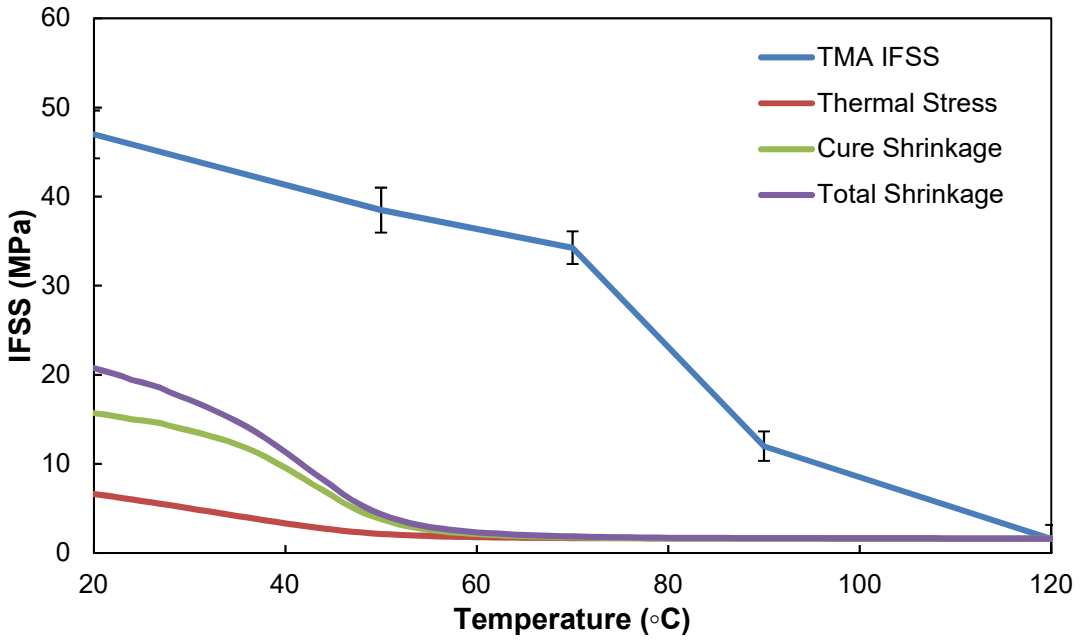

Figure 7.22 - Updated plot for contribution of residual stresses plot to IFSS for R ≈ 0.5.

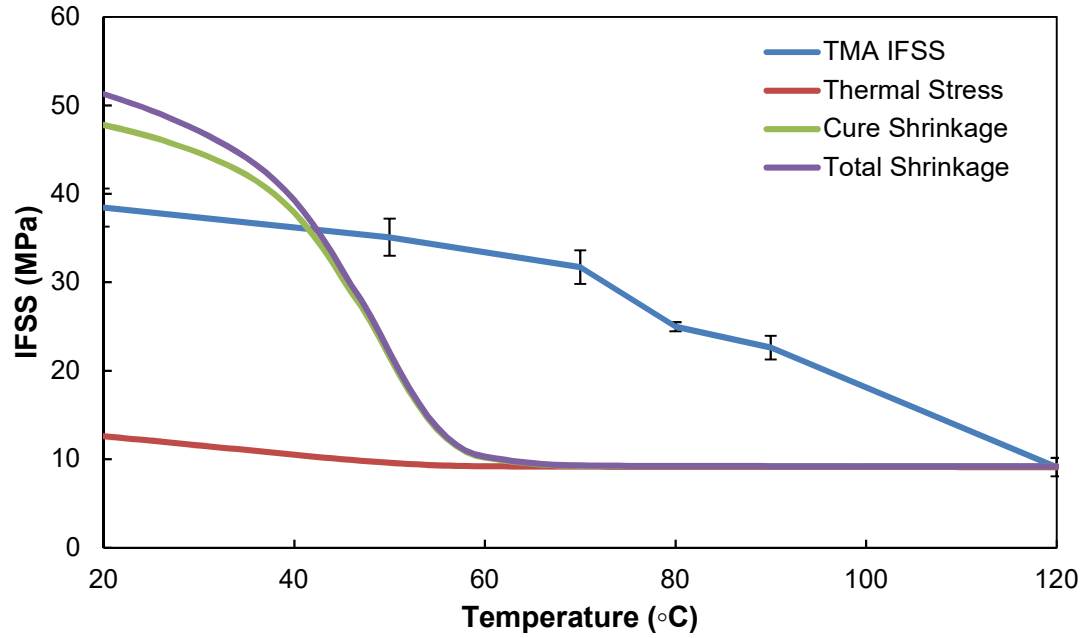

Figure 7.23 - Updated plot for contribution of residual stresses plot to IFSS for R ≈ 2.0.

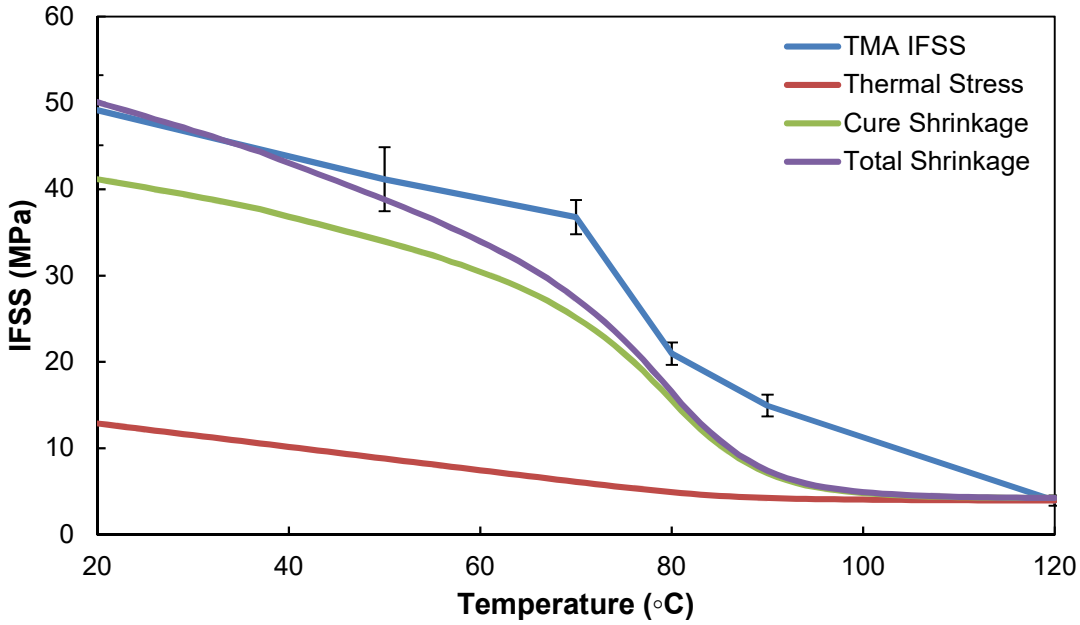

Figure 7.24 - Updated plot for contribution of residual stresses plot to IFSS for R ≈ 1.0 with a coefficient of static friction = 0.75.

Analysing the data presented in the different figures several of the conclusions regarding the accuracy of the model in Chapter 6 appear consistent. Figure 7.21 shows that the results of the model correlate well with the measured IFSS results of the TMA microbond technique. Since the level of shrinkage measured was smaller than the original 8% assumed in Chapter 6, the contribution values appear smaller. However, if the coefficient of static friction is slightly increased from 0.6 up to 0.75 as shown in Figure 7.24 then the two plots are shown to correlate to a greater degree. Another potential reason for the lack of correlation in the temperature region above T_g may be due to the assumption made between the residual stress and the gel point by the model. In reality the transition of residual stresses being “frozen-in” once the gel point is crossed may not be clear cut. Given the visco-elastic nature of the polymer (or polymerising polymer) the “frozen-in” stress may start to build up even before the gel point, to give a more gradual increase in residual stress as observed in the IFSS data.

Overall these results would support the hypothesis that residual stresses can contribute significantly to the stress transfer capability of the interface. Figure 7.21 and Figure 7.24 suggest that there does exist a clear link between the IFSS and the residual stress contribution.

It can be seen that the contributions predicted by the model for R ≈ 0.5 and R ≈ 2.0 again appear to correlate poorly with the results produced by the TMA microbond method. This was also the case in Chapter 6, although the decrease in cure shrinkage for R ≈ 0.5 appears to have been impacted the most. It can be seen that the contribution of the residual stresses to the IFSS equates to only ≈ 20 MPa maximum. Compared to the 46 MPa measured at 20 °C this would confirm that other adhesion mechanisms must be at work in order to produce this value. In addition to this, both plots show that the residual stress contribution decreases before any notable drop in IFSS occurs. For R ≈ 0.5 the value for IFSS drops ≈ 70 °C, while the residual stress contribution is shown to have relaxed away ≈ 50 °C. In the case of R ≈ 2.0, the suggested contribution at 20 °C still appears notably larger than the measured IFSS. This was the case in the original model in Chapter 6 also. The contribution is then shown to relax away at ≈ 60 °C while the IFSS maintains a gradual decline. Both would suggest that the residual stress contribution is not the key contributor of the complex mechanisms at work at the interface, highlighting the limits of the model currently used. Compared to the results for R ≈ 1.0, it appears that the contribution of the residual stresses plays a more central role in defining the value for IFSS the nearer the R value is to stoichiometry. Once the ratio begins to deviate from this value, the significance of the residual stresses appears to decrease. However, the apparent limits of the model are directly linked to our lack of understanding regarding the T_g of an epoxy microdroplet. This is due to the model assuming that the T_g of the droplet is the same as the bulk value measured using DSC in Chapter 4. It has been shown in

the past by Zinck et al. [161] that the T_g of a thin film of resin differed from that of the bulk matrix. They also suggested that this affected their microbond results. As such this would provide an explanation for why the model works for R ≈ 1.0 but not for off-stoichiometric values. The possibility of this T_g scaling issue also being influenced by the R value would also explain why the results of the model decrease in correlation the further the R value deviates from stoichiometry.

Therefore, to move this research forward more work is required to study the T_g value of epoxy microdroplets to identify whether the values differ from the bulk matrix. It would also be of interest to investigate whether the R value influences this scaling factor further, since R ≈ 1.0 would not appear to be as affected as the off-stoichiometric ratios. Further study of the friction coefficient of the APS coated fibres (fibre 1) would also be beneficial to gain a measurable value that could be used for the model. Studies into the influence of the R value on wettability and contact angle would also be recommended.

7.6 Summary and conclusions

In conclusion, in this chapter it has been shown that a novel technique using hot-stage microscopy can be used to measure the cure shrinkage of a minute epoxy droplet upon a single fibre during its curing process. It was shown by two users that as the R value of the system was increased, the level of cure shrinkage that occurred increased. Thus, the contribution to the IFSS of the residual stresses formed due to this shrinkage could be influenced by matrix chemistry. The measured values using the technique were found to be noticeably larger than those reported in the literature, however this was due to technique measuring all possible shrinkage that would occur. To account for this the gel point for the different ratios was required to discern how much shrinkage could be frozen into the matrix structure.

Two other techniques from literature were employed to compare to the hot-stage method. A rheometry based technique was successful in allowing for the measurement of the gel point for different R values. It also appeared to show potential for measuring the level of cure shrinkage with a varying temperature profile. However, more work is required to fully perfect this method due to difficulties in defining the cross-over point for sample loading. The TMA method was unsuccessful, with the sample preparation being too difficult to reproduce consistently. Some favourable comparisons could be seen with work conducted using the technique in the past, however the dimension changes measured were significantly larger than any measured using the other techniques. Also, the TMA machine itself appeared to not be sufficiently sensitive to accurately measure the shrinkage of the epoxy resin sample.

The rheometry technique also showed that the gel point of the matrix system was influenced by the R value. As the R value was increased the gel point was shown to occur faster. Since the same schedule was used between the rheometer and hot-stage methods, the measured gel points could then be applied to the hot-stage data. Taking this into account, the measured values for $R \approx 0.5$, $R \approx 1.0$ and $R \approx 2.0$ were calculated and appeared consistent with values reported in the literature.

The recalculated residual cure shrinkage data for these ratios was then applied to the residual stress contribution model discussed in Chapter 6. It was shown that for $R \approx 1.0$, the model again showed good correlation with the measured IFSS results. This correlation was further improved when the coefficient of static friction was increased from 0.6 up to 0.75. However, the model again appeared inconsistent for the other two ratios, suggesting that circumstances change the further the R value deviates from the stoichiometric ratio.

Droplet deformations were discovered to occur in samples used for the microbond test, with the fraction of deformed droplets increasing with the amine content of the matrix system. This may be potentially due to the volatile nature of the modifier present in the Araldite 506® resin. Surprisingly, these deformations were shown to seemingly not influence the IFSS values measured during the study, with multiple samples having been tested with deformations and showing no adverse effects. Finally, it was concluded that more research is required to fully understand the cause of these deformations as well as any potential influence they may have on the measured IFSS between the fibre and matrix system.

Chapter 8. Conclusions and future work

8.1 Conclusions

8.1.1 The influence of matrix chemistry on thermomechanical and mechanical properties of the matrix

It was shown in Chapter 4 that the apparent R value had a major influence on all of the thermomechanical properties of the matrix studied. The cure kinetics of the epoxy system were analysed using DSC, with the heating rate of the curing process shown to distinctly influence the polymerisation reaction that occurred. Although higher heating rates were shown to result in a faster completion of the reaction, it was found that T_g was greater for rates below 5 °C/min. This confirmed that the heating rate of 2 °C/min during the standard curing procedure for samples was acceptable.

The R value was also shown to have a significant effect on the LCTE value of the matrix, especially when the temperature was above T_g. Above T_g, the LCTE magnitude was shown to reach a minimum at the stoichiometric ratio due to this ratio inducing the highest crosslink density. As the ratio deviated from R ≈ 1.0 the matrix crosslink density decreased, leading to an increase in LCTE. Below T_g, the R value appeared to have a less clear influence, with the LCTE values for excess epoxy ratios (R < 1) only appearing to be significantly influenced.

The final value for T_g was also shown to be greatly influenced by the R value of the matrix system, for both purities of hardener investigated. The maximum T_g value was recorded at a ratio slightly above the stoichiometric point (R ≈ 1.25), with good correlation shown between each of the measurement techniques used. The high purity TETA was shown to possess greater values of T_g measured for ratios around the stoichiometric point when compared to the standard purity TETA. The higher purity TETA was also shown to possess a lower activation energy value than standard purity

TETA, suggesting that it was moderately superior. Overall a degree of correlation was shown with past results in the literature, despite the differences in resin used. However, the values for T_g and activation energy (E_a) were notably lower than published values for other DGEBA/ TETA systems. It was concluded that this, along with the maximum T_g occurring slightly above stoichiometry, was due to the modified nature of the Araldite 506® resin.

Using dynamic mechanical analysis, the R value of the system was shown to also have some influence over the storage modulus (E') of the matrix. Ultimately the largest magnitude of E' was recorded at the stoichiometric ratio however ratios close to $R \approx 1.0$ possessed comparable values at lower temperatures. It was not until the ratio deviated sufficiently from $R \approx 1.0$ that E' was significantly impacted due to the significant drop in the T_g of the matrix.

Finally, a combination of FT-IR and Raman spectroscopy were used to quantify the influence of the R value on the potential molecular structure of the final matrix after curing. Analysis of the epoxy and amine groups remaining within non-stoichiometric reacted systems was carried out. The effect of post-curing on the level of these remaining groups was also studied. It was shown that systems mixed with excess epoxy did indeed possess a significant level of excess reactive epoxy groups remaining within the matrix and that these could undergo a further etherification reaction if exposed to elevated temperatures. For ratios where $R > 1$, primary amines were shown to dominate the thermoset reaction, with more secondary amine groups remaining in the system after curing. If $R >> 1$ then it was found that primary amine groups could also be found in the matrix after reaction due to over-saturation. It was concluded that both the excess epoxy and amine scenarios would result in reduced crosslink density of the matrix, which could explain the decrease in thermomechanical properties observed for the off-stoichiometric ratios.

8.1.2 The influence of matrix chemistry on GF – Epoxy Interface

It was shown in Chapter 5 that the R value had a major influence over the stress transfer capability of the interface. This was shown to be the case independent of the fibre sizing applied or the purity of TETA used. Although the chemistry of the fibre sizing was shown to influence the IFSS values measured, specifically the maximum value achievable and the R value at which it would occur, these differences were not as significant as changing the R value. Given the results, it was concluded that the R value of the matrix may have a greater influence than the chemistry of the fibre sizing in defining the level of adhesion between the fibre and the polymer. Hence it could be concluded that chemistry does indeed play a key role in defining the stress transfer capability of the interface in adhesion mechanisms other than just chemical bonding at the fibre surface.

A clear correlation was established between the IFSS value measured and the measured T_g value of the polymer matrix, suggesting a potential link between the two. This link was expanded upon by studying the formation of thermal residual stresses at the interface and how they could be interrelated to the stress transfer capability of the interface and R value respectively. It was shown how the decrease in IFSS with deviating R value could be correlated to a decrease in the contribution of the thermal residual stresses formed at the interface. This would suggest that thermal residual stresses can indeed contribute to the stress transfer capability of the interface. However, this contribution would only represent a portion of the total IFSS value measured and thus other mechanisms, such as cure shrinkage stresses, must also actively be playing a role.

8.1.3 The influence of matrix chemistry and temperature on GF – Epoxy Interface

The results presented in Chapter 6 showed that the R value, testing temperature and fibre silane coating could each influence the stress transfer capability of the interface. The IFSS was shown to possess an inversely dependent relationship with the testing temperature and was also influenced by the R value. At lower temperatures, (i.e. below the matrix T_g values measured in Chapter 4), the maximum IFSS value was shown to occur at the stoichiometric value. The magnitude of IFSS was then shown to decrease as the R value deviated further from this value. This was the case for both types of silane coated fibres. Again, this would suggest that the R value possesses a greater influence over interfacial adhesion than the coating of the fibre. However, a slight difference was observed in that when the testing temperature exceeded 70 °C a transition in IFSS was observed for the APS coated fibres. The GPS coated fibre data differed in that the observed trend appeared significantly more linear with increases in temperature. This would suggest that although the R value appears to have the greater influence overall, the chemistry of the sizing can still play a role in defining the stress transfer capability of the interface. This would agree with the observed conclusions taken from the microbond data in Chapter 5.

It was also observed that at temperatures well above T_g a small value of IFSS still existed, despite the residual stresses having potentially relaxed away completely. Interestingly, at these higher temperatures the magnitude of IFSS appeared to be possess a linear relationship with the level of amine present within the epoxy system. Larger R values were shown to possess greater IFSS values once the testing temperature increased above the T_g value. It was hypothesized that the magnitude of IFSS being greater for excess amine ratios (R > 1) results from a combination of an

increase in the level of hydrogen bonding and a variation in the shear failure behaviour of the matrix due to the differing crosslink densities.

Using Nairn's model, a correlation was shown to exist between the IFSS values measured and the potential total contribution of residual stresses due to cure and thermal shrinkage. The correlation was shown to be particularly good at the stoichiometric ratio for both the APS and GPS coated fibres studied. However, as the ratios deviated further from R ≈ 1.0 the degree of correlation was shown to decrease. It was concluded that assumptions made by the model appeared to be oversimplifications once the R value deviated significantly from the stoichiometric value. The potential contribution of cure shrinkage stresses to the interface was shown to be large enough that more research was required to address some of the unknowns and assumptions. Specifically, more work regarding the link between cure shrinkage, the R value and the gel point of the polymer was required to ascertain the potential total contribution to the strength of the interface.

8.1.4 The influence of matrix chemistry on cure shrinkage of polymer matrix

In Chapter 7 it was shown that a novel technique using hot-stage microscopy could be used to measure the cure shrinkage of a minute epoxy droplet on a single fibre during the curing process. Good correlation between data gathered by two users showed that the technique was repeatable. The results showed that as the R value was increased, the level of cure shrinkage that would occur increased. This would mean that contribution to the IFSS from the residual stresses formed due to chemical cure shrinkage could be influenced by the R value.

The measured values using the technique were found to be noticeably larger than those reported in the literature, however it was concluded that this was due to the

methodology. Unlike other cure shrinkage techniques, the hot-stage method was shown to measure the level of shrinkage from the start of the curing process, through the gel point and then finishing once the polymer had effectively cured. Any residual stress that would form due to cure shrinkage before the gel point would likely relax away rather than be frozen into the network. As such the residual stress forming fraction of the shrinkage that occurs during the curing process is typically measured from the gel point on, as is done in other comparable techniques. To account for this the gel point for the different ratios was required to discern what level of the cure shrinkage was potentially frozen into the matrix structure.

Two other techniques from literature were employed to compare to the hot-stage method. Ultimately the TMA method proved unsuccessful, with the sample preparation being too difficult to reproduce consistently. The TMA machine itself appeared to not be sensitive enough to accurately measure the shrinkage of the sample consistently.

A rheometry based technique showed potential for measuring the level of cure shrinkage with a varying temperature profile. Previously any cure shrinkage work conducted using rheometry was done at a constant heating rate or constant temperature, with no prior tests using a full curing schedule with multiple heating ramps. As such there were difficulties in defining the cross-over point for sample loading due to the changing temperature profiles and R values. It was concluded that with more input the technique could be successfully adapted to function with a varying temperature profile, as was done using the hot-stage technique.

The use of a rheometer also allowed for the measurement of the gel point for different R values. As the R value was increased the gel time was shown to reduce. Since the same schedule was used between the rheometer and hot-stage methods, the

measured gel times could then be applied to the hot-stage data. Taking this into account, the measured values for R ≈ 0.5, R ≈ 1.0 and R ≈ 2.0 were recalculated and appeared consistent with values reported in the literature.

The recalculated residual cure shrinkage data for the R values studied was then applied to the residual stress contribution model discussed in Chapter 6. It was shown that for R ≈ 1.0, the model again showed good correlation with the measured IFSS results. This correlation was further improved when the coefficient of static friction was increased from 0.6 up to 0.75. However, the model again appeared inconsistent for the other two ratios, suggesting that circumstances change the further the R value deviates from the stoichiometric ratio.

During the course of the project droplet deformations were discovered to occur in samples used for the microbond test, with the fraction of deformed droplets increasing with the amine content of the matrix system. Surprisingly, these deformations were shown to seemingly not influence the IFSS values measured during the study, with multiple samples having been tested with deformations and showing no adverse effects. One hypothesis was that these deformations were caused by the build-up of residual stress within the microdroplet during the curing process. Overall it was concluded that more research is required to fully understand the cause of these deformations as well as any potential influence they may have on the measured IFSS between the fibre and matrix system.

8.1.5 Overall conclusions

Through the research conducted during this project it can be concluded that the R value of the epoxy system has a major influence over the level of adhesion that exists between the fibre and the polymer matrix. Across multiple fibres it was shown that changing the R value significantly affected the apparent IFSS value measured. The

effect was shown to be of a greater magnitude than that of changing the sizing chemistry of the fibre. This would suggest that although chemical bonding may be an active adhesion mechanism, it may not be the dominant mechanism when it comes to defining the stress transfer capability of the interface as was once thought. Moreover, the potential for variance in the level of sizing applied to the surface of the fibre could lead to localised changes in the R value of the matrix within the interface region. It could be that these localised changes in chemistry are greatly influencing the material properties of the matrix within the interface, leading to changes in its ability to effectively transfer stresses.

In addition to the influence that the R value has over the IFSS value, it was also shown to possess a considerable degree of influence over several key thermomechanical properties of the interface. These include the T_g, storage modulus (E'), gel point and LCTE values as well as the level of chemical shrinkage that occurs during the curing process. The clear correlation shown between the measured IFSS values and T_g for different R values would certainly suggest that the two must be related to some degree. Furthermore, all the properties discussed above influence the level of residual stress that will form due to thermal and cure shrinkage. As such the hypothesis that the contribution of these residual stresses could be influenced by matrix chemistry was shown to be correct. This would correlate with what was shown to occur for the IFSS values measured and satisfy the two current arguments regarding residual stress contribution at the interface, these being that (i) chemistry must play an active role in defining the contribution of the residual stresses and (ii) that the contribution itself is significant to the stress transfer capability of the interface overall.

However there still appears to be a missing element within the residual stress contribution theory regarding ratios where R deviates significantly from stoichiometry. At these points the adhesion mechanisms appear to change, with current known

mechanisms such as chemical bonding not providing acceptable solutions for the degree of variance of IFSS observed. The data collected from the TMA microbond work highlighted that the IFSS value decreased significantly at comparable temperatures for different R values. This is despite the fact that the T_g of each ratio would vary greatly and thus one would expect the magnitude of IFSS to decrease greatly at different points. One potential solution could be that the T_g of a microdroplet differs from that measured within the DSC, thus explaining the apparent discrepancy observed and why the residual stress models for off-stoichiometric ratios appear to not correlate. Another potential solution relates to the nature of the polymer above T_g and the difficulty in measuring an accurate representation of adhesion for what would now be a rubbery state polymer. Our understanding of the adhesion mechanisms at work between a glass fibre and a rubbery state polymer is considerably less than that of a polymer in its glass state; thus the mechanisms could differ significantly.

8.2 Future Work

8.2.1 The influence of matrix chemistry on thermomechanical and mechanical properties of the matrix

The results of Chapter 4 overall showed that the R value possessed a significant level of influence over the thermomechanical properties of the system studied. However, it was noted that the values measured for T_g were significantly smaller than those recorded in literature for other DGEBA/ TETA systems. It was concluded that this was due to the modified nature of the Araldite 506 ® resin studied. As such it would be desirable to carry out a similar investigation into the influence of R on the thermomechanical properties of an unmodified DGEBA resin to confirm whether this was the correct conclusion. Confirming that this relationship with R occurs for other DGEBA resins would also be beneficial to ensure it is not a localised phenomenon occurring only for the Araldite 506 ®/ TETA system.

In light of the findings of the residual stress model, an in-depth study into the T_g of the microdroplets is also required to ascertain whether it differs significantly from the bulk matrix as the R value is changed. It is clear from the findings in Chapter 5 that the measured IFSS and T_g of the microdroplets must be related to some degree but how exactly the two fit within the residual stress model needs to be expanded upon further. The correlation for the model for R values close to $R \approx 1.0$ would suggest that this may only be a major issue once the R value deviates significantly away from this value. This study may directly lead to a further investigation using thermal gravimetric analysis (TGA) to study whether the TETA curing agent has potential for vaporising during the curing process. This would lead to the true R value of the droplet deviating from what was originally assigned. Changes to the T_g of a microdroplet could specifically be linked to changes to its R value, with a potential cause for this being vaporization of the curing agent. If this were the case, then this could explain why the residual stress model for $R >> 1$ shows a poor degree of correlation.

Further testing regarding the influence of the R value on the mechanical properties of the matrix would also be recommended. Specifically, the use of macromechanical tests such as tensile testing and impact testing would be of interest. Given the results presented in Chapter 4 it would be expected that the R value would exert significant influence over properties such as the Young's modulus and the fracture toughness of the material. Fracture toughness is understood to be a key property when it comes to defining the strength of the interface in the composites industry and as such would be primary importance. If the influence of temperature could be investigated in combination with this study then this would provide a better understanding of what may be occurring to the minute samples tested in the TMA, especially at the extreme R values.

Whilst the FT-IR and Raman studies conducted did provide data that was beneficial for understanding the molecules present within the polymer for different R values after curing, it was understood that there were certain limitations associated with the techniques. The sample quality used for the analysis proved adequate for mIR and nIR analysis but not for Raman. Overall the sample quality could certainly be improved. Thus, a more in-depth study, with the design of a mould to produce samples specific to mIR, nIR and Raman would be beneficial to allow for a more accurate study to be fully completed. In addition, the introduction of other potential variables such as different curing schedules for samples, different resins systems, different heating rates and the use of the high purity TETA would each provide interesting avenues regarding how they change the degree to which there are remaining reactive epoxy and amine groups within the polymer after curing.

8.2.2 The influence of matrix chemistry on GF – Epoxy Interface

The results of Chapter 5 showed that the R value significantly influenced the IFSS value measured using the microbond technique for the Araldite 506®/TETA system. The obvious next step regarding this investigation would be to study whether the R value possessed a comparable level of influence over the IFSS value for another DGEBA resin system. This would remove the possibility that the observed relationship is localised to this one system.

In the same vein it would be beneficial to carry out a comparable matrix stoichiometry study using other interface characterization techniques, both micromechanical and macromechanical. It is accepted that the microbond techniques possesses certain limitations which other test methods do not possess. As such, if the same relationship between the stress transfer capability of the interface and the R value was observed using other techniques then this would remove any doubt regarding its role in defining the level of fibre-matrix adhesion.

One of the issues typically observed when using the microbond test relates to the degree of data scatter that occurs during the test. It was observed when conducting the microbond test within the TMA using fixed blades that the degree of scatter of the data collected was significantly smaller than that for the regular microbond test. This in turn led to the undergraduate investigation presented in Appendix A to compare the adjustable blade setup to a new fixed blade design. The results were inconclusive due to a manufacturing error regarding the fixed blade setup, however it was felt that if this was repeated the fixed blade setup would prove superior in terms of the quality of data collected. The reasoning behind this hypothesis relates to the size of the remaining meniscus of samples after de-bonding has occurred. It was found, using SEM analysis, that the meniscus for fixed blade samples was considerably smaller. This in turn leads to a more accurate value of the embedded area being tested which does not need to be corrected afterwards, as was typically the case for the adjustable blade setup. As such a more in-depth study into the comparison between the two blade setups would be beneficial into enhancing the current microbond technique used.

A point of interest identified during the literature review was that the wettability of the fibre can play an important role in defining the level of interfacial adhesion. In Chapter 5 it was shown that R value and the sizing chemistry of the fibre could both influence the level of interfacial adhesion. Glass fibre sizings are typically designed to possess superior wettability with the polymers they are meant to bond with, to promote the maximum level of bonding. It would be of interest to investigate the wettability of the different fibres studied to gauge whether the wettability findings correlate with those shown for the IFSS values. Furthermore, it would be beneficial to study the wettability of these fibres by dipping them into the epoxy system mixed at different R values. Judging by the influence that the R value possesses over a large degree of the matrix

properties, it might be expected to influence the ability of the system to wet upon the fibre. This would be particularly significant during the sample preparation process for the microbond process, where the formation of minute droplets of epoxy resin is one of the key variables.

Finally, it was noted from the literature review that one of the less touched upon subjects regarding the interface is its effect on the long term micromechanical fatigue performance of the composite. Variables of the interface, such as the chemistry of the fibre sizing, are accepted as playing a key role in defining most of the parameters which influence the long-term performance of composites subjected to environmental exposure and fatigue loading. Given the apparent role of the R value in dictating the stress transfer capability of the interface it may also be expected to contribute to the fatigue performance of the material. As such a novel fatigue study using dynamic mechanical analysis could be carried out to ascertain the role of the R value in defining the long-term strength of the interface using a microdroplet sample. This would also allow for the role of humidity to be studied regarding its influence over the stress transfer capability of the interface for an epoxy system with varying R values. In addition to this, the act of artificially ageing the interface of a sample has been conducted in the literature [13,264–267] however little research has been conducted into the role of the R value in this scenario. Thus, it would be beneficial to understand how the R value may influence the long-term performance of a GF/Epoxy composite.

8.2.3 The influence of matrix chemistry on cure shrinkage of polymer matrix

Chapter 7 introduced a novel method for studying the level of cure shrinkage that occurred for the Araldite 506®/ TETA system during the curing process. A natural next step in the investigation would be to carry out a comparable study using a different DGEBA resin to quantify whether similar levels of shrinkage would occur.

This would aid in confirming whether the hot-stage microscopy technique is a viable method for measuring cure shrinkage across a range of different systems. Specifically, this will aid in confirming whether no material is lost due to the volatile nature of the resin components. Given the differences shown in Chapter 4 when using the high purity TETA, it would also be of interest to study whether the hardener purity would have any effect on the level of shrinkage that would occur for a microdroplet.

Further research regarding the effect of the R value on the gel point of the matrix would also be beneficial. Due to time constraints with the equipment, only three R values were studied compared to the typical number of seven throughout the rest of the project. This would allow for each of the measurements made using the hot-stage method to be updated to reflect the level of shrinkage that would occur after the gel point.

Future work with the rheometer would also allow for more effort to be placed in developing the technique for measuring cure shrinkage with a varying temperature profile. Despite the difficulties encountered, towards the end of the experimental session it was felt that by making slight alterations to the procedure the technique would provide a viable comparison to the hot-stage method. Specifically, rather than defining the triggering point of gelling to a consistent value across each R value, instead the operator would manually track the moduli values as was done during the gel point experiments. Once they crossed, the operator would trigger the next stage of the procedure, where the load would be applied, and the gap width measured to gain the value of shrinkage. This change would hopefully remove the variability seen in the results in Chapter 7 where it was clear that the load was typically being applied before the sample had gelled to a satisfactory level. This was shown to have occurred at different levels from sample to sample across all ratios studied and thus represented the major difficulty with the method currently.

Considering the observations made regarding droplet deformations, it is recommended that future research should be focussed on studying this phenomenon in more detail to decipher the root cause of these deformations and whether they possess any influence on the final performance of a microbond sample. Potential avenues of research include further SEM analysis of the cured epoxy using forms other than minute droplets to examine whether these deformations scale or whether they occur only for droplets. In addition to this, analysis of different epoxy systems is also required to find out whether the phenomenon is specific to the Araldite 506® resin used in this thesis. Another interesting question would be whether the large variation in individual values of IFSS might be related to what type and severity of deformation that each individual droplet exhibited. Finite element analysis of droplet deformations would allow for us to understand how in theory these deformations could influence the strength of the microdroplet samples. Modelling of the failure mechanics for such samples would also be of interest to understand why it appears that such deformations do not ultimately affect the IFSS values measured for certain samples.

References

[1] R.-M. Wang, S.-R. Zheng, Y.-P. Zheng, R.-M. Wang, S.-R. Zheng, Y.-P. Zheng, Introduction to polymer matrix composites, in: Polym. Matrix Compos. Technol., 2011: pp. 1–548. doi:10.1533/9780857092229.1.

[2] J.L. Thomason, Glass Fibre Sizings: A Review of the Scientific Literature, Blurb Inc, 2012. http://www.blurb.co.uk/b/6244677-glass-fibre-sizings.

[3] F.T. Wallenberger, J.C. Watson, H. Li, Glass Fibers, ASM Hanb. 21: Compos (2001) 27–34.

[4] R.A. Pethrick, Polymer Science and Technology for Engineers and Scientists, in: Polym. Sci. Technol. Eng. Sci., Wiley, 2010: pp. 1–185. doi:10.1017/CBO9781107415324.004.

[5] A.T. DiBenedetto, Tailoring of interfaces in glass fiber reinforced polymer composites: a review, Mater. Sci. Eng. A. 302 (2001) 74–82. doi:10.1016/S0921-5093(00)01357-5.

[6] F.R. Jones, A Review of Interphase Formation and Design in Fibre-Reinforced Composites, 2010. doi:10.1163/016942409X12579497420609.

[7] J.-K. Kim, Y.-W. Mai, Characterization of interfaces, in: Eng. Interfaces Fiber Reinf. Compos., Elsevier, 1998: pp. 5–41. doi:10.1016/0250-6874(81)80012-1.

[8] P.J. Herrera-Franco, L.T. Drzal, Comparison of methods for the measurement of fibre/matrix adhesion in composites, Composites. 23 (1992) 2–27. doi:10.1016/0010-4361(92)90282-Y.

[9] L.J. Broutman, Measurement of the Fiber-Polymer Matrix Interfacial Strength, Interfaces Compos. ASTM STP 452. (1969) 27–41.

[10] M. Dey, J.M. Deitzel, J.W. Gillespie, S. Schweiger, Influence of sizing formulations on glass/epoxy interphase properties, Compos. Part A Appl. Sci. Manuf. 63 (2014) 59–67. doi:10.1016/j.compositesa.2014.04.006.

[11] L.T. Drzal, M. Madhukar, Fibre-matrix adhesion and its relationship to composite mechanical properties, J. Mater. Sci. 28 (1993) 569–610.

doi:10.1007/BF01151234.

[12] R.J. Gray, C.D. Johnston, The effect of matrix composition on fibre/matrix interfacial bond shear strength in fibre-reinforced mortar, Cem. Concr. Res. 14 (1984) 285–296. doi:10.1016/0008-8846(84)90116-9.

[13] R. Plonka, E. Mäder, S.L. Gao, C. Bellmann, V. Dutschk, S. Zhandarov, Adhesion of epoxy/glass fibre composites influenced by aging effects on sizings, Compos. Part A Appl. Sci. Manuf. 35 (2004) 1207–1216. doi:10.1016/j.compositesa.2004.03.005.

[14] J.L. Thomason, L. Yang, Temperature dependence of the interfacial shear strength in glass-fibre polypropylene composites, Compos. Sci. Technol. 71 (2011) 1600–1605. doi:10.1016/j.compscitech.2011.07.006.

[15] J.L. Thomason, L. Yang, Temperature dependence of the interfacial shear strength in glass-fibre epoxy composites, Compos. Sci. Technol. 96 (2014) 7–12. doi:10.1016/j.compscitech.2014.03.009.

[16] J.A. Nairn, Thermoelastic analysis of residual stresses in unidirectional, high-performance composites, Polym. Compos. 6 (1985) 123–130. doi:10.1002/pc.750060211.

[17] R.S. Raghava, Thermal expansion of organic and inorganic matrix composites: A Review of theoretical and experimental studies, Polym. Compos. 9 (1988) 1–11. doi:10.1002/pc.750090102.

[18] H.D. Wagner, J.A. Nairn, Residual thermal stresses in three concentric transversely isotropic cylinders: application to composites containing a interphase., Compos. Sci. Technol. 57 (1997) 1289–1302. doi:10.1016/S0266-3538(97)00058-4.

[19] L. Di Landro, M. Pegoraro, Carbon fibre thermoplastic matrix adhesion, J. Mater. Sci. 22 (1987) 1980–1986. doi:10.1007/BF01132927.

[20] D.A. Biro, G. Pleizier, Y. Deslandes, Application of the microbond technique: Effects of hygrothermal exposure on carbon-fiber/epoxy interfaces, Compos. Sci. Technol. 46 (1993) 293–301. doi:10.1016/0266-3538(93)90163-B.

[21] J. Jakobsen, M. Jensen, J.H. Andreasen, Thermo-mechanical

characterisation of in-plane properties for CSM E-glass epoxy polymer composite materials – Part 1: Thermal and chemical strain, Polym. Test. 32 (2013) 1350–1357. doi:10.1016/j.polymertesting.2013.08.010.

[22] L. Di Landro, M. Pegoraro, Evaluation of residual stresses and adhesion in polymer composites, Compos. Part A Appl. Sci. Manuf. 27 (1996) 847–853. doi:10.1016/1359-835X(96)00046-2.

[23] Y.A. Chekanov, V.N. Korotkov, B.A. Rozenberg, E.A. Dhzavadyan, L.M. Bogdanova, Cure shrinkage defects in epoxy resins, Polymer. 36 (1995) 2013–2017. doi:10.1016/0032-3861(95)91446-E.

[24] H. Ismail, S. Shuhelmy, M.R. Edyham, The effects of a silane coupling agent on curing characteristics and mechanical properties of bamboo fibre filled natural rubber composites, Eur. Polym. J. 38 (2002) 39–47. doi:10.1016/S0014-3057(01)00113-6.

[25] J.A. Ramos, N. Pagani, C.C. Riccardi, J. Borrajo, S.N. Goyanes, I. Mondragon, Cure kinetics and shrinkage model for epoxy-amine systems, Polymer. 46 (2005) 3323–3328. doi:10.1016/j.polymer.2005.02.069.

[26] H. Petersen, Investigation of sizing - from glass fibre surface to composite interface, PhD Thesis. Technical University of Denmark, 2017.

[27] B. Ellis, Introduction to the chemistry, synthesis, manufacture and characterization of epoxy resins, in: B. Ellis (Ed.), Chem. Technol. Epoxy Resins, 1993 Editi, Springer, 2012: pp. 1–35.

[28] D.N. Dang, S. Cohendoz, S. Mallarino, X. Feaugas, S. Touzain, Effects of curing program on mechanical behavior and water absorption of DGEBA/TETa epoxy network, J. Appl. Polym. Sci. 129 (2013) 2451–2463. doi:10.1002/app.38843.

[29] W.R. Ashcroft, Curing agents for epoxy resins, in: B. Ellis (Ed.), Chem. Technol. Epoxy Resins, 1993 Editi, Springer, 2012: pp. 37–70.

[30] G. Nikolić, S. Zlatkovic, M. Cakic, S. Cakić, C. Lacnjevac, Z. Rajic, Fast Fourier Transform IR Characterization of Epoxy GY Systems Crosslinked with Aliphatic and Cycloaliphatic EH Polyamine Adducts, Sensors (Basel). 10

(2010) 684–696. doi:10.3390/s100100684.

[31] B. Ellis, The kinetics of cure and network formation, in: B. Ellis (Ed.), Chem. Technol. Epoxy Resins, 1993 Editi, Springer, 2012: pp. 72–113.

[32] C.C. Riccardi, R.J.J. Williams, A kinetic scheme for an epoxy-amine reaction with simultaneous etherification, J. Appl. Polym. Sci. 32 (1986) 3445–3456. doi:10.1002/app.1986.070320208.

[33] L. Xu, J.R. Schlup, Etherification versus amine addition during epoxy resin amine cure: An in situ study using near-infrared spectroscopy, J. Appl. Polym. Sci. 67 (1997) 895–901. doi:10.1002/(SICI)1097-4628(19980131)67:5<895::AID-APP15>3.0.CO;2-N.

[34] N. Sbirrazzuoli, A. Mititelu-Mija, L. Vincent, C. Alzina, Isoconversional kinetic analysis of stoichiometric and off-stoichiometric epoxy-amine cures, Thermochim. Acta. 447 (2006) 167–177. doi:10.1016/j.tca.2006.06.005.

[35] S.L. Simon, J.K. Gillham, Reaction Kinetics and TTT Cure Diagrams for Off-Stoichiometric Ratios of a High-Tg Epoxy/ Amine System, J. Appl. Polym. Sci. 46 (1992) 1245–1270. doi:10.1002/app.1992.070460714.

[36] L.C. Chan, H.N. Nae, J.K. Gillham, Time-temperature-transformation (TTT) diagrams of high Tg epoxy systems: Competition between cure and thermal degradation, J. Appl. Polym. Sci. 29 (1984) 3307–3327. doi:10.1002/app.1984.070291109.

[37] J.K. Gillham, Formation and Properties of Thermosetting and High Tg Polymeric Materials, Polym. Eng. Sci. 26 (1986) 1429–1433. doi:10.1002/pen.760262012.

[38] J.K. Gillham, G. Wisanrakkit, The glass transition temperature (Tg) as an index of chemical conversion for a High-Tg amine/epoxy system: Chemical and diffusion-controlled reaction kinetics.pdf, J. Appl. Polym. Sci. Volume 41 (1990) 2885–2929. doi:10.1002/app.1990.070411129.

[39] J.B. Enns, J.K. Gillham, Effect of the Extent of Cure on the Modulus, Glass Transition, Water Absorption, and Density of an Amine-Cured Epoxy., J. Appl. Polym. Sci. 28 (1983) 2831–2846. doi:10.1002/app.1983.070280914.

[40] S. Montserrat, Vitrification and Further Structural Relaxation in the Isothermal Curing of an Epoxy-Resin, J. Appl. Polym. Sci. 44 (1992) 545–554. doi:10.1002/app.1992.070440319.

[41] T. Koike, Dielectric Relaxation During Isothermal Curing of Epoxy Resin with an Aromatic Amine, J. Appl. Polym. Sci. 44 (1992) 679–690. doi:10.1002/app.1992.070440415.

[42] Q. Wang, B.K. Storm, L.P. Houmøller, Study of the isothermal curing of an epoxy prepreg by near-infrared spectroscopy, J. Appl. Polym. Sci. 87 (2003) 2295–2305. doi:10.1002/app.11711.

[43] P. Sharma, V. Choudhary, A.K. Narula, Curing of epoxy resin using imide-amines, J. Appl. Polym. Sci. 101 (2006) 3503–3510. doi:10.1002/app.24580.

[44] D. Rosu, C.N. Cascaval, F. Mustata, C. Ciobanu, Cure kinetics of ternary blends of epoxy resins studied by nonisothermal DSC data, Thermochim. Acta. 383 (2002) 119–127. doi:10.1002/app.29781.

[45] V.L. Zvetkov, Comparative DSC kinetics of the reaction of DGEBA with aromatic diamines . I . Non-isothermal kinetic study of the reaction of DGEBA with m -phenylene diamine, Polymer. 42 (2001) 6687–6697. doi:http://dx.doi.org/10.1016/S0032-3861(01)00160-4.

[46] R.A. Pethrick, E.A. Hollins, I. McEwan, E.A. Pollock, D. Hayward, P. Johncock, Effect of Cure Temperature on the Structure and Water Absorption of Epoxy/Amine Thermosets, Polym. Int. 39 (1996) 275–288. doi:10.1002/(SICI)1097-0126(199604)39:4<275::AID-PI508>3.0.CO;2-I.

[47] T.P. Skourlis, R.L. McCullough, An experimental investigation of the effect of prepolymer molecular weight and stoichiometry on thermal and tensile properties of epoxy resins, J. Appl. Polym. Sci. 62 (1996) 481–490. doi:10.1002/(SICI)1097-4628(19961017)62:3<481::AID-APP6>3.0.CO;2-M.

[48] F. Meyer, G. Sanz, A. Eceiza, I. Mondragon, The effect of stoichiometry and thermal history during cure on structure and properties of epoxy networks, Polymer. 36 (1995) 1407–1414. doi:10.1016/0032-3861(95)95918-Q.

[49] F. Gonzalez Garcia, B.G. Soares, V.J.R.R. Pita, R. Sanchez, J. Rieumont,

Mechanical Properties of Epoxy Networks Based on DGEBA and Aliphatic Amines, J. Appl. Polym. Sci. 106 (2007) 2047–2055. doi:10.1002/app.24895.

[50] F. Fernandez-Nograro, A. Valea, R. Llano-Ponte, I. Mondragon, Dynamic and Mechanical Properties of DGEBA/PP Amine based Epoxy Resins as a function of Stoichiometry, Eur. Polym. J. 32 (1996) 257–266. doi:10.1016/0014-3057(95)00122-0.

[51] M.R. Vanlandingham, R.F. Eduljee, J.W. Gillespie Jr., Relationships between stoichiometry, microstructure, and properties for amine-cured epoxies, J. Appl. Polym. Sci. 71 (1999) 699–712. doi:10.1002/(sici)1097-4628(19990131)71:5<699::aid-app4>3.0.co;2-d.

[52] J.R.M. D'Almeida, S.N. Monteiro, Role of the resin matrix/hardener ratio on the mechanical properties of low volume fraction epoxy composites, Adv. Perform. Mater. 4 (1997) 285–295. doi:10.1023/A:1008625121464.

[53] J.R.M. D'Almeida, S.N. Monteiro, The Effect of the resin/hardener ratio on the compressive behavior of an epoxy system, Polym. Test. 15 (1996) 329–339. doi:10.1016/0142-9418(95)00037-2.

[54] J.R.M. D'Almeida, S.N. Monteiro, The resin/hardener ratio as a processing parameter for modifying the mechanical behaviour of epoxy-matrix/glass microsphere composites, Compos. Sci. Technol. 58 (1998) 1593–1598. doi:10.1016/S0266-3538(97)00223-6.

[55] J.R.M. D'Almeida, S.N. Monteiro, The Influence of the Amount of Hardener on the Tensile Mechanical Behavior of an Epoxy System, Polym. Adv. Technlogies. 9 (1998) 216–221. doi:10.1002/(SICI)1099-1581(199803)9:3<216::AID-PAT746>3.0.CO;2-S.

[56] J.R.M. D'Almeida, W.G. de Menezes, S. Neves Monteiro, Ageing of the DGEBA / TETA Epoxy System with off-Stoichiometric Compositions 2 . Experimental Methods And Materials, Mater. Res. 6 (2003) 415–420. doi:10.1590/S1516-14392003000300017.

[57] G.R. Palmese, R.L. McCullough, Effect of epoxy-amine stoichiometry on cured resin material properties, J. Appl. Polym. Sci. 46 (1992) 1863–1873. doi:10.1002/app.1992.070461018.

[58] F. Bignotti, S. Pandini, F. Baldi, R. De Santis, Effect of the Resin/Hardener Ratio on Curing, Structure and Glass Transition Temperature of Nanofilled Epoxies Fabio, Polym. Compos. 32 (2011) 1034–1048. doi:10.1002/pc.

[59] M.R. Gude, S.G. Prolongo, A. Urena, Effect of the epoxy/amine stoichiometry on the properties of carbon nanotube/epoxy composites, J. Therm. Anal. Calorim. 108 (2012) 717–723. doi:10.1007/s10973-011-2056-x.

[60] D.U. Shah, P.J. Schubel, Evaluation of cure shrinkage measurement techniques for thermosetting resins, Polym. Test. 29 (2010) 629–639. doi:10.1016/j.polymertesting.2010.05.001.

[61] L. Khoun, P. Hubert, Cure Shrinkage Characterization of an Epoxy Resin System by Two in Situ Measurement Methods, Polym. Compos. 31 (2010) 1603–1610. doi:10.1002/pc.

[62] Y. Nawab, S. Shahid, N. Boyard, F. Jacquemin, Chemical shrinkage characterization techniques for thermoset resins and associated composites, J. Mater. Sci. 48 (2013) 5387–5409. doi:10.1007/s10853-013-7333-6.

[63] K.F. Schoch, P.A. Panackal, P.P. Frank, Real-time measurement of resin shrinkage during cure, Thermochim. Acta. 417 (2004) 115–118. doi:10.1016/j.tca.2003.12.027.

[64] H. Yu, S.G. Mhaisalkar, E.H. Wong, Cure shrinkage measurement of nonconductive adhesives by means of a thermomechanical analyzer, J. Electron. Mater. 34 (2005) 1177–1182. doi:10.1007/s11664-005-0248-5.

[65] S. V. Hoa, P. Ouellette, T.D. Ngo, Determination of Shrinkage and Modulus Development of Thermosetting Resins, J. Compos. Mater. 43 (2009) 783–803. doi:10.1177/0021998308102035.

[66] J.-K. Kim, Y.-W. Mai, Introduction, in: Eng. Interfaces Fiber Reinf. Compos., Elsevier, 1998: pp. 1–4. doi:10.1016/S0065-230X(09)04001-9.

[67] L. Yang, A Physical Approach To Interfacial Strength In Fibre Reinforced Thermoplastic Composites, PhD Thesis. University of Strathclyde, 2011.

[68] F.E. Bartell, H.J. Osterhof, Determination of the Wettability of a Solid by a Liquid, Ind. Eng. Chem. 19 (1927) 1277–1280. doi:10.1021/ie50215a026.

[69] T. Young, An Essay on the Cohesion of Fluids, Philos. Trans. R. Soc. London. 95 (1805) 67–87.

[70] L.T. Drzal, The interphase in epoxy composites, in: K. Dusek (Ed.), Epoxy Resins Compos. II, 1st ed., Springer-Verlag Berlin Heidelberg, 1986: pp. 1–32.

[71] K. Van De Velde, P. Kiekens, Wettability and surface analysis of glass fibres, Indian J. Fibre Text. Res. 25 (2000) 8–13.

[72] K. Szymczyk, A. Zdziennicka, J. Krawczyk, B. Jańczuk, Wettability, adhesion, adsorption and interface tension in the polymer/surfactant aqueous solution system. I. Critical surface tension of polymer wetting and its surface tension, Colloids Surfaces A Physicochem. Eng. Asp. 402 (2012) 132–138. doi:10.1016/j.colsurfa.2012.02.054.

[73] S. Rebouillat, B. Letellier, B. Steffenino, Wettability of single fibres - beyond the contact angle approach, Int. J. Adhes. Adhes. 19 (1999) 303–314. doi:10.1016/S0143-7496(99)00006-8.

[74] K. Szymczyk, A. Zdziennicka, J. Krawczyk, B. Ja??czuk, Wettability, adhesion, adsorption and interface tension in the polymer/surfactant aqueous solution system: II. Work of adhesion and adsorption of surfactant at polymer-solution and solution-air interfaces, Colloids Surfaces A Physicochem. Eng. Asp. 402 (2012) 139–145. doi:10.1016/j.colsurfa.2012.02.055.

[75] M. Giraud, T. Nguyen, X. Gu, M.R. Vanlandingham, Effects of stoichiometry and epoxy molecular mass on wettability and interfacial microstructures of amine-cured epoxies, in: 24th Annu. Meet. Adhes. Soc., National Institute of Standards and Technology, Williamsburg, 2001: pp. 260–262.

[76] P. Chen, C. Lu, Q. Yu, Y. Gao, J. Li, X. Li, Influence of fiber wettability on the interfacial adhesion of continuous fiber-reinforced PPESK composite, J. Appl. Polym. Sci. 102 (2006) 2544–2551. doi:10.1002/app.24681.

[77] J.L. Thomason, The interface region in glass fibre-reinforced epoxy resin composites: 3. Characterization of fibre surface coatings and the interphase, Composites. 26 (1995) 487–498. doi:10.1016/0010-4361(95)96806-H.

[78] W.A. Zisman, Contact Angle, Wettability, and Adhesion, in: F.M. Fowkes (Ed.), Advances in Chemistry; American Chemical Society, 1964: pp. 1–51. doi:10.1021/ba-1964-0043.

[79] E.P. Plueddemann, Reminiscing on silane coupling agents, J. Adhes. Sci. Technol. 5 (1990) 261–277. doi:10.1163/156856191X00350.

[80] J.G. Williams, M.E. Donnellan, M.R. James, W.L. Morris, Properties of the interphase in organic matrix composites, Mater. Sci. Eng. A. 126 (1990) 305–312. doi:10.1016/0921-5093(90)90137-R.

[81] H.C. Tsai, A.M. Arocho, L.W. Gause, Prediction of fiber-matrix interphase properties and their influence on interface stress, displacement and fracture toughness of composite material, Mater. Sci. Eng. A. 126 (1990) 295–304. doi:https://doi.org/10.1016/0921-5093(90)90136-Q.

[82] X. Gao, R.E. Jensen, W. Li, J. Deitzel, S.H. McKnight, J.W. Gillespie, Effect of Fiber Surface Texture Created from Silane Blends on the Strength and Energy Absorption of the Glass Fiber/Epoxy Interphase, J. Compos. Mater. 42 (2008) 513–534. doi:10.1177/0021998307086203.

[83] F. Awaja, M. Gilbert, G. Kelly, B. Fox, P.J. Pigram, Adhesion of polymers, Prog. Polym. Sci. 34 (2009) 948–968. doi:10.1016/j.progpolymsci.2009.04.007.

[84] J.L. Thomason, L. Yang, Temperature dependence of the interfacial shear strength in glass- fibre epoxy composites., Compos. Sci. Technol. 96 (2014) 7–12. doi:10.1016/j.buildenv.2006.10.027.

[85] L.G. Zhao, N.A. Warrior, A.C. Long, A micromechanical study of residual stress and its effect on transverse failure in polymer-matrix composites, Int. J. Solids Struct. 43 (2006) 5449–5467. doi:10.1016/j.ijsolstr.2005.08.012.

[86] H. Li, J.C. Watson, Continuous Glass Fibres for Reinforcement, in: P. Richet (Ed.), Encycl. Glas. Sci. Technol. Hist. Cult., John Wiley & Sons, 2018.

[87] F.T. Wallenberger, Commercial and Experimental Glass Fibers, in: Fiberglass Glas. Technol. Energy-Friendly Compos. Appl., 2010: pp. 1–474. doi:10.1007/978-1-4419-0736-3.

[88] B.D. Agarwal, L.J. Broutman, K. Chandrashekhara, Analysis and Performance of Fiber Composites, 2006. doi:10.1002/pol.1980.130181011.

[89] S.. Saidpour, M.O.. Richardson, Glass fibre coating for optimum mechanical properties of vinyl ester composites, Compos. Part A Appl. Sci. Manuf. 28 (1997) 971–975. doi:10.1016/S1359-835X(97)00071-7.

[90] R.C. Zhuang, T. Burghardt, R. Plonka, J.W. Liu, E. Mäder, Affecting glass fibre surfaces and composite properties by two stage sizing application, Express Polym. Lett. 4 (2010) 798–808. doi:10.3144/expresspolymlett.2010.96.

[91] B. Fernandez, A. Arbelaiz, A. Valea, F. Mujika, I. Mondragon, A comparative study on the influence of epoxy sizings on the mechanical performance of woven carbon fiber-epoxy composites, Polym. Compos. 25 (2004) 319–330. doi:10.1002/pc.20026.

[92] Z. Dai, F. Shi, B. Zhang, M. Li, Z. Zhang, Effect of sizing on carbon fiber surface properties and fibers/epoxy interfacial adhesion, Appl. Surf. Sci. 257 (2011) 6980–6985. doi:10.1016/j.apsusc.2011.03.047.

[93] E.K. Drown, H. Al Moussawi, L. Drzal, Glass fiber sizings and their role in fiber-matrix adhesion, J. Adhes. Sci. Technol. 5 (1991) 865–881. doi:10.1163/156856191X00260.

[94] M. Tanoglu, S.H. McKnight, G.R. Palmese, J.W. Gillespie, Effects of glass-fiber sizings on the strength and energy absorption of the fiber/matrix interphase under high loading rates, Compos. Sci. Technol. 61 (2001) 205–220. doi:10.1016/S0266-3538(00)00195-0.

[95] C. Sellitti, S. Vargui, E. Martuscelli, D. Fabbro, Wettability of glass fibres with different sizings and their adhesion to unsaturated polyester matrices, J. Mater. Sci. 22 (1987) 3477–3484. doi:10.1007/BF01161445.

[96] P. Jenkins, Investigation of the Strength Loss of Heat Treated Glass Fibre, PhD Thesis. University of Strathclyde, 2016.

[97] J.-K. Kim, Y.-W. Mai, Surface treatments of fibers and effects on composite properties, in: Eng. Interfaces Fiber Reinf. Compos., Elsevier, 1998: pp. 171–

237.

[98] J. Perdigão, G. Gomes, I.K. Lee, The effect of silane on the bond strengths of fiber posts, Dent. Mater. 22 (2006) 752–758. doi:10.1016/j.dental.2005.11.002.

[99] S. Debnath, S.L. Wunder, J.I. McCool, G.R. Baran, Silane treatment effects on glass/resin interfacial shear strengths, Dent. Mater. 19 (2003) 441–448. doi:10.1016/S0109-5641(02)00089-1.

[100] L. Yang, J.L. Thomason, Effect of silane coupling agent on mechanical performance of glass fibre, J. Mater. Sci. 48 (2012) 1947–1954. doi:10.1007/s10853-012-6960-7.

[101] H.F. Wu, D.W. Dwight, N.T. Huff, Effects of silane coupling agents on the interphase and performance of glass-fiber-reinforced polymer composites, Compos. Sci. Technol. 57 (1997) 975–983. doi:10.1016/S0266-3538(97)00033-X.

[102] B. Yu, Z. Jiang, X.Z. Tang, C.Y. Yue, J. Yang, Enhanced interphase between epoxy matrix and carbon fiber with carbon nanotube-modified silane coating, Compos. Sci. Technol. 99 (2014) 131–140. doi:10.1016/j.compscitech.2014.05.021.

[103] T. Jesionowski, A. Krysztafkiewicz, Influence of silane coupling agents on surface properties of precipitated silicas, Appl. Surf. Sci. 172 (2001) 18–32. doi:10.1016/S0169-4332(00)00828-X.

[104] Y. Xie, C.A.S. Hill, Z. Xiao, H. Militz, C. Mai, Silane coupling agents used for natural fiber/polymer composites: A review, Compos. Part A Appl. Sci. Manuf. 41 (2010) 806–819. doi:10.1016/j.compositesa.2010.03.005.

[105] C. Kaynak, C. Celikbilek, G. Akovali, Use of silane coupling agents to improve epoxy-rubber interface, Eur. Polym. J. 39 (2003) 1125–1132. doi:10.1016/S0014-3057(02)00381-6.

[106] S. Park, J.S. Jin, Effect of Silane Coupling Agent on Interphase and Performance of Glass Fibers/Unsaturated Polyester Composites, J. Colloid Interface Sci. 242 (2001) 174–179. doi:10.1006/jcis.2001.7788.

[107] A.K. Ghosh, E. Bertels, K. Allaer, D. Van Hemelrijck, B. Verheyde, B. Goderis, W. Van Paepegem, J. Degrieck, B. Van Mele, Effect of Silane Coupling Agent on Interfacial Strength of Stainless Steel, in: 16th Eur. Conferance Compos. Mater., Seville, 2014: pp. 1–5.

[108] J. Berg, F.R. Jones, The role of sizing resins, coupling agents and their blends on the formation of the interphase in glass fibre composites, Compos. Part A Appl. Sci. Manuf. 29 (1998) 1261–1272. doi:10.1016/S1359-835X(98)00091-8.

[109] J.L. Thomason, Glass Fibre Sizing: A Review of Size Formulation Patents, Blurb Inc, 2015. http://www.blurb.co.uk/b/6244662-glass-fibre-sizing.

[110] J.L. Koenig, H. Emadipour, Mechanical characterization of the interfacial strength of glass-reinforced composites, Polym. Compos. 6 (1985) 142–150. doi:10.1002/pc.750060303.

[111] D. Hull, T.W. Clyne, An Introduction to Composite Materials, Cambridge University Press, 1996.

[112] Edwin P. Plueddemann, Composite Materials Volume 6: Interfaces in Polymer Matrix Composites, Academic Press, 1974.

[113] H. Ishida, J.L. Koenig, Fourier transform infrared spectroscopic study of the silane coupling agent/porous silica interface, J. Colloid Interface Sci. 64 (1978) 555–564. doi:https://doi.org/10.1016/0021-9797(78)90398-3.

[114] H. Ishida, J.L. Koenig, An investigation of the coupling agent/matrix interface of fiberglass reinforced plastics by fourier transform infrared spectroscopy, J. Polym. Sci. Polym. Phys. Ed. 17 (1979) 615–626. doi:10.1002/pol.1979.180170405.

[115] H. Ishida, J.L. Koenig, Effect of hydrolysis and drying on the siloxane bonds of a silane coupling agent deposited on E-glass fibers, J. Polym. Sci. Polym. Phys. Ed. 18 (1980) 233–237. doi:10.1002/pol.1980.180180206.

[116] C.-H. Chiang, H. Ishida, J.L. Koenig, The structure of γ-aminopropyltriethoxysilane on glass surfaces, J. Colloid Interface Sci. 74 (1980) 396–404. doi:https://doi.org/10.1016/0021-9797(80)90209-X.

[117] M.K. Antoon, J.L. Koenig, Irreversible effects of moisture on the epoxy matrix in glass-reinforced composites, J. Polym. Sci. Polym. Phys. Ed. 19 (1981) 197–212. doi:10.1002/pol.1981.180190202.

[118] C. Chiang, J.L. Koenig, Fourier transform infrared spectroscopic study of the adsorption of multiple amino silane coupling agents on glass surfaces, J. Colloid Interface Sci. 83 (1981) 361–370. doi:https://doi.org/10.1016/0021-9797(81)90331-3.

[119] H. Ishida, C. Chiang, J.L. Koenig, The structure of aminofunctional silane coupling agents: 1. γ-Aminopropyltriethoxysilane and its analogues, Polymer. 23 (1982) 251–257. doi:https://doi.org/10.1016/0032-3861(82)90310-X.

[120] S.R. Culler, H. Ishida, J.L. Koenig, The silane interphase of composites: Effects of process conditions on γ-aminopropyltriethoxysilane, Polym. Compos. 7 (1986) 231–238. doi:10.1002/pc.750070406.

[121] Y.-T. Liao, A study of glass fiber–epoxy composite interfaces, Polym. Compos. 10 (1989) 424–428. doi:10.1002/pc.750100606.

[122] K.-P. Hoh, H. Ishida, J.L. Koenig, Spectroscopic studies of the gradient in the silane coupling agent/matrix interface in fiberglass-reinforced epoxy, Polym. Compos. 9 (1988) 151–157. doi:10.1002/pc.750090209.

[123] K. Albert, B. Pfleiderer, E. Bayer, R. Schnabel, Characterization of chemically modified glass surfaces by 13C and 29Si CP/MAS NMR spectroscopy, J. Colloid Interface Sci. 142 (1991) 35–40. doi:https://doi.org/10.1016/0021-9797(91)90031-3.

[124] C. Jones, C.J. Kiely, S.S. Wang, The characterization of an SCS6/Ti–6Al–4V MMC interphase, J. Mater. Res. 4 (1989) 327–335. doi:10.1557/JMR.1989.0327.

[125] D. Wang, F.R. Jones, P. Denison, TOF SIMS and XPS study of the interaction of hydrolysed γ-aminopropyltriethoxysilane with E-glass surfaces, J. Adhes. Sci. Technol. 6 (1992) 79–98. doi:10.1163/156856192X00070.

[126] D. Wang, F.R. Jones, Surface analytical study of the interaction between $γ$-amino propyl triethoxysilane and E-glass surface, J. Mater. Sci. 28 (1993)

2481–2488. doi:10.1007/BF01151683.

[127] T.H. Cheng, F.R. Jones, D. Wang, Effect of fibre conditioning on the interfacial shear strength of glass-fibre composites, Compos. Sci. Technol. 48 (1993) 89–96. doi:10.1016/0266-3538(93)90123-X.

[128] D. Wang, F.R. Jones, P. Denison, A tof sims study of the incorporation of aluminium into the silane coating on e-glass fibres, Catal. Today. 12 (1992) 375–383. doi:https://doi.org/10.1016/0920-5861(92)80052-O.

[129] E.P. Plueddemann, Adhesion Through Silane Coupling Agents, J. Adhes. 2 (1970) 184–201. doi:10.1080/0021846708544592.

[130] Edwin P. Plueddemann, Silane Coupling Agents, 2nd ed., Springer, 1982. http://www.springer.com/gb/book/9780306434730.

[131] M.E. Schrader, Radioisotopic Studies of Bonding at the Interface, J. Adhes. 2 (1970) 202–212. doi:10.1080/0021846708544593.

[132] A. Haque, M. Shamsuzzoha, F. Hussain, D. Dean, S2-Glass/Epoxy Polymer Nanocomposites: Manufacturing, Structures, Thermal and Mechanical Properties, J. Compos. Mater. 37 (2003) 1821–1837. doi:10.1177/002199803035186.

[133] J. Zhang, S. Deng, Y. Wang, L. Ye, L. Zhou, Z. Zhang, Effect of nanoparticles on interfacial properties of carbon fibre-epoxy composites, Compos. Part A Appl. Sci. Manuf. 55 (2013) 35–44. doi:10.1016/j.compositesa.2013.08.005.

[134] G.M. Odegard, T.C. Clancy, T.S. Gates, Modeling of the mechanical properties of nanoparticle/polymer composites, Polymer. 46 (2005) 553–562. doi:10.1016/j.polymer.2004.11.022.

[135] V. Nguyen, A. Vaughan, P. Lewin, A. Krivda, The effect of resin stoichiometry and nanoparticle addition on epoxy/silica nanodielectrics, IEEE Trans. Dielectr. Electr. Insul. 22 (2015) 895–905. doi:10.1109/TDEI.2015.7076790.

[136] E. Mader, S. Zhandarov, S.L. Gao, X.F. Zhou, S.R. Nutt, S. Zhandarov, Bond strength measurement between glass fibres and epoxy resin at elevated temperatures using the pull-out and push-out techniques, J. Adhes. 78 (2002) 547–569. doi:Doi 10.1080/00218460290010313.

[137] P. Sae-Oui, U. Thepsuwan, K. Hatthapanit, Effect of curing system on reinforcing efficiency of silane coupling agent, Polym. Test. 23 (2004) 397–403. doi:10.1016/j.polymertesting.2003.10.002.

[138] P.P. Parlevliet, H.E.N. Bersee, A. Beukers, Residual stresses in thermoplastic composites—A study of the literature—Part I: Formation of residual stresses, Compos. Part A Appl. Sci. Manuf. 37 (2006) 1847–1857. doi:10.1016/j.compositesa.2005.12.025.

[139] L. Yang, J.L. Thomason, The thermal behaviour of glass fibre investigated by thermomechanical analysis, J. Mater. Sci. 48 (2013) 5768–5775. doi:10.1007/s10853-013-7369-7.

[140] J.T. Zhang, M. Zhang, S.X. Li, M.J. Pavier, D.J. Smith, Residual stresses created during curing of a polymer matrix composite using a viscoelastic model, Compos. Sci. Technol. 130 (2016). doi:10.1016/j.compscitech.2016.05.002.

[141] M. Detassis, a. Pegoretti, C. Migliaresi, H.D. Wagner, Experimental evaluation of residual stresses in single fibre composites by means of the fragmentation test, J. Mater. Sci. 31 (1996) 2385–2392. doi:10.1007/BF01152951.

[142] A. Takaku, R.G.C. Arridge, The effect of interfacial radial and shear stress on fibre pull-out in composite materials, J. Phys. D. Appl. Phys. 6 (2002) 2038–2047. doi:10.1088/0022-3727/6/17/310.

[143] J.A. Nairn, P. Zoller, Matrix solidification and the resulting residual thermal stresses in composites, J. Mater. Sci. 20 (1985) 355–367. doi:10.1007/BF00555929.

[144] M. Detassis, A. Pegoretti, C. Migliaresi, Effect of temperature and strain rate on interfacial shear stress transfer in carbon/epoxy model composites, Compos. Sci. Technol. 53 (1995) 39–46. doi:10.1016/0266-3538(94)00069-7.

[145] M.M. Shokrieh, A.R.G. Mohammadi, The importance of measuring residual stresses in composite materials, Woodhead Publishing Limited, 2014. doi:10.1533/9780857098597.1.3.

[146] K.S. Kim, H.T. Hahn, Residual stress development during processing of graphite/epoxy composites, Compos. Sci. Technol. 36 (1989) 121–132. doi:10.1016/0266-3538(89)90083-3.

[147] K.D. Cowley, P.W.R. Beaumont, The measurement and prediction of residual stresses in carbon-fibre/polymer composites, Compos. Sci. Technol. 57 (1997) 1445–1455. doi:10.1016/s0266-3538(97)00048-1.

[148] G.R. Palmese, R.L. Mccullough, N.R. Sottos, Relationship between interphase composition, material properties, and residual thermal stresses in composite materials, J. Adhes. 52 (1995) 101–113. doi:10.1080/00218469508015188.

[149] L. Yang, J.L. Thomason, Development and application of micromechanical techniques for characterising interfacial shear strength in fibre-thermoplastic composites, Polym. Test. 31 (2012) 895–903. doi:10.1016/j.polymertesting.2012.07.001.

[150] M.R. Piggott, Why interface testing by single-fibre methods can be misleading, Compos. Sci. Technol. 57 (1997) 965–974. doi:10.1016/S0266-3538(97)00036-5.

[151] M.R. Piggott, Why the fibre/polymer interface can appear to be stronger than the polymer matrix, Compos. Sci. Technol. 57 (1997) 853–857. doi:10.1016/S0266-3538(96)00151-0.

[152] L. Yang, J.L. Thomason, Interface strength in glass fibre-polypropylene measured using the fibre pull-out and microbond methods, Compos. Part A Appl. Sci. Manuf. 41 (2010) 1077–1083. doi:10.1016/j.compositesa.2009.10.005.

[153] B. Liu, Z. Liu, X. Wang, G. Zhang, S. Long, J. Yang, Interfacial shear strength of carbon fiber reinforced polyphenylene sulfide measured by the microbond test, Polym. Test. 32 (2013) 724–730. doi:10.1016/j.polymertesting.2013.03.020.

[154] J.P. Craven, R. Cripps, C. Viney, Evaluating the silk/epoxy interface by means of the Microbond Test, Compos. Part A Appl. Sci. Manuf. 31 (2000) 653–660. doi:10.1016/S1359-835X(00)00042-7.

[155] A. Wada, H. Fukuda, Microbond Test for the Fiber/Matrix Interfacial Shearing Strength, in: 12th Int. Conf. Compos. Mater., Paris, 1999: pp. 1–8.

[156] H. Wang, H. Wang, W. Li, D. Ren, Y. Yu, An improved microbond test method for determination of the interfacial shear strength between carbon fibers and epoxy resin, Polym. Test. 32 (2013) 1460–1465. doi:10.1016/j.polymertesting.2013.09.017.

[157] N.S. Choi, J.E. Park, Fiber/matrix interfacial shear strength measured by a quasi-disk microbond specimen, Compos. Sci. Technol. 69 (2009) 1615–1622. doi:10.1016/j.compscitech.2009.03.012.

[158] B. Morlin, T. Czigany, Cylinder test: Development of a new microbond method, Polym. Test. 31 (2012) 164–170. doi:10.1016/j.polymertesting.2011.10.007.

[159] S. Sockalingam, G. Nilakantan, Fiber-matrix interface characterization through the microbond test: A review, Int. J. Aeronaut. Sp. Sci. 13 (2012) 282–295. doi:10.5139/IJASS.2012.13.3.282.

[160] B. Miller, P. Muri, L. Rebenfeld, A microbond method for determination of the shear strength of a fiber/resin interface, Composites. 18 (1987) 267. doi:10.1016/0010-4361(87)90471-X.

[161] P. Zinck, H.D. Wagner, L. Salmon, J.F. Gerard, Are microcomposites realistic models of the fibre / matrix interface? II . Physico-chemical approach, Polymer. 42 (2001) 6641–6650. doi:10.1016/S0032-3861(00)00871-5.

[162] G. Pandey, C.H. Kareliya, R.P. Singh, A study of the effect of experimental test parameters on data scatter in microbond testing, J. Compos. Mater. 46 (2012) 275–284. doi:10.1177/0021998311410508.

[163] H. Heilhecker, W. Cross, R. Pentland, C. Griswold., J.J. Kellar, L. Kj, The Vice Angle in the Microbond Test, J. Mater. Sci. Lett. 19 (2000) 2145–2147. doi:10.1023/a:1026787012473.

[164] M. Nishikawa, T. Okabe, K. Hemmi, N. Takeda, Micromechanical modeling of the microbond test to quantify the interfacial properties of fiber-reinforced composites, Int. J. Solids Struct. 45 (2008) 4098–4113.

doi:10.1016/j.ijsolstr.2008.02.021.

[165] H.F. Wu, C.M. Claypool, An analytical approach of the microbond test method used in characterizing the fibre-matrix interface, J. Mater. Sci. Lett. 10 (1991) 260–262. doi:10.1007/BF00735651.

[166] H.F. Wu, C.M. Claypool, A finite-element model of the use of the microbond test method for characterization of composite interfacial properties, J. Mater. Sci. Lett. 10 (1991) 1072–1075. doi:10.1007/BF00720128.

[167] Z. Liu, X. Yuan, A.J. Beck, F.R. Jones, Analysis of a modified microbond test for the measurement of interfacial shear strength of an aqueous-based adhesive and a polyamide fibre, Compos. Sci. Technol. 71 (2011) 1529–1534. doi:10.1016/j.compscitech.2011.06.001.

[168] D. Yang, Y. Sheng, J. Ye, Y. Tan, Discrete element modeling of the microbond test of fiber reinforced composite, Comput. Mater. Sci. 49 (2010) 253–259. doi:10.1016/j.commatsci.2010.05.003.

[169] C.T. Chou, U. Gaur, B. Miller, The effect of microvise gap width on microbond pull-out test results, Compos. Sci. Technol. 51 (1994) 111–116. doi:10.1016/0266-3538(94)90161-9.

[170] R.J. Day, J. V. Cauich Rodrigez, Investigation of the micromechanics of the microbond test, Compos. Sci. Technol. 58 (1998) 907–914. doi:10.1016/S0266-3538(97)00197-8.

[171] S. Sockalingam, M. Dey, J.W. Gillespie, M. Keefe, Finite element analysis of the microdroplet test method using cohesive zone model of the fiber/matrix interface, Compos. Part A Appl. Sci. Manuf. 56 (2014) 239–247. doi:10.1016/j.compositesa.2013.10.021.

[172] J.T. Ash, W.M. Cross, D. Svalstad, J.J. Kellar, L. Kjerengtroen, Finite element evaluation of the microbond test: Meniscus effect, interphase region, and vise angle, Compos. Sci. Technol. 63 (2003) 641–651. doi:10.1016/S0266-3538(02)00256-7.

[173] B.. Carroll, The accurate measurement of contact angle, phase contact areas, drop volume, and Laplace excess pressure in drop-on-fiber systems, J.

Colloid Interface Sci. 57 (1976) 488–495. doi:10.1016/0021-9797(76)90227-7.

[174] S.F. Zhandarov, E. V. Pisanova, The local bond strength and its determination by fragmentation and pull-out tests, Compos. Sci. Technol. 57 (1997) 957–964. doi:10.1016/S0266-3538(97)00037-7.

[175] Y. a. Gorbatkina, V.G. Ivanova-Mumjieva, Adhesion of polymers to fibers: Further elaboration of pull-out method, Polym. Sci. Ser. D. 2 (2009) 214–216. doi:10.1134/S1995421209040054.

[176] A.K. Patrikis, M.C. Andrews, R.J. Young, Analysis of the single fibre pull out test by the use of Raman spectroscopy. Part 1 Pull out of aramid fibres from an epoxy resin, Compos. Sci. Technol. 52 (1994) 387–396. doi:10.1016/0266-3538(95)00030-5.

[177] J.K. Kim, C. Baillie, Y.W. Mai, Interfacial debonding and fibre pull-out stresses - Part I Critical comparison of existing theories with experiments, J. Mater. Sci. 27 (1992) 3143–3154. doi:10.1007/BF01116004.

[178] J.P. Favre, M.C. Merienne, Characterization of fibre/resin bonding in composites using a pull-out test, Int. J. Adhes. Adhes. 1 (1981) 311–316. doi:10.1016/0143-7496(81)90025-7.

[179] T. Ramanathan, A. Bismarck, E. Schulz, K. Subramanian, Investigation of the influence of acidic and basic surface groups on carbon fibres on the interfacial shear strength in an epoxy matrix by means by single-fibre pull-out test, Compos. Sci. Technol. 61 (2001) 599–605. doi:10.1016/S0266-3538(00)00239-6.

[180] M.R. Piggott, The single-fibre pull out method: its advantages, interpretation and experimental realization, Compos. Interfaces. 1 (1993) 211–223. doi:10.1163/156855493X00086.

[181] C.I. Wang, Fracture mechanics of single-fibre pull-out test, J. Mate Rials Sci. 32 (1997) 483–490. doi:10.1023/A:1018534323464.

[182] S.-Y. Fu, C.-Y. Yue, X. Hu, Y.-W. Mai, Analyses of the micromechanics of stress transfer in single- and multi-fiber pull-out tests, Compos. Sci. Technol.

60 (2000) 569–579. doi:10.1016/S0266-3538(99)00157-8.

[183] L.M. Zhou, J.K. Kim, Y.W. Mai, On the single fibre pull-out problem: effect of loading method, Compos. Sci. Technol. 45 (1992) 153–160. doi:10.1016/0266-3538(92)90037-4.

[184] W. Beckert, B. Lauke, Finite element calculation of energy release rate for single-fibre pull-out test, Comput. Mater. Sci. 5 (1996) 1–11. doi:10.1016/0927-0256(95)00052-6.

[185] S. Zhandarov, E. Mäder, Analysis of a pull-out test with real specimen geometry. Part I: matrix droplet in the shape of a spherical segment, J. Adhes. Sci. Technol. 27 (2013) 430–465. doi:10.1080/01694243.2012.715730.

[186] W. Beckert, B. Lauke, Critical discussion of the single-fibre pull-out test: does it measure adhesion?*, Compos. Sci. Technol. 57 (1998) 1689–1706. doi:http://dx.doi.org/10.1016/S0266-3538(97)00107-3.

[187] D. Tripathi, F.R. Jones, Single fibre fragmentation test for assessing adhesion in fibre reinforced composites, J. Mater. Sci. 33 (1998) 1–16. doi:10.1023/A:1004351606897.

[188] M. Detassis, E. Frydman, D. Vrieling, X.F. Zhou, H.D. Wagner, J.A. Nairn, Interface toughness in fibre composites by the fragmentation test, Compos. Part A Appl. Sci. Manuf. 27 (1996) 769–773. doi:10.1016/1359-835X(96)00045-0.

[189] J. Zhang, D.L. He, H.D. Wagner, E. Wiesel, J.B. Bai, Interfacial studies of carbon fiber/epoxy composites using single fiber fragmentation test, Compos. Interfaces. 20 (2013) 421–429. doi:10.1080/15685543.2013.807148.

[190] H.D. Wagner, J.A. Nairn, M. Detassis, Toughness of interfaces from initial fiber-matrix debonding in a single fiber composite fragmentation test, Appl. Compos. Mater. An Int. J. Sci. Appl. Compos. Mater. 2 (1995) 107–117. doi:10.1007/BF00569253.

[191] X.F. Zhou, H.D. Wagner, S.R. Nutt, Interfacial properties of polymer composites measured by push-out and fragmentation tests, Compos. - Part A

Appl. Sci. Manuf. 32 (2001) 1543–1551. doi:10.1016/S1359-835X(01)00018-5.

[192] S. Deng, L. Ye, Y.-W. Mai, H.-Y. Liu, Evaluation of fibre tensile strength and fibre/matrix adhesion using single fibre fragmentation tests, Compos. Part A Appl. Sci. Manuf. 29 (1998) 423–434. doi:10.1016/S1359-835X(97)00094-8.

[193] D. Tripathi, F.R. Jones, Measurement of the load-bearing capability of the fibre/matrix interface by single-fibre fragmentation, Compos. Sci. Technol. 57 (1997) 925–935. doi:10.1016/S0266-3538(97)00016-X.

[194] A. Awal, G. Cescutti, S.B. Ghosh, J. Müssig, Interfacial studies of natural fibre/polypropylene composites using single fibre fragmentation test (SFFT), Compos. Part A Appl. Sci. Manuf. 42 (2011) 50–56. doi:10.1016/j.compositesa.2010.10.007.

[195] R. Joffe, J.A. Andersons, L. Wallström, Strength and adhesion characteristics of elementary flax fibres with different surface treatments, Compos. Part A Appl. Sci. Manuf. 34 (2003) 603–612. doi:10.1016/S1359-835X(03)00099-X.

[196] F.G. Torres, M.L. Cubillas, Study of the interfacial properties of natural fibre reinforced polyethylene, Polym. Test. 24 (2005) 694–698. doi:10.1016/j.polymertesting.2005.05.004.

[197] R.J. Sager, P.J. Klein, D.C. Lagoudas, Q. Zhang, J. Liu, L. Dai, J.W. Baur, Effect of carbon nanotubes on the interfacial shear strength of T650 carbon fiber in an epoxy matrix, Compos. Sci. Technol. 69 (2009) 898–904. doi:https://doi.org/10.1016/j.compscitech.2008.12.021.

[198] Y. Huang, R.J. Young, Analysis of the fragmentation test for carbon-fibre/epoxy model composites by means of Raman spectroscopy, Compos. Sci. Technol. 52 (1994) 505–517. doi:https://doi.org/10.1016/0266-3538(94)90033-7.

[199] J. Scherf, H.D. Wagner, Interpretation of fiber fragmentation in carbon/epoxy single fiber composites: Possible fiber pre-tension effects, Polym. Eng. Sci. 32 (1992) 298–304. doi:10.1002/pen.760320410.

[200] W. Liu, S. Zhang, L. Hao, X. Zhao, W. Jiao, F. Yang, R. Wang, Effect of Fiber

Surface on the Interfacial Properties for Carbon Fiber Reinforced Polymer Composites, Polym. Polym. Compos. 22 (2014) 283–288.

[201] P. Feillard, G. Désarmot, J.P. Favre, A critical assessment of the fragmentation test for glass/epoxy systems, Compos. Sci. Technol. 49 (1993) 109–119. doi:10.1016/0266-3538(93)90050-Q.

[202] J.-H. You, W. Lutz, H. Gerger, A. Siddiq, A. Brendel, C. Höschen, S. Schmauder, Fiber push-out study of a copper matrix composite with an engineered interface: Experiments and cohesive element simulation, Int. J. Solids Struct. 46 (2009) 4277–4286. doi:10.1016/j.ijsolstr.2009.08.021.

[203] K. Goto, I. Kawahara, H. Hatta, Y. Kogo, I. Shiota, Measurement of fiber/matrix interface properties of C/C composites by single fiber and fiber bundle push-out methods, Compos. Interfaces. 12 (2005) 603–616. doi:10.1163/156855405774327894.

[204] N. Chandra, C.R. Ananth, Analysis of interfacial behavior in MMCs and IMCs by the use of thin-slice push-out tests, Compos. Sci. Technol. 54 (1995) 87–100. doi:10.1016/0266-3538(95)00040-2.

[205] A.F. Kalton, D.B. Miracle, T.W. Clyne, The Effect of Interfacial Strength on the Response of Ti MMCs to Single Fibre Push-Out and Transverse Tensile Testing, Key Eng. Mater. 127–131 (1997) 659–670. doi:10.4028/www.scientific.net/KEM.127-131.659.

[206] A. Battisti, D. Esqué-de los Ojos, R. Ghisleni, A.J. Brunner, Single fiber push-out characterization of interfacial properties of hierarchical CNT-carbon fiber composites prepared by electrophoretic deposition, Compos. Sci. Technol. 95 (2014) 121–127. doi:10.1016/j.compscitech.2014.02.017.

[207] R.J. Kerans, T.A. Parthasarathy, F. Rebillat, J. Lamon, Interface Properties in High-Strength Nicalon/C/SiC Composites, As Determined by Rough Surface Analysis of Fiber Push-Out Tests, J. Am. Ceram. Soc. 81 (1998) 1881–1887. doi:10.1111/j.1151-2916.1998.tb02561.x.

[208] C. Medina M, J.M. Molina-Aldareguía, C. González, M.F. Melendrez, P. Flores, J. LLorca, Comparison of push-in and push-out tests for measuring interfacial shear strength in nano-reinforced composite materials, J. Compos.

Mater. 50 (2016). doi:10.1177/0021998315595115.

[209] T. Köck, A. Brendel, H. Bolt, Interface reactions between silicon carbide and interlayers in silicon carbide-copper metal-matrix composites, J. Nucl. Mater. 362 (2007) 197–201. doi:10.1016/j.jnucmat.2007.01.022.

[210] J.-K. Kim, Y.-W. Mai, Measurements of interface/interlaminar properties, in: Eng. Interfaces Fiber Reinf. Compos., Elsevier, 1998: pp. 43–92.

[211] ASTM D 2344/D 2344M, Standard Test Method for Short-Beam Strength of Polymer Matrix Composite Materials, i (2016) 1–8. doi:10.1520/D2344.

[212] S. Ogihara, Y. Sakamoto, J. Koyanagi, Evaluation of Interfacial Tensile Strength in Glass Fiber/Epoxy Resin Interface using the Cruciform Specimen Method, J. Solid Mech. Mater. Eng. 3 (2009) 1071–1080. doi:10.1299/jmmp.3.1071.

[213] S. Ogihara, J. Koyanagi, Investigation of combined stress state failure criterion for glass fiber/epoxy interface by the cruciform specimen method, Compos. Sci. Technol. 70 (2010) 143–150. doi:10.1016/j.compscitech.2009.10.002.

[214] G.P. Tandon, R.Y. Kim, V.T. Bechel, Fiber – Matrix Interfacial Failure Charcterization Using a Cruciform-shaped Specimen, J. Compos. Mater. 36 (2002) 2667–2691. doi:10.1106/002199802028686.

[215] A. Smits, D. Van Hemelrijck, T.P. Philippidis, A. Cardon, Design of a cruciform specimen for biaxial testing of fibre reinforced composite laminates, Compos. Sci. Technol. 66 (2006) 964–975. doi:10.1016/j.compscitech.2005.08.011.

[216] J. Koyanagi, H. Nakatani, S. Ogihara, Comparison of glass-epoxy interface strengths examined by cruciform specimen and single-fiber pull-out tests under combined stress state, Compos. Part A Appl. Sci. Manuf. 43 (2012) 1819–1827. doi:10.1016/j.compositesa.2012.06.018.

[217] J. Koyanagi, S. Ogihara, Temperature dependence of glass fiber/epoxy interface normal strength examined by a cruciform specimen method, Compos. Part B Eng. 42 (2011) 1492–1496.

doi:10.1016/j.compositesb.2011.04.041.

[218] ASTM E1356-08, Standard Test Method for Assignment of the Glass Transition Temperatures by Differential Scanning Calorimetry, (2008) 1–4. doi:10.1520/E1356-08R14.2.

[219] ASTM E698-16, Standard Test Method for Kinetic Parameters for Thermally Unstable Materials Using Differential Scanning Calorimetry and the Flynn/Wall/Ozawa Method, (2016). doi:10.1520/E0698-16.2.

[220] T. Ozawa, Kinetic analysis of derivative curves in thermal analysis, J. Therm. Anal. 2 (1970) 301–324. doi:10.1007/BF01911411.

[221] ASTM E831-12, Standard Test Method for Linear Thermal Expansion of Solid Materials by, (2000) 1–5. doi:10.1520/E0831-12.2.

[222] ASTM E1545-11, Standard Test Method for Assignment of the Glass Transition Temperature by Thermomechanical Analysis, (2011) 1–5. doi:10.1520/E1545-11.2.

[223] ASTM D5023-07, Standard Test Method for Plastics: Dynamic Mechanical Properties: In Flexure (Three- Point Bending), (2001) 1–3. doi:10.1520/D5023-07.1.

[224] ASTM E1640-13, Standard Test Method for Assignment of the Glass Transition Temperature By Dynamic Mechanical Analysis, (2013) 1–6. doi:10.1520/E1640-13.2.

[225] Y. Li, K.L. Pickering, R.L. Farrell, Determination of interfacial shear strength of white rot fungi treated hemp fibre reinforced polypropylene, Compos. Sci. Technol. 69 (2009) 1165–1171. doi:10.1016/j.compscitech.2009.02.018.

[226] G.M. Wu, Y.T. Shyng, S.F. Kung, C.F. Wu, Oxygen plasma processing and improved interfacial adhesion in PBO fiber reinforced epoxy composites, Vacuum. 83 (2009) S271–S274. doi:10.1016/j.vacuum.2009.01.080.

[227] H. Dannenberg, W.R. Harp, Determination of Cure and Analysis of Cured Epoxy Resins, Anal. Chem. 28 (1956) 86–90. doi:10.1021/ac60109a028.

[228] J. Mijovic, S. Andjeli6, S. Andjelic, A study of reaction kinetics by near-

infrared spectroscopy. 1. Comprehensive analysis of a model epoxy/amine system, Macromolecules. 28 (1995) 2787–2796. doi:10.1021/ma00112a026.

[229] N. Poisson, G. Lachenal, H. Sautereau, Near-and mid-infrared spectroscopy studies of an epoxy reactive system, Vib. Spectrosc. 12 (1996) 237–247. doi:10.1016/0924-2031(96)00027-6.

[230] G. Nikolic, S. Zlatkovic, M. Cakic, S. Cakic, C. Lacnjevac, Z. Rajic, Fast fourier transform IR characterization of epoxy GY systems crosslinked with aliphatic and cycloaliphatic EH polyamine adducts, Sensors. 10 (2010) 684–696. doi:10.3390/s100100684.

[231] M. González-González, J.C. Cabanelas, J. Baselga, Applications of FTIR on Epoxy Resins - Identification, Monitoring the Curing Process, Phase Separation and Water Uptake, in: Infrared Spectrosc. – Mater. Sci. Eng. Technol., InTech, 2012: pp. 261–284. doi:10.5772/2055.

[232] G. Lachenal, A. Pierre, N. Poisson, FT-NIR spectroscopy: Trends and application to the kinetic study of epoxy/triamine system (Comparison with DSC and SEC results), Micron. 27 (1996) 329–334. doi:10.1016/S0968-4328(96)00022-4.

[233] E. Duemichen, M. Javdanitehran, M. Erdmann, V. Trappe, H. Sturm, U. Braun, G. Ziegmann, Analyzing the network formation and curing kinetics of epoxy resins by in situ near-infrared measurements with variable heating rates, Thermochim. Acta. 616 (2015) 49–60. doi:10.1016/j.tca.2015.08.008.

[234] M. Erdmann, V. Trappe, H. Sturm, U. Braun, E. Duemichen, Cure conversion of structural epoxies by cure state analysis and in situ cure kinetics using nondestructive NIR spectroscopy, Thermochim. Acta. 650 (2017) 8–17. doi:10.1016/j.tca.2017.01.010.

[235] J.L. Koenig, P.T.K. Shih, Raman studies of the glass fiber-silane-resin interface, J. Colloid Interface Sci. 36 (1971) 247–253. doi:10.1016/0021-9797(71)90169-X.

[236] D. Puglia, L. Valentini, J.M. Kenny, Analysis of the cure reaction of carbon nanotubes/epoxy resin composites through thermal analysis and Raman spectroscopy, J. Appl. Polym. Sci. 88 (2003) 452–458.

doi:10.1002/app.11745.

[237] P.T.K. Shih, J.L. Koenig, Raman studies of the hydrolysis of silane coupling agents, Mater. Sci. Eng. 20 (1975) 137–143. doi:10.1016/0025-5416(75)90142-1.

[238] L. Merad, M. Cochez, S. Margueron, F. Jauchem, M. Ferriol, B. Benyoucef, P. Bourson, In-situ monitoring of the curing of epoxy resins by Raman spectroscopy, Polym. Test. 28 (2009) 42–45. doi:10.1016/j.polymertesting.2008.10.006.

[239] J.A. Bennett, R.J. Young, The effect of fibre–matrix adhesion upon crack bridging in fibre reinforced composites, Compos. Part A Appl. Sci. Manuf. 29 (1998) 1071–1081. doi:10.1016/S1359-835X(98)00045-1.

[240] J.D. Keenan, J.C. Seferis, J.T. Quinlivan, Effects of moisture and stoichiometry on the dynamic mechanical properties of a high???performance structural epoxy, J. Appl. Polym. Sci. 24 (1979) 2375–2387. doi:10.1002/app.1979.070241206.

[241] R. Hardis, J.L.P. Jessop, F.E. Peters, M.R. Kessler, Cure kinetics characterization and monitoring of an epoxy resin using DSC, Raman spectroscopy, and DEA, Compos. Part A Appl. Sci. Manuf. 49 (2013) 100–108. doi:10.1016/j.compositesa.2013.01.021.

[242] S. Vyazovkin, N. Sbirrazzuoli, Mechanism and Kinetics of Epoxy−Amine Cure Studied by Differential Scanning Calorimetry, Macromolecules. 29 (1996) 1867–1873. doi:10.1021/ma951162w.

[243] E.G. Karayannidou, D.S. Achilias, I.D. Sideridou, Cure kinetics of epoxy-amine resins used in the restoration of works of art from glass or ceramic, Eur. Polym. J. 42 (2006) 3311–3323. doi:10.1016/j.eurpolymj.2006.08.025.

[244] M. Munz, H. Sturm, W. Stark, Mechanical gradient interphase by interdiffusion and antiplasticisation effect - Study of an epoxy/thermoplastic system, Polymer. 46 (2005) 9097–9112. doi:10.1016/j.polymer.2005.06.098.

[245] P. Sharma, V. Choudhary, A.K. Narula, Curing of Epoxy Resin Using Imide-Amines, J. Appl. Polym. Sci. 101 (2006) 3503–3510. doi:10.1002/app.24580.

[246] Y.F. Li, M.Z. Xiao, Z. Wu, K. Peng, C.M. Han, W. Xiang, J.Y. Dai, Effects of epoxy/hardener stoichiometry on structures and properties of a diethanolamine-cured epoxy encapsulant, IOP Conf. Ser. Mater. Sci. Eng. 137 (2016) 012012. doi:10.1088/1757-899X/137/1/012012.

[247] Y. Calventus, S. Montserrat, J.M. Hutchinson, Enthalpy relaxation of non-stoichiometric epoxy-amine resins, Polymer. 42 (2001) 7081–7093. doi:10.1016/S0032-3861(01)00133-1.

[248] F.-M. Kong, C.M. Walkup, R.J. Morgan, Structure—Property Relations of Polyethertriamine-Cured Bisphenol-A-diglycidyl Ether Epoxies, in: R.S. Bauer (Ed.), Epoxy Resin Chem. II, American Chemical Society, 1983: pp. 211–227. doi:10.1021/bk-1983-0221.ch011.

[249] R. Bansil, M.K. Gupta, Effect of varying crosslinking density on polyacrylamide gels, Ferroelectrics. 30 (1980) 63–71. doi:10.1080/00150198008209489.

[250] R. Mezzenga, A. Luciani, Phase Separation and Gelation of Epoxy Resin / Hyperbranched Polymer Blends, Polym. Eng. Sci. 42 (2002) 249–257. doi:10.1002/pen.10945.

[251] J. Parameswaranpillai, A. George, J. Pionteck, S. Thomas, Investigation of Cure Reaction, Rheology, Volume Shrinkage and Thermomechanical Properties of Nano-TiO 2 Filled Epoxy/DDS Composites, J. Polym. 2013 (2013) 1–17. doi:10.1155/2013/183463.

[252] J. Mijovit, S. Andielit, J.M. Kenny, In situ Real-time Monitoring of Epoxy / Amine Kinetics by Remote Near Infrared Spectroscopy, Polym. Adv. Technol. 7 (1996) 1–16. doi:10.1002/(SICI)1099-1581(199601)7:1<1::AID-PAT480>3.0.CO;2-N.

[253] B.A. Rozenberg, Kinetics, thermodynamics and mechanism of reactions of epoxy oligomers with amines, in: K. Dušek (Ed.), Epoxy Resins Compos. II, Springer Berlin Heidelberg, Berlin, Heidelberg, 1986: pp. 113–165. doi:10.1007/BFb0017916.

[254] S. Swier, G. Van Assche, W. Vuchelen, B. Van Mele, Role of Complex Formation in the Polymerization Kinetics of Modified Epoxy−Amine Systems,

Macromolecules. 38 (2005) 2281–2288. doi:10.1021/ma047796x.

[255] G. Socrates, Infrared and Raman characteristic group frequencies: tables and charts, 3rd ed., Wiley-Blackwell, 2004.

[256] J.L. Thomason, L.J. Adzima, Sizing up the interphase: An insider's guide to the science of sizing, Compos. Part A Appl. Sci. Manuf. 32 (2001) 313–321. doi:10.1016/S1359-835X(00)00124-X.

[257] J.L. Thomason, L. Yang, D. Bryce, R. Minty, An exploration of the relationship of chemical and physical parameters in the micromechanical characterisation of the apparent interfacial strength in glass fibre epoxy systems, IOP Conf. Ser. Mater. Sci. Eng. 139 (2016) 012048. doi:10.1088/1757-899X/139/1/012048.

[258] P. Zinck, E. Mäder, J.F. Gerard, Role of silane coupling agent and polymeric film former for tailoring glass fiber sizings from tensile strength measurements, J. Mater. Sci. 36 (2001) 5245–5252. doi:10.1023/A:1012410315601.

[259] Q. Wu, M. Li, Y. Gu, S. Wang, L. Yao, Z. Zhang, Effect of Sizing on Interfacial Adhesion of Commercial High Strength Carbon Fiber-Reinforced Resin Composites, Polym. Polym. Compos. 37 (2016) 254–261. doi:10.1002/pc.

[260] C. Li, K. Potter, M.R. Wisnom, G. Stringer, In-situ measurement of chemical shrinkage of MY750 epoxy resin by a novel gravimetric method, Compos. Sci. Technol. 64 (2004) 55–64. doi:10.1016/S0266-3538(03)00199-4.

[261] J. Zhao, P. Yu, S. Dong, The influence of crosslink density on the failure behavior in amorphous polymers by molecular dynamics simulations, Materials (Basel). 9 (2016). doi:10.3390/ma9040234.

[262] S.P. Reilly, J.L. Thomason, Effects of silane coating on the properties of glass fibre and glass fibre reinforced epoxy resin, 14th Eur. Conf. Compos. Mater. ECCM14. (2010) 7–10. http://strathprints.strath.ac.uk/20626/1/strathprints020626.pdf.

[263] G. Tesoro, Yulong Wu, Silane coupling agents: the role of the organofunctional group, J. Adhes. Sci. Technol. 5 (1991) 771–784.

doi:10.1163/156856191X00206.

[264] G.M. Odegard, A. Bandyopadhyay, Physical aging of epoxy polymers and their composites, J. Polym. Sci. Part B Polym. Phys. 49 (2011) 1695–1716. doi:10.1002/polb.22384.

[265] A. Hodzic, J.K. Kim, A.E. Lowe, Z.H. Stachurski, The effects of water aging on the interphase region and interlaminar fracture toughness in polymer-glass composites, Compos. Sci. Technol. 64 (2004) 2185–2195. doi:10.1016/j.compscitech.2004.03.011.

[266] G.H.D. Tonoli, V.D. Pizzol, G. Urrea, S.F. Santos, L.M. Mendes, V. Santos, V.M. John, M. Frías, H. Savastano, Rationalizing the impact of aging on fiber--matrix interface and stability of cement-based composites submitted to carbonation at early ages, J. Mater. Sci. 51 (2016) 7929–7943. doi:10.1007/s10853-016-0060-z.

[267] M. De Monte, C. Cruz, L. Yang, J. Thomason, Aging of the fiber-matrix interface in glass-fiber-reinforced polyamide 66 composites - experiments and modelling, in: Eur. Congr. Comput. Methods Appl. Sci. Eng., Crete Island, Greece, 2016.

[268] K.A. Downes, J.L. Thomason, A method to measure the influence of humidity and temperature on the interfacial adhesion in polyamide composites, Compos. Interfaces. 6440 (2015) 1–10. doi:10.1080/09276440.2015.1059114.

Appendix A: Influence of microbond test setup on IFSS

Introduction

After extensive work with the Instron adjustable microbond and TMA fixed microbond setups discussed in subchapter 3.3 it was decided to study whether it was plausible to improve the Instron method by changing the microbond rig setup. The primary difficulty with the adjustable rig was in the alignment of the two separate shearing blades, whilst this issue was removed in the TMA setup by using fixed blades. This work was conducted by an undergraduate student, Andrew Paxton, under the supervision of myself and Professor James Thomason.

Literature Review

The Microbond Test Setup

Previous research has shown that there are many factors relating to the set-up of the microbond experiment as well as the specimens tested which influence the outcomes and reliability of the measured IFSS value [150,162,169]. It is not uncommon for the microbond experiment to display large scatter in the data produced due to the difficulty in being able to consistently control certain variables within the experiment. Previous works have also suggested that this is due to the control of “some unexpected experimental parameter” [14] and varying droplet size due to human error [268]. This data scatter can be one of the potential drawbacks of the technique when compared to other micromechanical methods. A schematic provided in Figure A.1 [172] showing the setup of the microbond experiment, rotated horizontally, displays the different parameters that may influence the measured IFSS value.

Heilhecker et al [163] has shown that the vice or blade angle, ϕ in the figure above, has the most significant impact on the state of shear loading at the interphase region and therefore on the measured IFSS value. Finite element analysis (FEA) represents a useful technique for modelling the loading distribution across the droplet and the microbond blades with Ash et al [172] and Nishikawa [164] having both used FEA to simulate a microbond experiment.

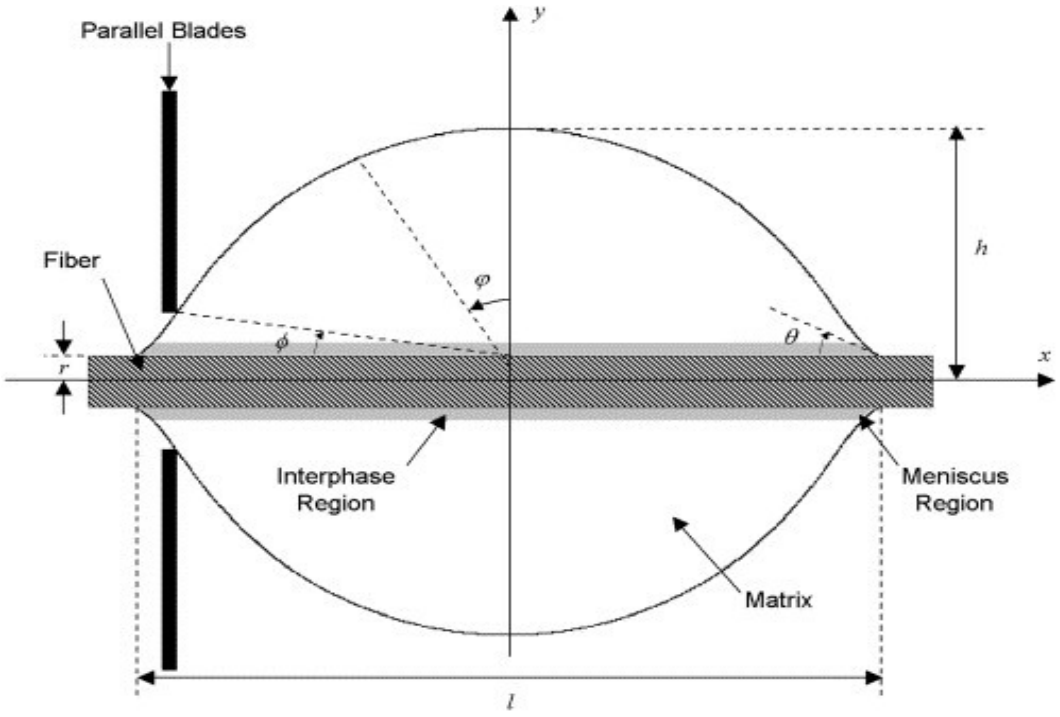

Figure A.1 - Schematic of geometric parameters of microbond test. Where l is embedded length, r is fibre radius, h is the droplet radius, θ is the contact angle, φ is the angle from the y-axis, ϕ is the vice angle.

Ash [172] was able to produce the plot shown in Figure A.2 through simulation showing the maximum von-Mises Stress in MPa along the distance of the interphase region from the point closest to the blades at different angles. From Figure A.2 it can be seen that with an increasing vice angle the combined stresses along the interphase region decrease as they are distributed throughout the diameter of the droplet and, in order to cause yielding at the interphase, a larger load would have to be exerted. This

emphasises the importance that the design of the shearing blade has in the overall experimental setup.

While in practice these parameters are hard to control manually at such a small scale, it nevertheless suggests that smaller vice angles are preferred for the microbond experiment to obtain accurate results of maximum load. Other factors, such as the geometry of the droplet and meniscus effects caused at the ends by capillary forces during droplet application, influence the measured maximum stress value. However, as samples are often made by hand these parameters are harder to account for in the overall setup.

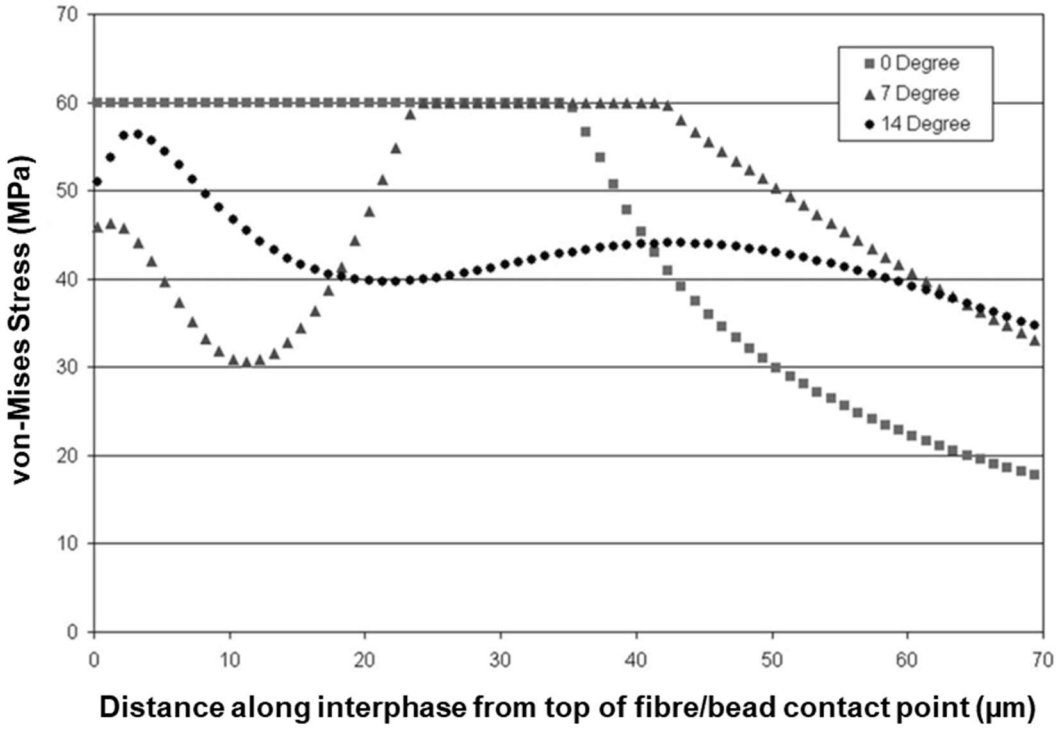

Figure A.2 - von-Mises stress at interphase region with varying blade angle.

Shearing Blade Designs

The primary goal of this section of work was to design a fixed blade method capable of functioning with the Instron 3342 universal testing machine to allow for a

comparison to be made against the adjustable blade setup used for the bulk of the microbond research conducted in this thesis. There were multiple different designs in the literature which could be used to construct the fixed blade method, with Figure A.3 [67] detailing the more promising designs. A further design taken into consideration was the fixed blade setup used for the TMA microbond technique discussed in subchapter 3.3.2 [14,15]. A set of shearing plates was adapted to fit inside a Thermomechanical Analyser (TMA) oven with the capability to accommodate droplets of various diameters while allowing easy placement of the fibre within the vice. In addition, Thomason et al [14,15] found that the setup produced data sets with low scatter as well as good R^2 values. This was also shown to be the case for the results discussed in subchapter 6.2, with the data scatter appearing smaller than for the adjustable setup.

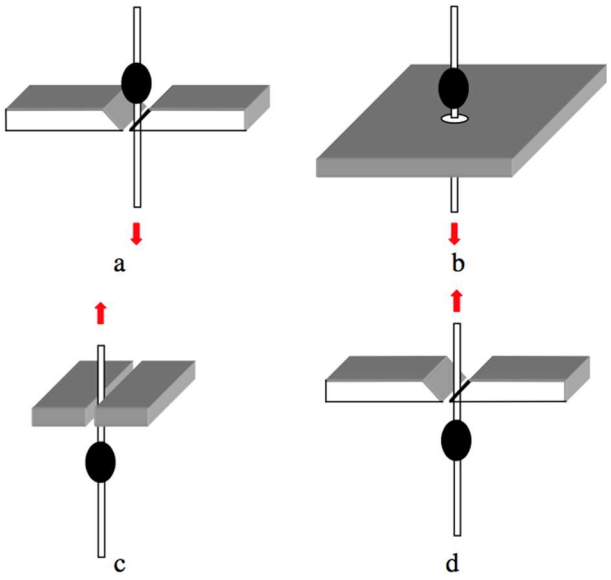

Figure A.3 - Different potential fixed blade microbond designs.

As a result of these findings, the TMA fixed blade design was used as a starting point to base the initial concepts on for the adaptation of the fixed blade method for the standard microbond experiment under regular climate conditions.

Experimental

This study focussed on the design, manufacture and testing of a fixed blade microbond setup for the Instron tensile testing machine to compare with the technique discussed in section 3.3.1. As a result, the sample preparation and testing procedure used were as discussed in section 3.3.1, with the only difference now being that the rig was fixed instead of adjustable. Fibre 1 was selected for the comparison, since this was the fibre that had been studied most with the adjustable method. The R value selected was the stoichiometric ratio. The results would then be compared with tests done using the adjustable rig by the same operator, (Andrew), as well as the findings discussed in Chapter 5.

Fixed Blade Design

As was discussed, the crucial aspect of producing a reliable testing method was in ensuring the accurate design of the shearing blade. The accurate measurement and production of the fixed blades proved challenging due to the microscale at which the test functions at. Minute differences in blade width or alignment could result in a large error during the test. It was agreed between myself and Andrew that the design had to meet several design criteria in order for it to be suitable for microbond experimental work:

i. The material used for the blades had to possess a high stiffness to ensure effective shearing of the matrix droplet. Although very small loads are capable of de-bonding the droplet during the test, any potential movement or deformation of the blades during the test could have a significant impact on the final result obtained.

ii. The design had to possess a parallel bottom shearing face, with knife edges to accommodate the fibre pull-out technique and provide an equally distributed shearing force.

iii. The design had to accommodate droplets and fibres of various diameters.

Several design concepts were initially created by hand and then modelled using Creo Parametric CAD modelling software with an example shown in Figure A.4. Originally, it was planned to manufacture the blade from one piece of metal to ensure flatness and parallel alignment of the bottom shearing face. However, such a design proved to be too demanding to manufacture within the University given the time constraints of the project, thus the design was simplified to be similar to that designed for the TMA microbond technique.

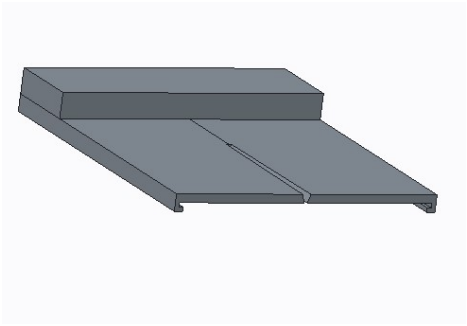

Figure A.4 - CAD model of final fixed blade design.

Under microscopy the blades were positioned together with the angled edges aligned. Glue was then placed on the top of each plate and the brace placed on top. Whilst the glue was setting a small slit was formed, keeping the rear parts of the blade in contact with each other. The process took place on a flat glass surface to ensure the shearing faces of both plates were maintained on the same plane. This process was completed for several iterations and ran with practice test samples until the gap between the fixed blades was small enough to accommodate droplets in the region of 40-80 μm diameter.

To maintain a similarity between the fixed blade design and the original adjustable design, high carbon content stainless steel was used for the blade material. Two knife edges were also grinded at one edge of each plate to accommodate the fibre pull-out technique and the edges and surfaces were polished to remove any surface deformities that may lead to potential errors. An image of the fixed blades after completion is provided in Figure A.5.

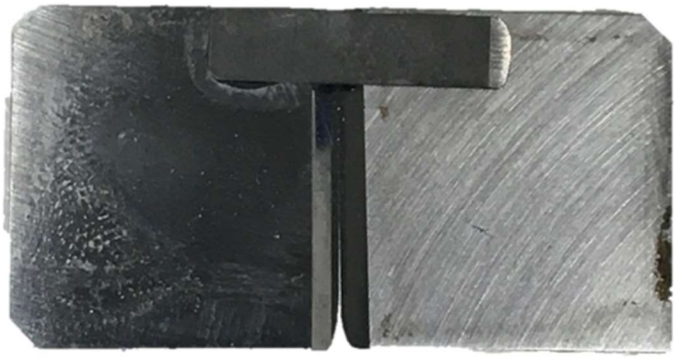

Figure A.5 - Image of fixed blade final design.

Microbond Rig Design

Following the successful design and manufacture of the fixed blade setup it was then necessary to design a rig that would allow it to be installed onto the Instron tensile testing machine. As with the fixed blade setup it was agreed between myself and Andrew that the rig be designed to meet a number of different criteria to ensure accurate measurement:

i. The rig design had to be able to support the fixed blade in a way that the plates could exert a downward shearing force without displacement or movement.
ii. The rig design also had to be able to fit on the Instron tensile testing machine used for the experiment.
iii. The rig design had to be able to adjust the position of the blade to accommodate for varying positioning of the sample. Since the sample is

suspended on the hook of the Instron, it was required that the blade position be slightly adjustable to ensure the sample met the angled edges of the blade.

As with the fixed blades, the design of the rig underwent multiple different iterations to ensure it met the conditions specified as well as to simplify the manufacturing process. CAD models and technical drawings, such as that shown in Figure A.6, were produced at each stage. Aluminium was chosen as the material for manufacture due to its good corrosive resistant properties and light weight.

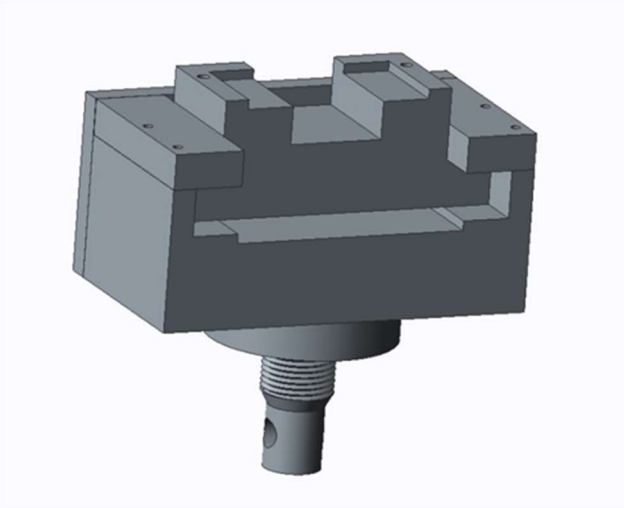

Figure A.6 - CAD model of final rig design.

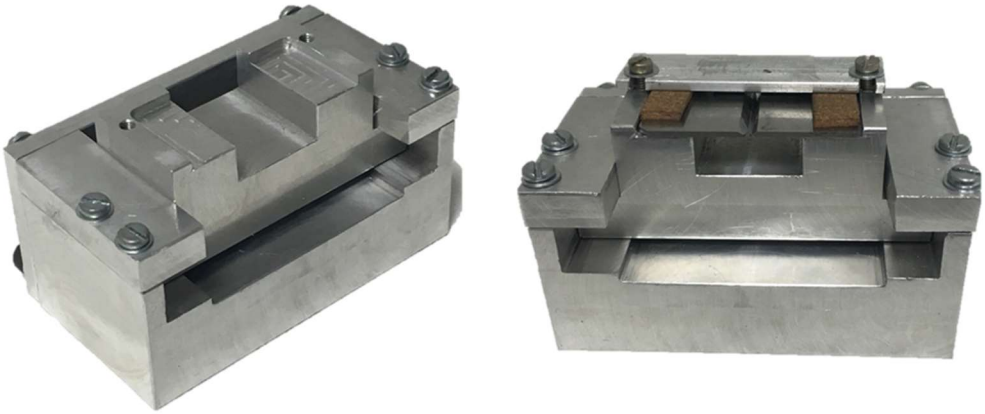

Figure A.7 - Image of final manufactured rig and rig with fixed blade.

After manufacture the individual parts were bolted together. The edges of the top step had to be hand-filed slightly to better accommodate the blade and a thin aluminium clamp was used to fix the blade in place whilst testing. Holes were drilled and threaded into the bottom base to accommodate the base screw from the current moveable rig. This allowed the design to be fitted on to the Instron tensile testing machine. An image of the final rig design after manufacture as well as with the fixed blades in place can be seen below in Figure A.7.

Results and Discussion

The primary method of comparison used were the load/ displacement plots produced by the microbond test as well as their respective coefficient of determination (R^2) values for defining how close the data was to the fitted regression line of the plot. The average IFSS values produced from the data were also compared. Figure A.8 shows the load/displacement plot for the samples tested using the adjustable blade rig and Figure A.9 shows the load/displacement plot for the samples tested using the fixed blade rig.

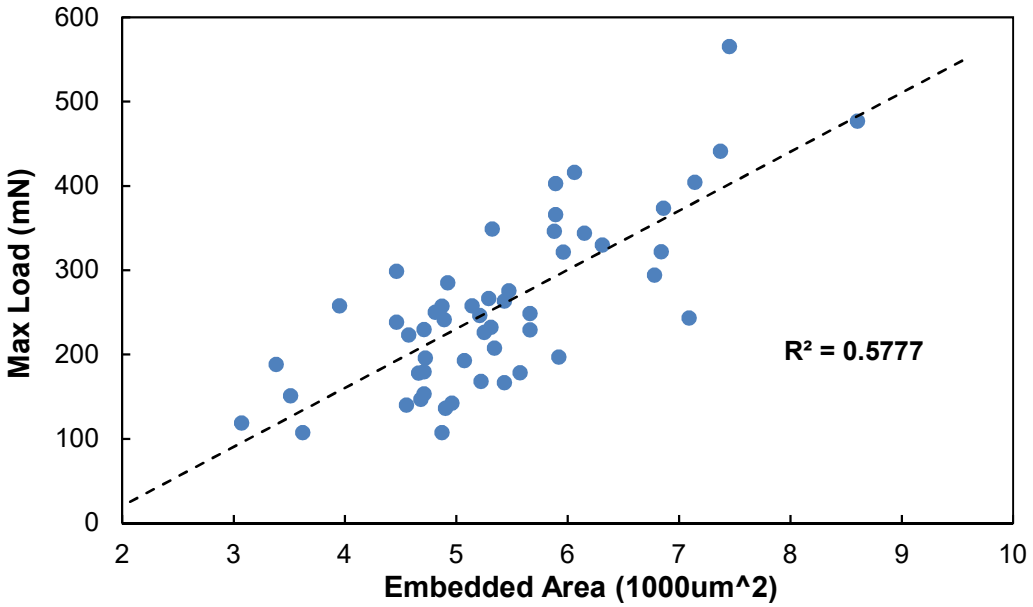

Figure A.8 - Load/Displacement Plot using adjustable blade setup.

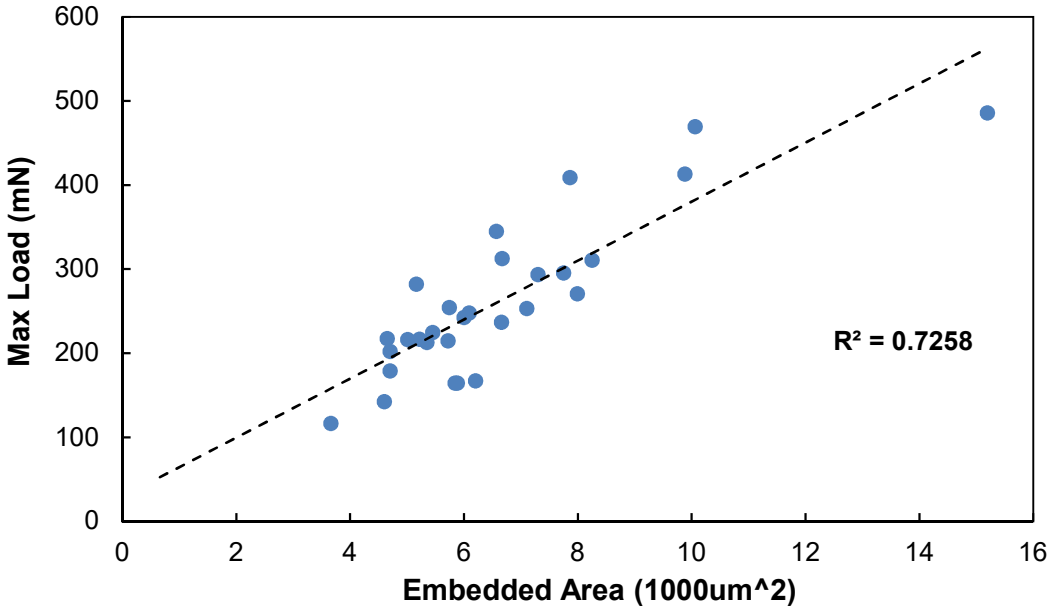

Figure A.9 - Load/Displacement Plot using fixed blade setup.

It can be seen that data collected using the fixed blade setup possesses a larger R^2 value, suggesting that the technique produces a more reliable test. It should be stated that the adjustable blade method provided 53 successful tests with 7 samples being neglected due to fibre breakage whilst for the fixed blade technique only 30 of the 60 samples were classified as successful tests. The others were neglected due to fibre breakage. Thus, judging from the two plots, it can be see that the fixed blade setup appears more consistent for the successful samples, however it results in more fibre breakages.

The mean IFSS value obtained for the adjustable technique was 47 MPa compared to the 40 MPa obtained using the fixed blade technique. Both appear lower than the 52 MPa recorded for the stoichiometric ratio in section 5.2 as shown in Table A.1. This would agree with the plot discussed in subchapter 6.2 regarding the comparison between the TMA microbond setup and the Instron adjustable setup. It was shown how the fixed blades of the TMA microbond setup produced IFSS values of slightly lesser size, but with less scatter without the need to measure any remaining

meniscus. It is notable however that the error recorded for the data collected by Minty appears smaller than that collected by Paxton for both setups. This can be attributed to operator error/experience, as well as the data produced by Minty having undergone further analysis using SEM imaging as discussed in subchapter 3.3.

Testing method	Average IFSS Value (MPa)	Standard Deviation	Successful Samples	95% Confidence Limits	Operator
Adjustable Blade	47	12.4	53	3.42	Paxton
Fixed Blade	40.1	7.8	30	2.91	Paxton
Adjustable Blade	51.8	6.6	57	1.75	Minty

Table A.1 - Comparison of IFSS data collected using the two techniques.

A possible explanation for the superior levels of scatter for the fixed blade setup is the parallel alignment of the bottom shearing face. A microscopic image comparison of both blades shows the alignment of the fixed blade (Figure A.10) is considerably better that of the adjustable setup without adjustment (Figure A.11). It can be seen that comparing the two figures, Figure A.11 shows a notable misalignment between the two adjustable blades compared to the fixed blades shown in Figure A.10. Even with a small misalignment of the blades, a moment force may be introduced due to offset loading. Therefore, the droplet would not solely be experiencing a shearing force and thus would be likely to de-bond before its true maximum de-bond strength was measured.

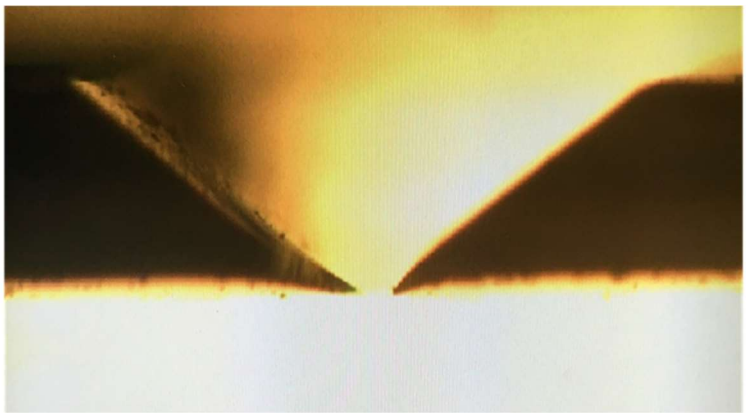

Figure A.10 - Microscopic image of fixed blade alignment.

Figure A.11 - Microscopic image of adjustable blade misalignment (prior to corrections).

This is the primary difficulty in working with the adjustable setup when compared to the more consistent fixed blade setup. Since the design requires the blades to be adjustable this requires several other moving parts to allow this to be achievable. Each of the different parts may be found to fatigue over time, introducing errors to the system. For instance, the left blade was found to naturally hang lower within the rig than the right blade as shown in Figure A.11, and could only be raised through retracting the blade. As such a specific method of adjusting the left blade first, retracting it and then adjusting the right blade had to be followed to produce the proper alignment. It has been noted that the adjustable setup will typically require re-alignment after around six months to ensure the blades had not drifted further. The

setup and alignment process of the adjustable setup was also found to be an extremely sensitive procedure, requiring a degree of experience and investment of time before being able to be carried out successfully. This can potentially add the possibility for further human error.

Figure A.12 shows the adjustable setup after the proper adjustments have been made to the blades, with it shown to compare more favourably to the fixed blades. However, it does appear that having the adjustable blades will introduce a degree of variability to the experimental process, hampering the reproducibility of the test and likely resulting in the higher degree of scatter shown in Figure A.8.

Figure A.12 - Microscopic image of adjustable blade alignment (after corrections).

Analysis using scanning electron microscopy provides support to this hypothesis, with Figure A.13 showing a de-bonded droplet using the adjustable setup and Figure A.14 showing a de-bonded droplet using the fixed setup respectively. It can be seen in Figure A.13 that the droplet has successfully de-bonded, yet it has left a remaining meniscus at its original position on the fibre. This remaining meniscus left over can be seen to be not symmetrical and shows that the crack in the matrix droplet has propagated at an angle which could potentially be a result of the misalignment of the two blades. As such the true embedded length of the fibre within the droplet would be

smaller than that measured originally and used for the calculation. Thus, after analysis the IFSS value would be increased and the degree of scatter likely decreased. The samples shown in Figure A.8 did not undergo this analysis hence this may explain the large difference between the results gained by myself and Andrew Paxton shown in Table A.1.

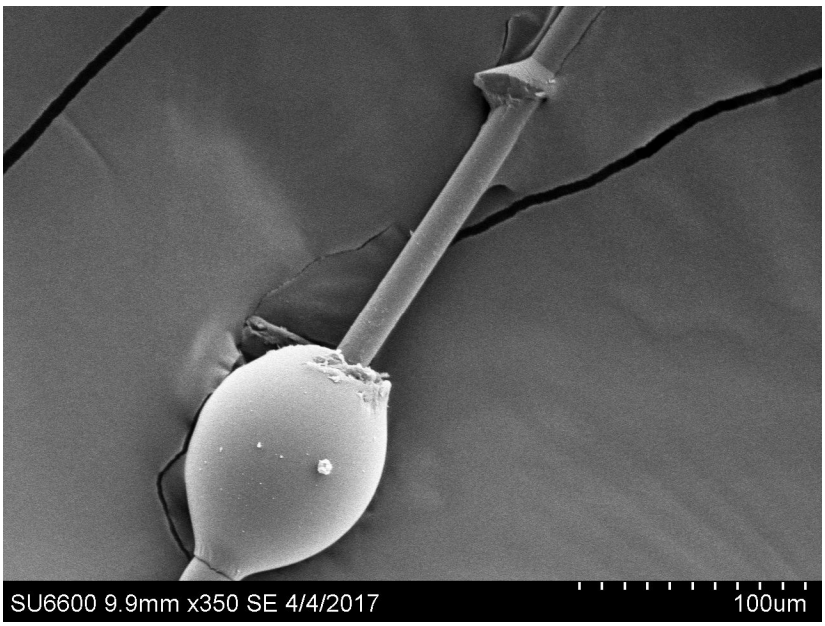

Figure A.13 – De-bonded droplet using the adjustable blades rig

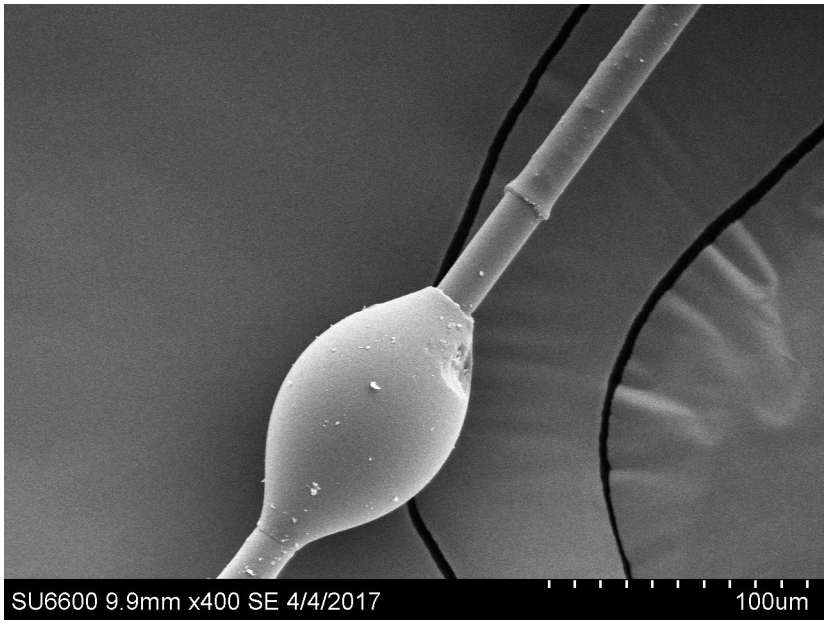

Figure A.14 - De-bonded droplet using the fixed blades rig

Figure A.14 shows a droplet having successfully de-bonded with no remaining meniscus. As such the true embedded length of the droplet was equal to that originally measured, hence giving a more accurate reading for IFSS with less scatter.

Yet it must also be stated that although the fixed blade method gave less scatter than the adjustable method, much fewer successful tests were achieved, with only 30 out of a set of 60 being suitable for use compared to 53 for the adjustable blades. Most of the test failures were found to occur due to the practicality of placing the fibre in the slot of the fixed blade by hand. The process of placing the fibre was tedious and time consuming, mostly due to the sample not always lying perfectly vertical. This made placing it in the slot and then sliding the blade over the identified droplet challenging without damaging the fibre. This process was further complicated by the fibre catching on the blade edges whilst the sliding part was being adjusted as well as by the presence of other droplets within close proximity to the indented one making it hard to place it beneath the shearing plates. The two former issues are not typically encountered when using the adjustable method.

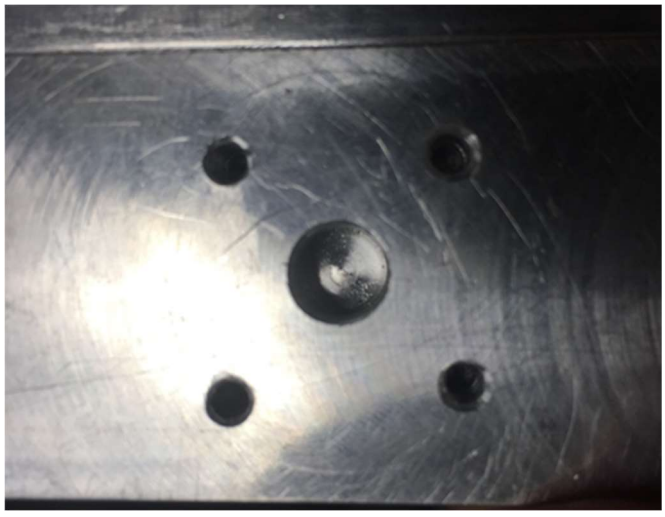

Figure A.15 - Image of manufacturing defect.

In addition, it was found that during manufacture a mistake was made in the exact placement of holes drilled on the bottom of the rig to fit the base screw. Two of the

holes were slightly offset and not square as intended as shown in Figure A.15. This meant that the rig and blade sat at an angle during the testing and the direction of loading was not in-line with the direction of vertical displacement. This would have led to twisting of the fibres during loading and explained the high number of fibre breakages. This may also explain why the IFSS value measure for the fixed blade setup was significantly smaller than that measured for the adjustable blade setup.

Summary and Conclusions

In conclusion it was found that there was a significant difference in the results produced by using two different microbond blade setups. The data from the adjustable microbond setup was shown to possess large levels of scatter and therefore a larger degree of error, with this attributed to parameters that are hard to control. Droplet geometry and size as well as blade angle and alignment represent variables that are difficult to keep constant whilst working on such a small scale, with slight differences magnified in the resulting IFSS measured. The fixed blade method was shown to produce data with lower levels of scatter and higher R^2 values, however the practicality of placing the droplet was found to be time-consuming and challenging in terms of avoiding fibre breakage. As such although the quality of the data produced by the fixed blade method was superior, there was also less of it.

Lower IFSS values than expected were obtained using both methods when compared to those discussed in Chapter 5. The adjustable method produced an average IFSS of 47 MPa which was comparable to the expected value of around 52 MPa. A potential explanation for the error between the results was that the samples tested in this study did not undergo any further analysis after testing to assess the size of the true embedded length of the de-bonded droplet. The adjustable method was shown to produce samples which regularly left a tell-tale meniscus at the original position of the

droplet prior to testing. As such, the embedded length used in the calculation of the IFSS was likely larger than the actual true embedded length, resulting in a smaller IFSS recorded IFSS value.

In contrast the fixed blade method showed a much lower average IFSS value than expected, at only 40 MPa, with the tested samples showing no signs of leaving any meniscus at the point of de-bond. Yet the significantly lower IFSS may be attributed to a number of causes, such as the mistake in the manufacture of the rig which may have led to fibre twisting, as well as any potential damage to the fibre during the placing of the sample. Thus, despite the decrease in error shown for the fixed blade setup and the better quality of the de-bonded samples after testing it was difficult to draw a conclusion on whether the setup was superior to the current adjustable method. It was shown to produce more consistent data, however, the practicality of the technique proved challenging and the final values measured for IFSS were significantly lower than those for the current method. Despite this it is highly recommended that further research be conducted into this topic, since the manufacturing defect in the fixed blade setup very likely impacted the loading of the microbond samples, resulting in the lower IFSS.

Future Work

Future work would focus on the remanufacture of the fixed blade rig to correct the placement mistake of the inserts to fit the base screw. This would ensure the loading is collinear with the direction of displacement of the fibre and remove the possibility that this may be influencing the results obtained by the fixed blade. This would also potentially decrease the number of sample breakages due to twisting, leading to more data overall.

It would also be recommended that a micrometer or similar device be incorporated into the design to allow for more sensitive adjustment of the sliding part over the identified droplet during fibre placement. This may help to decrease the time spent placing a sample as well as potentially reduce the number of breakages due to the fibre coming into unwanted contact with the blades.